MONASH University

Fronto-striato-thalamic Circuits, Dopamine, and the Psychosis Continuum

Kristina Sabaroedin

Grad Dip (Hons) Psychology

A thesis submitted for the degree of Doctor of Philosophy

at Monash University in 2020

Faculty of Medicine, Nursing, and Health Sciences

School of Psychological Sciences

Copyright notice

Abstract

The symptoms of psychosis are proposed to lie on a continuum of severity, ranging from psychosis-like experiences (PLEs) on the least severe end of the continuum, through prodromal at-risk mental states and first episode psychosis (FEP), to schizophrenia at the extreme end. Dysfunction of fronto-striato-thalamic (FST) circuits is central to the emergence of psychosis. Two FST circuits that are particularly relevant to the symptoms of psychosis are the dorsal 'associative' circuit, linking the dorsolateral prefrontal cortex with the dorsal striatum, and the ventral 'limbic' circuit, linking the orbital and ventromedial prefrontal cortices and subcortical limbic structures (e.g., hippocampus and amygdala) with the nucleus accumbens. Altered connectivity of the dorsal and ventral circuits has consistently been demonstrated in various cohorts along the psychosis continuum. The onset of psychosis is thought to be driven by a dysregulation of dopamine signalling within these circuits. The general aim of this thesis was to systematically investigate the connectivity of FST circuits across the psychosis continuum.

After a review of relevant background literature in Chapter 1, Chapter 2 presents an investigation of the associations between corticostriatal functional connectivity and PLEs in a large community sample of healthy adults who underwent high resolution resting-state functional magnetic resonance (fMRI) scanning. Functional connectivity is defined as statistical dependencies between regional physiological signals, and is widely used to probe brain circuit dysfunction. Positive and negative dimensions of PLEs were derived from a data reduction method applied to an extensive battery of PLE measurements assessing a wide array of subclinical symptoms. Positive symptom-like PLEs were associated with reduced functional connectivity of the dorsal circuit; namely, between dorsal striatal regions and the primary motor and prefrontal cortices, specifically the dorsolateral prefrontal and anterior cingulate cortices. This finding was consistent with prior work in clinical patients and high-

risk groups, thus establishing the dorsal corticostriatal function as a putative neural marker of symptom severity across a broad spectrum of the psychosis continuum.

Chapter 3 develops a model of FST effective connectivity across different stages of the psychosis continuum and in relation to striatal dopaminergic function. Effective connectivity refers to the causal influence that one neuronal system exerts over another. Thus, unlike functional connectivity, it is able to distinguish bottom-up from top-down influences within FST circuitry. This is important in light of ongoing debates in the literature about whether psychotic symptoms and dopamine dysfunction arise from deficient top-down regulation of subcortical systems by cortical areas or abnormal bottom-up signalling from deeper subcortical structures. To overcome this limitation, spectral dynamic causal modelling (DCM) was used to identify causal interactions in dorsal and ventral FST circuitry in a healthy group with PLEs, anti-psychotic naïve FEP patients, and patients with established schizophrenia. The healthy group with PLEs also underwent a concurrent positron emission tomography with [^{18}F]DOPA to examine associations between FST connections and striatal dopamine synthesis capacity. Early phases of psychosis were associated with prominent disruption of subcortical connectivity, particularly of the thalamus and the midbrain. Cortical dysfunction emerged later in the illness. Midbrain and thalamic connectivity were associated with positive symptoms across the continuum, and also with striatal dopamine synthesis. This finding supports the primary role of subcortical and midbrain dysfunction in the early stages of psychosis.

Having established a working model of FST effective connectivity across the psychosis continuum, Chapter 4 returns to the study of subclinical PLEs, using item response theory (IRT), a technique for refining self-report measurements to derive a high-precision characterization of nine distinct PLE dimensions, thereby providing a high-resolution characterization of subclinical symptomatology. These dimensions included positive symptom-like constructs related to delusions, hallucinations, cognitive disorganisation, and body image aberration; and negative symptom-like constructs related to anhedonia, asociality, avolition, blunted affect, and alogia. Using spectral DCM to link these dimensions to dorsal and ventral FST effective connectivity revealed that all dimensions of positive PLEs were associated with striatothalamic connectivity, suggesting an important role for the striatal filtering of information flow in positive PLE expressions. Subclinical delusions and

hallucinations were also associated with ascending influence of the amygdala on the cortex, whereas dimensions pertaining to delusions and cognitive disorganisation were associated with connections spanning both dorsal and ventral FST circuits. Associations with negative PLE dimensions were restricted to subcortical components of the ventral circuit and implicated the nucleus accumbens. Bottom-up influences from the midbrain were not prominently associated with PLE dimensions, suggesting a mechanistic distinction between subclinical and clinical symptom expressions across the continuum.

Taken together, these findings demonstrate that the connectivity of FST circuits is implicated across different stages of the psychosis continuum. This thesis identifies a prominent role for subcortical dysconnectivity and midbrain disinhibition in early illness, cortical disruption in established illness, a prominent role of striatothalamic influence in both subclinical and clinical positive symptoms and striatal dopamine synthesis, and dysconnectivity of subcortical limbic circuits in negative PLEs. The findings support a neurobiological continuum of psychosis at the level of connected neural circuits, rather than specific brain regions or connections, and suggest that dysfunction of subcortical circuitry in particular may play a primary role in disease pathophysiology.

Acknowledgements

This thesis is only possible with the help of my fantastic supervision team. First and foremost, I would like to extend the warmest gratitude to my primary supervisor Prof. Alex Fornito. I appreciate your patience, kindness, and generosity. Your rigorous training is invaluable, and I hope it will help me build a solid foundation as a researcher. I would like to thank Dr. Kevin Aquino for your support, enthusiasm and positive attitude. You have made this journey more enjoyable. Last but not least, I would like to thank Prof. Mark Bellgrove for all the opportunities you have given me.

I am thankful for all my colleagues and friends whom I have met through the PhD for your camaraderie. Finishing a PhD during a pandemic has been challenging. I really appreciate the friendship, the Netflix parties, the gifts, crafternoons, WhatsApp chats, and company, both in person and on Zoom, during this difficult time. I am also extremely grateful for all the friends who have known me for years. Thank you for your friendship and support. You remind me that I can always take on whatever life throws at me and rise above.

I would like to thank my father who instils in me good work ethics from a young age and also for encouraging me to follow my own path. I am deeply grateful to my mother who values education and always encourages me to see the world. Thank you to my sister—the one who should have been doing a PhD—for the company and for putting up with my mischief.

Last but not least, I would like to thank the *yang* to my *yin,* Hannes Almgren, for all your support and patience. Hopefully we close this physical distance soon.

Publications during enrolment

_____

1. Pani, S. M., **Sabaroedin, K.,** Tiego, J., Bellgrove, M., & Fornito, A. (2020). A multivariate analysis of the association between corticostriatal functional connectivity and psychosis-Like experiences in the General Community. *Psychiatry Research: Neuroimaging.* 111202.
2. Brosnan, M.B., **Sabaroedin, K.**, Silk, T., Genc, S., Newman, D. P., Loughnane, G. M., Fornito, A., O Conell, R. G., & Bellgrove, M. (2020). Dorsal fronto-parietal connectivity underpins evidence accumulation during perceptual decisions in humans. *Nature Human Behaviour,* 1-12.
3. Aquino, K., Fulcher, B., Parkes, L., **Sabaroedin, K.**, & Fornito, A. (2020). Identifying and removing widespread signal deflections from fMRI data: Rethinking the global signal regression problem. *NeuroImage*, 116614.
4. **Sabaroedin, K.**, Tiego, J., Parkes, L., Sforazzini, F., Finlay, A., Johnson, B., Pinar, A., Cropley, V., Harrison, B.J., Zalesky, A., Pantelis, C., Bellgrove, M., & Fornito, A. (2019). Functional connectivity of corticostriatal circuitry and psychosis-like experiences in the general community. *Biological Psychiatry*, *86*(1), 16-24.
5. Den Ouden, L., Kandola, A., Suo, C., Hendrikse, J., Costa, R., Watt, M. J., Lorenzetti, V., Chye, Y., Parkes, L., **Sabaroedin, K**., & Yücel, M. (2018). The influence of aerobic exercise on hippocampal integrity and function: Preliminary findings of a multi-modal imaging analysis. *Brain Plasticity*. Advance online publication. doi: 10.3233/BPL-170053

In submission

1. **Sabaroedin, K.,** Razi, A., Chopra, S., Tran, N., Pozaruk, A., Chen, Z., Finlay, A., Nelson, B., Allott, K., Alvarez-Jimenez, M., Graham, J., Baldwin, L., Tahtalian, S., Yuen, H.P., Harrigan, S.,

Cropley, V., Sharma, S., Saluja, B., Williams, R., Pantelis, C., Wood, S.J., O'Donoghue, B., Francey, S., McGorry, P., Aquino, K., & Fornito, A. Effective connectivity of fronto-striato-thalamic circuitry across the psychosis continuum. *Submitted to The American Journal of Psychiatry on December 7th, 2020*

2. Zhang, X., Chye, Y., Braganza, L., Fontenelle, L., Harrison, B.J., Parkes, L., **Sabaroedin, K.,** Maleki, S., Yucel., M., & Suo, C. Severity related to neuroanatomical alteration across symptom dimensions in obsessive-compulsive disorder. *Submitted to Journal of Affective Disorders Reports on December 7th, 2020*
3. Deco, G., Aquino, K., Arnatkevičiūtė, A., Oldham, S., **Sabaroedin, K.,** Kringelbach, M. L., & Fornito, A. Dynamical consequences of regional heterogeneity in the brain's transcriptional landscape. *Submitted to Science Advances on October 29th, 2020*
4. Chopra, S., Fornito, A**.**, Francey, S. M., O'Donoghue, B., Cropley, V., Nelson, M., Graham, J., Baldwin, L., Tahtalian, S., Yuen, H. P., Allott, K., Alvarez-Jimenez, M., Harrigan, S., **Sabaroedin, K.,** Pantelis, C., Wood, S., & McGorry, P. Differentiating the effect of medication and illness on brain volume reductions in first-episode psychosis: A longitudinal, randomized, triple-blind, placebo-controlled MRI study. *Submitted to Neuropsychopharmacology on September 29th, 2020.*

Declarations

_____

I hereby declare that this thesis contains no material that has been accepted for the award of any other degree or diploma at any university or equivalent institution. To the best of my knowledge, this thesis contains no material previously published or written by any other person, except where due references were acknowledged in this thesis.

This thesis includes one original paper published in a peer reviewed journal, one paper in submission for publication, and one paper in preparation for publication. The core theme of this thesis is the investigation of the connectivity of fronto-striato-thalamic circuitry in the psychosis continuum. The ideas, development, and writing of all papers in thesis, including the preparation of figures, were the principal responsibility of myself, a student working within the School of Psychological Sciences, under the primary supervision of Prof. Alex Fornito with the co-supervision of Dr. Kevin Aquino and Prof. Mark Bellgrove. The inclusion of co-authors reflects and acknowledges the active collaborative efforts in the production of the publications included in this thesis. In the case of Chapters 2–3, my contribution to the work involved the following:

Ch	Publication Title	Status	Nature and % of student contribution	Co–authors and % of contribution	Co–authors Monash student
2	Functional Connectivity of Corticostriatal Circuitry and Psychosis-like Experiences in the General Community	Published	75% – Concept & design, all data cleaning and analysis, writing of manuscript, data collection	1. Jeggan Tiego 5% 2. Linden Parkes 1% 3. Francesco Sforazzini 1% 4. Amy Finlay 1% 5. Beth Johnson 1% 6. Ari Pinar 1% 7. Vanessa Cropley 1% 8. Ben J. Harrison 1% 9. Andrew Zalesky 1% 10. Christos Pantelis 1% 11. Mark Bellgrove 1% 12. Alex Fornito 10%	Yes 1. Jeggan Tiego* 2. Linden Parkes* 3. Ari Pinar*
3	Effective Connectivity of Fronto-striato-thalamic Circuitry Across the Psychosis Continuum	Submitted	70% – Concept & design, all data cleaning and analysis, writing of manuscript	1. Adeel Razi 5% 2. Sidhant Chopra 2% 3. Nancy Tran 2% 4. Andrii Pozaruk 2% 5. Zhaolin Chen 0.45% 6. Amy Finlay 0.45% 7. Barnaby Nelson 0.45% 8. Kelly Allott 0.45% 9. Mario Alvarez-Jimenez 0.45% 10. Jessica Graham 0.45% 11. Lara Baldwin 0.45% 12. Steven Tahtalian 0.45% 13. Hok P Yuen 0.45% 14. Susy Harrigan 0.45% 15. Vanessa Cropley 0.45% 16. Sujit Sharma 0.45% 17. Bharat Saluja 0.45% 18. Christos Pantelis 0.45% 19. Stephen Wood 0.45% 20. Brian O'Donoghue 0.45% 21. Shona Francey 0.45% 22. Patrick McGorry 0.45% 23. Robert Williams 0.45% 24. Kevin Aquino 0.45% 25. Alex Fornito 10%	Yes 1. Sidhant Chopra

* Co-authors were students at Monash University at time of publication, but have graduated since then

Sections of published or submitted papers have been renumbered for a consistent presentation of the thesis.

Student

Kristina Sabaroedin

Date: 16th December 2020

The undersigned hereby certifies that the above declaration correctly reflects the nature and extent of the of the student's and co-author's contribution to this work. In instances where I am not the responsible author, the respective contribution of authors was made in agreement with the responsible author.

Primary supervisor

Prof. Alex Fornito

Date: 16th December 2020

Contents

CHAPTER 1 ..... **1**

INTRODUCTION **1**

1.1. The Psychosis Continuum 2
1.1.1. Symptoms of psychosis 2
1.1.2. Biological evidence for a psychosis continuum 3
1.2. Schizophrenia: a dysconnectivity of brain networks 5
1.3. Fronto-striato-thalamic circuits 6
1.4. Dysconnectivity of ventral and dorsal FST circuits in psychosis 8
1.5. Fronto-striato-thalamic dysconnectivity, dopamine dysfunction, and psychosis 11
1.6. Is the primary pathology bottom-up or top-down? 14
1.7. Dynamic causal modelling 16
1.8. Aims and overview of the thesis 16

CHAPTER 2 ..... **20**

FUNCTIONAL CONNECTIVITY OF CORTICOSTRIATAL CIRCUITRY AND PSYCHOSIS-LIKE EXPERIENCES IN THE GENERAL COMMUNITY **20**

Abstract 21
2.1. Introduction 21
2.2. Methods and materials 24
2.2.1. Participants 24
2.2.2. Measures of PLEs 25
2.2.3. Principal component analysis 25
2.2.4. Neuroimaging data acquisition and pre-processing 26
2.2.5. Definition of seed regions of interest 26
2.2.6. Functional connectivity analysis 26
2.3. Results 27
2.3.1 Principal component analysis 27
2.3.2. Corticostriatal functional connectivity 29
2.4. Discussion 32
2.4.1. Dorsal corticostriatal coupling and PLEs 32
2.4.2. Ventral corticostriatal coupling and PLEs 35
2.4.3. Limitations 35
2.4.4. Conclusions 36
2.5. Acknowledgements and disclosures 37
2.6. Article information 37

CHAPTER 3 ..... **39**

EFFECTIVE CONNECTIVITY OF FRONTO-STRIATO-THALAMIC CIRCUITRY ACROSS THE PSYCHOSIS CONTINUUM **39**

Abstract 40
3.1. Introduction 41
3.2. Methods and materials 43
3.2.1. Participants 43
3.2.2. Symptom measures 43
3.2.3. MRI/PET processing and analysis 44
3.2.4. Dynamic causal modelling 44

3.3. RESULTS 46
3.3.1. Participant demographic details 46
3.3.2. Group differences in effective connectivity 47
3.3.3. Associations with positive symptomatology 49
3.3.4. Associations with negative symptomatology 50
3.3.5. Associations with striatal dopamine synthesis capacity 51
3.4. DISCUSSION 52
3.4.1. Effective dysconnectivity of fronto-striato-thalamic circuits across the psychosis continuum 52
3.4.2. Associations with symptoms 53
3.4.3. Associations with striatal dopamine synthesis capacity 54
3.4.4. Limitations 55
3.4.5. Conclusions 56

CHAPTER 4 57

EFFECTIVE CONNECTIVITY OF FRONTO-STRIATO-THALAMIC CIRCUITRY AND DIMENSIONS OF PSYCHOSIS-LIKE EXPERIENCES 57

ABSTRACT 58
4.1. INTRODUCTION 58
4.2. METHODS AND MATERIALS 62
4.2.1. Participants 62
4.2.2. Measures of PLEs 62
4.2.3. Parametric unidimensional item response theory analysis 63
4.2.4. Neuroimaging acquisition and preprocessing 66
4.2.5. Dynamic causal modelling 66
4.3. RESULTS 69
4.3.1. Participants 69
4.3.2. Item response theory 70
4.3.3. Effective connectivity associations with positive PLEs 73
4.3.4. Effective connectivity associations with negative PLEs 76
4.4. DISCUSSION 78
4.4.1. FST effective connectivity and positive PLEs 79
4.4.2. FST effective connectivity and negative PLEs 80
4.4.3. Limitations and future directions 82
4.4.4. Conclusions 82

CHAPTER 5 83

GENERAL DISCUSSION AND CONCLUDING REMARKS 83

5.1. GENERAL DISCUSSION 83
5.1.1. FST effective connectivity and dopaminergic function in psychosis 84
5.1.2. Evidence for a neurobiological continuum across a broad spectrum of symptom severity 86
5.1.3. Implications for models of psychosis 89
5.2. LIMITATIONS AND FUTURE DIRECTIONS 90
5.3. CONCLUSIONS 91

APPENDIX A 93

APPENDIX B 108

APPENDIX C 128

REFERENCES 144

Chapter 1

Introduction

Psychosis is a distressing syndrome that encompasses symptoms which disrupt an individual's connection with reality. Psychosis can be a feature of various psychiatric disorders; however, it is primarily associated with psychotic spectrum disorders. A prototypical psychotic disorder is schizophrenia. Schizophrenia is a heterogeneous illness with a prevalence rate of up to 0.46% in the general population (Jablensky, 2000; Keshavan et al., 2011). It leads to poor quality of life, reduced mortality, increased risk of suicide, homelessness, and employment (Chesney et al., 2014; Laursen et al., 2012; Rosenheck et al., 2006). Due to its complex nature and large variability in prognosis, schizophrenia remains one of the most challenging disorders to define and treat (Owen et al., 2016).

In recent years, attention has been drawn to the fact that many symptoms of these disorders may have a continuous distribution with experiences in the general community, giving rise to the concept of a psychosis continuum. The least extreme end is occupied by subthreshold or psychosis-like experiences (PLEs) that can occur in otherwise healthy individuals living in the general community, while severe psychotic disorders such as schizophrenia sit at the opposite end (Grant et al., 2018). Early illness phases such as the prodrome, also known as an at-risk mental state (ARMS) (Goulding et al., 2013; Yung et al., 2005), and a first episode of psychosis (FEP), are thought to sit between the extreme ends of the continuum. Phenomenological and neurobiological studies have provided much support for the psychosis continuum (Taylor et al., 2020; Verdoux & Van Os, 2002). However, there has been a debate whether the distribution of symptoms continues into the general population due to differing conceptualization of health and disease, validity of measures for PLEs, as well as the clinical utility of subthreshold PLEs (Grant et al., 2018; Kraemer et al., 2004; Verdoux & Van Os, 2002). Subtle

differences in putative neurobiological markers of psychosis across the continuum have also been identified, leading to call for further research (Nelson et al., 2013).

This thesis investigates the role of fronto-striato-thalamic (FST) circuits in the emergence of psychotic symptoms, in distinct stages across the psychosis continuum. These circuits are thought to play a central role in the pathogenesis of psychosis. The remainder of this chapter will provide a general background to the psychosis continuum, its neurobiology, and the potential role of FST circuits in particular. The discussion provides a context for the three subsequent empirical chapters that follow.

1.1. The Psychosis Continuum

1.1.1. Symptoms of psychosis

The core features of psychosis are defined by so-called positive symptoms that can be described as excessive perceptual experiences such as unusual thoughts, persistent beliefs, and sensory experiences such as hallucinations and delusions (Andreasen & Olsen, 1982). Although often transient, positive symptoms encompass the cardinal features of a psychotic disorder (Guloksuz & Van Os, 2018). In subthreshold PLEs, positive-like symptoms include mild delusions, hallucination, and body image aberration (Chapman et al., 1978; Mason & Claridge, 2006; Peters et al., 2004; Stefanis et al., 2002). They can occur as isolated experiences or enduring personality traits, usually referred to as schizotypy (Kwapil & Barrantes-Vidal, 2015). In the prodromal phase, positive symptoms become more distressing, instigating help-seeking behaviours (Yung & McGorry, 1996). Positive symptoms in the FEP stage become exacerbated and they are sustained for at least four weeks (Fusar-Poli et al., 2017). The presence of positive symptoms in chronic schizophrenia is highly variable, with relapses and remissions occurring in patients (Johnstone et al., 1986; Owen et al., 2016). In clinical cases, positive symptoms can be efficiently treated by antipsychotics (Seeman & Lee, 1975).

People with psychotic illness also show negative symptoms, which are deficits in normal functioning that include anhedonia, alogia, and social withdrawal (Kirkpatrick et al., 2006). Negative symptoms can be challenging to detect in early phases of psychosis, and are notoriously difficult to treat, leading to worse functional impairment and poorer prognosis (Malla & Payne, 2005; van Os & Kapur, 2009; Velthorst et al., 2014). Negative subclinical symptoms can co-occur with positive PLEs,

although measurements of negative PLEs pose several challenges as they have been found to show low associations with the clinical symptoms (Lincoln et al., 2017; Schlier et al., 2015). In a ten-year longitudinal study, negative PLEs were linked to higher social impairment in healthy individuals (Kwapil et al., 2013). In chronic schizophrenia, negative symptoms are persistent and lead to worse functioning, social and occupational impairment, and reduced quality of life (Liddle, 1987). Currently, there is no effective pharmacological treatment for negative symptoms. Although not included as part of the diagnostic criteria, cognitive deficits are also pervasive across the psychosis continuum, and can manifest long before the onset of illness (Lewandowski et al., 2011).

The emergence of symptoms on the less extreme end of the continuum may increase vulnerability for progressing into the severe end of the continuum. PLEs, with a prevalence rate of up to 8% in the general population, increase the risk for psychotic spectrum disorders and impaired functioning (Barrantes-vidal et al., 2015; Kwapil et al., 2013; Kwapil & Barrantes-vidal, 2018; van Os et al., 2009; Vollema et al., 2002). Although not a disorder in itself, the onset of psychosis is associated with an increased risk of developing formal psychotic disorders such as schizophrenia, in addition to other comorbid disorders and poor functional outcomes (Kelleher & Cannon, 2016; Malla & Payne, 2005; Upthegrove et al., 2010; Yung & McGorry, 1996). Thus, the psychosis continuum provides an important framework in understanding risk factors, pathogenesis, and progression of psychotic disorders that may aid early identification and intervention (Wood et al., 2011).

1.1.2. Biological evidence for a psychosis continuum

Genes play a major contribution to the risk for schizophrenia with heritability estimates of around 85% (Cardno & Gottesman, 2000; Visscher et al., 2008). The largest genome-wide association study (GWAS) of schizophrenia on a sample of up to 150,000 individuals (36,989 cases and 113,075 controls) revealed over a hundred of common genetic risk variants involved in synaptic signalling, pruning, and development of the brain (Howes et al., 2015; Ripke et al., 2014; Sekar et al., 2016; Yang et al., 2005). This finding posits that a substantial fraction of genetic risk for schizophrenia is polygenic, being attributable to the cumulative effect of common variants, in combination with rare mutations and copy number variations of large effects (Purcell et al., 2009; Tansey et al., 2015). A corollary of the polygenic

model of schizophrenia risk is that disease liability is normally distributed in the population (Plomin et al., 2009). Thus, consistent with the phenomenological conceptualisation of a continuum of psychosis symptoms, the extant quantitative and molecular genetic evidence is consistent with a model in which people with schizophrenia have an increased number of risk genes and thus represent the extreme end of a continuous symptom distribution, with less severe PLEs reflecting an underlying genetic vulnerability to schizophrenia (Vollema et al., 2002). Indeed, polygenic risk (PGR) scores of schizophrenia explain up to 7% of variance in genetic liability in the general population (Ripke et al., 2014).

Using longitudinal data, PGR scores of schizophrenia have been associated with greater cognitive decline between childhood and adulthood as well as lower IQ in late adulthood (McIntosh et al., 2013), in accordance with the prevalence of cognitive dysfunction in schizophrenia (Lewandowski et al., 2011). However, PGR associations with subclinical symptoms have been mixed. PGR scores were not found to be associated with positive PLEs (Mistry et al., 2018); however, in a large sample of healthy youths, they explained 0.5% variance in negative PLEs (Jones et al., 2016). However, as risk variants encode synaptic pathways and brain development (Ripke et al., 2014; Sekar et al., 2016; Skene et al., 2018), studies investigating the association between PGR and brain function or morphology have found promising evidence for the continuity of neurobiological substrates of psychosis. Higher PGR scores in healthy samples were associated with increased activation in the dorsolateral prefrontal cortex (DLPFC) during a working memory task adults (Walton et al., 2014), reduced cortical thickness and early cannabis use in youths (French et al., 2015), and reduced activation in the ventral striatum during a decision-making task in healthy adults (Lancaster et al., 2016). These findings are consistent with known evidence of DLPFC dysfunction, impaired ventral striatal signal, grey matter loss, and cannabis use in clinical cohorts (Arseneault et al., 2002; Fornito et al., 2009; Juckel et al., 2006; Potkin et al., 2009). The following sections will focus on evidence for neurobiological continuities across the psychosis continuum.

1.2. Schizophrenia: a dysconnectivity of brain networks

The human brain consists of 100 billion neurons interconnected in complex networks across multiple spatial and temporal scales (Essen & Tononi, 2016). Psychiatric and neurological disorders arise from disruptions of human brain networks, and thus understanding the connectivity of brain networks is central to uncovering the pathogenesis and neurobiological progression of various illnesses (Essen & Tononi, 2016; Fornito et al., 2015). The advancement of non-invasive neuroimaging methods has provided new approaches to comprehensively map brain networks (Fornito et al., 2012; Sporns, 2013).

Brain connectivity can be measured at the level of structure or function. Structural connectivity is defined as anatomical connections linking different neuronal populations (Sporns et al., 2004). It can be derived from measuring white matter projections across multiple spatial scales, ranging from local circuitry to long-range connections encompassing topologically distant brain regions (Sporns et al., 2004). Functional connectivity refers to statistical dependencies (most commonly quantified using Pearson correlations) between physiological signals recorded from two or more discrete brain regions (Friston, 1994). The most popular tool for measuring functional connectivity in living patients is functional magnetic resonance imaging (fMRI). fMRI evaluates the contrast in magnetic properties of oxygenated and deoxygenated blood, also known as blood-oxygen-level-dependent (BOLD) signal, as a proxy for neural activity (Liégeois & Elward, 2020). Historically, fMRI studies employed a task in the scanner to investigate differences in stimulus-evoked brain activity between patients and healthy controls. Although still a popular method, task fMRI poses some limitations as some tasks can be challenging for patient groups (Fornito & Bullmore, 2010). In recent years, the use of more passive, so-called resting-state paradigms, in which fMRI signals are recorded in the absence of a specific task, have become a very popular tool for assessing different aspects of network dysfunction in psychotic and other psychiatric disorders (Fornito & Bullmore, 2010).

Schizophrenia is proposed to arise from a dysconnectivity of brain networks (Friston, 1999). Using resting-state fMRI, altered functional connectivity in corticostriatal circuits, fronto-parietal, cingular-opercular, cerebellar, and default mode network has been found in healthy first-degree relatives of schizophrenia patients, youths with severe PLEs, ARMS, FEP, and schizophrenia patients (Dandash et al., 2014; Li et al., 2017; Lord et al., 2012; Repovs et al., 2011; Sarpal et al., 2015;

Satterthwaite et al., 2015; Skåtun et al., 2017; Wang et al., 2014; Wolf et al., 2015). Increased functional connectivity of the PFC, the default mode network, and limbic regions has been reported in youths with PLEs and patients in early phases of psychosis (Anticevic et al., 2015; Jalbrzikowski et al., 2019; Kraguljac et al., 2016; Satterthwaite et al., 2015). At the same time, reduced functional connectivity of cingulo-opercular regions, fronto-parietal network, sensory, and somatomotor systems has been found in cohorts spanning different phases of the psychosis continuum (Dong et al., 2018; Lewandowski et al., 2019; Satterthwaite et al., 2015; Skåtun et al., 2017). These findings implicate a consistent set of neural systems as being relevant to psychosis in subclinical and clinical groups, with alterations in connectivity emerging at an early age.

While these studies suggest that brain network dysfunction is widespread in psychosis, it is as yet unclear whether this dysfunction originates within a focal neural circuit and then spreads to encompass other areas, or whether the dysfunction has a distributed origin. One set of neural circuits that have been the subject of particular focus as a site of early pathology in psychosis are the brain's FST systems, which play diverse roles in cognition and behaviour, and are heavily influenced by the neurotransmitter dopamine, the primary target of all antipsychotic drugs available today.

1.3. Fronto-striato-thalamic circuits

FST circuits are a set of discrete yet integrated neural circuits that topographically connect the frontal cortex with the striatum, comprising the caudate and putamen, along a ventromedial-dorsolateral gradient (Alexander et al., 1986; Haber, 2016; Marquand et al., 2017; Quartarone et al., 2019). Each FST circuit subserves a specific function and collectively they are involved in several key processes such as executive functions, emotional processing, salience attribution, and motor control (Alexander et al., 1986; Haber, 2016; Marquand et al., 2017). Two FST circuits that are frequently associated with symptoms of the psychosis continuum are the ventral "limbic" and the dorsal "associative" circuits.

The ventral FST circuit links the orbitofrontal cortex (OFC), ventromedial prefrontal cortex (VMPFC) with the nucleus accumbens of the ventral striatum (Haber & Knutson, 2009). The nucleus accumbens also receives projections from subcortical limbic structures (i.e., hippocampus and amygdala) (Chang & Grace, 2014; Grace, 2016; Lodge & Grace, 2006). The ventral circuit is heavily

implicated in reward, motivational, and emotional processing (De la Fuente-Fernández et al., 2002; Haber et al., 2000; Hurd & Hall, 2005). The dorsal FST circuit links the dorsolateral prefrontal cortex (DLPFC) with the dorsal "associative" striatum (i.e., caudate nucleus and the putamen) (Alexander, 1986). However, connections from various cortical regions also overlap in the dorsal striatum, rendering this region as an information integration hub for FST circuits (Balleine et al., 2007; Haber, 2016; Joel & Weiner, 2000). Thus, the dorsal circuit contributes to executive functions and information integration (Balleine et al., 2007; Graybiel, 1998). Information from both the ventral and dorsal striatum projects back to the cortex through the pallidum and substantia nigra pars reticulata, and the thalamus (Figure 1.1) (Alexander, 1986; Gerfen & Bolam, 2010).

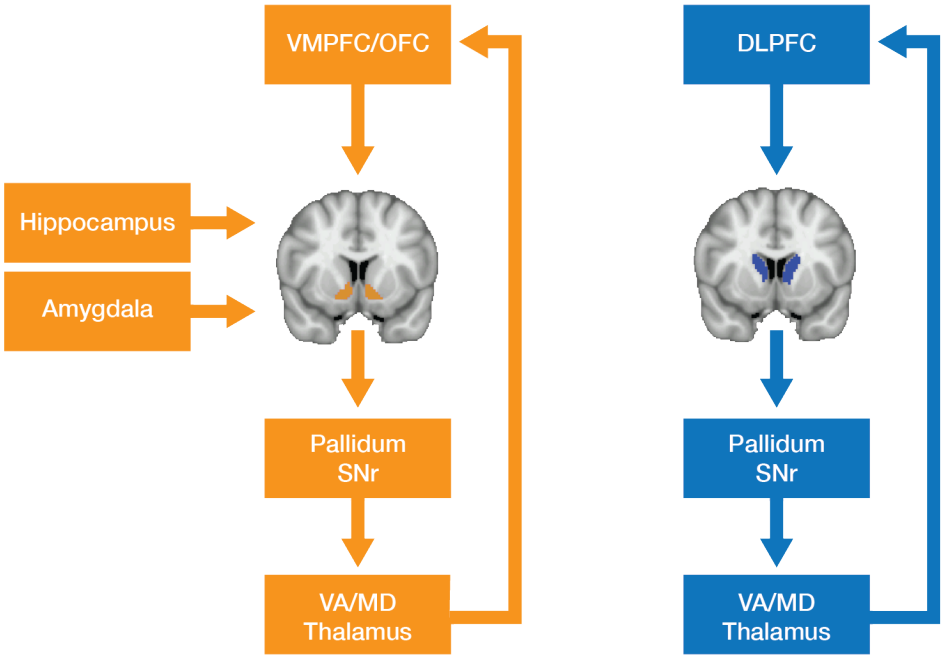

Figure 1.1. Ventral and dorsal FST circuits. The ventral circuit is shown on the left and the dorsal circuit is on the right. Anatomical locations of ventral and dorsal regions of the striatum are shown on the axial slices. Information from the cortex flows to the striatum, and back to the cortex through the pallidum, substantia nigra pars reticulata, and to the thalamus. The hippocampus and amygdala also send projections to the ventral striatum. VMPFC: ventromedial prefrontal cortex; OFC: orbitofrontal cortex; DLPFC: dorsolateral prefrontal cortex; SNr: substantia nigra pars reticulata; VA: ventral anterior; MD: mediodorsal.

In addition to prefrontal connections, the striatum receives vast dopaminergic innervation from the midbrain, and in turn, the midbrain receives most of its projections from the striatum (Haber et al., 2000). Pathways from the ventral tegmental area (VTA) and the substantia nigra (SN) in the midbrain form the mesolimbic and nigrostriatal pathways with the dorsal and ventral striatum, respectively (Hurd & Hall, 2005; Lerner et al., 2015). Striatal inputs also converge on the midbrain, allowing information to flow across the striatum (Haber et al., 2000). As the striatum receives most of the dopaminergic projections in the brain, dopamine is a potent modulator of FST circuit function and its innervation of the striatum facilitates associative learning, reward valuation, information integration, and information filtering (Haber, 2003; Maia & Frank, 2017; Robbins & Everitt, 1992; Wolfram Schultz, 2016).

1.4. Dysconnectivity of ventral and dorsal FST circuits in psychosis

Using resting-state fMRI, functional connectivity of FST circuits can be investigated using different methods. A popular approach in inferring functional connectivity is the seed-based approach. This approach includes using a mask, or seed, to extract time-series from a region of interest and estimating correlations of the time-series with physiological signals in other regions of the brain (Fox et al., 2005; Joel et al., 2011). Functional connectivity of FST circuits can be estimated by using seeds placed in various regions of the circuits, either in the striatum, limbic regions encompassed in the ventral circuit, or in the thalamus.

Resting-state functional connectivity studies using seeds located in the ventral striatum, variably placed in either the nucleus accumbens, ventral caudate or putamen regions, have found increased connectivity of the ventral circuit in ARMS, FEP patients and their unaffected first-degree relatives compared to healthy controls. In ARMS and first-degree relatives of FEP patients, increased connectivity was found between the ventral putamen and inferior frontal regions including the VMPFC (Dandash et al., 2014; Fornito et al., 2013). FEP patients have been found to demonstrate increased functional connectivity between the ventral caudate, including the nucleus accumbens, with the OFC and insula, and this increase was positively associated with positive and negative symptom severity and longer duration of untreated psychosis (Fornito et al., 2013; Sarpal et al., 2017). Higher positive PLEs were associated with increased functional connectivity of the ventral circuit comprising the ventral

putamen, cingulate and superior frontal gyrus, consistent with ARMs and first-degree relatives of FEP patients (Wang et al., 2018). Increased functional connectivity of the ventral circuit in the earlier stages of psychosis along the continuum is consistent with reports of aberrant ventral striatal activity and grey matter loss in established schizophrenia (Morris et al., 2012; Stegmayer et al., 2014).

Using seeds places in subcortical limbic regions, altered functional connectivity with the frontal cortex has also been reported across the continuum. Reduced functional connectivity of the amygdala with the OFC was found in established schizophrenia (Anticevic, Tang, et al., 2014). However, in the earlier stages of psychosis, the amygdala exhibited increased functional connectivity with the ventrolateral PFC, frontal pole, thalamus, and brainstem in ARMS and FEP patients (Anticevic, Tang, et al., 2014; Kim et al., 2020). Similar findings were also reported in youths with PLEs (Jalbrzikowski et al., 2019). The anterior hippocampus, on the other hand, demonstrated increased functional connectivity with cortical areas including the medial PFC in established schizophrenia (Zhou et al., 2008), whereas increased functional connectivity of the hippocampus in individuals with PLEs was restricted to subcortical regions including the striatum and thalamus (Kozhuharova et al., 2020). Using other neuroimaging methods, dysconnectivity between subcortical limbic regions with the PFC has also been reported. For the amygdala, increased activation was reported in at-risk youths during an emotional processing task in the scanner and this was accompanied with reduced activation of inferior frontal regions (Gee et al., 2012). For the hippocampus, resting cerebral blood flow of this region was increased in at-risk individuals (Allen et al., 2016) and this was accompanied with PFC inhibition that was linked with increased medial prefrontal GABA levels in individuals who transitioned to psychosis (Modinos et al., 2018). Together, these results suggest that dysconnectivity of the ventral circuit is not limited to alterations implicating the ventral striatum, but also between limbic areas with prefrontal regions, suggesting a dysfunction in emotional processing across the continuum of severity.

In the dorsal FST circuit, reduced functional connectivity between the dorsal caudate and the DLPFC was found in FEP patients and their unaffected first-degree relatives, ARMSs, and chronic unmedicated patients (Dandash et al., 2014; Fornito et al., 2013; Horga et al., 2016). In FEP patients, reduced functional connectivity between the dorsal caudate, bilateral DLPFC, and left medial PFC, was associated with the severity of positive symptoms (Fornito et al., 2013). ARMS individuals with higher

levels of positive symptoms also exhibited reduced functional connectivity between the dorsal caudate, left rostromedial PFC and right DLPFC compared to healthy controls (Dandash et al., 2014). Following treatment in FEP patients, improvement of psychotic symptoms was accompanied with increased functional connectivity between the right dorsal caudate and right DLPFC, suggesting a contribution of dorsal circuit disruption in the onset of psychosis symptoms (Sarpal et al., 2015). Functional connectivity of the dorsal circuit has not been extensively associated with subthreshold symptoms, although reduced functional connectivity with posterior regions has been found in a large sample of healthy adults with PLEs (Wang et al., 2018b).

The thalamus plays a central role in relaying information between the striatum and the cortex, and thus changes in functional connectivity of this region also reflect alterations in FST circuits (Haber & McFarland, 2001; Sherman, 2016). Largely consistent with the findings of dorsal striatum connectivity, reduced functional connectivity of the thalamus was reported with PFC regions encompassing the cognitive control network (i.e., the medial PFC, DLPFC, and ACC) in at-risk individuals, FEP, and schizophrenia patients (Anticevic et al., 2014; Li et al., 2017; Welsh et al., 2010; Woodward & Heckers, 2016). Reduced connectivity with prefrontal and cerebellar regions were pronounced in at-risk patients who converted to psychosis (Anticevic et al., 2015). Notably, implicated cortical regions include areas that are functionally segregated into the dorsal and ventral FST circuits, but functionally connected as part of a canonical brain network such as the cognitive control network (Cole & Schneider, 2007). This suggests that the thalamus is involved in modulating connectivity across cortical regions, and thus this structure may be a promising site to investigate cortico-cortico integration (Sherman, 2016). Furthermore, there is a lack evidence for altered functional connectivity of the thalamus in PLEs, suggesting that dysconnectivity of this region is associated with clinical presentations of symptoms.

Together, these findings indicate that alterations in FST connectivity can be found in varying stages across the psychosis continuum. Functional connectivity of the ventral FST circuit was implicated in groups at all stages of severity, with increased functional connectivity of the ventral striatum and prefrontal regions featuring prominently. Reduced functional connectivity of the dorsal circuit was established in at-risk and clinical groups; however, this has not been demonstrated in healthy

people with PLEs. This is at odds with the finding of healthy first-degree relatives of patients demonstrating reduced functional connectivity of this circuit (Fornito et al., 2013). Based on the continuous distribution of genetic risk, a consistent pattern of connectivity should be extended to the general population with PLEs. The paucity of evidence supporting a link between dorsal FST connectivity and PLEs may reflect issues surrounding the measurement of subclinical symptoms in the general population, which rely on a wide range of self-report measures. Such measures can be confounded by lack of insight (Pavlova & Uher, 2020), over-reporting and misinterpretation of questions (Verdoux & Van Os, 2002), and items are often dichotomised to measure the presence or absence of latent dimensional traits, thus failing to provide accurate estimates of severity (van der Sluis et al., 2010). Therefore, further investigation using more robust methods in the measurement of subclinical symptoms is warranted to investigate functional connectivity of the dorsal circuit in PLEs.

1.5. Fronto-striato-thalamic dysconnectivity, dopamine dysfunction, and psychosis

Dysregulation of dopamine has long been thought to play a central role in the onset of psychotic symptoms. All antipsychotics block the uptake of dopamine by binding to dopamine D2 receptors in the striatum (Seeman, 1992). Moreover, compounds that increase synaptic dopamine concentrations such as ketamine and amphetamine increase striatal dopamine release and elicit psychotic symptoms in otherwise healthy individuals (Lieberman et al., 1987). These established findings indicate that dopamine hyperactivity contributes to psychosis onset.

Dopamine neurons are located in the midbrain, with widespread projections to the ventral and dorsal striatum and to the cortex through the mesolimbic, nigrostriatal, and mesocortical pathways, respectively (Haber et al., 2000; Hurd & Hall, 2005; Thierry et al., 1976). At baseline, or during normal contexts, dopamine neurons exhibit tonic firing which is described as a spontaneously occurring spike activity driven by membrane currents of dopamine neurons (Grace & Bunney, 1984). The tonic activity of dopamine neurons is controlled by the inhibitory action of GABA, thus preventing the neurons from firing spontaneously (Grace & Bunney, 1985). The tonic activity of dopamine neurons regulates baseline dopamine concentration in the striatum. In salient contexts, such as during a presentation of unexpected rewards, dopamine neurons switch to phasic activity, characterised by a transient, high

amplitude, burst spike firing pattern which releases dopamine (Floresco et al., 2003; Grace, 1991). This phasic firing depends on glutamatergic input on dopamine neurons (Floresco et al., 2003). Phasic dopamine firing is thought to represent learning, goal driven behaviour, and salience attribution (Schultz et al., 1993). An important point to note is that only neurons that were tonically active can switch to phasic firing, thus tonic activity governs the responsivity of the dopamine system (Grace, 1991).

Aberrantly increased tonic activity of dopamine neurons in the striatum is thought to lead to inappropriate phasic firing of dopamine neurons irrespective of context, resulting in the misattribution of salience that gives rise to psychotic symptoms (Frith, 2005; Heinz & Schlagenhauf, 2010; Kapur, 2003; Maia & Frank, 2017). Earlier work hypothesized that dopamine dysfunction implicates the mesolimbic pathway, and that this dysfunction is thought to disrupt the role of the ventral striatum in attributing salience, thus contributing to the onset of psychosis (Kapur, 2003). Additionally, antipsychotics were found to exert its efficacy by acting selectively on the mesolimbic dopamine system (Lidsky, 1995). Animal work has also found that dopamine activity in limbic regions was selectively increased due to impaired corticolimbic feedback following prefrontal lesions of mesocortical projections (Pycock et al., 1980; Weinberger, 1987). However, recent evidence supporting a role for the dorsal striatum in associative learning and evidence from in-vivo imaging studies in patients has questioned the mesolimbic theory (McCutcheon et al., 2019).

Striatal dopamine activity can be measured in-vivo using positron emission tomography (PET) imaging using the tracer 3,4-dihydroxy-6-[^{18}F]-fluoro-L-phenylalanine ([^{18}F]DOPA) to measure presynaptic dopamine synthesis capacity (Grace, 2016; Weinstein et al., 2017). Elevations in dopamine synthesis capacity in the associative striatum have been reported in at-risk individuals, especially in those who transition to psychosis (Egerton et al., 2013; Howes et al., 2009; Howes, Bose, Turkheimer, Valli, Egerton, Stahl, et al., 2011; Mizrahi et al., 2014). The findings of elevated dopamine synthesis in the associative striatum challenge the mesolimbic dysfunction as a primary risk suggested by earlier work, and the findings that delusions and hallucinations are associated with aberrant dopaminergic signalling in the ventral striatum (Kapur, 2003; Maia & Frank, 2017; Winton-Brown et al., 2014). Reports of elevated dopamine synthesis for the ventral striatum have been restricted to patients with established schizophrenia (Kumakura et al., 2007; McGowan et al., 2004). It may be that striatal

dopamine dysfunction is a general feature of clinical illnesses on the psychosis continuum, with elevated dopamine synthesis in the dorsal striatum being a distinct feature of the at-risk phase. The dorsal striatum is an integrative hub, and thus its dysfunction may elicit failures in cognitive, emotional, and sensory integration that contribute to psychosis onset (McCutcheon et al., 2019).

Dopamine controls information flow from the striatum to the thalamus by modulating the activity of striatal GABAergic medium spiny neurons, which constitute approximately 95% of neurons in the striatum (Carlsson et al., 1999; Kemp & Powell, 1971; Surmeier et al., 2007). These ascending striatothalamic pathways are classified into the direct and indirect pathways (Figure 1.2). The excitatory direct pathway expresses D1 dopamine receptors and it relays information from the striatum to the medial pallidum, before terminating in the thalamus. D2 receptors are expressed in the inhibitory indirect pathway, and the output of this pathway inhibits the medial pallidum indirectly via the lateral pallidum and the subthalamic nucleus, preventing information transmission to the thalamus (Gerfen & Surmeier, 2011; Keeler et al., 2014). Dopamine dysregulation in the striatum may result in an imbalance of signalling along these pathways, thus contributing to positive and negative symptoms (Carlsson et al., 1999).

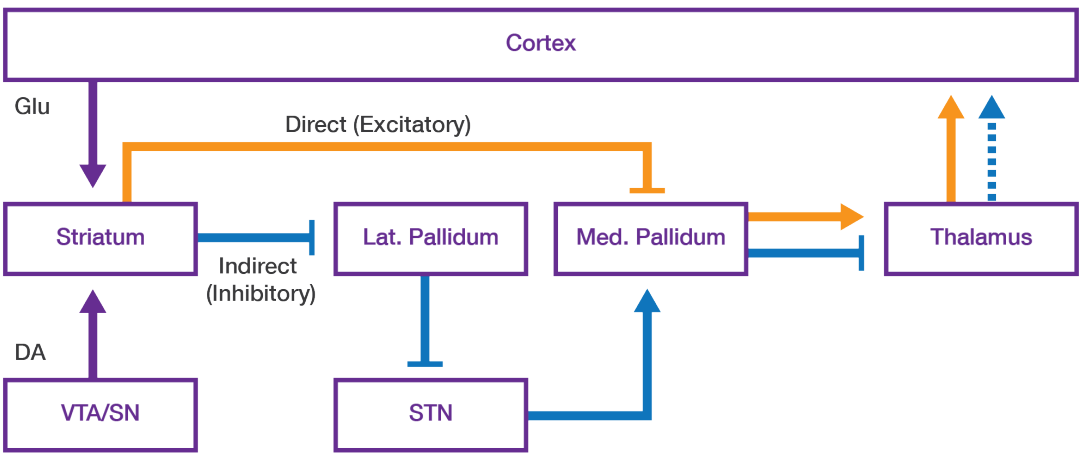

Figure 1.2. Direct and indirect striatothalamic pathways. The direct pathway (orange arrows) consists of D1 receptors acting on striatal medium spiny neurons. Its excitatory mechanism is executed by inhibiting the GABAergic output of the medial pallidum to the thalamus, thus allowing information being relayed on to the cortex. The indirect pathway (blue arrows) consists of D2 receptors acting on striatal medium spiny neurons. Its inhibitory action is performed by diminishing the inhibitory control of the lateral pallidum on the subthalamic nucleus, thus allowing the latter structure to send glutamatergic

input to the medial pallidum. This excitatory action of the subthalamic nucleus results in a GABAergic output sent from the medial pallidum to the thalamus, which effectively prevents information to be relayed on to the cortex (dashed blue arrow). VTA: ventral tegmental area; SN: substantia nigra; STN: subthalamic nucleus; Glu: glutamate; DA: dopamine.

1.6. Is the primary pathology bottom-up or top-down?

Developmental models propose that dysregulation of subcortical dopamine emerges from a loss of top-down control of the cortex or subcortical limbic regions on the midbrain (Lodge & Grace, 2011; Weinberger, 1987). This top-down disruption is proposed to occur early in development and both rodent and non-human primate studies have shown that early lesions of the DLPFC and the hippocampus can indeed remain functionally silent until post-puberty (Goldman & Alexander, 1977; Lipska et al., 1995). Lesions of the cortex are thought to disrupt mesocortical dopamine projections, leading to deficits in cortical dopamine which elicits a compensatory response of the cortex, thus initiating inappropriate top-down feedback to the midbrain (Weinberger, 1987). Indeed cortical lesions were found to give rise to increased dopamine turnover and up-regulation of post-synaptic receptors in the midbrain (Pycock et al., 1980). Additionally, rodents receiving lesions of the hippocampus after birth demonstrated impaired sensorimotor gating post-puberty, a behavioural deficit that arises from dopamine hyperactivity (Lipska et al., 1995).

Consistent with the developmental prefrontal lesion hypothesis, several human neuroimaging studies have shown that prefrontal disruption is often accompanied by elevated subcortical dopamine. In both schizophrenia and FEP patients, elevated striatal dopamine activity was found to be accompanied by reduced glutamate metabolites and neuronal integrity in the PFC (Bertolino et al., 2000; Jauhar et al., 2018). In at-risk groups, cerebral blood flow in the striatum and prefrontal regions were inversely related (Kindler et al., 2017), and elevated striatal dopamine was associated with reduced IQ and functional deficits of the PFC during a working memory task (Fusar-Poli, Howes, et al., 2010; Howes et al., 2009). Reduced functional connectivity of the midbrain with the cortex in unmedicated schizophrenia patients has also been reported, consistent with the proposed compromise of the mesocortical pathway (Cadena et al., 2018; Hadley et al., 2014; Yoon et al., 2013).

Disruptions in the balance of prefrontal glutamate and GABA disrupts the inhibitory and excitatory control of the cortex on the midbrain, and indeed rodent work has found that blocking

prefrontal GABA receptors lead to increased striatal dopamine (Carlsson et al., 1999; Karreman & Moghaddam, 1996). In addition to the cortex, limbic regions such as the hippocampus and the amygdala also influence the top-down inhibition of the midbrain (Grace, 2016). A rodent methylazoxymethanol acetate (MAM) developmental model of psychosis discovered that hyperactivity of ventral subiculum of the hippocampus caused by GABA dysfunction sends augmented glutamatergic excitatory innervation to the nucleus accumbens, which inhibits the control of the pallidum on midbrain and increases dopamine population activity (Lodge & Grace, 2007). The amygdala, on the other hand, inhibits hyperactivity of the midbrain in response to chronic stress (Chang & Grace, 2014).

The translation of the MAM model is relevant to the onset of psychosis and neuroimaging evidence in humans have found that dysregulation of subcortical dopamine is related to aberrant hippocampal, and by extension, medial temporal lobe activity in ARMS groups (Modinos et al., 2015). Hippocampal glutamate levels and activity of this region were negatively associated with dopamine synthesis in the associative striatum of ARMS patients, especially in a subgroup that transitioned to psychosis (Roiser et al., 2013; Stone et al., 2010). Dysregulation of the hippocampus is thought to contribute to be a key contributor to psychosis symptoms and cognitive disorganisation that is pervasive across the psychosis continuum (Olypher et al., 2006).

Consistent with animal work, neuroimaging evidence in humans demonstrates that dysfunction of various neurotransmitter systems that span the cortex and subcortex contribute to psychosis onset (e.g., Carlsson & Carlsson, 1990; Fusar-Poli et al., 2011; Modinos et al., 2015). However, a limitation of neuroimaging is that the evidence, at best, is correlational. Therefore, despite the evidence fitting in with animal work, top-down disruption as a primary risk in psychosis cannot be inferred. Mounting evidence of striatal dopamine dysregulation associated with psychosis risk, and the finding that the DRD2 gene, which is strongly expressed in the striatum, contains a genome-wide risk variant for schizophrenia, challenge the proposed top-down model (Egerton et al., 2013; Howes et al., 2009; Howes, Bose, Turkheimer, Valli, Egerton, Valmaggia, et al., 2011; Mizrahi et al., 2014; Ripke et al., 2014). Delineating directional influences that perturb brain circuits in distinct stages of psychosis is an important future direction in the field, as it allows the understanding of the pathogenesis and progression of psychosis, as well as uncovering potential targets for early treatment.

1.7. Dynamic causal modelling

Functional connectivity is an undirected measure of coupled neuronal activity that cannot uncover the causal influences in FST circuits that are relevant to different phases of psychosis and symptom expressions. To overcome this limitation, one would ideally map patterns of effective connectivity within FST systems. Effective connectivity refers to the causal influence that one neural system exerts over another (Friston, 2011). Dynamic causal modelling (DCM) is a popular method for inferring effective connectivity using fMRI and relies on a generative neuronal model, coupled with an observation model, to estimate the strength of effective connectivity among (hidden) neuronal systems, given the haemodynamic signals measured with fMRI (Buxton et al., 1998; Friston et al., 2003) In recent years, the development of spectral DCM, which models effective connectivity in the cross-spectral domain for resting-state fMRI data, has allowed efficient estimation of effective connectivity networks during resting-state paradigms (Razi et al., 2015). Spectral DCM demonstrates robust construct validity and has been utilised to estimate endogenous effective connectivity of brain networks (Almgren et al., 2018; Preller et al., 2019; Razi et al., 2015; Zhou et al., 2017), as well as effective connectivity of frontoparietal, hippocampal, and anterior cingulate cortex (ACC) networks in FEP and established schizophrenia (Chahine et al., 2017; Cui et al., 2015; Uscatescu et al., 2020). However, a detailed characterization of FST effective connectivity across the psychosis continuum is lacking.

1.8. Aims and overview of the thesis

Psychosis symptoms are proposed to lie on a continuum of severity that is accompanied by neurobiological changes. The brain's FST systems, particularly the dorsal and ventral circuits, are relevant to the emergence of psychotic symptoms. Functional connectivity of these circuits has been investigated in clinical populations across varying phases of psychosis. The broad aim of this thesis is to systematically investigate the connectivity of FST circuits across the psychosis continuum. In particular, this thesis addresses the gaps in the current body of work by first testing for associations between PLEs and FST functional connectivity, and then developing a more refined model of FST

effective connectivity that can be used to probe this circuitry across the psychosis continuum. This thesis consists of three empirical chapters and a discussion section as below.

Chapter 2 first tests for associations between FST functional connectivity and PLEs in a large, non-clinical sample. FST circuits are central to psychosis onset and reduced functional connectivity of the dorsal FST circuit has been demonstrated in ARMS, FEP patients and their first-degree relatives (Dandash et al., 2014; Fornito et al., 2013), and indirectly in schizophrenia patients through the investigation of thalamus functional connectivity (Anticevic, Cole, et al., 2014; Li et al., 2017; Welsh et al., 2010; Woodward & Heckers, 2016). However, the association between functional connectivity of the dorsal circuit and PLEs is unclear and there is a lack of evidence for a continuum of altered dorsal FST functional connectivity in the general population, which is inconsistent with the proposed continuous distribution of symptom severity. Extending striatal connectivity to the entire cortex, this chapter aimed to investigate functional connectivity of corticostriatal circuits in tracking the expression of subclinical symptoms in non-clinical individuals. Critically, positive and negative dimensions of PLEs were derived from a data reduction method applied to an extensive measurement battery of PLEs to assess a wide variety of subclinical symptoms. Consistent with previous findings in clinical samples (Dandash et al., 2014; Fornito et al., 2013), positive PLEs were associated with reduced functional connectivity of the dorsal corticostriatal circuit, namely between the dorsal regions of the striatum and the primary motor and prefrontal cortices, including the DLPFC and the ACC. This chapter thus establishes the dorsal corticostriatal circuit as a putative marker of psychotic symptoms across the continuum of severity.

Building on these findings, Chapter 3 examines effective connectivity across different stages of the psychosis continuum, and in relation to striatal dopaminergic function. Animal models propose that subcortical dopamine dysfunction arises from a loss of top-down control of the cortex and limbic regions over the midbrain (Lodge & Grace, 2007; Weinberger, 1987). Despite converging correlational evidence supporting a top-down model from human neuroimaging work, there is accumulating evidence that bottom-up abnormalities may also be prominent, based on links between elevated dorsal striatum dopamine and psychosis risk, and the identification of schizophrenia risk variants in the DRD2 gene (Egerton et al., 2013; Howes et al., 2011; Howes et al., 2009; Mizrahi et al., 2014; Ripke et al., 2014).

This chapter thus uses DCM for resting-state fMRI data to examine the relative contributions of top-down and bottom-up signalling in FST dysfunction across the continuum. Using spectral DCM, both top-down and bottom-up influences of the dorsal and ventral circuits, as outlined in Figures 1.1 and 1.2, were identified in a healthy group with PLEs, antipsychotic-naïve FEP patients, and patients with established schizophrenia. FST connections were also associated with presynaptic dopamine levels, measured by [^{18}F]DOPA in concurrent PET imaging, in the dorsal and ventral striatum of the healthy sample. The findings indicate that compared to other phases, early phases of psychosis are associated with prominent disruption of subcortical connectivity, with midbrain and thalamic connectivity being robustly associated with positive symptoms across the continuum, as well as with dopamine synthesis capacity in the striatum. These findings align with a prominent role for both top-down and bottom-up subcortical regulation of dopamine as playing an important role early in the emergence of psychotic symptoms, with limited evidence for dysregulation of top-down cortical control mechanisms.

Having established a working model of FST effective dysconnectivity across stages of the psychosis continuum, Chapter 4 provides a more detailed characterization of how the model of FST effective connectivity in the preceding chapter relates to PLEs in non-clinical individuals. It applies a refined approach for characterizing the structure of PLEs into nine dimensions using item response theory (Reise et al., 2005), thus increasing the phenotypic resolution of the analysis. Spectral DCM revealed that striatothalamic connections were associated with all positive PLE dimensions. Delusions and hallucinations implicated ascending influence of the amygdala on the cortex, meanwhile causal influences associated with cognitive disorganisation and body image aberration were restricted to subcortical regions. Associations with negative PLE dimensions were restricted to the ventral circuit and implicated the nucleus accumbens, highlighting a prominent contribution of limbic circuitry in this domain. Increased midbrain influences were not associated with PLE dimensions, suggesting a mechanism distinct from clinical symptoms.

Chapter 5 presents an integrated discussion of the body of work presented in the preceding chapters. It outlines how the findings indicate that FST dysfunction is present across the psychosis continuum, that early dysfunction may lie in dysregulated subcortical systems in concert with dopaminergic dysfunction, and that while some continuities between clinical and subclinical

phenomena may be identified, they are not isomorphic. Collectively, these findings support a neurobiological continuum of psychosis that is evident at a systems-level, with dysfunction of subcortical circuitry as a primary feature of early pathophysiology.

Chapter 2

Functional Connectivity of Corticostriatal Circuitry and Psychosis-like Experiences in the General community

---

Sabaroedin, K., Tiego, J., Parkes, L., Sforazzini, F., Finlay, A., Johnson, B., Pinar, A., Cropley, V., Harrison, B.J., Zalesky, A., Pantelis, C., Bellgrove, M., & Fornito, A. (2019). Functional connectivity of corticostriatal circuitry and psychosis-like experiences in the general community. *Biological Psychiatry*, *86*(1), 16–24.

Preamble

Alterations in the functional connectivity of fronto-striato-thalamic (FST) circuits have been identified in clinical cohorts across the psychosis continuum. Associations between subclinical symptoms of psychosis and FST functional connectivity have been unclear. This chapter sought to investigate the association between psychosis-like experiences (PLEs) with functional connectivity of the striatum to the entire cortex in a large community sample of healthy adults. Using a data reduction method on an extensive battery of PLE measurements, the results demonstrate that reduced functional connectivity of the dorsal subdivision of the striatum with the primary motor and prefrontal cortices were associated with more severe positive-like symptoms. This finding is consistent with what has been found in clinical groups, suggesting that the dorsal circuit tracks the severity of positive symptoms across the psychosis continuum.

Supplementary materials for this chapter are in Appendix A.

Abstract

Background: Psychotic symptoms are proposed to lie on a continuum, ranging from isolated psychosis-like experiences (PLEs) in nonclinical populations to frank disorder. Here, we investigated the neurobiological correlates of this continuum by examining whether functional connectivity of dorsal corticostriatal circuitry, which is disrupted in psychosis patients and individuals at high risk for psychosis, is associated with the severity of subclinical PLEs.

Methods: A community sample of 672 adults with no history of psychiatric or neurological illnesses completed a battery of seven questionnaires spanning various PLE domains. Principal component analysis of 12 subscales taken from seven questionnaires was used to estimate major dimensions of PLEs. Dimension scores from principal component analysis were then correlated with whole-brain voxelwise functional connectivity maps of the dorsal striatum in a subset of 353 participants who completed a resting-state neuroimaging protocol.

Results: Principal component analysis identified two dimensions of PLEs that accounted for 62.57% of variance in the measures, corresponding to positive (i.e., subthreshold delusions and hallucinations) and negative (i.e., subthreshold social and physical anhedonia) symptom-like PLEs. Reduced functional connectivity between the dorsal striatum and prefrontal and motor cortices correlated with more severe positive PLEs. Increased functional connectivity between the dorsal striatum and motor cortex was associated with more severe negative PLEs.

Conclusions: Consistent with past findings in patients and individuals at high risk for psychosis, subthreshold positive symptomatology is associated with reduced functional connectivity of the dorsal circuit. This finding suggests that the connectivity of this circuit tracks the expression of psychotic phenomena across a broad spectrum of severity, extending from the subclinical domain to clinical diagnosis.

2.1. Introduction

Psychotic symptoms are proposed to follow a continuous distribution of severity, ranging from the absence of symptoms at one end to frank disorder at the other (Grant et al., 2018). Subthreshold psychosis-like experiences (PLEs) lie between these extremes (Kelleher & Cannon, 2011). Typically

characterized as attenuated (i.e., subclinical or subthreshold) forms of canonical positive symptoms (e.g., delusions and hallucinations), PLEs also encompass subclinical variation of the negative symptoms of schizophrenia, such as mild anhedonia (Barrantes-Vidal et al., 2013; Linney et al., 2003; MacDonald et al., 2001; Stefanis et al., 2002; Verdoux & Van Os, 2002). PLEs are predominantly transient (Cougnard et al., 2007; Hanssen et al., 2006); in cases of persistent expression, PLEs are thought to reflect an enduring personality dimension (Ettinger et al., 2014). The prevalence of PLEs in the general community reaches up to 8% (van Os et al., 2009), with higher incidences in the relatives of schizophrenia patients (Vollema et al., 2002), suggesting that one's liability for PLEs tracks vulnerability to clinical disorder. Severe PLEs may indeed progress into a help-seeking phase, as exemplified by the at-risk mental state (ARMS) for psychosis (Arseneault et al., 2002; Cannon et al., 2007; Kaymaz et al., 2012; Werbeloff et al., 2012; Yung & McGorry, 1996).

The continuum model of psychosis severity accords with evidence for a polygenic contribution to schizophrenia liability, which predicts a continuous population distribution of symptomatology (Lee et al., 2012; Plomin et al., 2009). It is also supported by neuroimaging evidence suggesting that subclinical and clinical phenomena share common neural correlates. The severity of PLEs in nonclinical samples correlates with variations in brain systems implicated in schizophrenia and various psychotic disorders, including frontotemporal, default mode, and cingulo-opercular systems (Corlett & Fletcher, 2012; Ettinger et al., 2012; Fusar-Poli, Broome, et al., 2010; Garrity et al., 2007; Henseler et al., 2010; Satterthwaite et al., 2015; Sheffield et al., 2016; White et al., 2010; Whitfield-Gabrieli et al., 2009; Wolthusen et al., 2018). Alterations of white matter integrity in the corpus callosum, thalamus, and parietal, language, and visual areas have also been commonly reported in studies of clinical and nonclinical individuals with subthreshold symptomatology (Jacobson et al., 2010; Skudlarski et al., 2013; Van Dellen et al., 2016). These findings suggest that a continuum of neural function may underlie a broad spectrum of symptom expression.

The brain's corticostriatal (CST) circuits are particularly relevant to the various cognitive and symptom dimensions of schizophrenia (Pantelis et al., 1992; Pantelis & Brewer, 1996). These parallel yet integrated circuits topographically connect frontal regions with the striatum, with feedback loops passing through the pallidum and thalamus (Alexander et al., 1986; Haber, 2016). The two CST circuits

that are most relevant to psychosis are the ventral and dorsal systems (Dandash et al., 2017; Grace, 2016). The ventral (limbic) system connects the orbitofrontal cortex, medial prefrontal cortex, and limbic structures of the brain (e.g., the hippocampus and amygdala) with the ventral striatum (Alexander et al., 1986; Draganski et al., 2008; Haber, 2016). This system is a major pathway for mesolimbic dopamine (Haber & Knutson, 2009) and has long been implicated in psychosis because of its role in reward processing and salience encoding (Kapur, 2003).

The dorsal (associative or cognitive) system links the dorsolateral prefrontal cortex (DLPFC) with the dorsal striatum (Alexander et al., 1986). Positron emission tomography studies indicate that both dopamine synthesis capacity and synaptic concentration are elevated prominently in the dorsal striatum of patients with schizophrenia (Kegeles et al., 2010), individuals in the ARMS phase (Fusar-Poli, Howes, et al., 2010; Howes et al., 2009), and healthy persons with increased liability for psychosis because of either genetic or environmental factors (Egerton et al., 2017; Huttunen et al., 2008). In ARMS, these elevations are present only in individuals who later transition to psychosis (Howes, Bose, Turkheimer, Valli, Egerton, Stahl, et al., 2011). These positron emission tomography findings are complemented by studies of striatal functional connectivity, which report reduced coupling of the DLPFC with dorsal caudate and putamen in patients with first-episode psychosis, their unaffected first-degree relatives, and individuals with ARMS (Dandash et al., 2014; Fornito et al., 2013). Similar changes have been found in patients with first-episode mania experiencing psychosis (Dandash et al., 2018), suggesting that dorsal CST dysfunction tracks the emergence of psychotic symptoms across diagnostic categories. Other studies focusing on thalamic connectivity support the association between changes in dorsal CST function with risk for psychosis (Anticevic, Cole, et al., 2014; Anticevic, Haut, et al., 2015; Woodward & Heckers, 2016). Changes of coupling in the dorsal CST circuit have also been correlated with the severity of both positive and negative symptoms in ARMS and clinical groups (Anticevic, Haut, et al., 2015; Dandash et al., 2014; Fornito et al., 2013), and they are often accompanied by increased coupling in the ventral CST circuit and thalamic sensorimotor systems (Anticevic, Cole, et al., 2014; Anticevic, Haut, et al., 2015; Fornito et al., 2013; Woodward & Heckers, 2016).

Together, these results indicate that reduced functional coupling of the dorsal CST system tracks the severity of psychotic symptom expression across a wide spectrum of illness severity that

spans individuals with genetic high risk for psychosis, individuals in the ARMS phase, and individuals who were clinically diagnosed with psychosis (Dandash et al., 2017). Here, we investigated whether CST function also tracks continuous subclinical variation in PLEs, ranging from the absence of PLEs to more severe experiences, in a large nonclinical sample. We combined resting-state functional magnetic resonance imaging with an extensive battery of PLE questionnaires measuring a broad array of subclinical phenomena related to schizophrenia symptomatology. Following evidence in clinical samples and individuals at high risk for psychosis (Dandash et al., 2014; Fornito et al., 2013), we hypothesized that reduced coupling between the dorsal striatum and prefrontal cortex would be associated with more severe PLEs, particularly those related to the positive symptoms of schizophrenia. Secondarily, we tested for other associations between dorsal and ventral striatal functional connectivity and PLE dimensions. In this exploratory analysis, we were particularly interested in determining whether increased coupling in the ventral system correlates with more severe PLEs, as suggested by work in individuals with genetic high risk for psychosis (Fornito et al., 2013).

2.2. Methods and materials

2.2.1. Participants

We recruited 672 participants (274 male subjects; age, mean ± SD 23.2 ± 4.89 years [range, 18–50 years]) from the general community to complete an online battery of PLE measures. To capture a broad range of PLE variation, ranging from the absence of PLEs to more severe subthreshold experiences, we included all participants with valid data from our measurement battery. All participants were right-handed with no personal history of neurological or psychiatric illness and no significant drug use (see Appendix A for further details). Recruitment was part of a larger genetics study that required participants to have all four grandparents of European descent (Pinar et al., 2018). The study was conducted in accordance with the Monash University Human Research Ethics Committee (reference number 2012001562). Each participant provided written informed consent following a thorough explanation of the study.

A subset of 379 participants with complete PLE measures underwent our resting-state functional magnetic resonance imaging protocol. Participants were subsequently excluded for scan

artifacts, poor scan quality, or excessive in-scanner head motion (details in Appendix A). The final sample with complete PLE measures and neuroimaging data comprised 353 participants (155 male subjects; median age [range], 22 years [18–50 years]; IQ range, 81–139, mean [SD] = 112 [11.6]).

2.2.2. Measures of PLEs

To sample a wide range of variation in PLEs, we used seven psychometrically validated self-report measures of subthreshold psychotic symptoms: the short-form Oxford-Liverpool Inventory of Feelings and Experiences (Mason et al., 2005); the Peters Delusion Inventory, 21-item version (Peters et al., 2004); the Community Assessment of Psychotic Experience (Stefanis et al., 2002); and four Chapman Scales measuring magical ideation, perceptual aberration, and social and physical anhedonia (Chapman et al., 1976, 1978a; Eckblad & Chapman, 1983). We chose these measures not only because they are commonly used for community samples but also because they capture dimensions of PLEs based on different conceptual models of subthreshold psychosis symptomatology. For the Peters Delusion Inventory and Community Assessment of Psychotic Experience, subscales measuring distress, preoccupation, and conviction were excluded from further analysis as they were redundant with the frequency scales (all $r < .85$). The battery yielded a total of 272 items spanning 12 subscales (Appendix A Table A1).

2.2.3. Principal component analysis

We used principal component analysis (PCA) of the subscale scores, with varimax rotation, as implemented in SPSS version 25 (IBM Corp., Armonk, NY), to derive data-driven estimates of the latent dimensions driving PLE variance in our sample. PCA was performed on the larger sample of 672 participants to obtain robust estimates of latent dimensions. The Kaiser-Meyer-Olkin test of sampling adequacy value was 0.87, indicating that the correlations between variables would yield reliable factors (Kaiser, 1974). Following PCA, component scores were extracted for all participants using the Anderson-Rubin method to ensure orthogonality (DiStefano et al., 2009).

2.2.4. Neuroimaging data acquisition and pre-processing

Multiband resting-state echo-planar images (620 volumes, 754-ms repetition time, 3-mm isotropic voxels) and anatomical T1-weighted scans (1-mm isotropic voxels) were acquired for each participant. The following pre-preprocessing steps were applied to the echo-planar images: 1) basic pre-processing in FSL FEAT that included removal of the first four volumes, rigid-body head motion correction, 3-mm spatial smoothing, and high-pass temporal filter (75-second cutoff); 2) removal of artifacts using FSL-FIX; 3) spatial normalization to the MNI152 template; and 4) spatial smoothing with a 6-mm full width at half maximum Gaussian kernel. After processing, the data were subjected to rigorous quality control for motion artifacts, as per past work (Parkes et al., 2018). Further details are presented in Appendix A.

2.2.5. Definition of seed regions of interest

In each hemisphere, six striatal regions of interest (ROIs) were seeded using 3.5-mm radius spheres that were delineated using a functional parcellation of the striatum (Di Martino et al., 2008), as per past work (Dandash et al., 2014; Fornito et al., 2013). For the caudate, three ROIs were seeded along a dorsoventral axis, including the dorsal caudate (x = ±13, y = 15, z = 9), the superior ventral caudate (x = ±10, y = 15, z = 0), and the inferior ventral caudate/nucleus accumbens (x = ±9, y = 9, z = -8). Three ROIs were seeded for the putamen along a similar axis, comprising the dorsocaudal putamen (DCP) (x = ±28, y = 1, z = 3), the dorsorostral putamen (x = ±25, y = 8, z = 6), and the ventrorostral putamen (x = ±20, y = 12, z = -3). Seeds in the dorsal CST system comprise the dorsal caudate, the dorsorostral putamen, and the DCP, whereas seeds in the ventral system comprise the inferior ventral caudate/nucleus accumbens, superior ventral caudate, and ventrorostral putamen. The mean time series of each region was then used for seed-related functional connectivity mapping. Further details on ROI definition are in Appendix A.

2.2.6. Functional connectivity analysis

First-level analysis was performed using SPM8 as previously described (Dandash et al., 2014; Fornito et al., 2013). For each participant, a general linear model containing the six seed-region time courses as

covariates was used to model blood oxygen level–dependent signal fluctuations in each voxel. Separate models were fitted for the left and right hemispheres, yielding a pair of brain maps for each striatal ROI. Parameter estimates from the first-level analysis were passed to a second-level general linear model to generate group-wide functional connectivity maps for each ROI. Covariates comprised component scores of orthogonal PLE dimensions derived from the PCA. Nuisance covariates included age, age squared, estimated full-scale IQ, sex, and mean framewise displacement as a measure of in-scanner motion (Power et al., 2012). Our analyses focused on mean effects collapsed across left and right striatal seeds to facilitate comparison with prior work (Dandash et al., 2014; Fornito et al., 2013). We note, however, that this approach may limit sensitivity to identify strongly lateralized effects.

Our primary hypothesis concerned the association between dorsal circuit connectivity and positive PLEs. We thus declared any associations between positive PLEs and functional connectivity of the dorsal circuit significant if they passed a threshold-free cluster enhancement (TFCE) (Smith & Nichols, 2009) corrected threshold of $p < .017$, determined using 5000 permutations, as implemented in FSL Randomise (Winkler et al., 2014). This threshold is a Bonferroni correction of the typical $p < .05$ threshold for the three seeds used to probe dorsal circuit connectivity. Our secondary hypotheses and other exploratory correlations were evaluated using a TFCE-corrected threshold of $p < .002$, which accounts for 24 comparisons in total (i.e., six seeds, two PLE dimensions, two contrast directions). To facilitate comparison with prior work in this area (Dandash et al., 2014; Fornito et al., 2013), we also report significant associations without accounting for cross-seed comparisons (i.e., those with TFCE-corrected $p < .05$). To avoid circular inference, which can inflate effect sizes, scatter plots of associations between PLEs and functional connectivity were visualized using a leave-one-subject-out approach (Esterman et al., 2010). See Appendix A for our results with $p < .05$ TFCE correction and leave-one-subject-out analysis details.

2.3. Results

2.3.1 Principal component analysis

PCA was performed on 12 subscales derived from seven PLE questionnaires completed by 672 participants (descriptive statistics and pairwise correlations between subscales are in Appendix A Table

A1). Based on the inflection in the scree plot (Appendix A Figure A1) (Osborne & Costello, 2005), we retained two principal components. The first component accounted for 42.87% of the variance, with high loadings from subscales measuring the positive dimension of psychosis-related experiences, including delusional ideation, unusual experiences, perceptual aberrations, and eccentric behaviour (i.e., positive PLEs). The second component accounted for 19.7% of the variance, with high loadings from subscales measuring the negative dimension of psychosis-related experiences (i.e., negative PLEs), including social and physical anhedonia. Component loadings are displayed in Table 2.1.

Table 2.1. Component Loadings of Subscales After Rotation

	Component	
Subscale	**1**	**2**
CAPE Positive	.88[a]	.01
Chapman Magical Ideation	.86 [a]	-.01
sO-LIFE Unusual Experiences	.86 [a]	.10
Peters Delusion Inventory	.85 [a]	.05
Chapman Perceptual Aberration	.78 [a]	.12
sO-LIFE Impulsive Nonconformity	.63 [a]	.17
CAPE Depressive	.53 [a]	.40
sO-LIFE Cognitive Disorganisation	.47 [a]	.49 [a]
sO-LIFE Introvertive Anhedonia	.03	.86 [a]
Chapman Social Anhedonia	.14	.79 [a]
Chapman Physical Anhedonia	-.19	.74 [a]
CAPE Negative	.40	.67 [a]
Eigenvalue	**5.14**	**2.36**
% of variance	**42.87**	**19.70**

CAPE, Community Assessment of Psychotic Experience; sO-LIFE, short-form Oxford-Liverpool Inventory of Feelings and Experiences.

[a] Loadings > .40.

2.3.2. Corticostriatal functional connectivity

Functional connectivity analysis was performed in 353 participants with functional magnetic resonance imaging data. Each striatal region showed functional connectivity profiles consistent with known anatomy and prior findings (Appendix A Figure A3) (Dandash et al., 2014; Di Martino et al., 2008; Fornito et al., 2013).

Dorsal CST functional connectivity and PLEs. As predicted, higher scores on the positive PLE dimension were associated with reduced functional connectivity between the dorsorostral putamen and the right DLPFC (i.e., anterior middle frontal gyrus) (Table 2.2, Figure 2.1). Higher positive PLE scores were also associated with reduced coupling between the dorsal caudate and left dorsal anterior cingulate cortex (ACC) and reduced coupling between the DCP and the right primary motor cortex (Table 2.2, Figure 2.1). Each of these results was statistically significant at the Bonferroni-corrected TFCE threshold of $p < .017$. Additional suggestive associations between dorsal circuit functional connectivity and positive PLEs at an uncorrected threshold of $p < .05$ TFCE are presented in Appendix A.

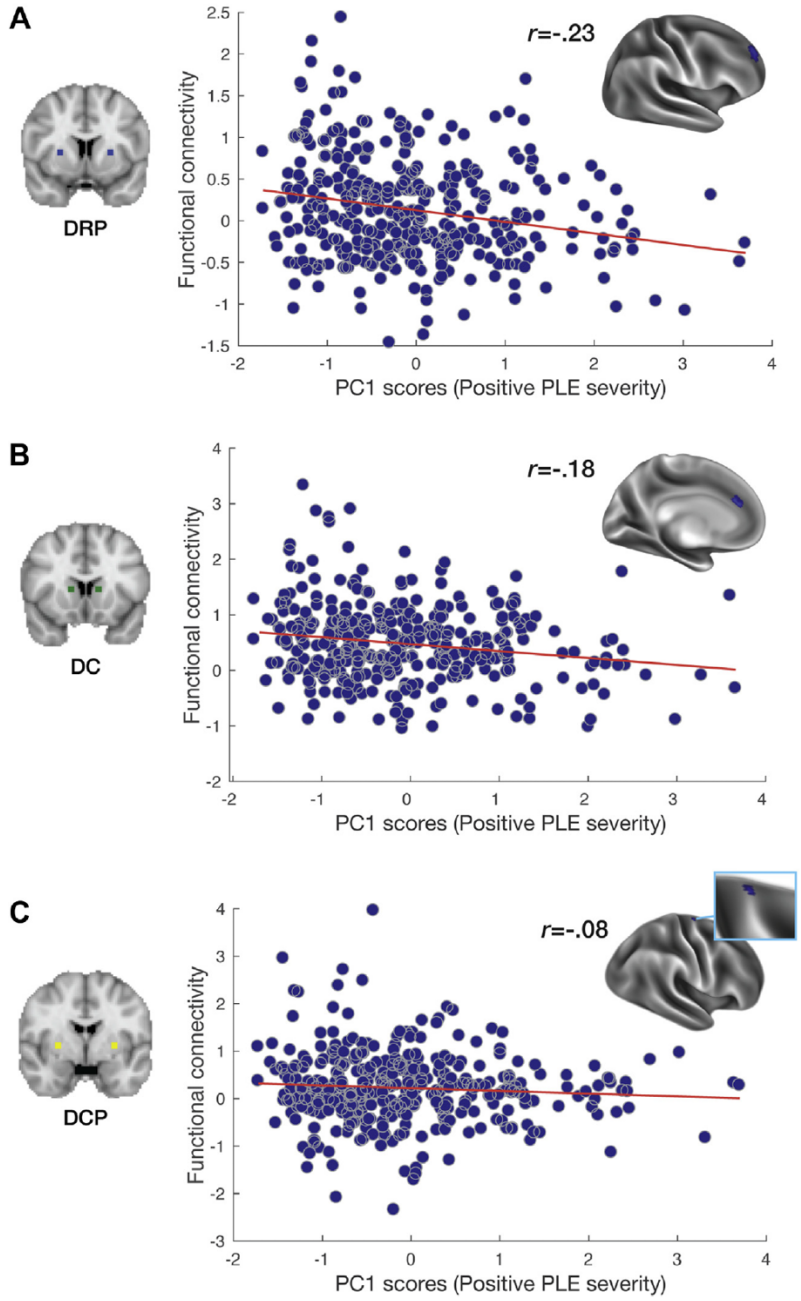

Figure 2.1. Associations between dorsal circuit functional connectivity and positive psychosis-like experiences (PLEs) (p < .017, threshold-free cluster enhancement corrected). Coronal slices in the left panels depict the location of striatal seed regions in the dorsal circuit. Cortical surface maps in the right panels depict the cortical sites for which functional connectivity with each seed correlates with positive PLE severity. Scatter plots depict the associations between positive PLE severity and functional connectivity between (A) the dorsorostral putamen (DRP) and right dorsolateral prefrontal cortex; (B) the dorsal caudate (DC) and left dorsal anterior cingulate cortex; and (C) dorsocaudal putamen (DCP) and primary motor cortex. Clusters on cortical surfaces are thresholded at $p < .017$ threshold-free cluster enhancement corrected. For visualization purposes, functional connectivity estimates and correlation coefficients were obtained using leave-one-subject-out analysis, thresholded at $p < .05$, threshold-free cluster enhancement corrected. PC, principal component.

PLEs and functional connectivity across dorsal and ventral CST circuits. Our exploratory analysis found a significant correlation between negative PLEs and increased functional connectivity between the DCP seeds and right primary motor area, TFCE corrected at $p < .002$ (Table 2.2, Figure 2.2). We did not find any significant association between PLEs and coupling within the ventral system after Bonferroni correction. Suggestive associations identified at an uncorrected threshold of $p < .05$ TFCE are presented in Appendix A.

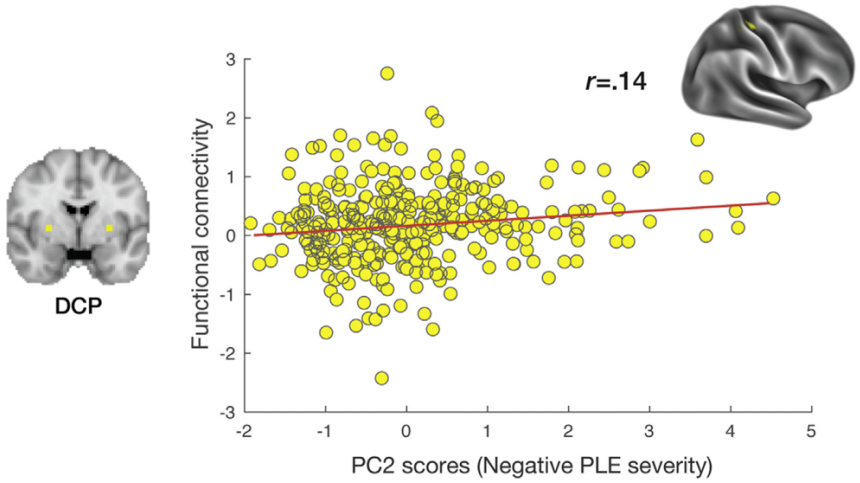

Figure 2.2. Association between dorsal functional connectivity and negative psychosis-like experiences (PLEs) (p <.002). Striatal seeds are shown in the axial slice in the leftmost panel. The scatter plot depicts the association between negative PLEs and functional connectivity between the dorsocaudal putamen (DCP) seed and right primary motor cortex. The cluster on the cortical surface was thresholded at $p < .002$, threshold-free cluster enhancement corrected. For visualization purposes, functional connectivity estimates and correlation coefficients were obtained using leave-one-subject-out analysis, thresholded at $p < .05$, threshold-free cluster enhancement corrected. PC, principal component.

Table 2.2. Regions Where Striatal Functional Connectivity Was Associated with PLEs

Seed	Region	MNI coordinates (x, y, z)	Max T-value	Cluster extent (voxels)	*p*
Dorsal circuit and positive PLEs -					
DRP	R anterior middle frontal gyrus	24, 54, 26	5.70	110	.002
DC	L dorsal anterior cingulate cortex	-8, 28, 26	4.98	26	.011
DCP	R primary motor cortex	22, -16, 74	4.88	22	.01
Dorsal circuit and negative PLEs +					
DCP	R primary motor cortex	34, -24, 52	5.07	44	.001

'+' sign indicates increased coupling in association with PLEs, while '-' indicates reduced coupling associated with PLEs. Clusters in the dorsal circuit that are associated with positive PLEs are thresholded at p <.017 TFCE corrected. Cluster associated with negative PLEs is thresholded at p <.002 TFCE corrected. R: right; L: left; DRP: dorso-rostral putamen; DC: dorsal caudate; DCP: dorso-caudal putamen; PLEs: Psychosis-like experiences.

2.4. Discussion

Corticostriatal systems have long been implicated in the pathophysiology of psychosis. Studies in independent samples present converging evidence that reduced coupling of the dorsal CST circuit is apparent across a broad spectrum of illness severity (Anticevic et al., 2014, 2015; Dandash et al., 2014; Fornito et al., 2013; Woodward & Heckers, 2016). Here, we show that reduced functional coupling in the dorsal CST circuit correlates with subclinical variation in PLEs related to positive symptomatology, consistent with a continuum of neural function that tracks the severity of symptom expression (Ettinger et al., 2014; Kelleher & Cannon, 2011; van Os et al., 2009) (see Figure 3 for a summary). Our comprehensive investigation of striatal functional connectivity also identified additional associations between PLEs and CST coupling that have not been observed in patients, suggesting a discontinuity for these phenotypes.

2.4.1. Dorsal corticostriatal coupling and PLEs

As hypothesized, higher levels of positive PLEs were associated with reduced coupling between the dorsal striatum and PFC. This association is broadly consistent with our past work in patients with first-

episode psychosis, persons with genetic high risk for psychosis, and individuals in the ARMS phase (Dandash et al., 2014; Fornito et al., 2013). However, the specific regions implicated in this past work show some differences with our current findings. Specifically, we have previously reported that first-episode patients, their unaffected relatives, and individuals with ARMS show reduced coupling between the dorsal caudate and the DLPFC, with patients and relatives also showing reduced coupling between the DCP and the DLPFC (Dandash et al., 2014; Fornito et al., 2013). Here, we found that positive PLEs were associated with reduced coupling between the dorsal caudate and the ACC and between the dorsorostral putamen and a more anterior region of the DLPFC. A summary and comparison of these findings is provided in Figure 2.3.

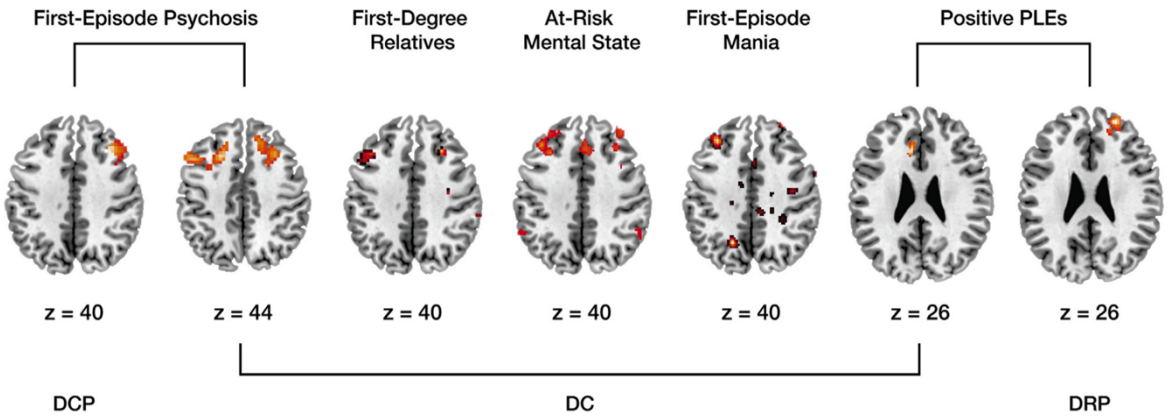

Figure 2.3. Functional connectivity of the dorsal circuit in persons experiencing different levels of illness severity. Axial slices show prefrontal regions where coupling within the dorsal circuit was reduced across a broad spectrum of severity, as identified in the current study and past findings. From left to right: regions in which coupling with the dorsocaudal putamen (DCP) and dorsal caudate (DC) were reduced in patients with first-episode psychosis compared with those in healthy control subjects [data from Fornito et al.2013]; regions of reduced coupling with the DC in healthy first-degree relatives of patients, individuals with at-risk mental state, and patients with first-episode mania with psychosis compared with those of healthy control subjects [data from Fornito et al. 2913, Dandash et al. 2014, and Dandash et al. 2018]; and findings from this study, showing regions where lower coupling with the DC and the dorsorostral putamen (DRP) was associated with more severe positive psychosis-like experiences (PLEs) (thresholded at $p < .05$, threshold-free cluster enhancement corrected, for visualization). The z-axis slice in Montreal Neurological Institute coordinates is shown beneath each image. The left hemisphere is on the left side of the images.

One explanation for these discrepancies is that variations in sample characteristics and image processing techniques may lead to slight changes in the localization of clinically relevant effects.

Another possibility is that our findings reflect a weak continuum model, in which PLEs are broadly related to the activity of the dorsal CST system, but the onset of frank illness arises only with dysfunction in very specific elements of this system—putatively, those involving the dorsal caudate and the DLPFC. It is also possible that our use of PCA to measure PLE severity, while capturing the dominant modes of variance across a wide battery of measures, may miss a more specific component of positive symptomatology that shows high behavioral and neurobiological continuity with clinical disorder. Better models of the latent dimensions underlying psychosis related psychopathology across the full range of illness severity will be required to clarify the relationship between clinical and subclinical phenotypes.

Nevertheless, the associations with dorsal circuit function and PLE severity implicate areas that have been shown in other work to be affected by schizophrenia and subthreshold symptomatology. Abnormal structure and function of the ACC are frequently reported in both patients and individuals at high risk for psychosis (Bora et al., 2011; Cadena et al., 2018; Fornito et al., 2009; Fornito, Yücel, et al., 2008; Fornito, Yung, et al., 2008; Reid et al., 2010; White et al., 2010). In addition, ACC dysfunction is linked to a failure to update prior beliefs based on sensory experience, which may induce hallucinations (Cassidy et al., 2018). Adolescents with high PLEs also show altered dorsal circuit activity during reward processing (Papanastasiou et al., 2018). Together, these findings motivate the need to develop a more refined understanding of how distinct elements of dorsal CST circuitry relate to specific types of PLEs and clinical symptoms.

After correcting for multiple comparisons, we also found that stronger negative PLEs were associated with increased functional connectivity between the DCP and the right sensorimotor cortex. This association was weak, however, with <1% of variance shared between the two measures. This finding differs from our prior report that negative symptoms correlate with reduced coupling between the dorsal caudate and DLPFC in patients with first-episode psychosis (Fornito et al., 2013). This divergence may be due to the nature of negative symptoms, which are complex and can be difficult to assess via self-report (Lincoln et al., 2017). Detailed investigation of the concordance between self-report and clinician-rated assessments of negative symptoms in both clinical and subclinical domains will be required to further clarify this phenotype.

2.4.2. Ventral corticostriatal coupling and PLEs

We did not find an association between PLEs and functional connectivity of the ventral circuit following multiple comparison correction. At a reduced threshold, we found associations between PLEs and ventral CST coupling that were restricted to the ventrorostral putamen–sensorimotor and visual circuit, such that increased functional connectivity was associated with higher negative and lower positive PLE scores (Appendix A Figure A5). The association with positive PLEs is consistent with disrupted frontostriatal connectivity leading to increased thalamic outflow to sensory cortices (Carlsson et al., 1999; Dandash et al., 2017). The concomitant association with negative PLEs implies that this increased outflow may be accompanied by psychomotor difficulties, which characterize many negative symptoms of schizophrenia (Dazzan et al., 2004; Emsley et al., 2003; Walther & Strik, 2012), given that CST circuits modulate goal-directed behaviour involving immediate physical action by coordinating motor with executive functions (Walther & Strik, 2012). However, these results should be regarded as tentative, and they require replication.

In contrast to our prior report that first-episode psychosis patients and their unaffected relatives showed increased coupling between the nucleus accumbens and the ventral frontal cortex (Fornito et al., 2013), we found no evidence for an association between the connectivity of this system and PLE severity. There is some evidence to suggest that this system may be tied to specific aspects of negative PLEs such as social anhedonia in subclinical groups (Wang et al., 2016). Our focus on dominant modes of PLE variance may have missed such specific effects.

2.4.3. Limitations

Over 90% of our sample was <30 years of age; hence, most participants have not passed through the maximal period of risk for schizophrenia (Loranger, 1984). As psychotic experiences in early adulthood have been found to predict later psychopathology (Rössler et al., 2007; Werbeloff et al., 2012), it is possible that some people in our cohort may develop the illness at a later stage. Our exclusion of individuals with a personal history of mental health treatment ensured that we sampled the subclinical range of symptom expression, but this means that we may not have sampled the more severe end of the

PLE spectrum. Our sample also included only righthanded individuals of European descent, which may limit the generalizability of the results.

Our two-component PCA solution parallels the well-known distinction between positive and negative symptoms in clinical populations, but it should be interpreted with some caveats. The simple two-factor solution may reflect an implicit bias in the PLE questionnaires to (over-)sample experiences related to positive and negative symptom dimensions of psychotic illness, which may inadvertently exclude other dimensions. A comprehensive assessment of clinical and subclinical symptomatology of psychosis may lead to a more refined model of the psychosis-risk phenotype.

Many of the associations between functional connectivity and PLEs were weak to moderate. It is possible that the strength of these association may increase with a more extensive sampling of the extreme end of the PLE spectrum. It is also likely that our PCA method, which focuses on common variance across instruments, may miss stronger associations with specific symptom domains. The strength of the associations identified here indicate that striatal functional connectivity cannot be used as a reliable predictor of PLE severity. However, when taken with findings in first-episode psychosis patients and individuals at high-risk for psychosis (Dandash et al., 2014; Fornito et al., 2013), our findings do suggest that dorsal corticostriatal dysconnectivity may represent a neurobiological mediator of a broad spectrum of psychosis symptom severity. Finally, in-scanner head motion exerts a pernicious effect on functional connectivity estimates (Ciric et al., 2017; Parkes et al., 2018; Power et al., 2012; Satterthwaite et al., 2012), but our extensive quality control procedures indicate that our findings could not be explained by motion artifact (see Appendix A).

2.4.4. Conclusions

Our findings indicate that variation in dorsal CST function tracks subclinical expression of positive PLEs in a nonclinical sample, paralleling the circuit-level changes seen in patients and high-risk groups. Together, these findings are consistent with a continuum of psychosis symptom severity that is apparent at the level of overt behaviour and underlying neurobiology, and which spans a broad spectrum of liability ranging from isolated experiences or attributional biases in otherwise healthy individuals to frank disorder in clinical populations.

2.5. Acknowledgements and disclosures

AFo was supported by the National Health and Medical Research Council (NHMRC) (Grant No. 1050504), Australian Research Council (Grant No. FT130100589), and the Sylvia and Charles Viertel Charitable Foundation. MB was supported by an NHMRC Senior Research Fellowship (Grant No. 1154378).

KS and AFo had full access to all the data in the study and take responsibility for the integrity of the data and the accuracy of data analysis.

AFo, MB, BJH, AZ, and CP were responsible for the study concept and design. KS and AFo drafted the manuscript. JT, AFi, BJ, AP, KS, MB, and AFo acquired the data. KS, AFo, JT, LP, and FS were responsible for the analysis and interpretation of the data.

MB, JT, VC, BJH, AZ, and CP conducted a critical revision of the manuscript for important intellectual content.

KS, JT, and AFo were responsible for statistical analysis. JT, AFi, and BJ provided administrative, technical, or material support. MB and AFo supervised.

We thank Chad Bousman, Dennis Velakoulis, Chao Suo, Kevin Aquino, Kate Thompson, Weile Sau, Jayden Bryan, and Erika Fortunato for their assistance in completing various phases of project planning, data collection, and analysis.

The authors report no biomedical financial interests or potential conflicts of interest.

2.6. Article information

From the Brain and Mental Health Research Hub (KS, JT, LP, AFi, AFo) and School of Psychological Sciences (KS, JT, LP, AFi, BJ, AP, MB, AFo), Monash Institute of Cognitive and Clinical Neurosciences, and Monash Biomedical Imaging (FS, AFo), Monash University; and Melbourne Neuropsychiatry Centre (VC, BJH, AZ, CP), Department of Psychiatry, The University of Melbourne, Victoria, Australia. Address correspondence to Kristina Sabaroedin, GradDip (Hons), Brain and Mental Health Research Hub, Monash University, 770 Blackburn Road, Clayton, Victoria 3168, Australia; E-mail: Kristina.Sabaroedin@monash.edu.

Received Oct 2, 2018; revised Jan 29, 2019; accepted Feb 13, 2019. Supplementary material cited in this article is available at https://doi.org/10.1016/j.biopsych.2019.02.013.

Chapter 3

Effective Connectivity of Fronto-striato-thalamic Circuitry Across the Psychosis Continuum

---

Sabaroedin, K., Razi, A., Chopra, S., Tran, N., Pozaruk, A., Chen, Z., Finlay, A., Nelson, B., Allott, K., Alvarez-Jimenez, M., Graham, J., Baldwin, L., Tahtalian, S., Yuen, H.P., Harrigan, S., Cropley, V., Sharma, S., Saluja, B., Williams, R., Pantelis, C., Wood, S.J., O'Donoghue, B., Francey, S., McGorry, P., Aquino, K., & Fornito, A. Effective connectivity of fronto-striato-thalamic circuitry across the psychosis continuum. *Under review in The American Journal of Psychiatry.*

Preamble

The findings of the previous chapter support a continuum fronto-striato-thalamic (FST) circuit dysconnectivity in psychosis. Dysfunction of dopamine activity within FST circuits is thought to play a central role in the emergence psychosis symptoms. Different models have been proposed to explain this dysfunction, variously ascribing a primary role to deficient top-down cortical and subcortical regulation of the midbrain or aberrant bottom-up signalling of deep brain structures. In this chapter, effective connectivity of FST circuitry was modelled to identify directed connectivity, or causal influences, within FST circuitry in different cohorts along the psychosis continuum. Striatal dopamine synthesis was also measured in a group of healthy individuals to investigate associations with FST effective connectivity. The early stage of psychosis is marked by a disruption of subcortical connectivity, particularly of the thalamus and midbrain, and that cortical dysfunction is apparent only in patients with established illness. Striatal dopamine synthesis capacity is linked to thalamic and midbrain connectivity. This chapter thus supports a primary role for dysfunction of bottom-up signalling in early phases of psychosis.

Supplementary materials for this chapter are in Appendix B.

Abstract

Objective: Aberrant dopaminergic activity within fronto-striato-thalamic (FST) circuits is thought to contribute to psychosis onset. It remains unclear whether primary abnormality arises from bottom-up subcortical signalling or impaired top-down cortical regulation. We mapped causal interactions (effective connectivity) of dorsal and ventral FST circuits across the psychosis continuum and identified connections associated with striatal dopamine synthesis.

Methods: Spectral dynamic causal modelling (DCM) for resting-state functional magnetic resonance imaging (fMRI) modelled FST effective connectivity in: (1) 46 antipsychotic-naïve first-episode psychosis (FEP) patients and 23 controls; (2) 36 established schizophrenia (SCZ) patients and 100 controls; and (3) 33 healthy individuals assessed for psychosis-like experiences (PLEs) with concurrent [^{18}F]DOPA positron emission tomography. DCM estimated FST connectivity in patients and their respective controls, associations with symptom severity in all cohorts, and with striatal [^{18}F]DOPA uptake in the PLE group.

Results: Patients commonly showed midbrain disinhibition and reduced top-down influence of thalamus on nucleus accumbens. Cortical dysfunction was only apparent in the SCZ group. Positive symptoms were primarily associated with bottom-up connectivity in FEP and a mixture of bottom-up and top-down connectivity in SCZ and PLE groups, with disinhibition of ventromedial prefrontal cortex and extrinsic connectivity of the midbrain implicated across all cohorts. Thalamic and midbrain connectivity were associated with striatal [^{18}F]DOPA uptake.

Conclusions: We identified a primary role for subcortical dysconnectivity in psychosis, with cortical dysfunction emerging in established illness. Effective connectivity of the midbrain and thalamus are robustly linked to positive symptom severity and striatal dopamine synthesis capacity, suggesting a central role in the emergence of psychotic symptoms.

3.1. Introduction

The symptoms of psychosis are proposed to lie on a continuum of severity, ranging from psychosis-like experiences (PLEs) at one end, through at-risk mental states (ARMS) to first episode psychosis (FEP) and chronic schizophrenia-spectrum illness at the other end (Grant et al., 2018). Dysfunction of fronto-striato-thalamic (FST) circuits linking the caudate and putamen with the prefrontal cortex is thought to be central to the emergence of psychotic symptoms (Anticevic, 2017; Dandash et al., 2014; Fornito et al., 2013; Haber, 2016; Pantelis et al., 1997; Sabaroedin et al., 2019). Two such circuits are particularly relevant: (1) a ventral 'limbic' system involved in emotional and reward processing, connecting the orbital and ventromedial prefrontal cortices and subcortical limbic structures (e.g., hippocampus and amygdala) with the nucleus accumbens (NAcc); and (2) a dorsal 'associative' system linking the dorsolateral prefrontal cortex (dlPFC) with the dorsal striatum, subserving associative learning and executive functions (Haber, 2016). Feedback loops passing through the pallidum and the thalamus connect both circuits back to the cortex (Haber, 2016).

The striatum in particular is a major target for dopamine projections from the ventral tegmental area (VTA) and substantia nigra (SN), with the ventral and the dorsal striatum respectively forming part of the mesolimbic and nigrostriatal pathways (Haber et al., 2000). Dysregulated dopamine signalling is proposed to contribute to psychosis onset by influencing the capacity of the striatum to filter and relay information to the thalamus, thus affecting broader FST function (Carlsson et al., 1999). In-vivo positron emission tomography (PET) has revealed elevated presynaptic dopamine synthesis capacity, measured using 3,4-dihydroxy-6-[^{18}F]-fluoro-L-phenylalanine ([^{18}F] DOPA), in the dorsal striatum of ARMS groups, especially in individuals who transition to psychosis (Howes, Bose, Turkheimer, Valli, Egerton, Stahl, et al., 2011). [^{18}F]DOPA elevations in the ventral striatum of schizophrenia patients and of ARMS individuals have also been reported (Allen, Chaddock, et al., 2012; McGowan et al., 2004).

This dopamine dysregulation is thought to alter functional connectivity of FST circuits across the psychosis continuum, as measured through resting-state functional magnetic resonance imaging (fMRI). Reduced functional connectivity between the dorsal striatum, thalamus, and dlPFC has been demonstrated in FEP patients and their unaffected first-degree relatives, ARMS individuals, chronic unmedicated patients, and healthy people with PLEs (Anticevic, 2017; Dandash et al., 2014; Fornito et

al., 2013; Horga et al., 2016; Sabaroedin et al., 2019). Increased functional connectivity between the ventral striatum, limbic regions, anterior cingulate cortex, ventromedial prefrontal and orbitofrontal cortices, was also found in these groups (Fornito et al., 2013; Kraguljac et al., 2016; Sarpal et al., 2017; Wang et al., 2018). Moreover, PET studies have identified direct correlations between prefrontal and medial temporal activation and striatal [^{18}F]DOPA levels (Fusar-Poli et al., 2011; Meyer-Lindenberg et al., 2002b; Modinos et al., 2015).

Functional connectivity quantifies statistical dependencies between regional physiological signals and does not distinguish causal interactions. It is therefore unclear whether FST dysfunction in psychosis arises from altered bottom-up signalling (i.e., from deep subcortical structures to higher subcortical or cortical areas) or disrupted top-down regulation of deeper subcortical systems. Evidence for a primary bottom-up pathology has been supported by studies reporting aberrant molecular function, activity, and functional connectivity of the midbrain across the psychosis continuum (Allen, Luigjes, et al., 2012; Hadley et al., 2014; Howes et al., 2013). Others have proposed that subcortical changes are secondary to deficient top-down control stemming from GABA/glutamate imbalance in the cortex or the hippocampus, leading to diminished top-down regulation of midbrain neurons (Carlsson et al., 1999; Lodge & Grace, 2007; Weinberger, 1987). Clinical studies have found correlations between impaired prefrontal function and elevated striatal dopamine synthesis in various groups along the psychosis continuum (McCutcheon et al., 2019). Altered activation and glutamate metabolites in the hippocampus, striatum, and midbrain of at-risk individuals have also been reported (Modinos et al., 2015), but these findings are largely correlational, making it difficult to disentangle top-down from bottom-up influences.

The relative influences on FST dysfunction in psychosis can be disentangled through models of circuit-level effective connectivity, which is defined as the causal influence that one neural system exerts over another (Friston et al., 2003). Effective connectivity is frequently inferred through dynamic causal modelling (DCM), which incorporates a Bayesian framework for identifying a generative model of directed, or causal, influences between regions comprising a distributed neural system (Friston et al., 2003). Here, we used spectral DCM (Razi et al., 2015) to characterize disruptions of dorsal and ventral FST effective connectivity across the psychosis continuum in antipsychotic-naïve FEP patients, people

with established schizophrenia (SCZ), and a non-clinical sample assessed for PLEs. We additionally used simultaneous fMRI-PET in the PLE cohort to identify which specific FST connections are associated with dorsal and ventral striatal [^{18}F]DOPA levels. This approach allowed us to cross-sectionally map effective dysconnectivity of FST circuits across the psychosis continuum and to identify putative directed influences associated with striatal dopamine synthesis capacity.

3.2. Methods and materials

3.2.1. Participants

Our analysis focused on three independent cohorts. The FEP cohort comprised antipsychotic-naïve patients and healthy controls (Francey et al., 2020). Separate analyses were also performed for a subgroup of FEP patients with schizophrenia diagnosis (FEP-SCZ). Data for established SCZ were obtained through the UCLA Consortium for Neuropsychiatric Phenomics open dataset (Poldrack et al., 2016). The PLE/[^{18}F]DOPA cohort comprised healthy participants recruited from the community who underwent concurrent PET/fMRI and completed the PLE assessment. Detailed information about the samples and recruitment is provided in Appendix B.

Participants were excluded from analyses if they had poor quality neuroimaging data or low variance explained by DCM. The PLE cohort represents a subset of the [^{18}F]DOPA group with PLE data. Exclusions at each step are detailed in Appendix B. Final sample numbers for each group are: 46 FEP patients (17 FEP-SCZ patients) and 23 controls, 51 SCZ patients and 100 controls, and 33 individuals in the PLE/[^{18}F]DOPA group PET (26 with complete PLE measures).

3.2.2. Symptom measures

We assessed positive symptoms using the positive frequency subscale of the Community Assessment of Psychotic Experience (CAPE) (Stefanis et al., 2002) for the PLE group and the positive subscale of Brief Psychiatric Rating Scale (BPRS) version 4 (Dazzi et al., 2016) for FEP and SCZ groups (details in Appendix B). Secondary analyses also considered negative symptoms using corresponding subscales from the same instruments.

3.2.3. MRI/PET processing and analysis

Echo-planar images (EPI) were preprocessed using FMRIPREP (version 1.1.1) (Esteban et al., 2019), with individual subjected to rigorous denoising and quality control for motion artifacts, as per past work (Parkes et al., 2018). Acquisition and processing details are in Appendix B.

PET data in the PLE/[^{18}F]DOPA group were acquired on a MR-PET Siemens Biograph scanner, following bolus injection of approximately 150 MBq of [^{18}F]DOPA. Patlak graphical analysis was used to quantify [^{18}F]DOPA influx rate constants (K_i^{cer} values) for dorsal and ventral striatal regions-of-interest (ROIs) (Parkes et al., 2017) (Appendix B Figure B1) relative to the cerebellum (Diedrichsen et al., 2009) in each participant's anatomical space. We only analysed the left hemisphere consistent with our DCM (see below). Further details are in Appendix B and Figure B2.

3.2.4. Dynamic causal modelling

ROI selection. ROIs spanning the dorsal and ventral FST and the midbrain were selected using stereotactic coordinates of past findings or of peak signals identified using functional connectivity, as outlined in Appendix B. We modelled 47 biologically plausible connections between eight ROIs (Figure 3.1). We focused on the left hemisphere given prior evidence of more consistent functional connectivity effects in left-lateralized FSTs (Dandash et al., 2014; Fornito et al., 2013).

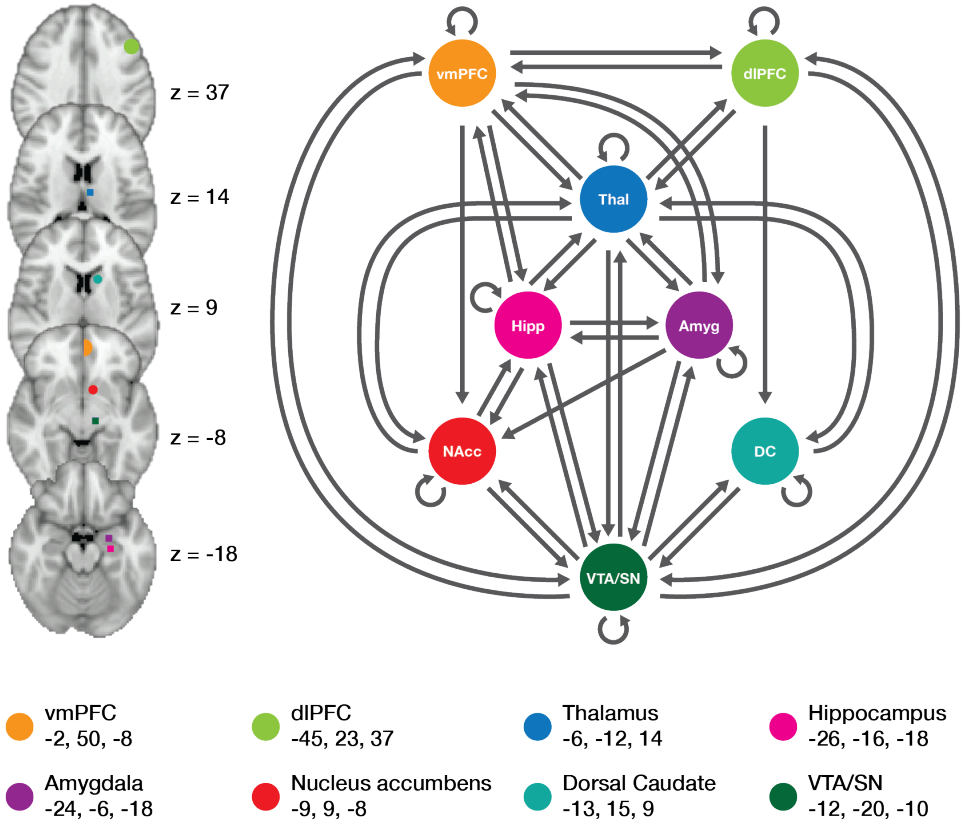

Figure 3.1. Parent model space of fronto-striato-thalamic systems encompassing dorsal and ventral circuits. Left shows anatomical locations of ROIs on axial slices. Right shows the parent model, including 47 biologically plausible connections including self-connections (circular arrows) for a network comprising eight regions. Centroids of ROIs in MNI coordinates (x, y, z) are presented in the bottom panel. VTA/SN: ventral tegmental area/substantia nigra (i.e., the midbrain).

Model estimation. We modelled effective connectivity in the spectral domain by fitting a complex cross spectral density using a generative model, parametrized by a power-law model of endogenous fluctuations, implemented in SPM12 (DCM 12; revision 7487) (Razi et al., 2015). Details are provided in Appendix B. Briefly, subject-specific first-level analyses were used to estimate directed (causal) influences between regions (in Hz), and the (inhibitory) recurrent or self-connectivity (i.e., self-inhibition) within each region. Following first-level model inversion, we excluded subjects with <75% variance explained by DCM for subsequent analyses.

Subject-specific connectivity parameters were then passed to a group-level general linear model (GLM) to estimate the designed effects and additive random effects of between-subject variability

(Friston et al., 2016). Second-level parametric empirical Bayes (PEB) models were run separately for each cohort. The FEP and SCZ were compared to their respective control group. Symptom correlates were modelled separately for each group, with both positive and negative symptoms included as covariates. Associations with [^{18}F]DOPA were modelled in the PLE cohort only, with dorsal and ventral striatal K_i^{cer} values as covariates. Age and sex were used as nuisance covariates for all models. Scanner site was also used as a covariate in the SCZ group. We only report effects with a posterior probability threshold above 0.95. PEB is a multivariate (Bayesian) GLM in which we fit all model parameters at once; hence, no correction for multiple comparisons is required. A typical effect size for effective connectivity between regions is 0.1 Hz (Razi et al., 2015). Technical details are in Appendix B.

3.3. Results

3.3.1. Participant demographic details

The demographic details of participants included in this study are in Table 3.1.

Table 3.1. Participants Descriptive Statistics

	PLE[a]	FEP			SCZ	
	(N = 33)	HC (n = 23)	FEP (n = 46)	FEP-SCZ (n = 17)	HC (n = 100)	Patients (n = 36)
Males, N (%)	15 (45.45)	14 (60.87)	20 (43.48)	9 (41.18)	55 (55)	26 (72.22)
Age, mean (SD)	22.30 (2.21)	21.74 (1.92)	19.12 (2.97)	20.51 (2.87)	30.6 (8.87)	35.81(8.49)
Age range	18 – 28	18 – 26	15 – 25	15 – 25	21 – 50	22 – 49
BPRS Total						
Mean (SD)	–	–	56.91 (10.34)	61.94 (9.41)	–	49.39 (14.03)
Range	–	–	38 – 80	46 – 80	–	26 – 77
BPRS Positive						
Mean (SD)	–	–	15.65 (4.19)	17.94 (4.31)	–	14.11 (6.17)
Range	–	–	10 – 27	13 – 27	–	5 – 29
BPRS Negative						
Mean (SD)	–	–	5.76 (2.6)	7 (3.16)	–	5.14 (2.54)
Range	–	–	3 – 12	3 – 12	–	3 – 11
CAPE Positive[b]						
Mean (SD)	23.04 (2.72)	–	–	–	–	–
Range	20 – 29	–			–	–
CAPE Negative[c]						
Mean (SD)	20.62 (5.22)	–	–	–	–	–
Range	14 – 37	–	–	–	–	–

[a] Demographics details are reported for the full sample with PET data. Demographics information for the sample subset included in the DCM-PLE analysis are: n = 26 (12 males), age mean (SD) = 21.81 (2.26), age range: 18 – 28 years old

[b, c] Measured in the sample subset included in the DCM-PLE analysis

3.3.2. Group differences in effective connectivity

FEP. Three differences were identified between FEP patients and controls (Figure 3.2A; Appendix B Table B1). Patients showed greater inhibitory influence of the thalamus on NAcc, weaker inhibitory influence of the amygdala on NAcc, and a disinhibition of ventral tegmental area/substantia nigra (VTA/STN). Similar differences were identified in the subset of FEP patients with a schizophrenia diagnosis (FEP-SCZ) (Appendix B Figure B3), compared to controls, who additionally showed

relatively stronger excitatory influence of VTA/STN on NAcc, stronger inhibitory influence of NAcc on hippocampus, and weaker self-inhibition within the amygdala. Cortical regions were not implicated in differences between FEP and controls.

SCZ. Similar to FEP, SCZ patients showed greater inhibitory influence of thalamus on NAcc and disinhibition of VTA/STN relative to controls (Figure 3.2B; Appendix B Table B1). SCZ patients also showed increased inhibitory influence of dlPFC on thalamus, of thalamus on hippocampus, and of VTA/STN on dorsal caudate (DC).

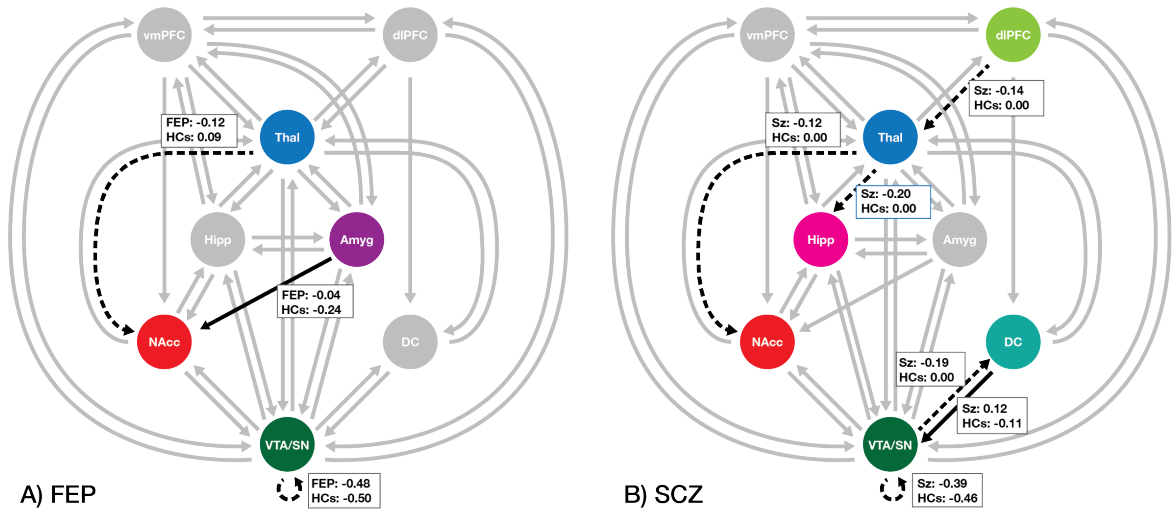

Figure 3.2. Group differences in fronto-striato-thalamic effective connectivity identified in the FEP (n = 46) and SCZ (n = 36) patients relative to their respective control groups. Differences in effective connectivity between FEP patients and healthy controls are shown in panel A, and patients with established schizophrenia and healthy controls are shown in panel B. Boxes show mean connectivity values in each group. For connections between regions, dashed arrows represent connections for which patients show a stronger inhibitory influence compared to controls; solid arrows represent connections for which patients show stronger excitatory, or weaker inhibitory, influence compared to controls. For self-connections, dashed arrows represent reduced inhibition (i.e., lower negative values) in patients compared to controls. Grey arrows represent modelled connections that were not (significantly) different from the prior. All connectivity parameters are in Hz, including self-connections. Connections were thresholded at Pp > 0.95 which represents strong evidence. DC: dorsal caudate; NAcc: nucleus accumbens: VTA/SN: ventral tegmental area/substantia nigra (midbrain).

3.3.3. Associations with positive symptomatology

FEP. Greater positive symptom severity (Figure 3.3, Appendix B Table B2) was predominantly associated with bottom-up connectivity. More severe positive symptoms were associated with stronger influence of VTA/SN on NAcc and amygdala, and of NAcc on VTA/SN; with weaker influence of VTA/SN on DC and hippocampus, of NAcc on hippocampus; and with reduced self-inhibition of the vmPFC and amygdala. The findings were consistent in the FEP-SCZ subgroup (Appendix B Figure B4, Table B2), Additionally, more severe positive symptoms were associated with weaker influence of DC on thalamus, hippocampus on amygdala, and dlPFC self-inhibition, and stronger influence of dlPFC on thalamus and thalamic self-inhibition. Self-connectivity of the amygdala was not associated with symptom severity in FEP-SCZ.

SCZ. Both top-down and bottom-up influences were associated with positive symptoms (Figure 3.3, Appendix B Table B2) in SCZ patients. Specifically, more severe positive symptoms were associated with stronger bottom-up influence of VTA/SN on dlPFC, of DC on thalamus, of thalamus on hippocampus, and of vmPFC on VTA/SN and hippocampus. Positive symptom severity was also associated with weaker bottom-up influence of VTA/SN on amygdala and of hippocampus on vmPFC; with weaker top-down influence of dlPFC on thalamus and of thalamus on VTA/SN; and with weaker self-inhibition of VTA/SN. The VTA/SN to amygdala connection and vmPFC self-connection were common between FEP and SCZ. When considering the FEP-SCZ subgroup, two additional connections—dlPFC-to-thalamus and DC-to-thalamus—were commonly implicated. Notably, the polarity of association was reversed in the FEP and SCZ cohorts for all of these connections except the vmPFC self-connection, suggesting that the link between positive symptoms and altered FST effective connectivity varies across illness stages.

PLEs. As with FEP and SCZ patients, the VTA/SN featured prominently albeit in different ways, with more severe PLEs associated with stronger bottom-up influence of this region on NAcc, and stronger top-down influence of dlPFC on VTA/SN, in addition to weaker VTA/SN self-inhibition (Figure 3.3,

Appendix B Table B3). PLE severity was also associated with stronger bottom-up influence of NAcc on thalamus, and of amygdala on hippocampus and VTA/SN; with weaker top-down influence of thalamus on hippocampus, of dlPFC on vmPFC, of amygdala on NAcc; and with weaker self-inhibition of amygdala, DC, and vmPFC.

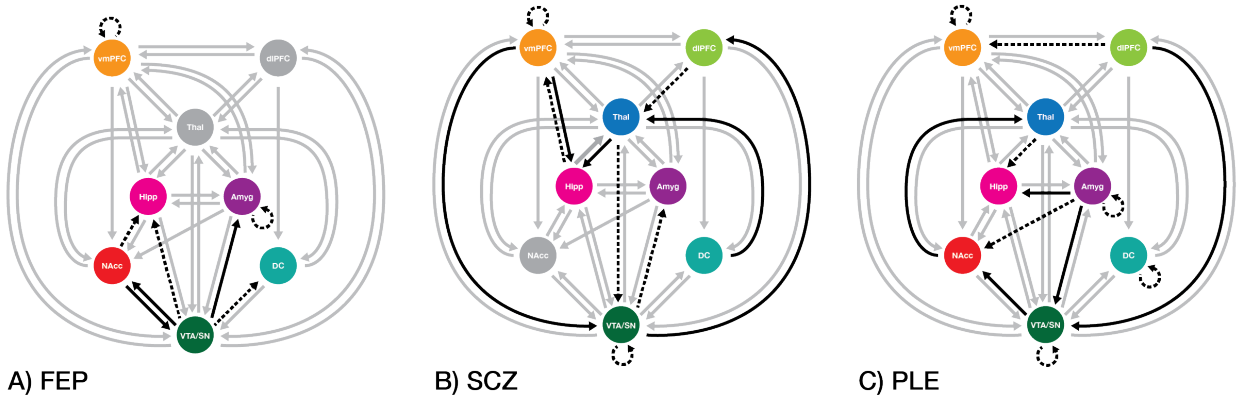

Figure 3.3. Associations between positive symptoms and fronto-striato-thalamic effective connectivity parameters in the FEP (n = 46), SCZ (n = 36), and PLE (n = 26) groups. Panels from left to right depict the results of PEB models mapping associations between FST effective connectivity and positive symptoms in (A) FEP, (B) SCZ, and (C) PLEs in a healthy cohort. For between-region connections, solid arrows denote positive associations and dashed arrows depict negative associations between effective connectivity parameters and symptoms/PLEs. For self-connections, dashed arrows denote negative associations such as more severe symptoms/PLEs were associated with reduced inhibition. Grey arrows show modelled associations that were not (significantly) different from the prior. Connections were thresholded at Pp > 0.95. DC: dorsal caudate; NAcc: nucleus accumbens: VTA/SN: ventral tegmental area/substantia nigra (midbrain).

3.3.4. Associations with negative symptomatology

Negative symptom correlations for the FEP, FEP-SCZ, SCZ, and PLE groups are presented in Appendix B Figure B5 and Tables B2–B3. Associations between symptom severity and amygdala self-inhibition was consistent across the last three groups, although the direction of the association was reversed in the SCZ compared to FEP-SCZ and PLE groups, which may be an effect of medication or illness progression.

3.3.5. Associations with striatal dopamine synthesis capacity

Dorsal striatum. Significant associations with dorsal striatal [^{18}F]DOPA implicated the thalamus (Figure 3.4; Appendix B Table B3). Specifically, higher [^{18}F]DOPA was associated with stronger thalamic self-inhibition, thalamic influence over the VTA/SN and DC, and amygdala over thalamus, in addition to weaker influence of DC on thalamus.

Ventral striatum. Ventral striatal [^{18}F]DOPA was associated with a distributed set of effective connections centred on midbrain and thalamus (Figure 3.4; Appendix B Table B3). Specifically, higher [^{18}F]DOPA was associated with weaker self-inhibition of NAcc and amygdala, weaker influence of these two regions on the thalamus, stronger self-inhibition of the VTA/SN and influence of this area on the vmPFC and DC, stronger influence of the hippocampus on VTA/SN and thalamus, and stronger self-inhibition of the DC.

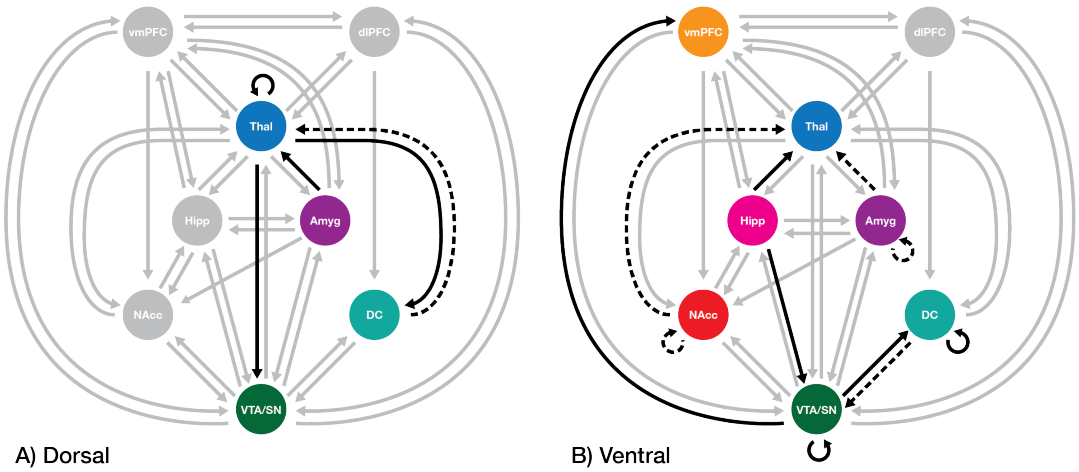

Figure 3.4. Associations between fronto-striato-thalamic connectivity and striatal dopamine synthesis capacity in the PLE group (n = 33). Panel A depicts connections associated with dopamine synthesis in the dorsal circuit. Panel B illustrates associations with dopamine synthesis in the ventral circuit. Solid arrows: positive associations between effective connectivity parameters and dopamine synthesis; dashed arrows: negative associations between effective connectivity parameters and dopamine synthesis; grey arrows: modelled connections that were not (significantly) different from the prior. Connections were thresholded at Pp > 0.95. DC: dorsal caudate; NAcc: nucleus accumbens: VTA/SN: ventral tegmental area/substantia nigra (midbrain).

3.4. Discussion

FST dysfunction has been identified across the psychosis continuum, but the influence of top-down versus bottom-up signalling within these circuits has been unclear. Using spectral DCM, we mapped the effective connectivity of dorsal and ventral FST circuits in FEP, established SCZ, and in association with subclinical PLEs. The two clinical groups showed consistent disinhibition of VTA/SN and top-down inhibitory influence of the thalamus on NAcc. Dysfunction of cortical regions was only identified in established illness. Positive symptomatology was associated with disinhibition of the vmPFC and VTA/SN connectivity across all groups. Moreover, concurrent PET-MRI of the PLE/[^{18}F]DOPA cohort revealed distinct circuits associated with dorsal and ventral dopamine synthesis capacity, with both tied to thalamic and VTA/SN connectivity. Collectively, our findings provide evidence of distinct FST connectivity profiles across the psychosis continuum, with dysfunction of subcortical systems featuring prominently in early illness stages and cortical abnormalities becoming more apparent later in the illness. Our findings also reveal that striatal dopamine synthesis capacity is closely tied to thalamic and midbrain connectivity.

3.4.1. Effective dysconnectivity of fronto-striato-thalamic circuits across the psychosis continuum

The clinical groups showed consistent evidence of VTA/SN disinhibition. In FEP, top-down connections to the VTA/SN were not implicated, suggesting an intrinsic bottom-up dysfunction. Midbrain disinhibition is consistent with elevated dopamine release in the striatum, suggesting that elevations in striatal dopamine synthesis reported by [^{18}F]DOPA and other PET studies across the psychosis continuum may be linked to intrinsic dysregulation of the midbrain (Lodge & Grace, 2007; McCutcheon et al., 2019). SCZ patients also showed increased inhibitory influence of VTA/SN over DC, which should yield a net disinhibition of striatal activity given that ~95% of striatal neurons are GABAergic (Gerfen & Bolam, 2010). Striatal disinhibition is expected to disrupt its capacity to filter information through the FST circuits (Carlsson et al., 1999). SCZ patients also showed increased top-down excitatory influence of DC over VTA/SN, which may reflect a compensatory response to regulate aberrant midbrain signalling to the DC. Our findings thus suggest that an early bottom-up midbrain

pathology may evolve to affect striatal function and potentially dysregulate feedback loops within dorsal and ventral FSTs with illness progression, although longitudinal data are required to test this hypothesis.

Both FEP and SCZ groups also showed increased inhibitory influence of thalamus over NAcc. Excitatory thalamostriatal projections provide feedback for the striatum to maintain bottom-up signalling to thalamus and cortex in support of specific actions or behaviors (Haber & McFarland, 2001). A greater inhibitory influence of thalamus on NAcc in both FEP and SCZ thus implies a dysregulation of the thalamostriatal feedback pathway. The relationship of this dysregulation with the intrinsic disinhibition of VTA/SN remains unclear.

We identified cortical dysconnectivity in SCZ, but not FEP patients, such that the SCZ group showed increased inhibitory influence of dlPFC over thalamus relative to controls. This result suggests that altered top-down regulation of cortex over subcortex may emerge in later illness stages. Indeed, it is possible that the increased inhibitory influence of dlPFC over thalamus reflects a compensatory response to dysregulated subcortical activity, but our design cannot disentangle the effects of illness progression from medication, given that FEP, but not SCZ, patients were antipsychotic naïve at assessment.

3.4.2. Associations with symptoms

Inhibition of the vmPFC was negatively associated with positive symptom severity across the FEP, SCZ, and PLE groups, highlighting a central role for corticolimbic activity across illness stages. Moreover, VTA/SN connectivity was consistently linked with symptom severity across all groups, aligning with our group difference analysis to suggest that midbrain dysfunction is a primary abnormality in psychosis. However, the specific connections implicated vary across the groups. In FEP, symptom severity was positively associated with influence of VTA/SN on amygdala, and influence of dlPFC on thalamus, and negatively associated with the influence of DC on thalamus (the last two associations were specific to FEP-SCZ). The polarity of these associations was reversed in SCZ. These differences may reflect a change in circuit dynamics with illness progression, differences in symptom severity between FEP and chronic stages (Leucht et al., 2005), or antipsychotic exposure in SCZ

patients. Nonetheless, our findings indicate that midbrain connectivity is robustly linked to positive symptom expression across illness stages.

Elements of FST connectivity in the PLE association map were more similar to positive symptom associations in FEP rather than SCZ, which may reflect the lack of antipsychotic exposure in the PLE and FEP groups. Across all three groups, consistency was greater at the regional rather than connection level. For instance, top-down connectivity of the dlPFC and amygdala to VTA/SN was linked with PLEs, whereas positive symptom severity in SCZ patients was associated with bottom-up influences of VTA/SN on the other two structures. These variations may reflect possible fundamental differences in the neural correlates of PLEs and clinical symptoms at different illness stages, an effect of medication in the SCZ group, or a combination of both.

There was less consistency across the cohorts with respect to associations between negative symptoms and effective connectivity, although the DLPFC and limbic regions were generally implicated. One particular challenge involves measuring negative PLEs via self-report measures (Pavlova & Uher, 2020).

3.4.3. Associations with striatal dopamine synthesis capacity

Dorsal and ventral striatal [^{18}F]DOPA levels were associated with effective connectivity of distinct elements of FST circuitry. All associations with dorsal striatal [^{18}F]DOPA involved the thalamus. Two such connections—one being from DC to thalamus and the other being the thalamic self-connection—were also identified as being associated with positive symptom severity in FEP-SCZ patients. The modulation of cortical and thalamic glutamatergic signals by dopamine in the striatum controls striatothalamic filtering and information flow to cortex via the thalamus, and its disruption is thought to play a key role in the pathogenesis of psychosis (Carlsson et al., 1999).

Connections associated with ventral striatal [^{18}F]DOPA were spread across both the ventral and dorsal systems. NAcc projections are widely distributed in the VTA/SN and can drive dopamine levels in the dorsal striatum (Haber et al., 2000). Accordingly, we found that ventral striatal [^{18}F]DOPA was associated with VTA/SN–DC connectivity and inhibition within these regions. VTA/SN–DC connectivity was also disrupted and SCZ patients and was associated with positive symptoms in FEP,

suggesting there may be a link between the NAcc's regulation of midbrain activity and dorsal circuit dysfunction in patients (Lodge & Grace, 2012). In summary, our PET results indicate that dopamine synthesis in the ventral striatum is associated with connectivity between the midbrain and the DC, whereas dopamine synthesis in the dorsal striatum is associated with striatothalamic interactions in the dorsal FST circuit.

3.4.4. Limitations

We used three independent samples to cross-sectionally characterize effective dysconnectivity across different stages of the psychosis continuum. This approach offers a test of consistency across cohorts, but inferences about the potential progression of circuit dysfunction must be confirmed longitudinally, especially given the difference in medication exposure, sample size, and symptom severity across the three cohorts. Additionally, differences in symptom associations found across the cohorts can only be compared qualitatively, as quantitative differences between groups would require direct between-group statistical comparisons outside of the PEB framework.

DCM offers a validated framework for modelling effective connectivity using fMRI that can be robustly performed on smaller sample sizes (Friston et al., 2016). DCM performed well in our data, explaining >75% of signal variance. Nonetheless, any model of effective connectivity should ideally be validated using gold-standard invasive methods. We also note that our PEB analysis of the PET data identifies associations with, but not causal influences on, striatal [^{18}F]DOPA.

We restricted our analysis to key left hemisphere FST regions implicated by prior work as relevant for psychosis. This focus facilitates efficient estimation of DCMs but may miss contributions from unmodelled areas. Recent improvements in the scalability of DCM (Frässle et al., 2017) may be used to derive a more comprehensive picture. Moreover, ultra-high-field imaging could be used to differentiate contributions of the VTA and SN, given the prominent role ascribed to the midbrain in our findings.

3.4.5. Conclusions

We identified a primary role for subcortical dysfunction in psychosis, with aberrant activity and connectivity of the midbrain, thalamus, and medial temporal areas emerging early and cortical dysconnectivity becoming apparent only in established illness. Effective connectivity of the midbrain and thalamus are strongly linked to positive symptom severity and striatal dopamine synthesis capacity, suggesting that they represent key elements of FST involvement in the pathogenesis of psychotic symptoms. Our findings show that aberrant bottom-up signalling emanating from the midbrain and dysconnectivity of subcortical regions play a prominent role in the pathogenesis of psychotic symptoms.

Chapter 4

Effective Connectivity of Fronto-striato-thalamic Circuitry and Dimensions of Psychosis-like Experiences

---

Sabaroedin, K., Tiego, J., Razi, A., Bellgrove, M., Aquino, K., & Fornito, A. Effective connectivity of fronto-striato-thalamic circuitry and dimensions of psychosis-like experiences. *Manuscript in preparation.*

Preamble

Having developed effective connectivity models of fronto-striato-thalamic (FST) circuitry across the psychosis continuum, this chapter revisited associations with psychosis-like experiences (PLEs). A high-resolution characterization of PLEs was derived through item response theory to examine the associations between specific dimensions of PLEs and FST effective connectivity. Nine dimensions spanning the positive- and negative-like symptoms were identified. Distinct dimensions from positive-like experiences consisting of subclinical delusions, cognitive disorganisation, and body image aberration were associated with striatothalamic connections. Distinct dimensions of negative PLEs comprising anhedonia, asociality, avolition, and alogia implicated the nucleus accumbens and associations were constrained to the subcortical regions within the ventral circuit. Bottom-up influence of the midbrain was not prominently associated with the PLE dimensions identified here, suggesting a distinct mechanistic process between clinical and subclinical symptoms along the psychosis continuum. Supplementary materials for this chapter are in Appendix C.

Abstract

Psychosis-like experiences (PLEs) in the general community are thought to be continuously distributed with the clinical symptoms of psychosis and thus provide an opportunity for understanding the pathogenesis of psychotic illnesses. Fronto-striato-thalamic (FST) circuits are central to the expression of psychosis symptoms and have been implicated in different stages of the psychosis continuum. Investigation of PLEs and FST connectivity have reported mixed findings, potentially due to the use of self-report measures for assessing PLEs, which yield coarse estimates of symptom dimensions. Furthermore, correlational methods have mainly been used to investigate FST connectivity, which cannot disentangle inter-regional causal influences within a brain network. This study aimed to derive high-resolution measures of distinct PLE dimensions and to investigate differential associations between PLEs and FST effective connectivity, which captures causal interactions between brain regions, in a large non-clinical sample. Item response theory (IRT) was used to obtain robust estimates of underlying latent dimensions of PLEs from a battery of questionnaires administered to 726 healthy participants. Effective connectivity of the FST system comprising the ventral and dorsal circuits was estimated using spectral dynamic causal modelling on resting-state fMRI data for a subset of participants who underwent neuroimaging (n = 352; 156 males; mean age [range] = 23.38 [18–50 years]). Positive PLEs comprising subthreshold delusions, cognitive disorganisation, body image aberration, and hallucinations were associated with effective connectivity of the striatothalamic pathway, suggesting the involvement of information filtering and integration in positive PLEs. Associations with negative PLE dimensions, namely anhedonia, asociality, avolition, and alogia, were restricted to the ventral circuit, highlighting a prominent contribution of limbic circuitry in this domain.

4.1. Introduction

Psychosis-like experiences (PLEs) are subclinical symptoms of schizophrenia and other psychotic disorders that occur in individuals who do not meet the threshold for a formal diagnosis (Grant et al., 2018). With a prevalence of up to 8% in the general community (van Os et al., 2009), PLEs are often transient, with persistent cases representing enduring personality traits (e.g. schizotypal personality) (Ettinger et al., 2014). The incidence of PLEs is higher in relatives of schizophrenia patients, suggesting

that PLEs mark a heightened risk of developing a psychotic disorder, and that they offer an opportunity to understand the pathogenesis of clinically significant illness (Barrantes-vidal et al., 2015; Vollema et al., 2002). PLEs can be grouped into experiences that mimic the positive and negative symptoms of clinical illness, and these dimensions are continuously distributed across clinical and non-clinical populations (Barrantes-Vidal et al., 2013; DeRosse & Karlsgodt, 2015; Stefanis et al., 2002; Verdoux & Van Os, 2002). Positive PLEs are characterized by subclinical delusions and hallucinations, and can include magical ideation, unusual perceptual experiences, and paranoia (Verdoux & Van Os, 2002). Negative PLEs encompass subthreshold negative-like symptoms such as mild anhedonia and social withdrawal (Chapman et al., 1976; Stefanis et al., 2002).

There is increasing evidence to suggest that both psychotic symptoms in clinical cases and PLEs in the general community are associated with variations in the structure and function of fronto-striato-thalamic (FST) circuits, which topographically link areas of frontal cortex with the striatum and thalamus along a ventromedial–to–dorsolateral topological gradient (Haber, 2016; Marquand et al., 2017). Two such circuits with particular relevance for PLEs are the ventral and the dorsal circuits. The ventral "limbic" circuit subserves emotional processes, reward valuation, and motivation by linking the ventral striatum with the ventromedial prefrontal cortex (VMPFC), orbitofrontal cortex (OFC), and subcortical limbic areas (i.e., hippocampus and amygdala) (Alexander, 1986; Draganski et al., 2008; Haber, 2016; Marquand et al., 2017). The dorsal "associative" circuit connects the dorsolateral prefrontal cortex (DLPFC) to the dorsal striatum and is involved in associative learning and executive functions (Haber, 2003). The striatum functions as a filter, relaying information back to the cortex through striatothalamic pathways that encompass the pallidum and thalamus (Carlsson et al., 1999; Haber, 2010). The striatum is also a major target for dopamine projections from the ventral tegmental area (VTA) and the substantia nigra (SN) of the midbrain, respectively forming the mesolimbic and nigrostriatal pathways with the ventral and dorsal striatum (Haber et al., 2000).

Resting-state functional magnetic resonance imaging (fMRI) has been widely used to examine associations between FST function, PLEs, and clinical illness. These studies primarily examine functional connectivity—i.e., statistical dependencies (often quantified with correlations) between signal fluctuations recorded in different brain regions—of the circuits to assess network function.

Presently, there are conflicting reports concerning the specificity of correlations between FST connectivity and distinct aspects of PLEs. One study conducting a principal component analysis of 12 PLE scales obtained from seven questionnaires identified positive and negative symptom-like PLE dimension, with the former associated with lower coupling in the dorsal circuit, particularly between the dorsal caudate and dorsal anterior cingulate cortex, and the latter associated with increased coupling between the dorsocaudal putamen and primary motor cortex (Sabaroedin et al., 2019). Re-analysis of this group using partial least squares regression to identify dimensions of common variance between the PLE scales and striatal functional connectivity indicated that reduced coupling of the dorsal circuit was associated with both positive and negative symptom-like domains (Pani et al., 2020). This latent variable implicated coupling between dorsal caudate and DLPFC, consistent with work in clinical cohorts (Dandash et al., 2014; Fornito et al., 2013). Other studies using single-scale measures of PLEs have found that positive PLEs are associated with reduced functional connectivity between the dorsal striatum and posterior cingulate cortex, but not prefrontal areas (Wang et al., 2018). The association between negative symptoms and FST dysfunction across the psychosis continuum is less established. Some reports suggest involvement of the ventral circuit across different illness stages (Fornito et al., 2013; Kraguljac et al., 2016; Wang et al., 2016), while others have found that negative PLEs are associated only with increased coupling within the dorsal circuit (Sabaroedin et al., 2019).

Part of the variability in findings concerning the link between PLEs and FST circuitry may reflect the nature of PLE measurements. Different self-reports have been used to quantify PLEs, with items measuring distinct components of positive symptoms typically aggregated into a subscale and coarsely estimated using summed scores, despite evidence that specific psychotic phenomenology are linked with distinct neurobiological processes (Corlett & Fletcher, 2012; Corlett et al., 2019; Diederen et al., 2012; Phillips & Silverstein, 2003). Additionally, dimensional latent traits are often measured by items with dichotomous options (i.e., true or false). These issues surrounding self-reports may lead to inaccurate estimation of PLEs, such that a person with mild experiences is forced to endorse a ‘true’ or ‘false’ option that does not capture the varying magnitude of their PLEs (van der Sluis et al., 2010), or the score for a person who experiences varying severity on distinct PLE dimensions is collapsed into

one general dimension score that lacks information of a person's varying trait expressions and where they sit on the multidimensional phenotypic continuum of psychosis.

A further limitation of studies using functional connectivity to examine FST circuits is that this method does not distinguish directional influences within a neural network (Friston et al., 2013). Competing hypotheses have proposed that psychosis symptoms arise either from bottom-up subcortical dopamine dysregulation or loss of top-down control over subcortical systems (Carlsson et al., 1999; Howes, Bose, Turkheimer, Valli, Egerton, Stahl, et al., 2011; Lodge & Grace, 2007). Effective connectivity is the causal influence that one neural system exerts over another, and models of effective connectivity can be used to parse the relative contributions of bottom-up and top-down signals (Friston, 1994). A popular method for inferring effective connectivity is dynamic causal modelling (DCM), which is a generative model embedded within a Bayesian framework for specifying directed, or causal, influences between brain regions (Friston et al., 2003). More recently, spectral DCM was developed as an approach to model effective connectivity in resting-state fMRI by estimating neuronal dynamics based on the cross-spectra of time-series (Razi et al., 2015). Recent work using DCM in FST circuits found that PLEs are associated with effective connectivity in both ventral and dorsal systems, with positive PLEs tied to a cascade of influence of the cortex over midbrain, the midbrain over nucleus accumbens, and the nucleus accumbens over thalamus, whereas negative PLEs were associated with a weaker influence of the cortex over the striatum (Sabaroedin et al., 2020). However, associations of specific PLE dimensions have not yet been considered.

The present study aimed to derive high-resolution measures of distinct PLE dimensions and to use spectral DCM to investigate the association between PLE dimensions and FST effective connectivity within a large non-clinical sample. Critically, PLEs were measured using a wide array of self-report scales, and item response theory (IRT) was used to obtain robust estimates of the underlying latent dimensions tapped by these scales. IRT is a collection of robust statistical methods that can be used to refine self-reports by defining the relationship between an unobserved continuous trait variable and the characteristics of a questionnaire item (Edelen & Reeve, 2007; Reise et al., 2005). It allows selection of only items that are informative with respect to an underlying latent trait, thus yielding a more accurate measure of that trait. Our analysis thus allowed us to disentangle the relative

contributions of top-down and bottom-up FST connectivity to distinct dimensions of PLEs measured in a non-clinical community sample.

4.2. Methods and materials

4.2.1. Participants

We recruited 726 participants (303 males; age mean [SD] = 23.32 [4.99]; age range = 18–50 years old) from the general community to complete an online battery of PLE measures. All participants were of European descent (defined as having all grandparents of European ancestry), right-handed with no personal history of neurological or psychiatric illness, and no significant drug use. The study was conducted in accordance with the Monash University Human Research Ethics Committee (reference number 2012001562). A subset of 379 participants with complete PLE measures underwent our resting-state fMRI protocol. Participants were subsequently excluded for either scan artifacts, poor scan quality, or excessive in-scanner head motion (criteria outlined below). The final fMRI sample comprised 352 participants (154 males; age mean [SD] = 23.38 [5.16]; age range =18–50 years; IQ range = 81–139, IQ mean [SD] = 112 [11.50]) with complete PLE measures and neuroimaging data.

4.2.2. Measures of PLEs

PLEs were assessed using psychometrically validated measures developed for use in the general community. The scales used included the Peters' Delusion Inventory-21 item version (PDI-21) (Peters et al., 2004), the Wisconsin Schizotypy Scales (WSS) measuring magical ideation, body image aberration, social and physical anhedonia (Chapman et al., 1976, 1978b; Eckblad & Chapman, 1983), the Community Assessment of Psychic Experiences (CAPE) (Stefanis et al., 2002), and the Oxford-Liverpool Inventory of Feelings and Experiences Short Form (*s*O-LIFE) (Mason et al., 2005). More information on the measures is outlined in Appendix C. Items from the seven measures were organized into dimensions that aligned with positive symptom dimensions widely recognized in the psychosis spectrum (American Psychiatric Association, 2013; van Os & Kapur, 2009): 1) delusions, 2) hallucinations, 3) cognitive disorganisation, and 4) body image aberration. We included body image

aberration as this dimension has been recognised as an important feature of clinical positive symptoms (Priebe & Röhricht, 2001), as well as in schizotypy (Lenzenweger, 2006). Similar steps were taken for items probing negative symptom dimensions. Items from the measures were pooled into five dimensions that aligned with what has been proposed by a wide body of research, resulting in five components: 1) anhedonia, 2) asociality, 3) avolition, 4) blunted affect, and 5) alogia (Kirkpatrick et al., 2006; Strauss et al., 2018; Strauss, Ahmed, et al., 2019; Strauss, Esfahlani, et al., 2019). Model fit and the uni-dimensionality of these item pools were assessed using IRT, as outlined in the following section.

4.2.3. Parametric unidimensional item response theory analysis

IRT is a collection of statistical methods for modelling the relationship between item-level data and the underlying constructs, or latent traits, that these items are proposed to measure. IRT is an ideal approach for improving psychometric precision in the measurement of psychological constructs, because it enables the performance of individual items in measuring the target latent trait to be empirically modelled (Reise & Rodriguez, 2016). Items with poor performance, as determined by several criteria discussed below, are removed and the model is re-estimated until all assumptions are satisfied, making IRT an iterative process (Toland, 2014). We performed parametric unidimensional IRT analysis in IRTPRO 4.2 using the Bock-Aitkin marginal maximal likelihood algorithm with expectation maximization for parameter estimation, which also accommodates partial or missing data (Bock & Aitkin, 1981; Cai et al., 2011).

To perform IRT estimation, dichotomous items from the PDI-21, WSS, and *s*O-LIFE were fitted using the 2-parameter logistic model (2PL), which fits: 1) a single slope parameter (α) for each item, and 2) one threshold parameter (β) (Edelen & Reeve, 2007; Reise & Rodriguez, 2016; Thomas, 2011). Polytomous items from the CAPE questionnaire were fitted using the graded response [GR] model, which is an extension of the 2PL model appropriate for ordered categorical data obtained from Likert scales (Samejima, 1969). The GR model estimates one slope parameter for each item and $k - 1$ threshold parameters, where k is the number of item response categories (Cai et al., 2011). Slope parameters are analogous to factor loadings and indicate how well an item discriminates between

different levels of the latent trait. These parameters are measured in logistic metric, generally within the range of $\pm$ 2.8, although they often exceed this range in clinical measurement (Reise & Rodriguez, 2016; Reise & Waller, 2009). Items with higher slope estimates are more discriminative between different levels of the latent trait being measured and therefore provide more precise measurement (i.e., reliability (r_{xx}) or Information (I); where $r_{xx} = 1 - (1/I)$) (Toland, 2014). Threshold parameters are analogous to item means in classical test theory and reflect the location (i.e., level of severity) on the distribution of the underlying trait, denoted theta (θ), where the probability of endorsing the response category is .5 (Reise et al., 2005). Threshold parameters are measured in a standardised metric where the population mean is 0 and the population standard deviation in 1 and typically range between -2 to +2, although these frequently exceed +3 in clinical measurements (Reise & Rodriguez, 2016; Reise & Waller, 2009; Thomas, 2011; Toland, 2014).

Item parameters from IRT estimation were used to generate option response functions (ORFs). ORFs are graphic representations of the probabilities of endorsing each item response category, with the x-axis of the graphs labelled 'theta' (θ), denoting the level of the measured latent trait, which is scaled to a mean of 0 and standard deviation of 1 (see Appendix C Figure C1 for an example of ORFs for items in the hallucination dimension). Dichotomous items with steep item response functions and polytomous items with steep and non-overlapping ORFs are more discriminative and provide more information about the latent trait (Toland, 2014).

Item parameters can also be used to generate item information functions (IIFs), which display the amount of information each item contributes additively at varying levels of the latent trait θ (Thomas, 2011; Toland, 2014). Item information is additive and can be combined to yield the test information function (TIF), which is a graphical representation of the combined measurement precision of items included in the model across the latent trait continuum (i.e., Appendix C Figures C2–C3) (Reise et al., 2005; Thomas, 2011). The relative impact of item removal on total precision of measurement along the latent trait continuum can therefore be evaluated with reference to the slope and threshold parameters, as well as by inspection of the ORFs, IIFs, and the TIF (Edelen & Reeve, 2007). In other words, these measures allowed us to identify the items that are most informative for a given latent trait, thus yielding a more refined measure of that trait.

Parametric IRT has a number of assumptions that must be satisfied for correct model estimation. The appropriate dimensionality assumption requires that the correct IRT model be chosen to reflect the number of latent dimensions underlying the pattern of item responses. In this case, we applied a unidimensional IRT model based on the assumption that participants' response patterns across the items could be reasonably explained by variance on a single underlying latent trait continuum by focusing on narrow homogenous constructs at the lowest level of the dimensional hierarchy of PLEs (Clark & Watson, 2019; Kotov et al., 2017; Toland, 2014). The monotonicity assumption for polytomous items was assessed by inspecting the ORFs for the CAPE items and ensuring that the probability of endorsement of each successive response category increased monotonically as a function of increasing severity of theta (Toland, 2014). Item-level performance, along with the functional form and local independence assumptions are evaluated prior to overall model fit in parametric IRT analysis (Essen et al., 2017; Toland, 2014). Fit of items to the 2PL or GR models was assessed with a generalization of the S-χ^2 item-fit statistic (Orlando & Thissen, 2003) at a recommended significance threshold for large samples (p <.01) (Stone & Zhang, 2003; Toland, 2014). Items were evaluated for local dependence (LD) based on standardized LD χ^2 statistics and removed when exceeding the recommended threshold (i.e. >10) (Cai et al., 2011).

Decisions to eliminate or retain items were made in consideration of multiple sources of information at each iteration, including slope and threshold parameter estimates, the ORFs and IIFs for each item and their overlap with other items, as well as local independence and model-data consistency. Items that had low slope parameters and contributed minimal or redundant information relative to other items, in combination with a violation of the functional form assumption (S- χ^2 p <.01) and/or local independence assumption (LD χ^2 statistics > 10), were removed. Assessment of model-level fit was evaluated with the bivariate root mean square error of approximation ($RMSEA_2$; ε_2) as an index of approximate fit (Cai et al., 2011; Maydeu-Olivares, 2015). A 90% confidence interval [90% *CI*] for the $RMSEA_2$ was calculated in *R* (https://www.R-project.org/) using the graphical extension with accuracy in parameter estimation package (https://www.R-project.org/). $RMSEA_2$ values below .05 are considered as evidence for close approximate fit.

Following model estimation, IRT scale score estimates were generated for each participant based on the pattern of responses and the item parameter estimates in the model using Bayesian estimation. Expected a posteriori (EAP) estimates were obtained, which is the mean of the latent trait (θ) posterior distribution given the observed response pattern (Bock & Mislevy, 1982). The EAP estimator provides very accurate estimates of population means given an observed response pattern, with a smaller average error than other estimators (Cai et al., 2011). The marginal reliability of the pattern response scores were used as indicators of the reliability of the estimates.

4.2.4. Neuroimaging acquisition and preprocessing

Participants were scanned at Monash Biomedical Imaging, Melbourne, Australia, on a 3 Tesla Siemens Skyra scanner equipped with a 32-channel head coil. Participants were instructed to lie in the scanner with eyes closed while maintaining wakefulness. Multiband resting-state echo-planar images (EPI; 620 volumes, 754 milliseconds repetition time, 3mm isotropic voxels) and anatomical T1-weighted scans (1mm isotropic voxels) were acquired for each participant. Preprocessing of the EPI images included: 1) basic preprocessing in FSL FEAT which included removal of the first four volumes, rigid-body head motion correction, 3mm spatial smoothing, and high-pass temporal filter (75 seconds cut-off); 2) removal of artifacts using FSL-FIX; 3) spatial normalization to the MNI152 template; and 4) spatial smoothing with a 4mm full-width half-maximum Gaussian kernel. Further details are outlined in our past work (Sabaroedin et al., 2019). Following preprocessing, all of our datasets were subjected to rigorous quality control for motion artifacts, as per past work (Parkes et al., 2018). In-scanner head motion was defined as excessive if either: 1) the mean framewise displacement is greater than 0.11mm, 2) the sum of suprathreshold spike in greater than 20%, or 3) if framewise displacement was greater than 2.5mm. Quality control procedures for this dataset were outlined in our previous work and yield minimal residual motion-related contamination (Sabaroedin et al., 2019).

4.2.5. Dynamic causal modelling

Regions of interest (ROIs) selection and time-series extraction. Eight ROIs spanning the dorsal and ventral FST circuits, and the midbrain, were selected using stereotactic coordinates of past findings or

of peak signals identified using functional connectivity. We used the same approach as in our recent study of clinical patients (Sabaroedin et al., 2020). The midbrain was included in the model as dopamine is a key modulator of FST circuits (Haber et al., 2000). Further details are outlined in Appendix C. MNI coordinates and voxel sizes of the ROIs are displayed in Table 4.1. Our model consisted of dorsal caudate (DC), nucleus accumbens (NAcc), DLPFC, VMPFC, thalamus, anterior hippocampus, amygdala, VTA/SN (i.e., midbrain). The dorsal and ventral striatum corresponded to the DC and the NAcc, respectively. Cortical ROIs were defined with a radius of 6mm and a 3.5mm radius was used for all subcortical ROIs, contained to the left hemisphere based on past work suggesting clinical effects in left-lateralized circuits (Dandash, et al., 2014; Fornito et al., 2013) The first eigenvariate of each region's time-series was extracted for DCM analysis. We specified a parent model that included all plausible biological connections including self (or recurrent) activity within each region, yielding 47 connections (Figure 4.1).

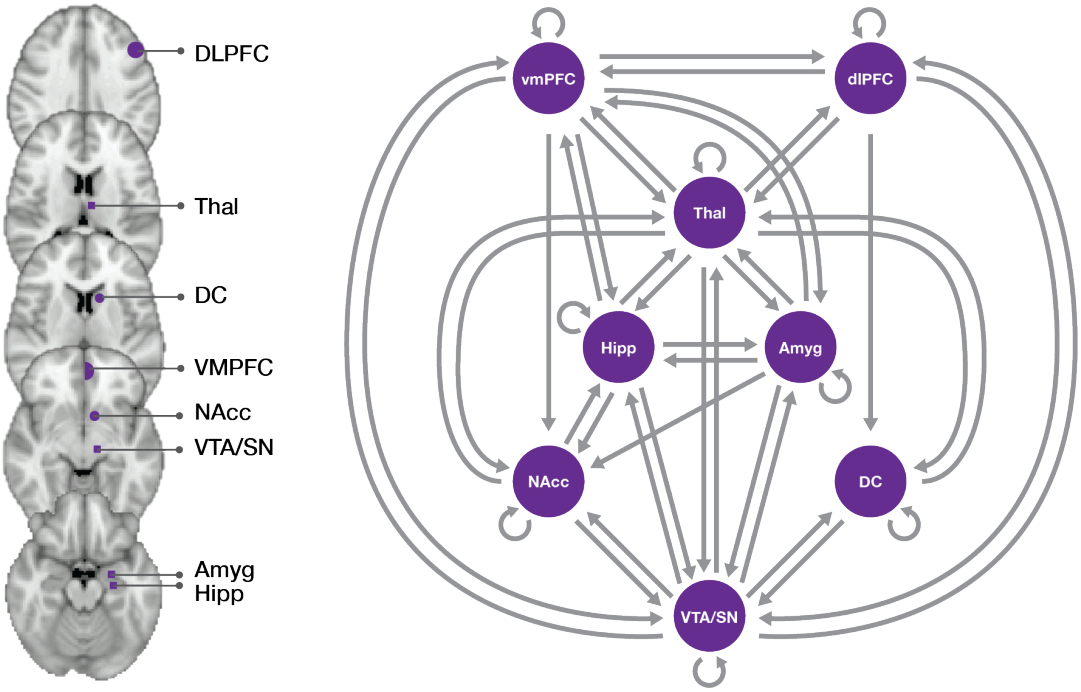

Figure 4.1. Parent model space of fronto-striato-thalamic systems encompassing dorsal and ventral circuits. Anatomical locations of regions of interest are shown on axial slices on the left. Model space on the right show modelled biological plausible connections, including the self-connections for each region, indicated by circular arrows.

Table 4.1. MNI Coordinates and Total Number of Voxels of DCM ROIs

Region	MNI coordinates	Voxels
Dorsal caudate (DC)	-13, 15, 9	22
Nucleus accumbens (NAcc)	-9, 9, -8	20
DLPFC	-45, 23, 37	136
VMPFC	-2, 50, -8	76
Thalamus (Thal)	-6, -12, 14	22
Amygdala (Amyg)	-24, -6, -18	27
Anterior hippocampus (Hipp)	-26, -16, -18	27
VTA/SN	-12, -20, -10	27

Model estimation. Effective connectivity was modelled in the spectral domain by fitting a complex cross spectral density using a parametrized power-law model of endogenous fluctuations, as implemented in SPM12 (DCM 12; r7487) (Friston et al., 2014; Razi et al., 2015) Details are provided

in Appendix C. Briefly, subject-specific first-level analyses were used to estimate causal (directed) influences between regions as defined in the model space (in Hz), and the (inhibitory) self-connectivity within each region. Self-connections were log-transformed to ensure prior negativity (i.e., inhibitory) constraints on self-connections. First-level inversion revealed that our model explained more than 75% variance in all participants. Subject-specific connectivity parameters were then passed to a group-level multivariate Bayesian general linear model (GLM) (i.e., parametric empirical Bayes) to estimate the designed effects and additive random effects of between-subject variability (Zeidman et al., 2019). IRT scale score estimates of positive PLE dimensions were entered into the group-level GLM as covariates. IRT scale score estimates with zero-inflated non-normal distributions (i.e., hallucinations and body image aberration) were binarized, with 0 indicating the absence of PLE, and 1 for the presence of PLEs (see Figures 4.3 and C4 in Appendix C for distributions of scores). Age and sex were used as nuisance covariates. A separate (Bayesian) GLM analysis was performed to assess associations with negative PLEs. A typical effect size for effective connectivity between regions is 0.1 Hz (Razi et al., 2015). It is important to note that this group-level analysis is based on fitting a (multivariate) Bayesian GLM which means that all model parameters are fitted at once, precluding the need for correction for multiple corrections. We report only effects with a posterior probability (Pp) threshold above 0.95, indicating strong evidence.

4.3. Results

4.3.1. Participants

Please refer to Table 4.2 for descriptive statistics of PLE questionnaires for our full sample and neuroimaging subsample. The number of participants with missing data in the items used to estimate IRT models are presented in Appendix C Table C1.

Table 4.2. Descriptive Statistics of Subscales in the Full and Neuroimaging Samples

	Full sample				Neuroimaging sample			
Subscales	**Min**	**Max**	**Mean (SD)**	**Median**	**Min**	**Max**	**Mean (SD**	**Median**
CAPE								
1. Positive	20	52	25.87 (4.68)	25	20	52	25.70 (4.70)	25
2. Negative	14	44	23.74 (5.65)	23	14	44	23.96 (5.82)	23
3. Depressive	8	27	13.90 (3.013)	13	8	27	13.83 (2.96)	13
WSS								
4. Magical Ideation	0	26	6.13 (4.74)	5	0	26	6.09 (4.59)	5
5. Phys Anhedonia	0	42	11.48 (6.98)	10	0	42	11.83 (7.20)	11
6. Perc Aberration	0	32	5.22 (5.27)	4	0	26	5.08 (5.10)	4
7. Soc Anhedonia	0	35	9.42 (6.42)	8	.0	35	9.64 (6.79)	8
sO-LIFE								
8. Unusual Experiences	0	12	2.85 (2.63)	2	0	12	2.88 (2.64)	2
9. Cog Disorganisation	0	11	4.74 (2.90)	5	0	11	4.68 (2.93)	5
10. Introvertive Anhedonia	0	10	1.62 (1.74)	1	0	9	1.69 (1.81)	1
11. Impulsive Nonconform	0	10	3.30 (2.07)	3	0	10	3.18 (2.11)	3
12. PDI	0	17	5.40 (3.50)	5	0	16	5.31 (3.44)	5

4.3.2. Item response theory

The model fit results of the IRT analyses are summarized in Appendix C Table C2 and the item parameter estimates are provided in Appendix C Tables C3–C11. In summary, all nine models provided a good fit to the data with respect to the $RMSEA_2$ and 90% *CI* (Maydeu-Olivares, 2015; Maydeu-Olivares & Joe, 2014). All the items retained for the nine phenotypic dimensions exhibited a good fit to the 2PL or GR models (i.e., $S\text{-}\chi^2$ p >.01), as well as local independence (LD χ^2 <10.0). The results also showed that the items retained had generally high slope parameters, providing reliable measurement of latent trait continua for each of the nine phenotypes. However, the threshold parameters revealed that most of the items provided maximum measurement precision at the upper end of the continuum, between the mean and three standard deviations above the mean, indicated by θ on the x-axis on the TIF graphs. Figures C2–C3 in Appendix C show that the information functions were peaked

towards the high end of the distribution for six of the nine phenotypes, meaning that the IRT scores for these phenotypes provided good precision in distinguishing high from low latent traits. IRT scores with lower measurement precision included cognitive disorganisation, avolition, and alogia (the latter which had low measurement precision across the latent trait continuum).

The histograms of the IRT scale score estimates revealed zero inflation for hallucinations, cognitive disorganisation, body image aberration, blunted affect, and alogia. In other words, a large proportion of the sample did not endorse an experience for these dimensions. There was also an indication of minor positive skew for the delusions, anhedonia, and asociality IRT scale score estimates. Distributions of IRT scores in the full sample are illustrated in Figure 4.2. Marginal reliability estimates for the scale scores we generally acceptable to good (r_{xx} = .74 - .84), except for hallucinations (r_{xx} = .50) and alogia (r_{xx} = .46).

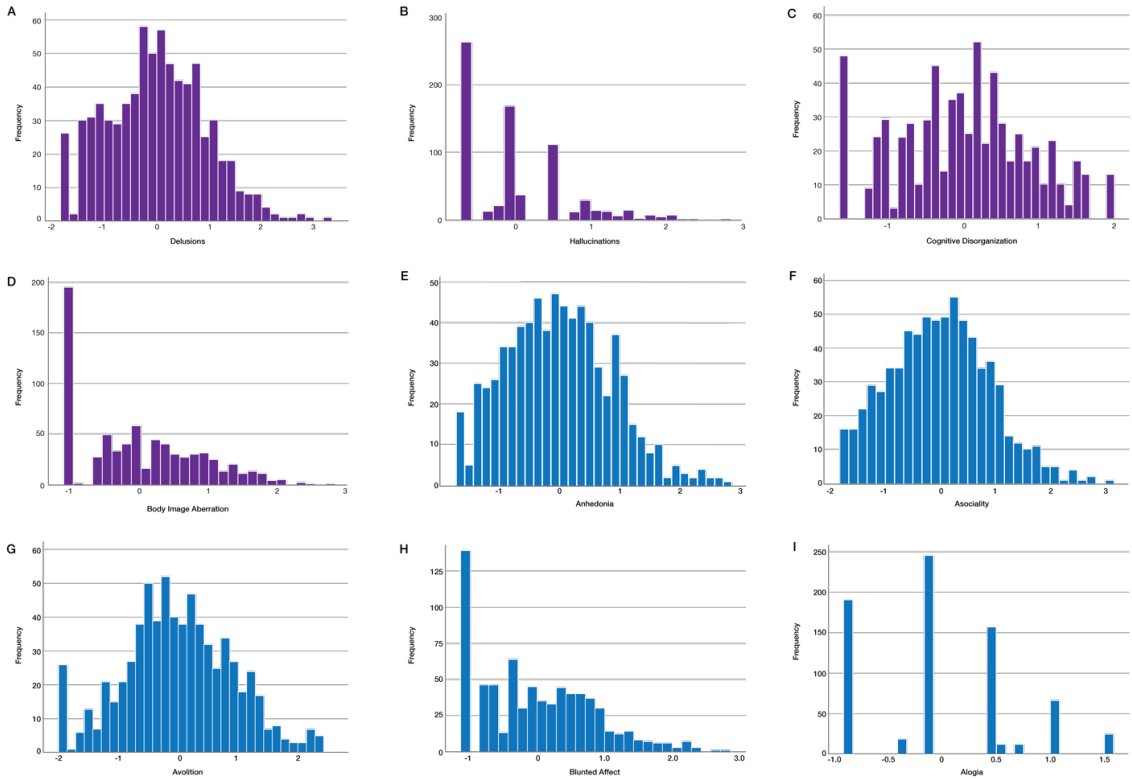

Figure 4.2. Histograms of item response theory scale scores estimates for positive and negative PLE dimensions in the large sample with questionnaire scores. Positive PLEs are portrayed in purple histograms, depicted in panels (A) delusions, (B) hallucinations, (C) cognitive disorganisation, and (D) body image aberration. All positive PLE histograms except for cognitive disorganisation comprises the full 726 participants. Cognitive disorganisation comprises 675 participants due to missing data. Negative PLEs are illustrated in blue histograms, depicted in panels (E) anhedonia, (F) asociality, (G) avolition,

(H) blunted affect, and (I) alogia**.** Due to missing data, avolition comprise 693 participants; asociality, blunted affect, and alogia consists of 724 participants. Anhedonia comprises the full 726 participants.

Figure 4.3 plots the IRT scale score estimates for all dimensions, as a function of participants' corresponding raw scores on the subscales. These scatterplots display the magnitude and variability in latent traits introduced by IRT scale scores compared to raw scores, thus providing richer information on the underlying dimension of these latent traits (Edwards, 2009). Correlation coefficients of IRT scores in our full sample are presented in Table 4.3, with most dimensions showing weak to moderate correlations with each other. Distributions of IRT scores in our imaging sample are presented in Appendix C Figure C4.

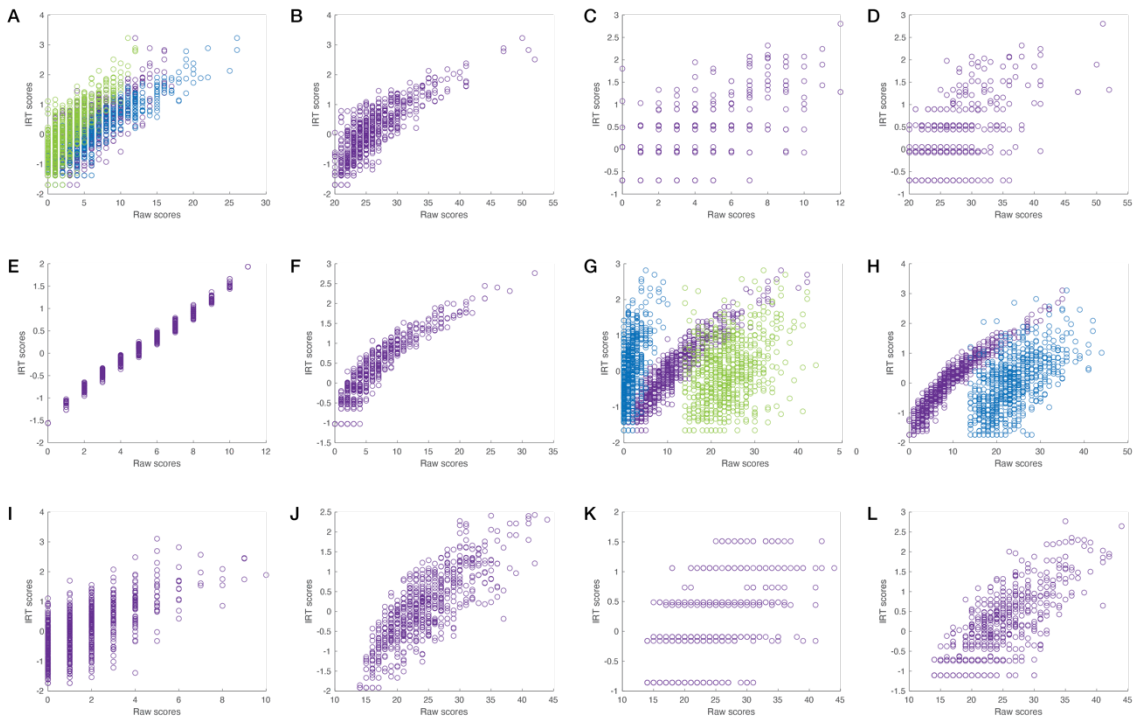

Figure 4.3. Scatterplots of IRT scores as a function of raw scores on corresponding subscales. Panels A–F depict IRT scores from the positive dimension: A) IRT scores for delusions as a function of raw scores from PDI-21 (purple), WSS Magical Ideation (blue), sO-LIFE Unusual Experiences (green); B) IRT scores for delusions as a function of raw scores from CAPE Positive subscale; C) IRT scores for hallucinations as a function of raw scores from sO-LIFE Unusual Experiences; D) IRT scores for hallucinations as a function of raw scores from CAPE Positive subscale; E) IRT scores for cognitive disorganisation as a function of raw scores from sO-LIFE Cognitive Disorganisation subscale; F) IRT scores for body image aberration as a function of raw scores from WSS Perceptual Aberration subscale. Panels G–L depict IRT scores from the negative dimension: G) IRT scores for anhedonia as a function of raw scores from WSS Physical Anhedonia (purple), sO-LIFE Introvertive Anhedonia (blue), and CAPE Negative (green); H) IRT scores for asociality as a function of raw scores

from WSS Social Anhedonia (purple) and CAPE Negative (blue) subscales; I) IRT scores for asociality as a function of raw scores from sO-LIFE Introvertive Anhedonia; J–L) IRT scores for avolition, alogia, and blunted effect, respectively, as a function of raw scores from CAPE Negative subscale.

Table 4.3. Correlation Coefficients (Spearman's Rho) of IRT Scores for All Participants with Complete Questionnaire Data (n = 675)

PLE dimension	1	2	3	4	5	6	7	8	9
1 Delusions	–								
2 Hallucinations	0.56**	–							
3 Cog dis	0.39**	0.28**	–						
4 Body image ab	0.62**	0.49**	0.37**	–					
5 Anhedonia	-0.05	0.02	0.16**	0.02	–				
6 Asociality	0.26**	0.16**	0.38**	0.31**	0.41**	–			
7 Avolition	0.38**	0.27**	0.64**	0.37**	0.15**	0.37**	–		
8 Blunted affect	0.33**	0.21**	0.28**	0.35**	0.26**	0.52**	0.43**	–	
9 Alogia	0.11*	0.07	0.31**	0.19**	0.23**	0.50**	0.29**	0.39**	–

* $p < 0.05$

** $p < 0.001$

4.3.3. Effective connectivity associations with positive PLEs

Delusional ideation. Subclinical delusions were associated with connections across the dorsal and ventral FST circuits (Fig 4.4A, Table 4.4). In the ventral circuit, higher levels of delusional ideation were associated with weaker bottom-up influence of the NAcc on thalamus, of amygdala on VMPFC, and of hippocampus on amygdala, as well as stronger influence of amygdala on hippocampus. In the dorsal circuit, delusional ideation was associated with stronger self-inhibition of the DLPFC and weaker influence of DC on midbrain.

Hallucinations. The presence of subclinical hallucination-like experiences was associated with inter-regional influences primarily located in the ventral FST circuit (Fig 4.4B, Table 4.4). More specifically,

hallucination severity was associated with stronger top-down influence of thalamus on NAcc and of hippocampus on VTA/SN, stronger bottom-up influence of amygdala on VMPFC, and weaker bottom-up influence of VTA/SN on NAcc.

Cognitive disorganisation. This dimension was associated with both the ventral and dorsal FST circuits (Fig 4.4C, Table 4.4). Specifically, more severe cognitive disorganisation was associated with weaker bottom-up influence of NAcc on hippocampus, and stronger influence of hippocampus on NAcc, of hippocampus on amygdala, and of DC on thalamus.

Body image aberration. The presence of body image aberration was associated with stronger top-down influence of both NAcc and DC on VTA/SN, and bottom-up influence of NAcc on thalamus (Fig 4.4D, Table 4.4).

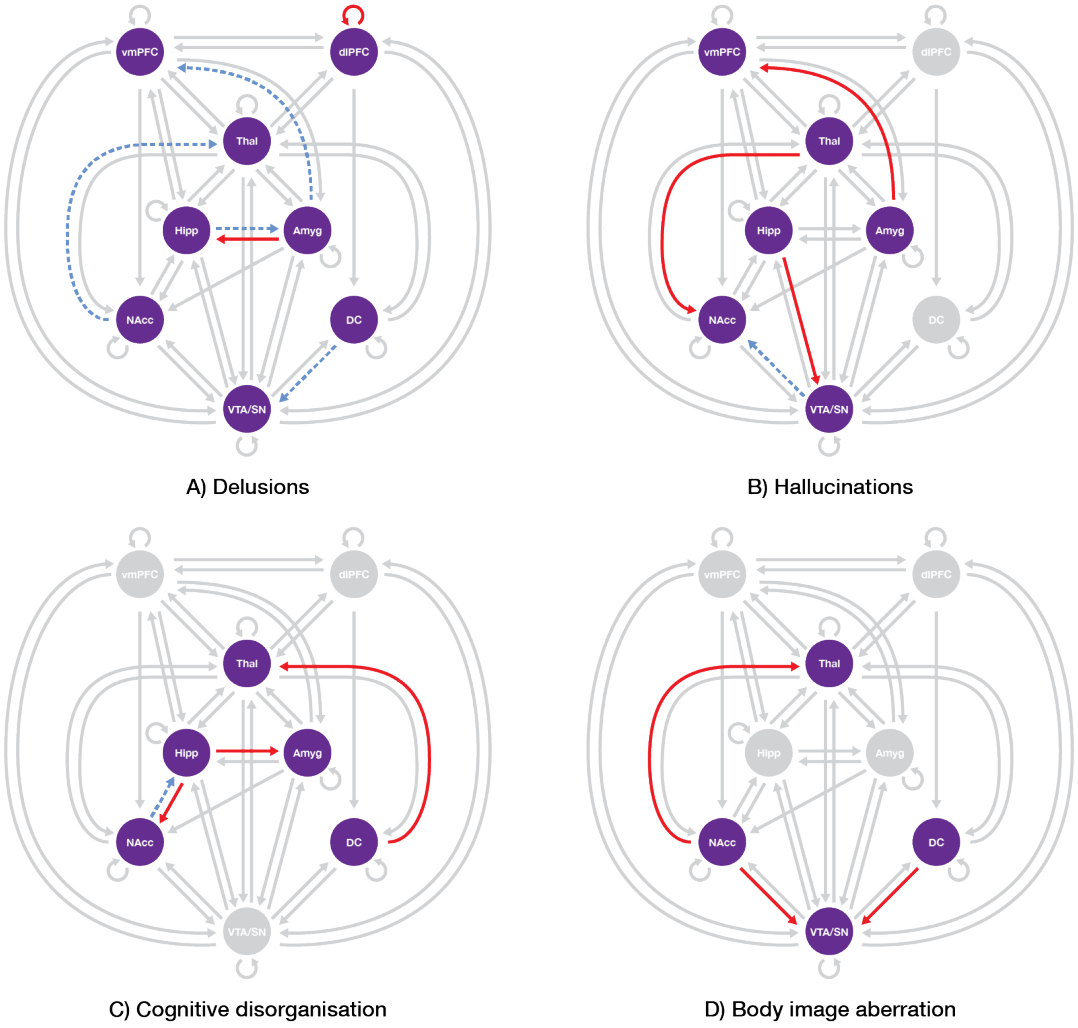

Figure 4.4. Associations between dimensions of positive PLEs and effective connectivity of FST circuits. Associations with delusions, hallucinations, cognitive disorganisation, and body image aberration are depicted in panels A, B, C, and D, respectively. Solid red arrows indicate connections that are positively associated with PLEs. Dashed blue arrows indicate connections that are negatively associated with PLEs. For self-connection, solid red arrow signifies increased self-inhibition associated with PLEs. Only connections with threshold of Pp > 0.95 are shown.

Table 4.4. Summary of Connections Associated with Positive PLEs

Connection	Positive (+) or negative (-) association	Effect size (Hz)*	90% Posterior Credible Interval (lower bound, upper bound)
Delusions			
DLPFC → DLPFC	+	*0.06*	*0.02, 0.11*
Amyg → VMPFC	-	0.06	-0,10, -.0.02
Amyg → Hipp	+	0.05	0.01, 0.09
Hipp → Amyg	-	0.08	-0.12, -0.03
DC → VTA/SN	-	0.06	-0.10, -0.02
NAcc → Thal	-	0.06	-0.10, -0.01
Hallucinations			
Amyg → VMPFC	+	0.07	0.03, 0.11
Thal → NAcc	+	0.06	0.02, 0.10
Hipp → VTA/SN	+	0.05	0.01, 0.09
Midbrain → NAcc	-	0.05	-0.09, -0.01
Cognitive disorganisation			
Hipp → Amyg	+	0.07	0.03, 0.11
Hipp → NAcc	+	0.05	0.01, 0.09
DC → Thal	+	0.04	0.00, 0.09
NAcc → Hipp	-	0.06	-0.10, -0.02
Body image aberration			
DC → VTA/SN	+	0.08	0.04, 0.12
NAcc → Thal	+	0.07	0.03, 0.12
NAcc → VTA/SN	+	0.06	0.02, 0.10

All connections have the posterior probability (free energy) value of 1.00.

* Connections between regions are in units of Hz. Self-connections are italicized, and values are in negative log-scale parameters to ensure that they are always negative, or inhibitory. A positive value for self-connection denotes increased inhibition, a negative value signifies reduced inhibition. A typical effect size for connectivity parameters is 0.1 Hz.

4.3.4. Effective connectivity associations with negative PLEs

Associations with negative PLEs are presented in Figure 4.5 and Table 4.5. All associations were restricted to subcortical regions within the ventral circuit. Greater anhedonia was associated with weaker influence of VTA/SN on hippocampus, and stronger influence of hippocampus on NAcc. Greater asociality was associated with stronger influence of amygdala on NAcc and weaker NAcc self-inhibition. More severe avolition was associated with stronger influence of NAcc on thalamus and of

hippocampus on amygdala. The presence of alogia was associated with weaker hippocampal self-inhibition, and top-down influence of NAcc on VTA/SN. We did not find any association between blunted affect and FST connectivity. The NAcc was commonly implicated across all other negative PLE dimensions.

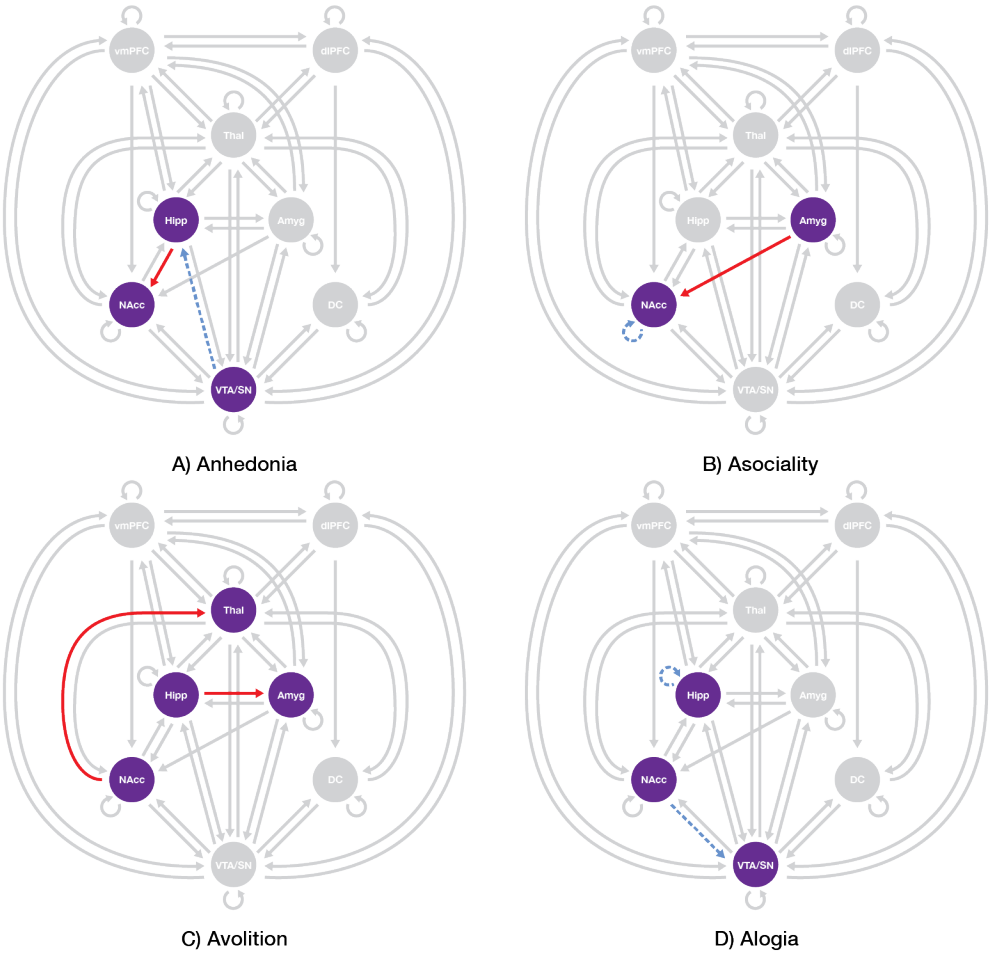

Figure 4.5. Associations between dimensions of negative PLEs and effective connectivity of FST circuits. Panels A–D depict associations with anhedonia, asociality, avolition, and alogia, respectively. Solid red arrows illustrate connections that are positively associated with PLEs. Dashed blue arrows indicate connections that are negatively associated with PLEs. For self-connections, dashed blue arrows mark reduced self-inhibition associated with negative-like experiences. Only connections that pass the prior probability threshold of 0.95 are shown.

Table 4.5. Summary of Connections Associated with Negative PLEs

Connection	Positive (+) or negative (-) association	Effect size (Hz)*	90% Posterior Credible Interval (lower bound, upper bound)
Anhedonia			
Hipp → NAcc	+	0.06	0.02, 0.10
VTA/SN → Hipp	-	0.05	-0.09, -0.01
Asociality			
Amyg → NAcc	+	0.06	0.02, 0.10
NAcc → NAcc	-	*0.05*	*-0.09, -0.01*
Avolition			
Hipp → Amyg	+	0.05	0.01, 0.09
NAcc → Thal	+	0.05	0.01, 0.10
Alogia			
Hipp → Hipp	-	*0.05*	*-0.09, -0.01*
NAcc → VTA/SN	-	0.07	-0.11, -0.04

All connections have the posterior probability (free energy) value of 1.00. Connections between regions are in units of Hz.

* Connections between regions are in units of Hz. Self-connections are italicized, and values are in negative log-scale parameters to ensure that they are always negative, or inhibitory. A positive value for self-connection denotes increased inhibition, a negative value signifies reduced inhibition. A typical effect size for connectivity parameters is 0.1 Hz.

4.4. Discussion

Variations in FST circuit function track symptom expressions across the psychosis spectrum (Anticevic, 2017; Dandash et al., 2014; Fornito et al., 2013; Pani et al., 2020; Sabaroedin et al., 2019), yet there have been some inconsistencies regarding PLEs correlations with dorsal and ventral FST connectivity. Here, we used an extensive battery of PLE measures and IRT to derive high-precision estimates of PLE dimensions. Spectral DCM evaluated differential associations of PLE dimensions with bottom-up and top-down connectivity in FST circuitry. All dimensions of positive PLEs implicated the striatothalamic pathways and, apart from hallucinations, were associated with effective connectivity distributed across the dorsal and ventral systems. Subthreshold delusions, cognitive disorganisation, and body image aberration were associated with bottom-up influence of the striatum on thalamus. Subthreshold hallucinations were associated with top-down influence of the thalamus on striatum. Distinct dimensions of negative PLEs were associated with effective connectivity that was restricted to the ventral FST circuit, with all but blunted affect being associated with NAcc function.

4.4.1. FST effective connectivity and positive PLEs

All dimensions of positive PLEs were associated with the effective connectivity of striatothalamic pathways. Delusions, cognitive disorganisation, and body image aberration were associated with bottom-up influence of the striatum on the thalamus, suggesting a contribution of information-filtering processes mediated by the striatum (Carlsson et al., 1999). Ventral striatal activity is thought to represent information updating (Nour et al., 2018; O'Doherty et al., 2004), and healthy individuals with higher delusional ideation have demonstrated reduced striatal signal during the presentation of salient stimuli (Corlett & Fletcher, 2012), suggesting that subthreshold delusional ideation is linked to a disruption of normative belief updating processes. Consistent with this idea, the influence of the NAcc on thalamus was associated with subthreshold delusions and body image aberration.

The dorsal striatum was implicated in cognitive disorganisation, with increased severity positively associated with influence of the DC on the thalamus, suggesting disruptions in sensory gating of the associative circuit (Carlsson et al., 1999). Hallucinations were the only positive PLE dimension positively associated with a top-down influence of the thalamus on NAcc, which may signify the relay of information from unmodelled sensorimotor FST circuits (Haber & McFarland, 2001). This is broadly consistent with previous work that has linked hallucinatory experiences with strong top-down prior beliefs modulating sensory states (Cassidy et al., 2018; Powers et al., 2017).

Positive PLEs have also been associated with aberrant dopamine signalling, especially in regions within the ventral FST circuit (Grant et al., 2013; Soliman et al., 2011). Accordingly, all dimensions of positive PLEs were associated with NAcc connectivity. This result aligns with the salience misattribution hypothesis (Kapur, 2003), in that it implies a link between PLE severity and dopaminergic signalling within FST circuitry. Under this hypothesis, hallucinations and delusions are thought to result from excessive striatal dopamine, which is thought to disrupt the encoding of uncertainty and matches between prior beliefs and incoming sensory information (Cassidy et al., 2018; Corlett et al., 2010; Kapur, 2003). In our analysis, only the hallucinations dimension was associated with bottom-up influence of the midbrain on NAcc. Hallucinations were also associated with stronger top-down influence of hippocampus on midbrain, whereas delusions and body image aberration were

associated with top-down influence of the striatum on the midbrain. Together, these results suggest that subcortical control over midbrain signalling may play a role in the expression of PLEs. Accordingly, D2 receptor dysfunction has been linked with body image aberration (Vulink et al., 2016) and increased dopamine release in the striatum and thalamus has been linked to disorganisation-related PLEs (Woodward et al., 2011). Consistent with this latter finding, we also found that body image aberration and cognitive disorganisation were associated with increased striatal influence on thalamus.

Effective connectivity of the hippocampus and amygdala were also associated with positive PLEs. Delusional ideation and hallucinations implicated bottom-up influence of the amygdala on VMPFC. Delusional ideation was additionally associated with reciprocal influences between the amygdala and the hippocampus. The involvement of the amygdala, especially with the concomitant influence of regions such as the hippocampus, VMPFC, and DLPFC, may reflect aberrant emotional processing associated with subthreshold paranoia (Corlett et al., 2010; Laviolette & Grace, 2006), which was measured in a large number of items in our PLE questionnaires. The hippocampus increases dopamine signalling in the context of novel stimuli (Kafkas & Montaldi, 2015; Lodge & Grace, 2006), and increased influence of the hippocampus on the midbrain associated with subthreshold hallucinations suggests that the hippocampal signalling may play a central role in this PLE dimension. The influence of hippocampus on amygdala and NAcc was also a prominent feature of cognitive disorganisation, which is compatible with models of cognitive disorganisation that have established a link between dysregulation of the hippocampus and disrupted cognitive processes (Olypher et al., 2006; Phillips & Silverstein, 2003).

4.4.2. FST effective connectivity and negative PLEs

Negative symptoms are challenging to define and studies identifying the neurobiological processes associated with this symptom domain have reported mixed results (Galderisi et al., 2015). Similarly, studies investigating associations between FST functional connectivity and subthreshold negative symptoms, quantified by aggregate scores of specific PLE dimensions, have also reported inconsistent findings (Pani et al., 2020; Sabaroedin et al., 2019, 2020).

Our fine-grained estimation of distinct PLE dimensions found that anhedonia, asociality, avolition, and alogia, were exclusively associated with ventral circuit effective connectivity, with the NAcc implicated as a central nexus across all domains. Negative symptoms have been linked with increased stress-induced dopamine release in the NAcc and reduced activity of this region in clinical groups, thus suggesting that the ventral circuit function is critically related to the pathophysiology of negative symptoms (Juckel et al., 2006; Soliman et al., 2008). Consistent with clinical findings, healthy individuals with greater physical anhedonia were found to exhibit increased striatal activity in response to stress (Soliman et al., 2011) and reduced ventral striatal activation in response to salient stimuli (Yan et al., 2016). Healthy individuals with social anhedonia have also demonstrated increased functional connectivity between the ventral striatum and PFC (Wang et al., 2016). Here, only avolition was associated with bottom-up FST connectivity—namely from the NAcc to the thalamus—which may reflect alterations in reward processing or habit formation (Haber, 2003).

Hippocampal effective connectivity was also associated with all negative PLE dimensions, except for asociality and blunted affect. This structure has mostly been associated with cognitive disorganisation and psychosis onset, with persistent negative symptoms in schizophrenia patients linked with reduced hippocampal grey matter volume (Lodge & Grace, 2006; Makowski et al., 2017; Olypher et al., 2006). The association between hippocampal connectivity and subthreshold negative symptoms has not been widely studied, although recently, reduced hippocampal subfield volume was reported in healthy youths with negative PLEs (Sahakyan et al., 2020), and reduced functional connectivity of the hippocampus and other subcortical structures were found in healthy people with more severe negative PLEs (Kozhuharova et al., 2020). Stress has a deleterious effect on the hippocampus, impairing cognition and memory performance (Kim & Yoon, 1998). Accordingly, healthy individuals showing both negative PLEs and cognitive disorganisation were found to be more reactive to stress (Grant & Hennig, 2020). The association between hippocampal connectivity and negative PLEs that we identify thus underscores a need to better understand the role of stress in influencing the long-term social and occupational outcomes that are tied to this symptom domain (Kwapil et al., 2013).

4.4.3. Limitations and future directions

Our strict recruitment criteria may have excluded individuals from the higher end of the PLE spectrum, which may reflect our modest effect sizes. However, our sample size is relatively large for the field, our data had high temporal resolution and were subjected to strict quality control, with the fitted DCMs explaining >75% of signal, suggesting that our findings are robust.

Work in subclinical cohorts has found effects in the right hemisphere (Corlett et al., 2006; Wang et al., 2018), which has been linked to the mechanistic processes of delusions (Gurin & Blum, 2017). As we were interested in the subclinical–clinical continuum, we modelled the left hemisphere given past evidence of more robust clinical findings in this hemisphere (Dandash, et al., 2014; Fornito et al., 2013). Regions such as orbitofrontal and anterior cingulate cortices, visual, and sensorimotor regions have been identified to contribute to distinct aspects of positive symptoms, and by extension, PLEs (Feinberg & Guazzelli, 1999; Fornito, Yung, et al., 2008; S. A. Grace et al., 2017; Miall & Wolpert., 1996). Recent developments in DCM allowing efficient model estimation for whole-brain networks (Frässle et al., 2017) may be used to extend this work to include all relevant regions and provide a more comprehensive understanding of the neural correlates of PLEs.

The combination of IRT with structural equation modelling could be used to uncover FST associations with higher order latent variables of PLEs. This approach was not explored here as our aim was to obtain dimensions of PLEs at the highest resolution.

4.4.4. Conclusions

We obtained high-precision estimates of discrete PLE dimensions, yielding nine distinct domains. Using spectral DCM, our models revealed that all positive PLE dimensions are associated with striatothalamic connections and, excluding hallucinations, are associated with effective connectivity distributed across the dorsal and ventral systems. These results suggest that the striatal filtering of information flow through FST circuits plays an important role in positive PLE expressions. Negative PLEs were associated with the ventral FST circuit, particularly connectivity of the NAcc and hippocampus, suggesting a close link between subthreshold negative symptoms and limbic system function.

Chapter 5

General Discussion and Concluding Remarks

———

5.1. General discussion

The overarching aim of this thesis was to systematically investigate the connectivity of fronto-striato-thalamic (FST) circuits across the psychosis continuum. Chapter 2 built on a series of studies in at-risk mental state (ARMS) individuals, first-episode psychosis (FEP) patients, and their first-degree relatives by examining whether FST functional connectivity correlates with psychosis-like experiences (PLEs) in a non-clinical sample. Supporting a neurobiological spectrum of function across the psychosis continuum, lower functional connectivity of the dorsal circuit was associated with more severe positive PLEs, as had been shown in clinical cohorts (Dandash et al., 2018; Dandash et al., 2014; Fornito et al., 2013). Chapter 3 aimed to overcome the limitations of functional connectivity analyses by using spectral dynamic causal modelling (DCM) to develop a model of FST effective connectivity across the psychosis continuum. FEP was associated with dysconnectivity of subcortical areas and prominent bottom-up influence of the midbrain, consistent with a major role for dopamine dysregulation in psychosis onset (Kapur, 2003; Maia & Frank, 2017). Psychotic symptoms in established schizophrenia patients were associated with more pervasive dysconnectivity of FST circuits that included cortical areas. Investigation of a non-clinical sample with [^{18}F]DOPA using positron emission tomography (PET) revealed that midbrain and thalamic connectivity were associated with dopamine synthesis capacity in the dorsal and ventral striatum. Having developed a model of FST effective connectivity, Chapter 4 revisited associations with PLEs by developing a high-resolution characterization of nine dimensions of PLEs, as derived through item response theory (IRT), to examine the specificity of associations between distinct aspects of PLEs and FST effective connectivity. While there was some

degree of specificity in the associations observed across dimensions, connectivity between the striatum and thalamus was consistently implicated in positive PLEs, suggesting that striatothalamic filtering (Carlsson et al., 1999) may be a core feature of subclinical psychotic symptoms. Across all cohorts along the psychosis continuum, negative symptomatology was associated with distinct sets of FST connections compared to positive symptoms and particularly involved limbic structures. The following sections outline some implications of the major findings, followed by limitations of this work and potential future directions.

5.1.1. FST effective connectivity and dopaminergic function in psychosis

The effective connectivity analysis revealed that, compared to controls, antipsychotic-naïve FEP patients demonstrated inter-regional causal influences that were limited to subcortical regions in the ventral circuit, including disinhibition of the midbrain. Disrupted bottom-up influence of the midbrain became more apparent in FEP patients with schizophrenia, who showed a more excitatory influence of the midbrain on nucleus accumbens. Associations with positive symptoms in FEP also featured bottom-up influences from the midbrain, with the midbrain's influence on the nucleus accumbens consistently demonstrated in both the entire FEP group and the schizophrenia subgroup. These findings are consistent with the dopamine hypothesis of psychosis, which proposes that the onset of psychosis can be attributed to hyperactivity of dopaminergic signalling (Kapur, 2003). The findings point to a primary disruption arising from aberrant midbrain signalling, potentially reflecting dopamine dysregulation in the early stage of illness.

The PET findings in healthy individuals in Chapter 3 indicated that dopamine synthesis in the ventral striatum is associated with the influence of the midbrain on the dorsal striatum. This is consistent with animal models, in which dopamine pathways from the midbrain influence the striatum in an ascending manner, with the nucleus accumbens sending the largest projection to the midbrain and the dorsolateral striatum receiving the most expansive dopaminergic projections (Haber et al., 2000). Rodent models have also demonstrated that increased dopaminergic activity in the midbrain influences dopamine projections to both the ventral and associative divisions of the striatum (Lodge & Grace, 2012). In line with this work, the findings of Chapter 3 indicated that the concomitant influence of the

nucleus accumbens on the midbrain, and the midbrain on the dorsal caudate, was associated with positive symptoms in FEP patients. In the subset of FEP patients with schizophrenia, the bottom-up influence of the dorsal caudate (DC) on thalamus was also implicated. This involvement of the dorsal striatum is coherent with various reports of elevated dopamine synthesis in the associative striatum of prodromal patients, with the elevations being more pronounced in those who converted to psychosis (Egerton et al., 2013; Howes et al., 2011; Howes et al., 2009; Mizrahi et al., 2014). Together with the PET results, the findings of this thesis indicate that positive symptom severity in the early stage of psychosis may reflect a pathology of the ventral striatum that influences the dorsal caudate through nigrostriatal pathways.

It is worth noting that the FST effective connectivity analysis in FEP demonstrated a negative association between positive symptoms and the midbrain's influence on the dorsal caudate. This result does not necessarily suggest that reduced dopaminergic transmission is associated with higher positive symptoms, which would counter current knowledge of the link between excessive dopamine activity and positive symptoms (Cassidy et al., 2018; Corlett et al., 2010). More specifically, the molecular basis of increased or decreased effective connectivity remains unclear. Dopamine in the striatum interacts with D1 or D2 receptors and, depending on the context, can activate either the direct excitatory or the indirect inhibitory striatal pathway (Gerfen & Surmeier, 2011). Stimulation of D1 receptors increases their excitability and promotes glutamatergic long-term potentiation, whereas stimulation of D2 receptors decreases their excitability and depresses excitatory neurons in the striatum (Gerfen & Surmeier, 2011). Accordingly, stimulation of direct or indirect pathways in rodents yields distinct blood-oxygen-level-dependent (BOLD) responses in the caudate and putamen, with greater fluctuations observed during D2 stimulation (Bernal-Casas et al., 2017). Thus, a negative association between symptom severity and midbrain–DC effective connectivity may reflect abnormally high levels of dopamine release causing an inhibitory effect in the striatum. Additionally, the observed negative association between positive symptoms and the DC's influence on thalamus in FEP-schizophrenia may indicate excessive signalling along the indirect striatothalamic pathway, which is thought to stem from overactive dopamine transmission in the dorsal striatum (Carlsson et al., 1999).

5.1.2. Evidence for a neurobiological continuum across a broad spectrum of symptom severity

The functional connectivity analysis of FST circuits and general PLE dimensions presented in Chapter 2 established initial evidence for a neurobiological continuum of psychosis focused on dorsal FST function, which extends to the general community. In Chapter 3, a general dimension of positive PLEs, measured using the CAPE positive subscale (Stefanis et al., 2002), was associated with inter-regional influences that were distributed across the dorsal and ventral FST circuits. The involvement of both circuits is consistent with emotional and cognitive contributions to PLEs (Debbané et al., 2009; Kerns, 2006). Notably, more severe positive PLEs were associated with greater top-down influence of DLPFC on midbrain, and bottom-up influence of the midbrain on nucleus accumbens, and of nucleus accumbens on thalamus. This finding suggests that positive PLEs are linked to a cascade of directed influences within FST circuitry, beginning with prefrontal regulation over midbrain function, and then influencing midbrain to thalamus via the striatum. Amygdala connectivity and dorsal caudate inhibition also played a role. These findings align with models positing that psychosis arises from disrupted cortical regulation of midbrain dopaminergic signalling (Weinberger, 1987) and highlights the utility of models of effective connectivity. However, if PLEs are to be considered a marker of latent vulnerability to clinical illness, this prominent role for top-down cortical regulation must be reconciled with the relative lack of cortical dysfunction identified in FEP patients.

Chapter 4 provided a more detailed consideration of the association between FST effective connectivity and distinct dimensions of PLEs, rather than focusing solely on aggregated summary scores. This analysis revealed a prominent role for bottom-up influences of the striatum on thalamus, specifically with dimensions pertaining to delusional ideation and cognitive disorganisation. Delusional ideation, including body image aberration, was associated with nucleus accumbens connectivity, which plays a role in information updating (Nour et al., 2018; O'Doherty et al., 2004), whereas cognitive disorganisation implicated the dorsal caudate, which subserves cognitive functions (Haber, 2003). Only subclinical hallucinations were associated with effective connectivity constrained to the ventral FST circuit, and featured top-down influence of the thalamus on nucleus accumbens. One major difference between the results in Chapters 3 and 4 is that the analysis of CAPE positive scores in Chapter 3 revealed

an association between the bottom-up influence of midbrain on the nucleus accumbens whereas this association was absent in Chapter 4's consideration of specific PLE dimensions. A direct comparison between the two is difficult, since Chapter 3 focused only on a single summary score for positive PLEs, whereas Chapter 4 developed more refined and less error-prone measures of specific PLE dimensions. Moreover, the large sample size in Chapter 4 comprised adult participants spanning a wider age range (18–50 years old) compared to the smaller sample of young adults in Chapter 3. It is thus possible that the association with midbrain connectivity in the younger healthy cohort may capture a feature associated with peak dopamine function, which occurs in this age range (Goldman-Rakic & Brown, 1982; Thompson et al., 2004; Weinberger, 1987).

Only subclinical delusions were associated with cortical influences, being positively associated with DLPFC inhibition. This result is consistent with past work reporting altered signalling of this region in healthy individuals with delusional ideation, suggesting the involvement of cognitive functions (Corlett & Fletcher, 2012; Fukuda et al., 2019). Top-down cortical influences were not linked with other positive PLE dimensions, contrasting the associations with CAPE scores in the healthy cohort in Chapter 3. IRT analysis in Chapter 4 identified that a large proportion of items in the CAPE positive subscale measure subclinical delusions. The associations with extrinsic DLPFC connectivity seen in Chapter 3 may be primarily driven by contributions to CAPE positive scores from delusional PLEs.

The investigation of negative PLEs throughout this thesis has yielded mixed results. Functional connectivity analysis revealed that increased connectivity of the dorsal circuit is associated with negative PLE severity. In Chapter 3, higher CAPE negative subscale scores (Stefanis et al., 2002) were associated with reduced top-down influence from cortex to striatum in both the dorsal and ventral circuits, as were reduced influence of amygdala and hippocampus on the midbrain, and greater midbrain self-inhibition. In Chapter 4, each of the specific negative PLE dimensions studied were associated exclusively with effective connectivity of ventral FST circuit, and prominently featured nucleus accumbens and hippocampal connectivity. Contradicting the findings of the previous chapter, specific dimensions of negative PLEs were not associated with cortical influences or bottom-up signalling from

the midbrain. These findings suggest that limbic system function is more closely associated with negative PLEs.

Several regions associated with PLEs were also linked with symptom severity in clinically diagnosed patients. The nucleus accumbens was consistently implicated in effective connectivity analyses across the cohorts. The ventral striatum has been linked to aberrant signalling and dopaminergic dysfunction in people at different stages of the psychosis continuum, and altered activity of this area has been correlated with the variations of both positive and negative symptoms (Juckel et al., 2006; Mohanty et al., 2005; Murray et al., 2008; Soliman et al., 2008, 2011; Yan et al., 2016). The thalamus was also consistently implicated. This region plays a role in relaying signals between the cortex and subcortex, and also between cortical regions, thus regulating cortical integration (Haber & McFarland, 2001; Sherman, 2016). Therefore, thalamic disturbances can influence the functioning of widespread neural systems, and vice versa, brain-wide disruptions may be reflected in thalamic dysregulation (Anticevic, 2017). The hippocampus, a region that is linked with psychosis onset, dopamine regulation, and expressions of symptoms along the psychosis continuum, was also repeatedly implicated in the effective connectivity models presented in this thesis (Harrison, 2004; Heckers & Konradi, 2015; Lieberman et al., 2018; Lodge & Grace, 2006).

The results of this thesis indicate that it is difficult to pinpoint a specific set of connections that are consistently associated with symptom expression across all stages of the severity continuum. In this sense, the findings support a neurobiological in a general, rather than specific sense, in which certain areas and circuits (e.g., midbrain, thalamus, nucleus accumbens, striatothalamic pathways) feature prominently, but in which the precise connections and nature of their involvement may vary across different stages. Some of these variations may be due to differences in medication status and other potential confounds. It is also possible that consistent neural correlates along the psychosis continuum are better captured at the level of regional activity, for instance as demonstrated by consistent variations in ventral striatal activity across cohorts (e.g., Juckel et al., 2006; Mohanty et al., 2005; Winton-Brown et al., 2017), rather than specific inter-regional connections. Furthermore, FST systems encompass deep subcortical and cortical regions, and capture various molecular systems, particularly the dopaminergic pathways, that mature at different stages of development (Goldman & Alexander, 1977; Larsen et al.,

2020; Østby et al., 2009; Sussman et al., 2016). The interaction of developmental effects with medication and illness progression, especially when comparing early stages of psychosis with established illness, should be taken into consideration when characterising FST connectivity along the psychosis continuum.

5.1.3. Implications for models of psychosis

Developmental animal models propose that cortical lesions occurring early in development disrupt dopamine transmission in the cortex, causing inappropriate top-down cortical signalling to the midbrain which induces hyperactivity of the subcortical dopamine system (Pycock et al., 1980; Weinberger, 1987). Dysregulation of the hippocampus, as demonstrated by the methylazoxymethanol (MAM) model in rodents, also compromises the control of subcortical limbic regions on the midbrain, thus dysregulating dopamine activity (Lodge & Grace, 2006). Effective connectivity of FST circuits in FEP, in comparison to healthy controls, revealed top-down influence of the thalamus and amygdala on the nucleus accumbens, accompanied with a disinhibition of the midbrain. FEP patients with schizophrenia additionally demonstrated excitatory bottom-up influence of the midbrain on the nucleus accumbens. These results partially fit with the MAM model with respect to the top-down influence of subcortical regions on the ventral striatum. However, contrary to this model, top-down influence of the hippocampus on the nucleus accumbens, or the nucleus accumbens on the midbrain, was not observed in FEP. The absence of altered efferent connectivity from these regions may be related to the illness stage investigated here. The MAM model is thought to be relevant to the prodromal phase of the illness (Modinos et al., 2015). It is plausible that the onset of FEP coincides with a compensatory amygdala response to downregulate prolonged dopamine hyperactivity (Chang & Grace, 2014; Grace, 2016). Accordingly, we found that FEP patients showed increased excitatory influence of the amygdala on the nucleus accumbens in Chapter 3.

The results in Chapter 3 also suggested that mesocortical system dysconnectivity was evident in established illness. Although cortical dysfunction is pervasive in schizophrenia (Meyer-Lindenberg et al., 2002a; Slifstein et al., 2015), the absence of altered top-down cortical influences in FEP is at odds with some developmental models (Pycock et al., 1980; Weinberger, 1987). The absence of a cortical

influence here may be due to several factors. As with the role of the hippocampus, it is possible that cortical dysregulation occurs earlier in the prodromal phase and may involve a distinct prefrontal area region that was not included in the effective connectivity models considered here. The anterior cingulate cortex, for instance, has been shown to exhibit alterations in morphology and connectivity prior to illness onset (Fornito, Yung, et al., 2008; Pettersson-Yeo et al., 2011). It is also worth mentioning that the FEP patients and their respective healthy controls in Chapter 3 were comprised mostly of adolescents, and this developmental age corresponds to a period of ongoing prefrontal maturation (Goldman-Rakic & Brown, 1982; Luna et al., 2001). Significant differences in DLPFC connectivity between patients and controls may appear at a later age, and abnormalities in mesocortical signalling seen in established illness may only emerge in adulthood, as longer-range projections myelinate and mature (Dosenbach et al., 2010).

In summary, although our findings suggest that dysregulation of top-down cortical control on mesolimbic dopamine may only emerge in later illness states, our analysis cannot completely rule out a role in triggering psychosis onset. A more comprehensive investigation of influences from a larger set of cortical regions, along with a sampling of cohorts from the prodromal stage, would be necessary to comprehensively test this developmental model. Our analyses provide stronger support for a prominent influence early in the illness of aberrant subcortical connectivity, and an intrinsic disinhibition of the midbrain in particular, which is consistent with abnormal bottom-up signalling as driving the emergence of psychotic symptoms.

5.2. Limitations and future directions

The work in this thesis, along with many other studies of the psychosis continuum, have largely focused on the cardinal positive symptomatology despite evidence proposing that positive PLEs, when they are not accompanied with negative PLEs or cognitive disorganisation, are not linked to distress or reduced functioning, and in some cases, may even lead to subjective wellbeing (Grant & Hennig, 2020; Mohr & Claridge, 2015). Instead, vulnerability for developing psychopathology in healthy people with PLEs has been linked to distress, negative symptoms, and cognitive disorganisation (Grant & Hennig, 2020; Horan et al., 2007). Although negative PLEs were investigated with respect to FST circuitry here, the

neurobiological basis of negative symptoms is less well understood (Galderisi et al., 2015). Thus, characterising brain circuits that are most sensitive to these risk factors may reveal consistencies in specific connections that are perturbed along the psychosis continuum.

Translation of developmental animal models proposing the loss of top-down control as a primary pathophysiological factor in psychosis onset may require direct validation in the prodromal stage (Lodge & Grace, 2006; Modinos et al., 2015; Weinberger, 1987). This thesis did not investigate at-risk groups. Mapping effective connectivity of FST circuits in this population may thus provide a fruitful avenue for refining pathophysiological models. Additionally, where this study evaluated cross-sectional differences in functional and effective connectivity across different stages of the psychosis continuum, a robust investigation of the neural correlates of illness progression should be pursued in longitudinal studies. Finally, the recent development of DCMs that are scalable to whole-brain networks (Frässle et al., 2017) will make it possible to survey effective connectivity across extended neural systems, including various regions that are implicated prior to illness onset such as the anterior cingulate cortex (Fornito, Yung, et al., 2008; Pettersson-Yeo et al., 2011), thereby providing a more complete picture of the circuit dysfunctions that may drive psychosis expression during different illness phases.

5.3. Conclusions

The findings presented in this thesis contribute to the understanding of the neurobiology of the psychosis continuum. They suggest that the psychopathological continuum of severity that has been observed in clinical studies shared similarities with a neurobiological continuum of FST circuit function, in which different levels of symptom severity are tied to the function of distinct FST sub-systems and regions, without there necessarily being a single connection or region that is continuously implicated across the entire illness spectrum. More specifically, this thesis identifies a prominent role for subcortical dysconnectivity and midbrain disinhibition early in the illness, a critical role for striatothalamic influences in regulating dopamine synthesis capacity in the striatum, and a role for cortical systems in later illness stages. Positive symptoms across the continuum are generally tied to midbrain and striatothalamic systems across dorsal and ventral circuits, whereas negative symptoms are more closely linked with ventral circuit and limbic functions. Despite some consistencies in the specific

FST regions implicated in the associations with both subclinical and clinical symptoms, there were differences in terms of the specific inter-regional connections that were linked to symptom severity in clinical and non-clinical individuals. This result suggests that while there may be continuity at the level of broad neural circuits, the specific circuit elements that are linked to symptom expression at different points along the psychosis continuum may vary, suggesting some discontinuity in their mechanistic bases. Overall, the findings support a neurobiological continuum of psychosis in a general systems-level, rather than specific inter-region connection-level. They also suggest that intrinsic dysfunction of subcortical circuitry may play a primary role in disease pathophysiology, and thus represents a promising target for treatment development.

Supplementary materials for Chapter 2

Appendix A

A.1. Supplementary methods and materials

Recruitment and exclusion criteria

Data collection was conducted between August 2013 to May 2017. We assessed participants for any lifetime history of psychiatric or neurological disorders, or psychotropic treatment, using a screening questionnaire and responses based on self-report. Additional exclusion criteria included regular use of recreational drugs for at least once a month or a history of drug abuse, and a significant blow to the head, signified by a loss of consciousness or memory. All of our participants were recruited from a healthy community sample and are functioning members of the community, were not taking psychotropic medication, and had no reason to lie about their medical history.

Missing values replacement for IQ scores

Full-scale IQ was estimated using the four-subtest version of the Wechsler Abbreviated Scale of Intelligence – Second Edition (WASI-II) (Wechsler, 2011). IQ scores were missing for 9 of 353 participants (2.5%). Little's Missing Completely at Random (MCAR) test was not significant (χ^2 (14) = 17.44, p = .23), indicating that the assumptions of MCAR were satisfied (Kitaichi et al., 2005; Little, 1988). To predict the missing IQ scores, regression analyses were conducted using the expected maximization algorithm implemented in IBM SPSS version 25. This method provides unbiased parameter estimates that account for missing values based on observed covariances in the data (Kitaichi et al., 2005). Predictor variables included age, sex, mean framewise displacement (FD), and 12 subscale scores from our measurement battery of psychosis-like experiences (PLEs).

Measures of psychosis-like experiences

The Oxford-Liverpool Inventory of Feelings and Experiences short-form (sO-LIFE) (Mason et al., 2005)**.** The sO-LIFE is a self-report measure of schizotypy traits in the general population. It consists of 43 items that are grouped into four dimensions: Unusual Experiences (12 items), Cognitive Disorganisation (11 items), Introvertive Anhedonia (10 items), and Impulsive Nonconformity (10 items). Each item is scored on a binary scale (0 = *'no'*; 1 = *'yes'*).

Peters Delusion Inventory 21-item (PDI-21) (Peters et al., 2004)**.** PDI-21 is a self-report measure assessing delusional ideation in the general population. The measure comprises four dimensions: PDI yes/no, distress, preoccupation, and conviction. For the present study, we used the PDI yes/no dimension to assess the presence of delusions in our sample. Items are measured on a binary scale (0 = *'no'*; 1 = *'yes'*), hence yielding a total score ranging from 0 to 21.

Community Assessment of Psychotic Experience (CAPE) (Stefanis et al., 2002)**.** CAPE is a self-report measure of subthreshold PLEs designed for the general population. It consists of 42 items that yield three dimensions of PLEs: positive, negative, and depressive. Positive experiences are measured by 20 items, negative experiences are measured by 14 items, and depressive experiences are measured by 8 items. A 4-point Likert scale measures the frequency of experiences (1 = *'never'*; 4 = *'nearly always'*). A separate score for each dimension can also be obtained by summing up the scores of a subscale yielding to possible maximum scores of 80, 32, and 56 for the positive, negative, and depressive subscales, respectively. A distress scale also accompanies each of the three dimensions of experiences, measured using a 4-point Likert scale (1 = '*not distressed'*; 4 = '*very distressed*').

Chapman Scales. Four subscales were administered to measure PLEs: 1) the magical ideation scale (Eckblad & Chapman, 1983) – 30 items measuring metaphysical beliefs, 2) the perceptual aberration scale (Chapman et al., 1978) – 35 items assessing perceptual abnormalities, 3) the physical anhedonia scale (Chapman et al., 1976) – 61 items measuring deficits in the ability to experience pleasure, and 4)

the revised social anhedonia scale (Chapman et al., 1976) – 40 items measuring social withdrawal or indifference.

Subthreshold depressive symptoms. We also measured depression scores using the Hospital Anxiety and Depression Scale (HADS) (Snaith, 2003). We did not find significant correlations between HADS Depression scores and both positive (r=-.02, p=.65) and negative (r=-.08, p=.13) PLEs, suggesting that our principal component scores were not influenced by depressive symptoms that are extrinsic to PLEs.

Neuroimaging data acquisition

Multiband T2*-weighted whole-brain echo-planar images (EPIs) were acquired for each participant using a 3T Siemens Skyra MRI scanner equipped with a 32-channel head coil, located at the Monash Biomedical Imaging facility, Melbourne, Australia. Participants were instructed to lie still in the scanner with eyes closed while maintaining wakefulness. A total of 620 functional volumes with 42 slices each were acquired per participant using an interleaved acquisition with the following parameters: repetition time (TR) of 754 milliseconds, echo time (TE) of 21 milliseconds, flip angle of 50°, multiband acceleration factor of 3, field of view (FOV) of 190mm, slice thickness of 3mm, and 3mm isotropic voxels. Anatomical T1-weighted images were also acquired for each participant using a 3-dimensional magnetic-prepared rapid gradient echo sequence. A total of 192 slices were acquired for each participant's T1-weighted images using an ascending acquisition with the following parameters: TR of 2300 milliseconds, TE of 2.07 milliseconds, flip angle of 9°, FOV of 256mm, and voxel size of $1mm^3$.

Preprocessing of EPI images

EPI images were initially preprocessed in FSL FEAT following a basic pipeline, which included removal of the first four volumes, rigid-body head motion correction, 3mm spatial smoothing to improve signal-to-noise ratio, and high pass temporal filter of 75s to remove slow drifts. Subsequently, spatial independent component analysis (ICA) was performed using FSL MELODIC. These components were used as inputs for FSL-FIX (Griffanti et al., 2014; Salimi-Khorshidi et al., 2014), an ICA-based denoising approach that uses an automated classifier to identify noise components

(representing signal contributions from head motion and various sources of scanner and physiological noise), and remove them from the data. This approach has been shown to successfully correct for motion and physiological noise, in addition to artifacts associated with multiband acceleration (Boyacioğlu et al., 2015; Griffanti et al., 2014).

The FSL-FIX classifier was trained using an independent cohort of 25 individuals (13 males; mean age = 25.56 years), acquired using identical scanner and acquisition protocol, in which each of over 2000 components were manually labelled as signal or noise. Components that correspond to motion, physiology, multiband artifact, white matter, and cerebrospinal fluid were classified based on their spatial characteristics, time-series fluctuations, and power spectra (Griffanti et al., 2017). The accuracy of the classifier in identifying nuisance components was verified in a subset of 15 individuals from our sample, yielding an accuracy estimate of 97%. Half the mislabelled components were false positives (i.e., noise classified as signal) which were less of a concern than the misclassification of signal as noise.

The time courses of components labelled as noise were used as nuisance regressors, along with 24 head motion parameters (6 rigid-body parameters, their backwards derivatives, and squared values of the 12 regressors) and the averaged signal taken from a mask of the entire brain (as well as the first derivative and squares of each). Prior work indicates that the last step results in better removal of motion artefact following FSL-FIX (Burgess et al., 2016), and is currently the most effective strategy for removing respiration-related signal changes in blood-oxygen-level dependent (BOLD) functional magnetic resonance (fMRI) data (Power et al., 2017).

Denoised functional data were spatially normalized to the International Consortium for Brain Mapping 152 template in Montreal Neurological Institute (MNI) space using ANTs (version 2.2.0) (Avants et al., 2011), via a three-step method: 1) registration of the mean realigned functional scan to the skull-stripped high resolution anatomical scan via rigid-body registration; 2) spatial normalization of the anatomical scan to the MNI template via a nonlinear registration; and 3) normalization of functional scan to the MNI template using a single transformation matrix that concatenates the transforms generated in steps 1 and 2. As a final step, spatially normalized functional images were

spatially smoothed with a 6mm full-width half-maximum Gaussian kernel using the AFNI (version 16) 3dBlurToFWHM function.

Motion exclusion and quality check of functional data

MRIQC (Esteban et al., 2017), an automated pipeline of quality checking of MRI scans, was initially used to assess the quality of our functional and structural data. Based on MRIQC reports and visual inspection of the data, scans from five participants containing artifacts and scans from four participants with missing volumes were excluded from further analysis.

To quantify the degree to which the denoised data contained residual contamination from head motion, we estimated the FD of each participant using the root mean squared volume-to-volume displacement of all voxels, derived from the six head motion parameter estimates (3 translations, 3 rotations) (Parkes et al., 2018). Typical motion exclusion thresholds (e.g., FD > 0.25mm (Satterthwaite et al., 2013)) are too lenient for our rapidly sampled data. We thus determined a threshold for identifying high motion volumes by concatenating all FD values from all participants into a single distribution and setting a threshold at the 75th percentile plus 1.5 times the interquartile range (an approach similar to that implemented in the fsl_motion_outliers function of the FSL toolbox). This approach yielded a threshold of FD > 0.11mm. Based on this value, participants were removed from further analysis using the following criteria: 1) their mean FD is greater than 0.11mm, 2) the sum of suprathreshold spikes is greater than 20%, or 3) if any FD is greater than 2.5mm (this value was adapted from previous work (Satterthwaite et al., 2013)). This procedure resulted in the exclusion of 32 individuals, resulting in a final sample of 353 people.

As all denoising pipelines for fMRI typically contain some residual level of motion contamination (Ciric et al., 2017; Parkes et al., 2018), we follow prior suggestions (Parkes et al., 2018) and report a series of quality control metrics to demonstrate the impact of motion of our findings. To generate these metrics, each participant's brain was parcellated into 333 cortical regions using the parcellation developed by Gordon et al (Gordon et al., 2016). For each of the 55,728 correlations between each pair of regions, we computed the cross-participant correlation between functional connectivity and mean FD. No connections showed a significant correlation with FD after correcting

for multiple comparison, and 7.9% were significant at $p <$. 05 uncorrected. The association between connectivity and FD also showed a negligible dependence on the distance between pairs of regions (ρ = -0.07; Figure S2). These results are comparable to the best performing denoising pipelines evaluated to date (Ciric et al., 2017; Parkes et al., 2018).

To further test of any residual effects of motion on functional connectivity estimates, we split the sample into three equally sized groups based on their mean FD values and calculated two-tailed t-contrasts assessing increases and decreases in functional connectivity in the groups with the highest (n = 117) and lowest (n = 117) mean FD values. No differences in functional connectivity were found between the groups. Moreover, the principal component scores describing PLE variance were not correlated with mean FD values (positive PLEs r = .03, p = .6; negative PLEs r = .06, p = .20). Together, these results indicate that motion confounds are well controlled in our analysis.

Details on the definition of seed regions of interest (ROIs)

The six ROIs were originally identified based on a meta-analysis of striatal activation in fMRI and PET studies (Postuma & Dagher, 2006). Based on activation peaks, the striatum was subdivided into to a dorsal and ventral caudate and a dorsal, ventral, and rostral putamen. The anatomical boundaries of these subregions were further refined in later work (Di Martino et al., 2008) by transforming the regions into MNI space, and ensuring that they are constrained within grey matter via visual inspection. For the caudate, three ROIs were seeded along a dorsoventral axis, including the dorsal caudate (DC; x = ±13, y = 15, z = 9), the superior ventral caudate (sVC; x = ±10, y = 15, z = 0), and the inferior ventral caudate/nucleus accumbens (iVC; x = ±9, y = 9, z = -8). Three ROIs were seeded for the putamen along a similar axis, comprising the dorso-caudal putamen (DCP; x = ±28, y = 1, z = 3), the dorso-rostral putamen (DRP; x = ±25, y = 8, z = 6), and the ventro-rostral putamen (VRP; x = ±20, y = 12, z = -3). We used the same coordinates as centroids for the 3.5mm radius spheres that were used as seeds in our analysis.

Leave-one-subject-out analysis

To visualize associations between functional connectivity and PLEs for specific clusters identified in our voxelwise analyses, we used a leave-one-subject-out (LOSO) analysis (Esterman et al., 2010). Specifically, the second-level general linear model was repeated 353 times, each time excluding one of the subjects. For our main analysis, a ROI was generated from key significant clusters (TFCE $p <.017$ corrected, 1000 permutations), and used as a mask to extract functional connectivity parameter estimates from the excluded subject. Significant clusters for our exploratory analysis were thresholded at TFCE $p <.002$ corrected, with 1000 permutations. These parameters estimates were then plotted as a function of PLE scores. This approach avoids the circular inference that can occur when visualizing scatterplots of brain-behaviour associations mapped at the voxel level (Kriegeskorte et al., 2009; Vul et al., 2017; Vul & Pashler, 2012).

A.2. Supplementary results

Associations significant at uncorrected levels

To facilitate comparison with past work, we report here associations between striatal functional connectivity and PLEs that are significant at $p <.05$, TFCE corrected, but did not survive Bonferroni correction across seeds and PLE dimensions.

Dorsal CST functional connectivity and PLEs. Higher positive PLEs were associated with reduced coupling between the DCP and left visual cortex, left posterior cingulate sulcus, and the right sensorimotor regions. Higher positive PLE scores were also linked with increased coupling between the DCP and regions of right medial PFC, frontal eye fields and frontal pole; and increased coupling between the DC and the lateral occipital cortex.

Higher scores on the negative PLE dimension were associated with increased functional connectivity between the dorsal striatum and sensorimotor areas; namely, between the DCP and right primary motor cortex, right superior temporal gyrus, and left occipital and somatosensory areas; and between the DC seed and right occipital cortex (Figure S4). Refer to Table S2 for a list of brain regions

in which functional connectivity with striatal seeds was significantly associated with PLEs at an uncorrected level.

Ventral CST functional connectivity and PLEs. Associations between PLEs and ventral system functional connectivity were limited to the VRP seeds. Specifically, higher positive PLEs were associated with lower functional connectivity between this region and left visual cortex (Table S2; Figure S5). Higher negative PLEs were associated with higher coupling between the VRP and bilateral sensorimotor cortex (Table S2; Figure S5), and lower coupling between the VRP and the right paracentral lobule (Table S2).

Table A1. Descriptive Statistics and Correlation Coefficients of Subscales Included in Principal Component Analysis (*N* = 672)

Subscales	Min	Max	Mean (SD)	1	2	3	4	5	6	7	8	9	10	11	12
CAPE															
1. Positive	20	52	25.94 (4.72)	–	.35[a]	.40[a]	.74[a]	-.10[b]	.64[a]	.18[a]	.72[a]	.29[a]	.06	.46[a]	.81[a]
2. Negative	14	44	23.74 (5.66)		–	.55[a]	.26[a]	.30[a]	.37[a]	.50[a]	.35[a]	.52[a]	.45[a]	.28[a]	.37[a]
3. Depressive	8	27	13.90 (3.01)			–	.35[a]	.11[b]	.36[a]	.21[a]	.40[a]	.53[a]	.26[a]	.40[a]	.43[a]
Chapman															
4. Magical Ideation	0	26	6.23 (4.78)				–	-.09[c]	.64[a]	.14[a]	.74[a]	.34[a]	.07[c]	.47[a]	.70[a]
5. Phys Anhedonia	0	42	11.50 (6.97)					–	-.01	.45[a]	-.05	.15[a]	.56[a]	.01	-.10[b]
6. Perc Aberration	0	32	5.21 (5.27)						–	.24[a]	.69[a]	.31[a]	.13[a]	.43[a]	.60[a]
7. Soc Anhedonia	0	35	9.36 (6.42)							–	.21[a]	.31[a]	.67[a]	.20[a]	.17[a]
sO-LIFE															
8. Unusual Experiences	0	12	2.86 (2.64)								–	.43[a]	.14[a]	.53[a]	.63[a]
9. Cog Disorganisation	0	11	4.75 (2.90)									–	.34[a]	.40[a]	.35[a]
10. Introvertive Anhedonia	0	10	1.62 (1.74)										–	.14[a]	.11[b]
11. Impulsive Nonconform	0	10	3.30 (2.08)											–	.43[a]
12. PDI	0	17	5.49 (3.49)												–

[a] $p < .001$

[b] $p < .01$

[c] $p < .05$

Table A2. Regions Where Striatal Functional Connectivity Was Associated with Psychosis-Like Experiences (p <.05 TFCE corrected)

Seed	Contrast	Region	MNI coordinates (x, y, z)	Max T-value	Cluster extent (voxels)	p
DC	Pos PLEs +	R lateral occipital cortex	42, -60, 24	4.98	37	.02
	Neg PLEs +	R occipital cortex	26, -82, 8	4.92	216	<.01
DCP	Pos PLEs -	R supplementary motor area	6, -4, 62	3.95	95	.03
		L visual association area	-6, -96, 24	4.71	68	.03
		R primary sensory area	10, -38, 78	4.18	57	.03
		L posterior cingulate sulcus	-16, -34, 50	4.32	56	.02
	Pos PLEs +	R medial prefrontal cortex	2, 44, 34	4.12	166	.03
		L frontal eye fields	-24, 30, 44	4.15	84	.03
		R frontal pole	16, 70, 2	4.97	33	.03
	Neg PLEs +	R superior temporal gyrus	66, -2, 6	4.74	91	.02
		L intraparietal sulcus	-26, -78, 24	5.14	66	.01
		L superior occipital gyrus	-20, -84, 38	4.05	47	.03
		L primary somatosensory area	-60, -14, 34	4.25	14	.04
		L parietal opercular	-52, -18, 18	4.66	11	.03
VRP	Pos PLEs -	L visual association area	-38, -92, 2	5.4	505	<.01
	Neg PLEs -	R paracentral lobule	2, -76, 42	4.72	58	.02
	Neg PLEs +	L primary somatosensory area	-60, -14, 30	4.78	890	<.01
		R postcentral sulcus	44, -30, 40	4.18	320	.01
		R precentral gyrus	12, -26, 68	5.16	240	.01
		R premotor cortex	50, -2, 26	4.19	201	.02
		R primary somatosensory area	44, -36, 62	4.44	114	.02
		R mid cingulate cortex	8, -18, 52	4.58	75	.02
		R primary somatosensory area	40, -12, 66	3.57	36	.04
		L frontal opercular	-58, -10, 6	4.35	28	.03
		R supplementary motor area	8, -14, 62	3.44	13	.04
		L posterior cingulate	-8, -26, 44	3.66	11	.04

List of brain regions showing significant associations at TFCE p <.05, not corrected for multiple comparisons. Only clusters with more than 10 voxels are listed. '+' sign indicates increased coupling in association with PLEs, while '-' indicates reduced coupling associated with PLEs. PLEs: Psychosis-Like Experiences; R: right; L: left; DRP: dorso-rostral putamen; DC: dorsal caudate; DCP: dorso-caudal putamen; VRP: ventro-rostral putamen.

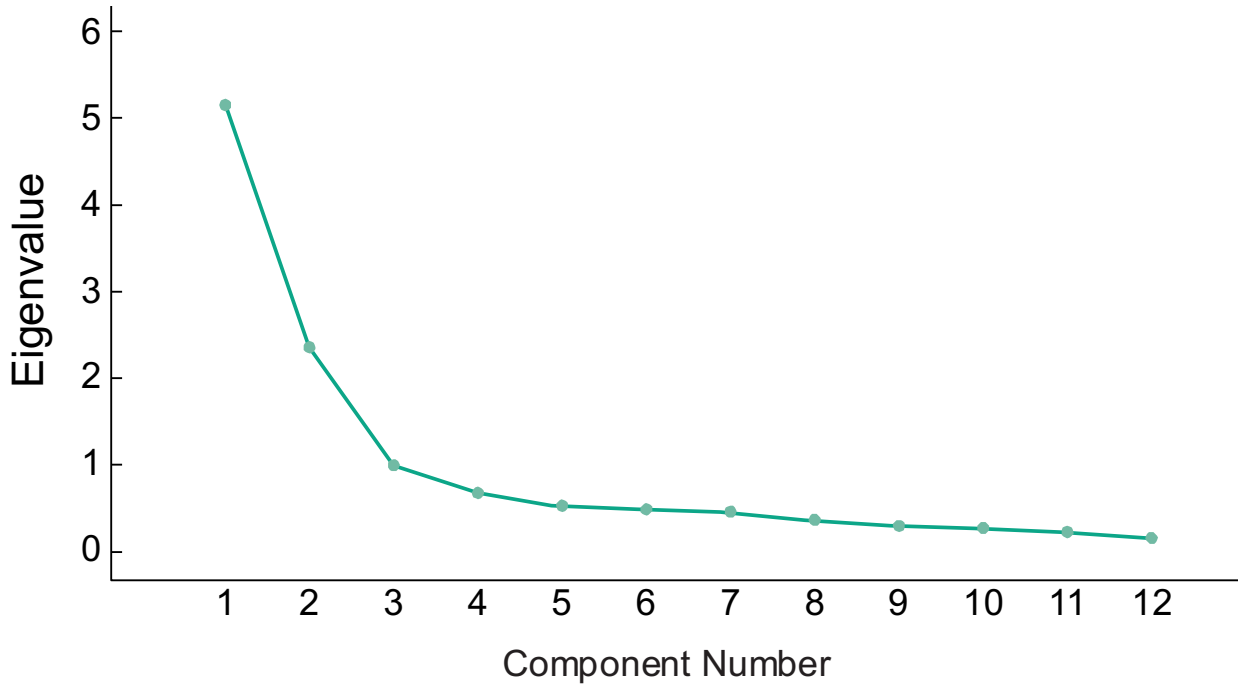

Figure A1. Scree plot of eigenvalues from principal component analysis of PLE measures. The x-axis depicts the component numbers identified in the principal component analysis, while the y-axis shows the eigenvalue of each component. Components above the point of inflection were retained. PLE: Psychosis-like experiences

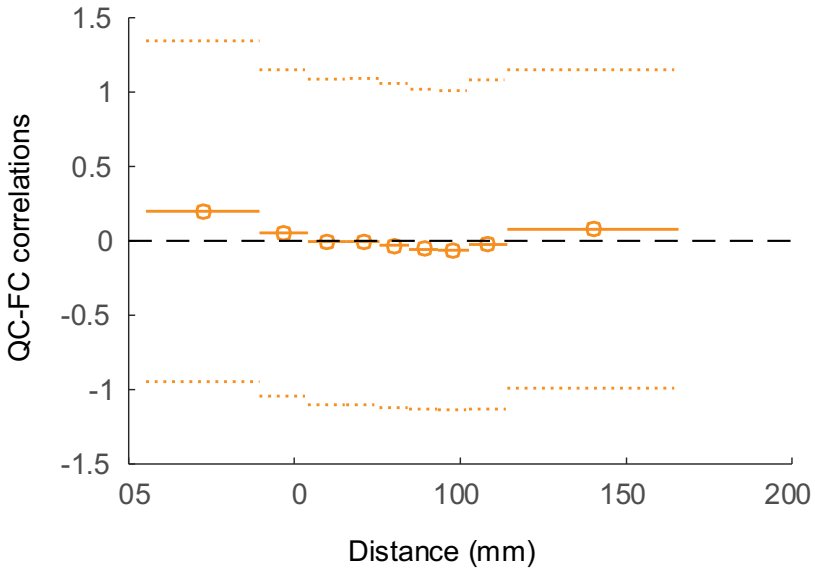

Figure A2. QC-FC distance dependence. Figure illustrates QC-FC distance dependence for the multiband EPI scans following preprocessing. QC-FC correlations were split into 10 equiprobable bins based on the distance between nodes in the Gordon parcellation. For each bin, circles depict the mean distance between edges. The mean and the standard deviation of the QC-FC correlations are represented by the solid and dotted lines, respectively.

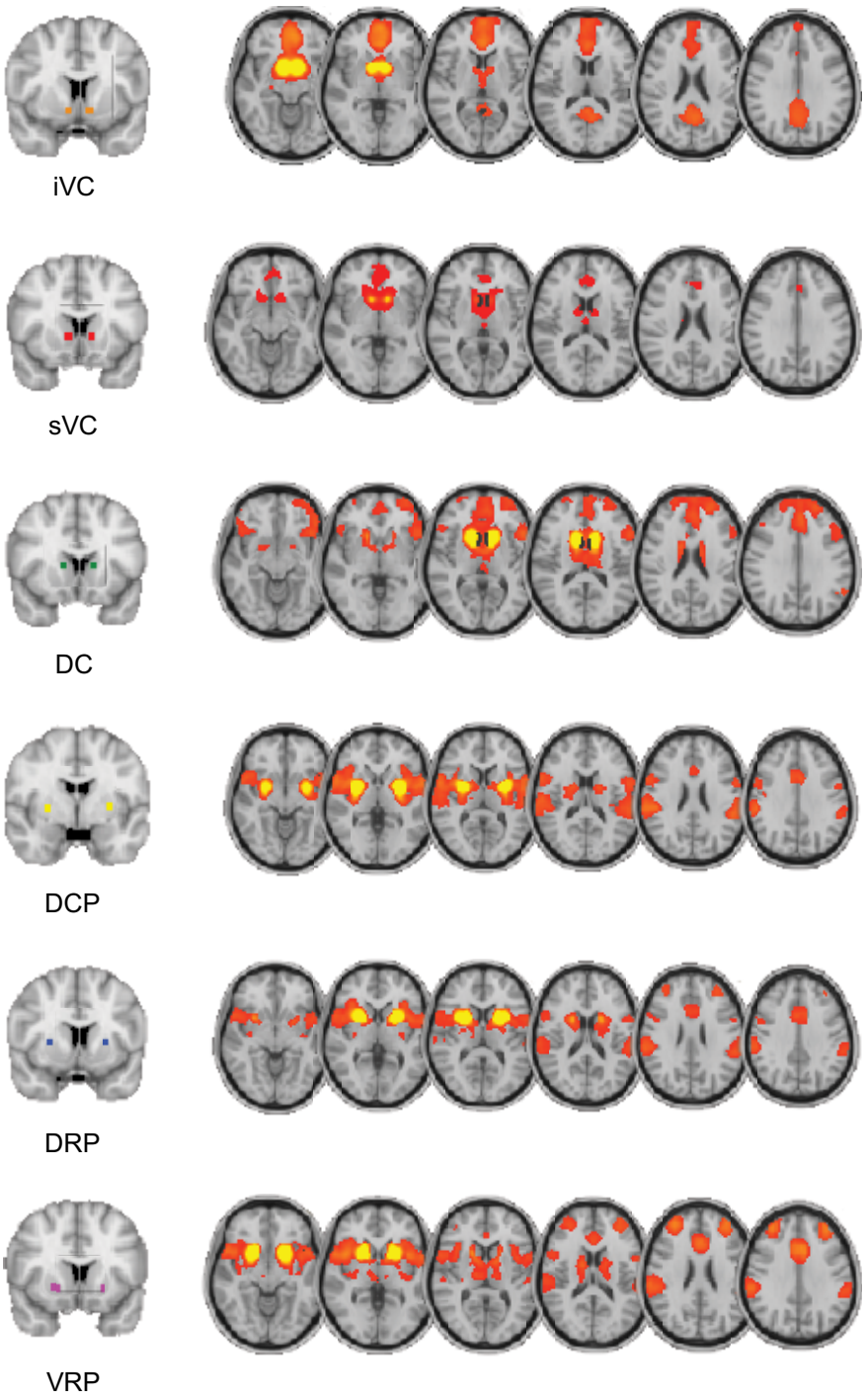

Figure A3. Main effect of seed regions on corticostriatal functional connectivity. Axial slices showing the main effect of striatal seed regions on corticostriatal functional connectivity. For the purpose of visualisation, images were thresholded at a TFCE corrected rate of $p < .001$, with 5000 permutations. The left hemisphere is on the right. iVC: inferior ventral caudate (i.e., nucleus accumbens); sVC: superior ventral caudate; DRP: dorso-rostral putamen; DC: dorsal caudate; DCP: dorso-caudal putamen; VRP: ventro-rostral putamen.

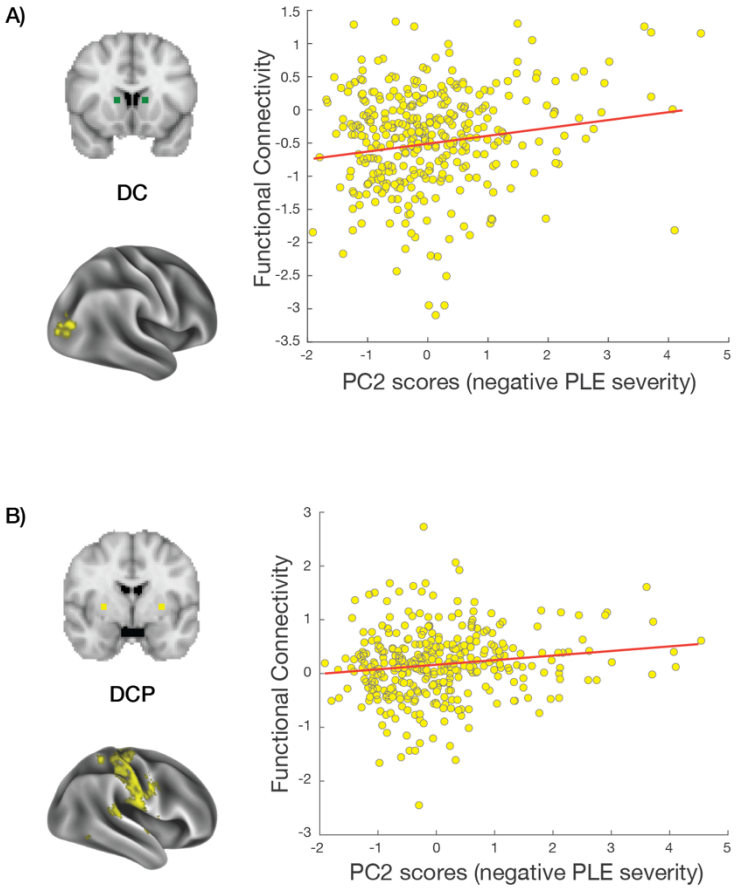

Figure A4. Positive associations between dorsal circuit functional connectivity and negative PLEs (p <.05 TFCE corrected). Functional connectivity between the dorsal striatum and the cortex that are associated with negative PLEs. Coronal slice in the top left of each panel depicts the location of striatal seed regions in the dorsal circuit. Cortical surface maps depict the cortical sites for which functional connectivity with each seed correlates with negative PLE severity. Scatterplots depict the associations between negative PLE severity and the functional coupling between (A) DC and right visual cortex, and (B) DCP and right motor region. Clusters are thresholded at p <.05 TFCE corrected. For visualization purposes, functional connectivity estimates were obtained using Leave-One-Subject-Out analysis. DC: dorsal caudate; DCP: dorso-caudal putamen; PC: principal component; PLEs: Psychosis-like experiences.

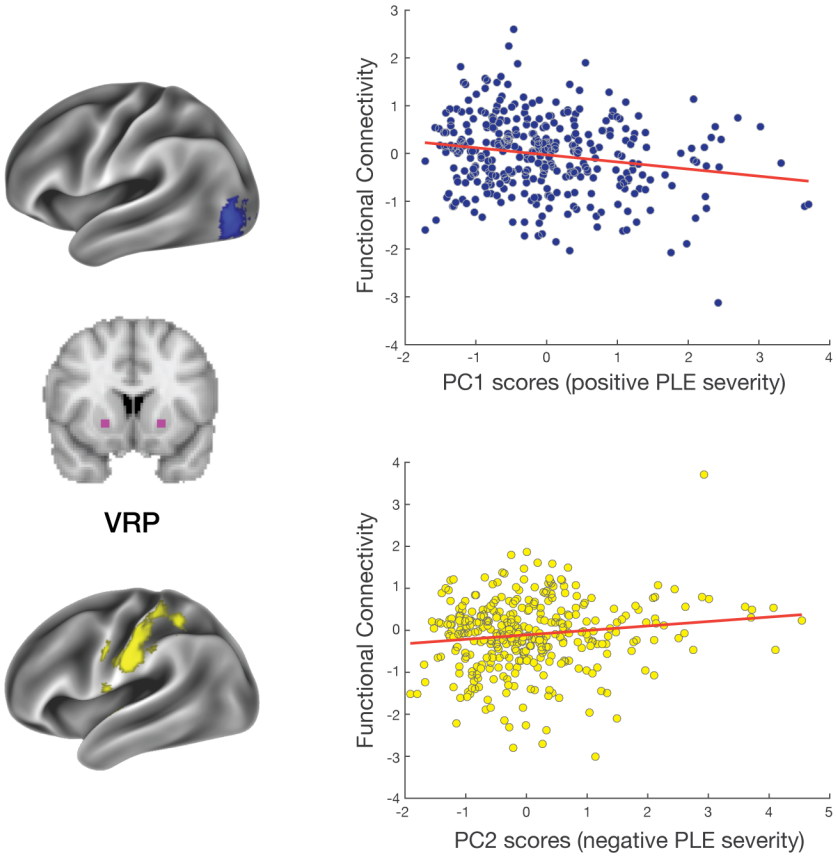

Figure A5. Associations between ventral circuit functional connectivity and PLEs (p <.05 TFCE corrected). Coronal slice in the centre of the left column depicts the location of striatal seed regions in the ventral circuit. Cortical surface maps show the cortical sites for which functional connectivity with the ventral seeds correlate with PLE severity. Blue scatterplot depicts the association between positive PLE and the functional coupling of VRP and left visual area. Yellow scatterplot depicts the association between negative PLEs and VRP and left somatosensory area. Clusters are thresholded as p <.05 TFCE corrected. For visualization purposes, functional connectivity estimates were obtained using a Leave-One-Subject-Out analysis. VRP: ventro-rostral putamen; PC: principal component; PLEs: Psychosis-like experiences.

Supplementary materials for Chapter 3

Appendix B

B.1. Supplementary methods and materials

Participants

FEP. FEP was defined as fulfilling Structured Clinical Interview for DSM-5 (SCID-5) criteria for a psychotic disorder. Patients with substance-induced psychosis were excluded in the present study. FEP diagnoses are in Table S2. Healthy controls had no history of psychiatric or neurological illness, as determined by self-reports, SCID, and the Comprehensive Assessment of At-Risk Mental States. All participants provided informed consent. For FEP patients, additional strict inclusion criteria include comprehension of English language, no contraindication to MRI scanning, less than six months of duration of untreated psychosis, living in stable accommodation, low risk to self or others (score of < 5 on the Brief Psychiatric Rating Scale version 4 (BPRS-4) Suicidality and Hostility subscales), and minimal previous exposure to antipsychotic medication (less than 7 days of use or lifetime 1750mg chlorpromazine equivalent exposure). For healthy controls, additional exclusion criteria included history of psychiatric or neurological illness in first-degree relatives and current use of psychotropic medications. Only baseline data were used in the present study. We also analysed a subsample of FEP patients with schizophrenia diagnoses (FEP-SCZ).

The initial sample size for this group was 61 patients and 27 controls. We excluded 5 patients with poor imaging data, 1 patient with high motion, 3 patients with DCM explaining <75% of the signal variance, and 6 patients with substance induced psychosis. This brought the final sample of patients included in the study to 46. A total of 17 FEP patients had a diagnosis of schizophrenia spectrum disorder (8 schizophrenia, 8 schizophreniform disorder and 1 schizoaffective disorders), making up a subset of FEP-SCZ patients. Other FEP patients were diagnosed with delusional disorder (n = 5), major depressive disorder with psychotic features (n = 10), psychotic disorder not otherwise specified (n = 13), and 1 patient had a missing diagnosis. For the control group, we excluded 3 individuals with high

motion (criteria outlined below), and 1 with DCM explaining <75% of the signal variance, resulting in a final sample of 23.

Established schizophrenia (SCZ). Data were obtained through the UCLA Consortium for Neuropsychiatric Phenomics open dataset (Poldrack et al., 2016). The initial sample consisted of 121 right-handed healthy controls and 51 schizophrenia patients. Healthy controls were excluded if they had a history of mental illness. Schizophrenia patients were excluded if they had comorbidity with either bipolar disorder or ADHD. Diagnoses were based on the DSM-IV and SCID-1.

We excluded 1 patient with poor imaging data, 9 with high motion, and 5 with DCM explaining <75% of the signal variance, resulting in a final sample of 36 patients. We excluded 6 controls with high motion and 15 with DCM explaining <75% of the signal variance, resulting in a final sample of 100 controls.

PLE/[^{18}F]DOPA. A total of 52 healthy participants were recruited from the community through online advertisements. Each participant provided informed consent. Exclusion criteria included current or history of psychiatric or neurological illnesses, significant medical history, intellectual disability, and first-degree relative with a mental illness. Participants underwent simultaneous resting-state fMRI and [^{18}F]DOPA PET.

Eight individuals did not complete the scanning protocol. We also excluded 3 participants with high motion and 5 participants with DCM explaining <75% of the signal variance. A total of 3 participants had unusable PET scans and 10 participants had missing PLE measures. This brought the final sample to 33 with fMRI and PET data and 26 with fMRI and complete PLE measures.

Symptom measures

Clinical symptoms. The Brief Psychiatric Rating Scale (BPRS) positive and negative subscales were used to respectively measure positive and negative symptoms in our clinical cohorts. The subscales were derived from a five factor solution outlined in Dazzi et al., 2016. The positive symptom subscale consists of five items: unusual thought content, suspiciousness, hallucinations, grandiosity, and bizarre

behaviour. The negative symptom subscale consists of three items: blunted affect, emotional withdrawal, and motor retardation. Each item is ranked on a Likert-like scale between 1 to 7, with a score of 1 denoting the absence of a measured symptom.

PLEs. Community Assessment of Psychotic Experience (CAPE) is a self-report measure of PLEs designed for the general population (Stefanis et al., 2002). The positive and negative frequency subscales were used to measure positive and negative PLEs, respectively. The frequency of positive experiences is measured by 20 items and negative experiences is measured by 14 items using A 4-point Likert scale (1 = *'never'*; 4 = *'nearly always'*). The maximum scores that can be yielded from the positive and negative subscales are 80 and 56, respectively.

Neuroimaging acquisition

FEP. Whole-brain T2*-weighed echo-planar images (EPIs) and anatomical T1-weighted (T1w) scans were acquired for each participant using a 3T Siemens Trio Tim scanner, equipped with a 32-channel head coil, located at the Royal Children's Hospital in Melbourne, Australia. Participants were instructed to lie still in the scanner while maintaining wakefulness with eyes closed. A total of 234 functional volumes with 37 slices each were acquired using the following parameters: repetition time = 2000ms; echo time = 32ms; flip angle = 90°; field of view = 210mm; slice thickness of 3.5 mm, and 3.3 x 3.3 x 3.55 mm voxels. A total of 176 slices were acquired for each participant's T1-weighted image using an interleaved acquisition using the following parameters: TR = 2.3s; TE = 2.98ms; flip angle of 9°; FOV of 256mm; voxel size of 1.1 x 1.1. x 1.2 mm.

SCZ. The CNP dataset (Poldrack et al., 2016) was acquired on one of two Siemens Trio 3T scanners located at the Ahmanson-Lovelace Brain Mapping Center and the Staglin Center for Cognitive Neuroscience at UCLA. Details of the resting-state EPI scan are TR = 2s, TE = 30ms , flip angle = 90°, 4mm slice thickness, 152 volumes with 34 slices each. Participants were instructed to keep their eyes

open. Details of the T1w scan are TR = 1.9s, TE = 2.26ms, flip angle of 90°, 176 slices with 1mm^3 voxels.

PLE/[^{18}F]DOPA. Data were acquired using a 3T Siemens Magnetom Biograph simultaneous MR-PET scanner equipped with a 20-channel head and neck coil at Monash Biomedical Imaging, Melbourne, Australia. Resting-state whole-brain T2*-weighed echo-planar image (EPIs) was also acquired for each subject using an interleaved acquisition with the following parameters: TR = 2.89s; TE = 30ms; 152 volumes with 44 slices per volume; flip angle = 90°; FOV = 190mm; slice thickness = 3mm; voxel size of 3mm^3. A high resolution T1w anatomical image was acquired for each subject using an ascending acquisition, with the following parameters: 176 slices; TR = 1640ms; TE = 2.34ms; flip angle = 8°; field of view (FOV) = 256mm; slice thickness = 1mm; voxel size = 1mm^3.

fMRIPREP preprocessing steps

fMRI and T1-weighted data were processed in the same way across all three cohorts using FMRIPREP software version 1.1.1 (Esteban et al., 2019). Each T1w scan was corrected for non-uniformity in intensity and subsequently skull stripped. Brain surfaces were reconstructed using FreeSurfer version 6.0.1. Tissue masks were generated using FreeSurfer. Spatial normalization of the skull stripped T1w images to the ICBM 152 Nonlinear Asymmetrical template version 2009c was performed using a nonlinear registration in ANTs version 2.1.0. Similarly, for each participant, tissue masks were registered from the surface space to the MNI template.

EPIs were slice-timed corrected using AFNI version 16.2.07 and realigned to a mean reference image using FSL. EPIs were distortion corrected using fieldmaps (phasediff-based workflow; https://fmriprep.readthedocs.io/en/stable/api/index.html#sdc-phasediff). For participants with missing fieldmaps, a "fieldmap-less" distortion correction was performed by co-registering the functional image to the intensity-inverted T1w image constrained with an EPI distortion atlas (Treiber et al., 2016). Following distortion correction, EPIs were co-registered with their corresponding T1w using boundary-based registration with nine degrees of freedom using the bbregister routine in FreeSurfer. The motion-

correcting transformations, field-distortion-correcting warp, EPI-to-T1w transformation, and T1w-to-MNI template warp were concatenated and applied in a single step using ANTs version 2.1.0. Independent component analysis (ICA) based denoising was performed using ICA-AROMA (Pruim et al., 2015). Following ICA-based denoising, signal corresponding to white matter and cerebrospinal fluid were also regressed from the data. Finally, the EPI data were high-pass filtered (temporal filter of 100s) and spatially smoothed using a 4mm full-width half-maximum kernel using the AFNI 3dBlurToFWHM function. In-scanner head motion was defined as excessive according to previously-defined stringent exclusion criteria (Parkes et al., 2018); namely, if any of the following were met: 1) mean framewise displacement (FD) > 0.20mm; (2) sum of suprathreshold FD spikes > 20%; and (3) any FD > 5mm. FD was calculated using the root mean squared volume-to-volume displacement of all voxels, derived from the six head motion parameter (3 translations, 3 rotations) (Parkes et al., 2018).

PET acquisition, reconstruction, and attenuation correction

All participants received carbidopa (150mg) and entacapone (400mg) orally 60 minutes before imaging to reduce the formation of radiolabelled metabolites that can cross the blood-brain barrier and thus confound tracer availability in the striatum (Hoffman et al., 1992; Ruottinen et al., 1995). Participants were instructed to lie still in the scanner with eyes closed.

The pseudo-CT attenuation correction method(Baran et al., 2018; Burgos et al., 2014) was used to correct PET images during image reconstruction. Dynamic PET images were reconstructed using the Siemens e7tools software with image volume size 344×344×127(2.09×2.09×2.03mm^3). The Ordinary Poisson-Ordered Subset Expectation Maximization (OP-OSEM) algorithm (3 iterations, 21 subsets) was used with the point spread function (PSF) for partial volume correction. A 5-mm FWHM Gaussian filter was applied to each 3D image volume. For correction of subject motion, the list mode dataset was first binned into 95 frames consisting of one 30-second background frame and ninety-four 60-second frames. Dynamic motion was corrected based on an image registration approach (Chen et al., 2019), where each frame was registered to the last frame using rigid-body transformation implemented in the FSL toolbox (Jenkinson et al., 2002). The final reconstructed dynamic PET images were registered to the corresponding T1 MPRAGE MRI image. Patlak graphical analysis was performed using Qmodeling

software (López-González et al., 2019; Patlak & Blasberg, 1985). The cerebellum was chosen as a reference region due to its low [^{18}F]DOPA uptake (Moore et al., 2003).

Regions of interest selection for dynamic causal modelling

Nucleus accumbens (NAcc) and dorsal caudate (DC). For the ventral and dorsal striatum, we seeded the NAcc and DC consistent with our previous works (Dandash, Harrison, et al., 2014; Fornito et al., 2013; Sabaroedin et al., 2019) using a functional parcellation of the striatum (Di Martino et al., 2008) that was delineated based on a meta-analysis of striatal activation in fMRI and PET studies (Postuma & Dagher, 2006).

dlPFC. To capture variations associated with subclinical symptoms, that may capture risk for psychosis, as well as disruptions in clinical groups, the dlPFC ROI was selected based on a peak in which functional connectivity with the DC was reduced in the healthy relatives of FEP patients compared to healthy controls (Fornito et al., 2013). This peak overlapped with an area that also showed reduced connectivity in patients.

vmPFC. To choose a region that was most relevant to the ventral circuit, we chose a peak in the vmPFC that showed strong functional connectivity with the NAcc in an independent cohort of 353 healthy adults (Sabaroedin et al., 2019).

Thalamus. The thalamus coordinate was selected from a peak in which functional connectivity with the dorsal caudate was reduced in ARMS individuals compared to healthy controls (Dandash, Harrison, et al., 2014).

Hippocampus, amygdala, and midbrain. ROIs for the three regions were selected using a similar method. Peak coordinates within anatomical masks for the hippocampus and amygdala were selected in a separate group-level functional connectivity analysis of each ROIs connectivity with the whole brain in an independent cohort of 353 individuals (Sabaroedin et al., 2019). For the hippocampus, we

chose the anterior region, using of a hippocampal mask provided in the Freesurfer package (Fischl et al., 2002). The anterior hippocampus is a hippocampal region that is most frequently implicated as dysfunctional in schizophrenia (Small et al., 2011), and it was defined as the region having the MNI coordinate of less than y = -22 (Zeidman & Maguire, 2017). Similar to the hippocampus, we used an amygdala mask provided in FreeSurfer. The midbrain mask was delineated based on the functional connectivity of the ventral tegmental (VTA) and substantia nigra (SN) with the whole brain (Murty et al., 2014). Due to the limited spatial resolution of fMRI images, we combined both of the dorsal and ventral midbrain regions and selected a functional connectivity signal peak in the same cohort that was used in the selection of our hippocampal, amygdala, and vmPFC ROIs.

Spherical ROIs were created with a radius of 6mm for cortical regions (i.e., dlPFC and vmPFC) and 3.5mm for each subcortical ROI. For vmPFC and thalamus ROIs with centroids that were close to the anatomical or functional boundary of the region, we used an anatomical mask from the FreeSurfer package when extracting the first eigenvariate for the ROIs to exclude signal from neighbouring regions.

Spectral dynamic causal modelling

Dynamic causal modelling (DCM) is a Bayesian framework that infers the directed (causal) connectivity among the neuronal systems – referred to as effective connectivity (Friston, 1994). A new DCM for resting state fMRI was recently proposed based upon a deterministic model that generates predicted cross spectra, referred to as spectral DCM. In order to model resting state activity —in the absence of external stimuli—a stochastic component capturing neural fluctuations is included in the model.

Mathematically, we can express the formulation of the stochastic generative model as a set of two equations. First is the neuronal state equation, namely

$$\dot{x}(t) = f(x(t), u(t), \theta) + v(t), \tag{S1}$$

and second is the observation equation, which is a static nonlinear mapping from the hidden physiological states in (1) to the observed BOLD activity, and is written as:

$$y(t) = h(x(t), \varphi) + e(t), \tag{S2}$$

where $\dot{x}(\mathrm{t})$ is the rate of change of the neuronal states $x(t)$, θ are unknown parameters (i.e., the effective connectivity) and $v(t)$ (resp. $e(t)$) is the stochastic process – called the state noise (resp. the measurement or observation noise) – modelling the random neuronal fluctuations that drive the resting state activity. In the observation equations, φ are the unknown parameters of the (haemodynamic) observation function and $u(t)$ represents any exogenous (or experimental) inputs that drive the hidden states, which are usually absent in resting state designs (Friston et al., 2014). Spectral DCM furnishes a constrained inversion of the stochastic model by parameterising the neuronal fluctuations $v(t)$. Spectral DCM simplifies the generative model by replacing the original timeseries with their second-order statistics (i.e., cross spectra). This means that, instead of estimating time varying hidden states, we are estimating their covariance, which is time invariant. Then we simply need to estimate the covariance of the random fluctuations, where a scale free (power law) form for the state noise (resp. observation noise) is used, motivated from previous work on neuronal activity (Beggs & Plenz, 2003; Shin & Kim, 2006; Stam & De Bruin, 2004), as follows:

$$\begin{aligned} g_v(\omega, \theta) &= \alpha_v \omega^{-\beta_v} \\ g_e(\omega, \theta) &= \alpha_e \omega^{-\beta_e} \end{aligned} \tag{S3}$$

Here, $\{\alpha, \beta\} \subset \theta$ are the parameters controlling the amplitudes and exponents of the spectral density of the neural fluctuations. The parameterisation of endogenous fluctuations means that the states are no longer probabilistic; hence the inversion scheme is significantly simpler, requiring estimation of only the parameters (and hyperparameters) of the model.

We used standard Bayesian model inversion to infer the parameters of the model in (1), (2) and (3), from the observed signal $y(t)$. The description of the Bayesian model inversion procedures based on variational Laplace can be found elsewhere (Friston et al., 2007; Friston et al., 2003; Razi & Friston, 2016).

Parametric Empirical Bayes

Empirical Bayes refers to the Bayesian inversion or fitting of hierarchical models. In hierarchical models, constraints on the posterior density over model parameters at any given level are provided by the level above. These constraints are called empirical priors because they are informed by empirical data. A hierarchical Parametric Empirical Bayes (PEB) model for DCM parameters has recently been introduced, which represents how individual (within-subject) connections derive from the subjects' group membership (Friston et al., 2016). Mathematically, for DCM studies with *N* subjects and *M* parameters per DCM, we have a hierarchical model, where the responses of the *i*-th subject and the distribution of the parameters over subjects can be modelled as:

$$
\begin{aligned}
y_i &= \Gamma_i^{(1)}(\theta^{(1)}) + \varepsilon_i^{(1)}, \\
\theta^{(1)} &= \Gamma^{(2)}\left(\theta^{(2)}\right) + \varepsilon^{(2)}, \\
\theta^{(2)} &= \eta + \varepsilon^{(3)},
\end{aligned}
\tag{S4}
$$

where, y_i is the BOLD time series from *i-th* subject *and* $\Gamma_i^{(1)}$ is a nonlinear mapping from the parameters of a model to the predicted response y, which in this study was the model in Eq. S1 above. $\varepsilon_i^{(1)}$ is independent and identically distributed (i.i.d.) observation noise (equivalent to $e(t)$ in Eq. S2). In this hierarchical form, *empirical priors* encoding second (between-subject) level effects place constraints on subject-specific parameters. The second level is a linear model where the random effects are parametrised in terms of their precision:

$$\Gamma^{(2)}\left(\theta^{(2)}\right) = (X \otimes W)\beta \,, \tag{S5}$$

where, $\beta \subset \theta$ are group means or effects encoded by a design matrix with between-subject, X, and within-subject, W, parts. The between-subject part encodes differences among subjects or covariates such as age, while the within-subject part specifies mixtures of parameters that show random effects. We assume that the first column of the design matrix is a constant term, modelling group means, and subsequent columns encode group differences.

Table B1. Summary of Group Differences in Fronto-striato-thalamic Effective Connectivity in FEP (n = 46), FEP-SCZ (n = 17), and SCZ (n = 36) Patients Respective to Healthy Controls

Connection	Increased (+) or decreased (-) in patients	Effect size (Hz)	90% Posterior Credible Interval (lower bound, upper bound)	Patients (mean)	Controls (mean)
FEP vs HCs					
Thal → NAcc	-	0.10	-0.20, -0.01	-0.12	0.09
Amyg → NAcc	+	0.11	0.02, 0.21	-0.04	-0.24
VTA/SN → VTA/SN	-	*0.14*	*-0.24, -0.03*	*-0.04 (-0.48)*	*0.00 (-0.05)*
FEP-SZ vs HCs					
Thal → NAcc	-	0.13	-0.24, -0.02	-0.14	0.00
Amyg → NAcc	+	0.12	0.02, 0.23	0.00	-0.24
Amyg → Amyg	-	*0.11*	*-0.23, 0.00*	*-0.17*	*0.00*
NAcc → Hipp	-	0.14	-0.25, -0.04	-0.29	0.00
VTA/SN→ NAcc	+	0.09	-0.02, 0.21	0.00	-0.14
VTA/SN→ VTA/SN	-	*0.08*	*-0.20, 0.03*	*-0.06* (-0.47)*	*0.07* (-0.54)*
SCZ vs HCs					
dlPFC → Thal	-	0.11	-0.19, -0.03	-0.14	0.00
Thal → Hipp	-	0.10	-0.18, -0.02	-0.20	0.00
Thal → NAcc	-	0.09	-0.17, -0.01	-0.12	0.00
VTA/SN → VTA/SN	-	*0.11*	*-0.21, -0.01*	*-0.26 (-0.39)*	*-0.09 (-0.26)*
VTA/SN → DC	-	0.13	-0.20, -0.03	-0.19	0.00
DC → VTA/SN	+	0.16	0.08, 0.24	0.12	-0.11

* denotes mean connections that were derived from the DCM PEB routine as these connections were removed in the subsequent Bayesian model averaging routine.

All connections have the posterior probability (free energy) value of 1.00

All parameters for between region connections are in Hz.

Self-connections are italicized, and values are log-transformed to ensure prior negativity (i.e., inhibitory) constraints on self-connections. A positive value for self-connection denotes increased inhibition, a negative value signifies reduced inhibition. Self-connection parameters in Hz are displayed in parentheses.

Table B2. Summary of Connections Associated with Severity of Clinical Symptoms in FEP (n = 46), FEP-SCZ (n = 17), and SCZ (n = 26) Patients

Connection	Positive (+) or negative (-) association	Effect size (Hz)	90% Posterior Credible Interval (lower bound, upper bound)
Positive symptoms			
FEP			
vmPFC → vmPFC	-	*0.16*	*-0.27, -0.06*
Amyg → Amyg	-	*0.08*	*-0.19, 0.02*
NAcc → Hipp	-	0.08	-0.19, 0.02
NAcc → VTA/SN	+	0.09	-0.01, 0.19
VTA/SN → NAcc	+	0.09	-0.02, 0.20
VTA/SN → Hipp	-	0.14	-0.24, -0.03
VTA/SN → Amyg	+	0.16	0.06, 0.27
VTA/SN → DC	-	0.08	-0.18, 0.03
FEP-SCZ			
vmPFC → vmPFC	-	*0.19*	*-0.32, -0.05*
dlPFC → dlPFC	-	*0.10*	*-0.23, 0.04*
dlPFC → Thal	+	0.12	-0.01, 0.26
Thal → Thal	+	*0.13*	*-0.01, 0.26*
Hipp →Amyg	-	0.14	-0.27, -0.01
NAcc → Hipp	-	0.10	-0.23, 0.04
NAcc → VTA/SN	+	0.12	-0.02, 0.25
DC → Thal	-	0.12	-0.25, 0.02
VTA/SN → NAcc	+	0.13	0.00, 0.26
VTA/SN → Hipp	-	0.14	-0.27, -0.01
VTA/SN → Amyg	+	0.10	-0.04, 0.23
VTA/SN → DC	-	0.12	-0.26, 0.01
SCZ			
vmPFC → vmPFC	-	*0.09*	*-0.20, 0.03*
vmPFC → Hipp	+	0.16	0.05, 0.27
vmPFC → VTA/SN	+	0.08	-0.03, 0.20
dlPFC → Thal	-	0.17	-0.28, -0.06
Thal → Hipp	+	0.10	-0.01, 0.21
Thal → VTA/SN	-	0.15	-0.26, -0.04
Hipp → vmPFC	-	0.09	-0.21, 0.02
DC → Thal	+	0.09	-0.01, 0.20
VTA/SN → VTA/SN	-	*0.16*	*-0.28, -0.04*
VTA/SN → Amyg	-	0.11	-0.22, 0.01

VTA/SN → dlPFC	+	0.11	0.00, 0.22
Negative symptoms			
FEP			
dlPFC → dlPFC	+	*0.11*	*0.00, 0.22*
Amyg → Thal	-	0.09	-0.19, 0.01
Amyg → Hipp	+	0.11	0.00, 0.21
Hipp → Hipp	+	*0.12*	*0.01, 0.22*
NAcc → NAcc	+	*0.10*	*0.00, 0.21*
DC → VTA/SN	-	0.09	-0.19, 0.01
VTA/SN → Thal	-	0.11	-0.22, -0.01
FEP-SCZ			
vmPFC → Amyg	-	0.18	-0.31, -0.05
dlPFC → dlPFC	+	*0.10*	*-0.03, 0.24*
dlPFC → Thal	+	0.10	-0.04, 0.23
Thal → Amyg	+	0.17	0.03, 0.30
Amyg → Amyg	+	*0.13*	*0.00, 0.27*
Amyg → Thal	-	0.11	-0.24, 0.03
Amyg → Hipp	+	0.11	-0.03, 0.24
Hipp → Hipp	+	*0.13*	*0.00, 0.27*
SCZ			
Thal → Thal	-	*0.16*	*-0.28, -0.05*
Thal → vmPFC	+	0.09	-0.01, 0.20
Amyg → Amyg	-	*0.16*	*-0.27, -0.04*
NAcc → NAcc	-	*0.09*	*-0.20, 0.03*
NAcc → Hipp	-	0.10	-0.21. 0.02
NAcc → VTA/SN	+	0.11	0.00, 0.22
VTA/SN → Hipp	-	0.13	-0.24, -0.02
VTA/SN → dlPFC	-	0.11	-0.22, 0.00

All connections have the posterior probability (free energy) value of 1.00

All parameters for between region connections are in Hz. Self-connections are italicized, and values are log-transformed to ensure prior negativity (i.e., inhibitory) constraints on self-connections. A positive value for self-connection denotes increased inhibition, a negative value signifies reduced inhibition.

Positive and negative symptoms measured with BPRS Positive and Negative subscales.

Table B3. Summary of Connections Associated with PLEs (n= 26) and Striatal Dopamine Synthesis (n = 33) in the Healthy PLE/[^{18}F]DOPA Cohort

Connection	Positive (+) or negative (-) association	Effect size (Hz)	90% Posterior Credible Interval (lower bound, upper bound)
Positive PLEs			
vmPFC → vmPFC	-	*0.08*	*-0.22, 0.05*
dlPFC → vmPFC	-	0.09	-0.22, 0.04
dlPFC → VTA/SN	+	0.14	0.00, 0.28
Thal → Hipp	-	0.11	-0.24, 0.03
Amyg → Amyg	-	*0.21*	*-0.35, -0.06*
Amyg → Hipp	+	0.11	-0.02, 0.25
Amyg → NAcc	-	0.20	-0.33, -0.06
Amyg → VTA/SN	+	0.11	-0.03, 0.25
NAcc → Thal	+	0.09	-0.05, 0.23
DC → DC	-	*0.13*	*-0.26, 0.00*
VTA/SN → VTA/SN	-	*0.13*	*-0.27, 0.01*
VTA/SN → NAcc	+	0.24	0.10, 0.38
Negative PLEs			
vmPFC→ Hipp	+	0.12	-0.02, 0.25
vmPFC→ NAcc	-	0.13	-0.27, 0.01
dlPFC → Thal	-	0.19	-0.32, -0.06
dlPFC → DC	-	0.13	-0.27, 0.01
Hipp → NAcc	+	0.15	0.01, 0.28
Hipp → VTA/SN	-	0.09	-0.22, 0.04
Amyg → Amyg	+	*0.08*	*-0.06, 0.22*
Amyg → vmPFC	+	0.13	-0.01, 0.26
Amyg → VTA/SN	-	0.10	-0.24, 0.04
NAcc → Hipp	-	0.08	-0.22, 0.05
DC → VTA/SN	+	0.11	-0.02, 0.25
VTA/SN → VTA/SN	+	*0.10*	*-0.04, 0.24*
VTA/SN → Hipp	+	0.09	-0.05, 0.22
VTA/SN → Amyg	+	0.09	-0.05, 0.22
VTA/SN→ NAcc	-	0.08	-0.21, 0.05
Dopamine Synthesis			
Dorsal Striatum			
Thal → Thal	+	*0.09*	*-0.05, 0.22*
Thal → VTA/SN	+	0.12	-0.01, 0.25
Amyg → Thal	+	0.11	-0.02, 0.24

Thal → DC	+	0.10	-0.04, 0.23
DC → Thal	-	0.13	-0.26, 0.00
Ventral Striatum			
Hipp → Thal	+	0.16	0.02. 0.30
Hipp → VTA/SN	+	0.16	0.02, 0.29
Amyg → Thal	-	0.12	-0.25, 0.02
NAcc → Thal	-	0.10	-0.24, 0.03
Amyg → Amyg	-	*0.14*	*-0.28, 0.00*
NAcc → NAcc	-	*0.14*	*-0.28, 0.00*
VTA/SN → DC	+	0.12	-0.01, 0.25
DC → VTA/SN	-	0.12	-0.24, 0.01
DC → DC	+	*0.10*	*-0.03, 0.23*
NAcc → NAcc	+	*0.10*	*-0.05, 0.25*
VTA/SN → vmPFC	+	0.15	0.01, 0.29

All connections have the posterior probability (free energy) value of 1.00

All parameters for between region connections are in Hz. Self-connections are italicized, and values are log-transformed to ensure prior negativity (i.e., inhibitory) constraints on self-connections. A positive value for self-connection denotes increased inhibition, a negative value signifies reduced inhibition.

Positive and negative PLEs measured using CAPE Positive and Negative subscales.

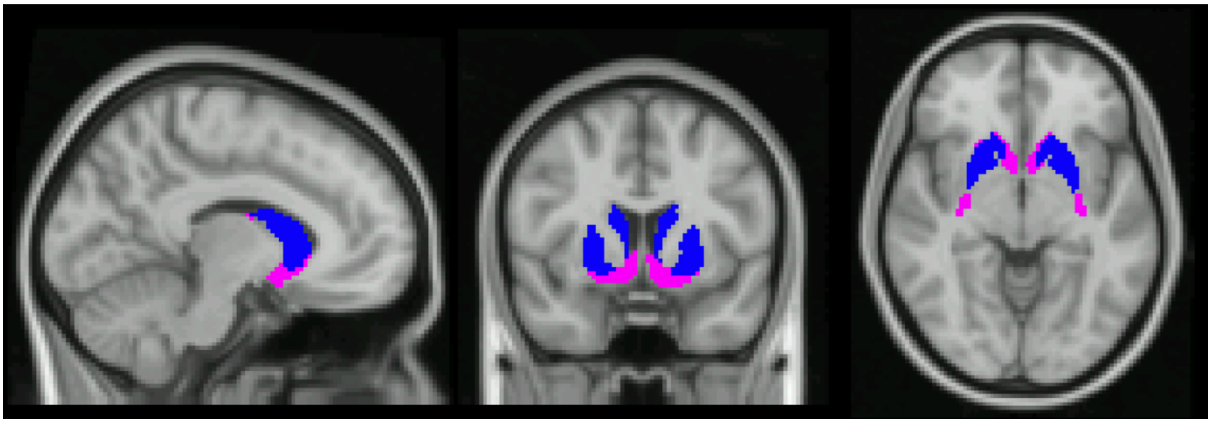

Figure B1. Parcellation of dorsal and ventral striatum used as regions of interest in PET quantification presented on the MNI 2mm template. The ventral striatum is in magenta and dorsal striatum is in blue. Striatal ROIs were registered to each person's anatomical template. PET analysis was restricted to the left hemisphere.

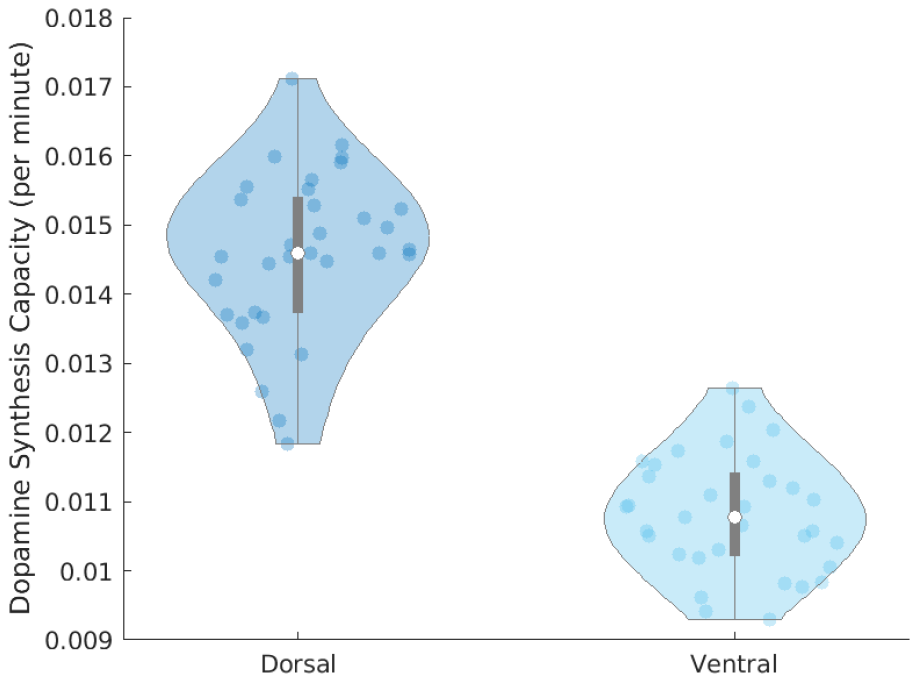

Figure B2. Dopamine synthesis values in dorsal and ventral striatal subdivisions in healthy participants. Distribution of dopamine synthesis values in the dorsal and ventral striatum. The central marks indicate median values. Gray boxes in the centre of violins indicate 25th and 75th percentile, respectively. The violins extend to extreme values that are not outliers.

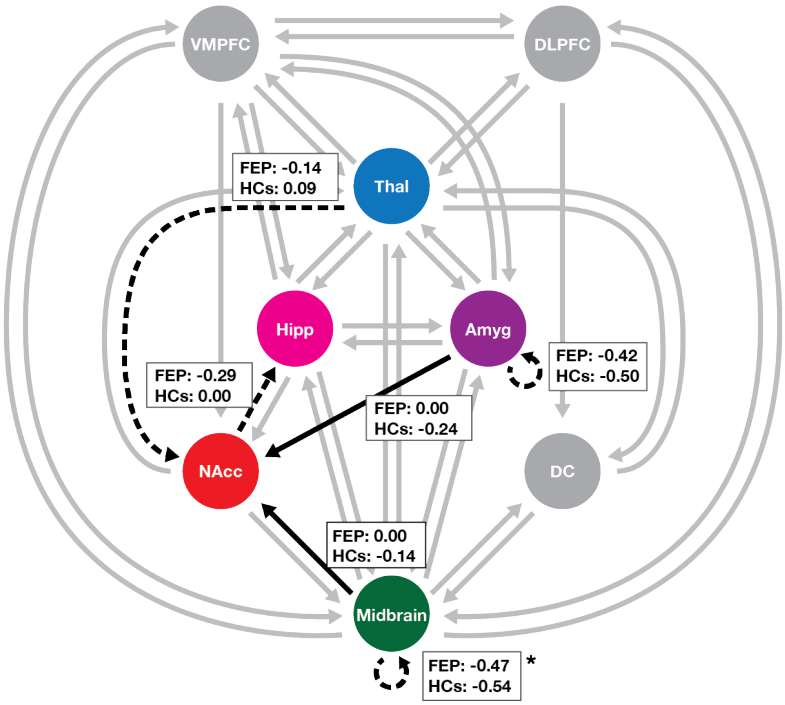

Figure B3. Group differences in effective connectivity parameters between FEP-SCZ patients (n = 17) and healthy controls (n = 23). Boxes show mean connectivity values in each group. Colours of regions in the top panel correspond with the colours in connectivity diagrams. For connections between regions, dashed arrows represent connections for which patients show a greater inhibitory influence compared to controls; solid arrow represents connections for which patients show greater excitatory, or less inhibitory, influence compared to controls. For self-connections, dashed arrows represent reduced inhibition (i.e., lower negative values) in patients compared to controls. Gray arrows represent modelled connections that were not (significantly) different from the prior. All connectivity parameters are in Hz, including self-connections. Connections were thresholded at Pp > 0.95.

* denotes mean connections that were derived from the DCM PEB routine as these connections were removed in the subsequent Bayesian model averaging routine.

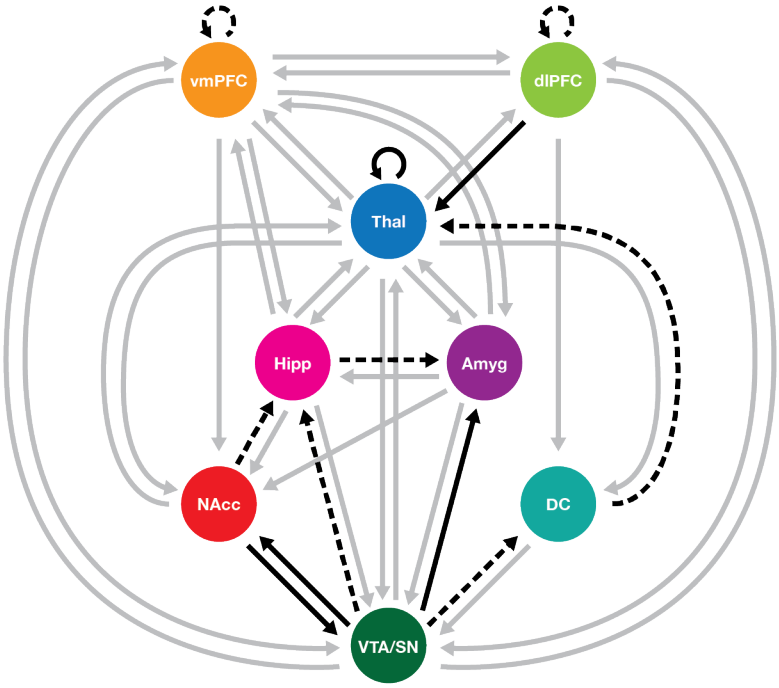

Figure B4. Associations between severity of positive psychosis-like experiences (PLEs) and effective connectivity parameters in FEP-SCZ patients (n = 17). Solid arrows: positive associations between effective connectivity parameters and positive PLEs; dashed arrows: negative associations between effective connectivity parameters and positive PLEs; grey arrows: associations that were not (significantly) different from the prior. Connections were thresholded at Pp > 0.95.

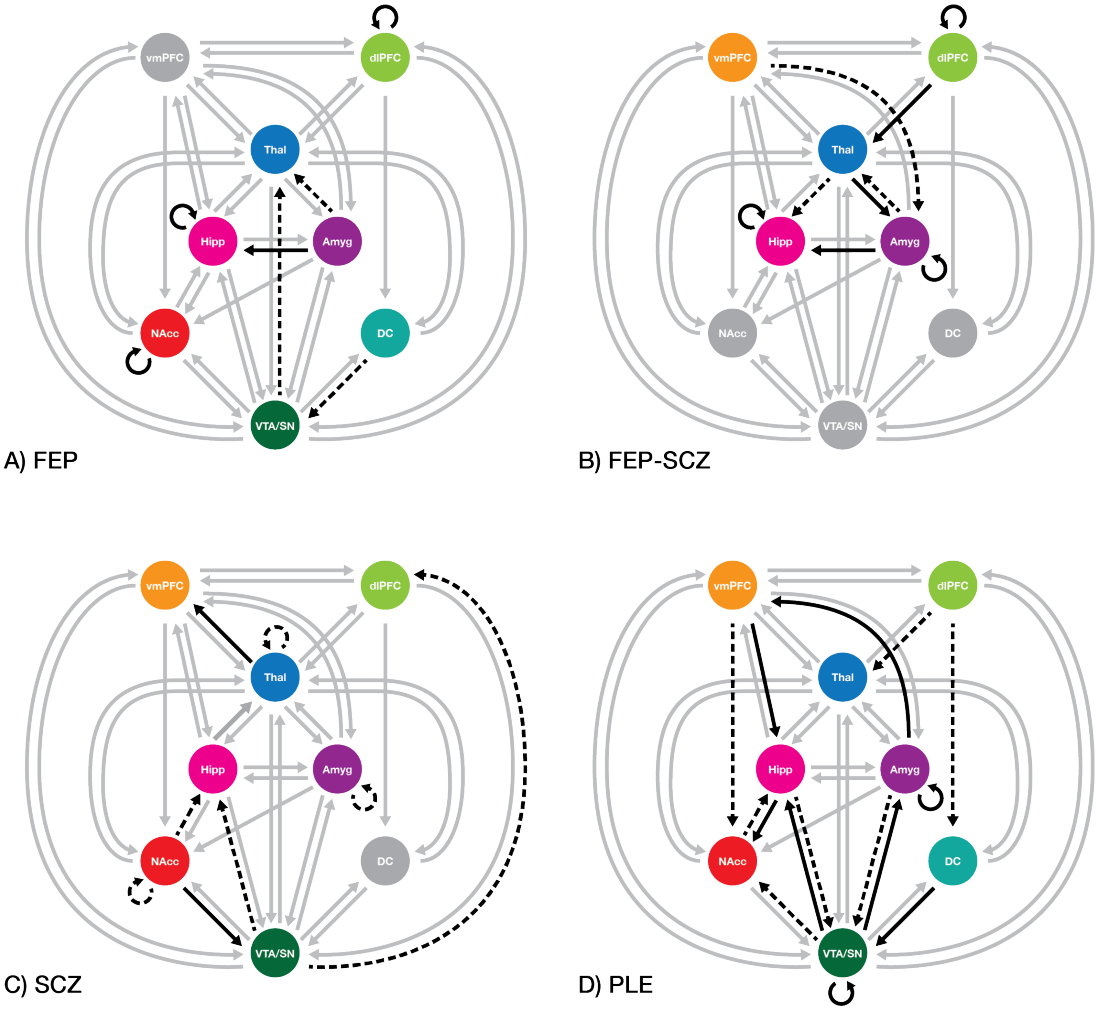

Figure B5. Associations between severity of negative symptomatology and effective connectivity parameters across all cohorts. Panels depict associations in (A) FEP (n = 46), (B) FEP-SCZ (n = 17), (C) SCZ (n = 36), and (D) PLE (n = 26) groups. Solid arrows: positive associations between effective connectivity parameters and negative PLEs/symptoms; sashed arrows: negative associations between effective connectivity parameters and negative PLEs/symptoms; grey arrows: associations that were not (significantly) different from the prior. Connections were thresholded at Pp > 0.95.

Supplementary materials for Chapter 4

Appendix C

C.1. Supplementary methods and materials

Measures of Psychosis-Like Experiences

The Oxford-Liverpool Inventory of Feelings and Experiences short-form (sO-LIFE) (Mason et al., 2005)**.** The sO-LIFE is a self-report measure of schizotypy traits in the general population. It consists of 43 items that are grouped into four dimensions: Unusual Experiences (12 items), Cognitive Disorganisation (11 items), Introvertive Anhedonia (10 items), and Impulsive Nonconformity (10 items). Each item is scored on a binary scale (0 = *'no'*; 1 = *'yes'*).

Peters Delusion Inventory 21-item (PDI-21) (Peters et al., 2004)**.** PDI-21 is a self-report measure assessing delusional ideation in the general population. The measure comprises four dimensions: PDI yes/no, distress, preoccupation, and conviction. For the present study, we used the PDI yes/no dimension to assess the presence of delusions in our sample. Items are measured on a binary scale (0 = *'no'*; 1 = *'yes'*), hence yielding a total score ranging from 0 to 21.

Community Assessment of Psychotic Experience (CAPE) (Stefanis et al., 2002)**.** CAPE is a self-report measure of subthreshold PLEs designed for the general population. It consists of 42 items that yield three dimensions of PLEs: positive, negative, and depressive. Positive experiences are measured by 20 items, negative experiences are measured by 14 items, and depressive experiences are measured by 8 items. A 4-point Likert scale measures the frequency of experiences (1 = *'never'*; 4 = *'nearly always'*). A separate score for each dimension can also be obtained by summing up the scores of a subscale yielding to possible maximum scores of 80, 32, and 56 for the positive, negative, and depressive

subscales, respectively. A distress scale also accompanies each of the three dimensions of experiences, measured using a 4-point Likert scale (1 = '*not distressed'*; 4 = '*very distressed*').

Wisconsin Schizotypy Scales. Four subscales were administered to measure PLEs: 1) the magical ideation scale (Eckblad & Chapman, 1983) – 30 items measuring metaphysical beliefs, 2) the perceptual aberration scale (Chapman et al., 1978) – 35 items assessing perceptual abnormalities pertaining to body image, 3) the physical anhedonia scale (Chapman et al., 1976) – 61 items measuring deficits in the ability to experience pleasure, and 4) the revised social anhedonia scale (Chapman et al., 1976) – 40 items measuring social withdrawal or indifference.

Regions of interest (ROIs) selection for dynamic causal modelling

Nucleus accumbens (NAcc) and dorsal caudate (DC). For the ventral and dorsal striatum, we seeded the NAcc and DC consistent with our previous works (Dandash, Harrison, et al., 2014; Fornito et al., 2013; Sabaroedin et al., 2019) using a functional parcellation of the striatum (Di Martino et al., 2008) that was delineated based on a meta-analysis of striatal activation in fMRI and PET studies (Postuma & Dagher, 2006).

DLPFC. To capture variations associated with risk for psychosis as well as disruptions in clinical groups, the DLPFC ROI was selected based on a peak in which functional connectivity with the DC was reduced in the healthy relatives of FEP patients compared to healthy controls (Fornito et al., 2013). This peak overlapped with an area that also showed reduced connectivity in patients.

VMPFC. To choose a region that was most relevant to the ventral circuit, we chose a peak in the VMPFC that showed strong functional connectivity with the NAcc in an independent cohort of 353 healthy adults (Sabaroedin et al., 2019).

Thalamus. The thalamus coordinate was selected from a peak in which functional connectivity with the dorsal caudate was reduced in ARMS individuals compared to healthy controls (Dandash, Harrison,

et al., 2014). For VMPFC and thalamus ROIs with centroids that were close to the anatomical or functional boundary of the region, we used an anatomical mask when extracting the first eigenvariate for the ROIs to exclude signal from neighbouring regions.

Hippocampus, amygdala, and midbrain. ROIs for the three regions were selected using a similar method. Peak coordinates within anatomical masks for the hippocampus and amygdala were selected in a group-level functional connectivity of the ROIs with the whole brain in a large independent cohort (Sabaroedin et al., 2019). For the hippocampus, we chose the anterior region using of a hippocampal mask provided in the Freesurfer package (Fischl et al., 2002). The anterior hippocampus is a hippocampal region that is most associated with schizophrenia (Small et al., 2011), and it was defined as the region having the MNI coordinate of less than y = -22 (Zeidman & Maguire, 2017). Similar to the hippocampus, we used an amygdala mask provided in Freesurfer. The midbrain mask was delineated based on the functional connectivity of the ventral tegmental (VTA) and substantia nigra (SN) (Murty et al., 2014). Due to the spatial resolution of fMRI images, we combined both of the dorsal and ventral midbrain regions and selected an activation peak in the same cohort that was used in the selection of our hippocampal, amygdala, and VMPFC ROIs.

Spectral dynamic causal modelling

Dynamic causal modelling (DCM) is Bayesian framework that infers the directed (causal) connectivity among the neuronal systems – referred to as effective connectivity. A new DCM for resting state fMRI was recently proposed based upon a deterministic model that generates predicted cross spectra, referred to as spectral DCM. In order to model resting state activity – in the absence of external stimuli – a stochastic component capturing neural fluctuations is included in the model.

Mathematically, we can express the formulation of the stochastic generative model as a set of two equations. First is the neuronal state equation, namely

$$\dot{x}(t) = f(x(t), u(t), \theta) + v(t), \tag{S1}$$

and second is the observation equation, which is a static nonlinear mapping from the hidden physiological states in (1) to the observed BOLD activity, and is written as:

$$y(t) = h(x(t), \varphi) + e(t), \tag{S2}$$

where $\dot{x}(\mathrm{t})$ is the rate of change of the neuronal states $x(t)$, θ are unknown parameters (i.e., the effective connectivity) and $v(t)$ (resp. $e(t)$) is the stochastic process – called the state noise (resp. the measurement or observation noise) – modelling the random neuronal fluctuations that drive the resting state activity. In the observation equations, φ are the unknown parameters of the (haemodynamic) observation function and $u(t)$ represents any exogenous (or experimental) inputs that drive the hidden states – that are usually absent in resting state designs (Friston et al., 2014). Spectral DCM furnishes a constrained inversion of the stochastic model by parameterising the neuronal fluctuations $v(t)$. Spectral DCM simplifies the generative model by replacing the original timeseries with their second-order statistics (i.e., cross spectra). This means, instead of estimating time varying hidden states, we are estimating their covariance, which is time invariant. Then we simply need to estimate the covariance of the random fluctuations; where a scale free (power law) form for the state noise (resp. observation noise) is used—motivated from previous work on neuronal activity (Beggs & Plenz, 2003; Shin & Kim, 2006; Stam & De Bruin, 2004)—as follows:

$$g_v(\omega, \theta) = \alpha_v \omega^{-\beta_v}$$

$$g_e(\omega, \theta) = \alpha_e \omega^{-\beta_e} \tag{S3}$$

Here, $\{\alpha, \beta\} \subset \theta$ are the parameters controlling the amplitudes and exponents of the spectral density of the neural fluctuations. The parameterisation of endogenous fluctuations means that the states are no longer probabilistic; hence the inversion scheme is significantly simpler, requiring estimation of only the parameters (and hyperparameters) of the model.

We used standard Bayesian model inversion to infer the parameters of the model in (1), (2) and (3), from the observed signal $y(t)$. The description of the Bayesian model inversion procedures based on variational Laplace can be found elsewhere for the interested readers (Friston et al., 2007; Friston et al., 2003; Razi & Friston, 2016) .

Parametric Empirical Bayes

Empirical Bayes refers to the Bayesian inversion or fitting of hierarchical models. In hierarchical models, constraints on the posterior density over model parameters at any given level are provided by the level above. These constraints are called empirical priors because they are informed by empirical data. A hierarchical Parametric Empirical Bayes (PEB) model for DCM parameters was recently introduced, which represents how individual (within-subject) connections derive from the subjects' group membership (Friston et al., 2016). Mathematically, for DCM studies with *N* subjects and *M* parameters per DCM, we have a hierarchical model, where the responses of the *i*-th subject and the distribution of the parameters over subjects can be modelled as:

$$y_i = \Gamma_i^{(1)}(\theta^{(1)}) + \varepsilon_i^{(1)} \qquad \text{(S4)}$$

$$\theta^{(1)} = \Gamma^{(2)}\left(\theta^{(2)}\right) + \varepsilon^{(2)}$$

$$\theta^{(2)} = \eta + \varepsilon^{(3)}$$

where, y_i is the BOLD time series from *i-th* subject *and* $\Gamma_i^{(1)}$ is a nonlinear mapping from the parameters of a model to the predicted response y, which in this study was the model in Eq. S1 above. $\varepsilon_i^{(1)}$ is independent and identically distributed (i.i.d.) observation noise (equivalent to $e(t)$ in Eq. S2). In this hierarchical form, *empirical priors* encoding second (between-subject) level effects place constraints on subject-specific parameters. The second level would be a linear model where the random effects are parameterised in terms of their precision:

$$\Gamma^{(2)}\left(\theta^{(2)}\right) = (X \otimes W)\beta$$

where, $\beta \subset \theta$ are group means or effects encoded by a design matrix with between X and within-subject W parts. The between-subject part encodes differences among subjects or covariates such as age, while the within-subject part specifies mixtures of parameters that show random effects. We assume that the first column of the design matrix is a constant term, modelling group means and subsequent columns encode group differences.

Table C1. Proportion of Participants with Missing Data for Variable Used as Indicators for the Bifactor Model of the Psychosis Spectrum

Variables	*N*	Missing		Univariate Outliers
		N	%	
Delusions SSE	726	0	0.0	0
Hallucinations SSE	726	0	0.0	0
Cognitive Disorganisation SSE	675	51	7.0	0
Perceptual Aberration SSE	726	0	0.0	0
Anhedonia SSE	726	0	0.0	0
Asociality SSE	724	2	0.3	0
Avolition SSE	693	33	4.5	0
Blunted Affect SSE	724	2	0.3	0
Alogia SSE	724	2	0.3	0

Note. $N = 727$. SSE = Item response theory scale score estimates. Little's MCAR test [$\chi^2(57) = 54.316$, $p = .576$]. One multivariate outlier [$\chi^2(11) = 31.313$, $p < .001$].

Table C2. Summary of Fit Statistics for Parametric Unidimensional Item Response Theory Models

Model	*df*	M_2	*p*	$RMSEA_2$ [90% *CI*]	-2**LL*	BIC
Delusions [1]					22954.80	23626.87
Hallucinations	271	48.60	.050	.020 [.013, .026]	3144.47	3253.00
Cognitive Disorganisation	44	66.81	.015	.020 [.000,.034]	9058.08	9207.31
Perceptual Aberration	350	644.99	<.001	.030 [.026, .034]	11583.24	11952.22
Anhedonia	739	1110.65	<.001	.030 [.027, .033]	21822.33	22336.27
Asociality	628	1117.43	<.001	.030 [.027, .033]	22604.51	23078.91
Avolition	164	288.46	<.001	.030 [.024, .036]	8816.31	9000.80
Blunted Affect	61	67.39	.267	.010 [.000, .025]	5746.77	5865.37
Alogia	1	2.45	.119	.040 [.000, 0.116]	2539.70	2579.24

Note. [1] Model fit statistics, including the M_2 and $RMSEA_2$, based on one- and two-way marginal tables could not be calculated for the Delusions scale due the large number of items and data sparsity. $N = 727$.

Table C3. Delusions Item Statistics and Parameter Estimates

SUBSCALE	ITEM	$S\text{-}\chi^2$	*df*	*p*	λ	*SE*	α	*se*	b_1	*se*	b_2	*se*	b_3	*se*
PDI-21	11	33.92	30	0.2832	0.56	0.1	1.16	0.18	2.42	0.28				
	14	29.62	31	0.5383	0.49	0.09	0.95	0.14	2.23	0.27				
	17	18.54	31	0.9623	0.57	0.09	1.19	0.16	2.02	0.21				
	21	31.55	27	0.2486	0.51	0.11	1.01	0.17	2.73	0.37				
WSS Magical Ideation	1	22.52	27	0.7113	0.59	0.1	1.23	0.18	2.41	0.27				
	3	48.73	32	0.0293	0.47	0.09	0.9	0.12	1.77	0.21				
	8	15.98	29	0.9759	0.56	0.07	1.14	0.12	0.37	0.08				
	9	26.25	29	0.6134	0.57	0.07	1.19	0.13	0.9	0.1				
	10	34.9	23	0.0531	0.67	0.06	1.54	0.15	0.05	0.07				
	12	38.97	29	0.1019	0.7	0.07	1.67	0.19	1.53	0.12				
	13	38.13	30	0.1461	0.68	0.07	1.59	0.17	1.28	0.1				
	14	20.97	29	0.8605	0.66	0.07	1.49	0.15	1.03	0.09				
	15	38.62	32	0.1948	0.45	0.09	0.84	0.12	1.8	0.23				
	17	29.65	31	0.5364	0.58	0.08	1.22	0.15	1.76	0.17				
	18	25.45	32	0.7879	0.56	0.08	1.13	0.14	1.74	0.18				
	20	36.44	31	0.2296	0.46	0.09	0.89	0.13	2.06	0.26				
	21	31.34	32	0.5011	0.54	0.08	1.09	0.14	1.81	0.19				
	24	27.95	28	0.4684	0.64	0.08	1.41	0.18	1.91	0.18				
	25	26.22	28	0.5623	0.72	0.07	1.75	0.21	1.67	0.13				
	27	26.26	26	0.4503	0.55	0.1	1.11	0.17	2.44	0.29				
	28	19.47	24	0.7272	0.81	0.06	2.35	0.29	1.66	0.11				
*s*O-LIFE Unusual Experiences	6	30.84	27	0.2772	0.71	0.08	1.71	0.22	1.82	0.15				
	10	19.41	18	0.3688	0.79	0.07	2.21	0.32	2.01	0.15				
	15	29.52	27	0.3352	0.64	0.07	1.41	0.15	0.66	0.08				
	27	35.97	27	0.1157	0.7	0.07	1.64	0.18	1.08	0.09				
	33	22.62	26	0.6555	0.73	0.06	1.81	0.19	1	0.08				
	38	15.47	24	0.9065	0.83	0.05	2.48	0.29	1.33	0.08				
	40	34.03	30	0.279	0.66	0.08	1.48	0.18	1.59	0.14				
CAPE Positive	5	34.47	32	0.3498	0.69	0.08	1.6	0.2	1.86	0.15	3.58	0.38	4.87	0.78
	6	66.53	63	0.3558	0.48	0.07	0.93	0.1	-1.35	0.16	2.16	0.21	4.63	0.51
	7	43.04	38	0.2636	0.5	0.09	0.97	0.13	1.75	0.2	4.69	0.61	7.23	1.34
	10	29.33	31	0.5534	0.65	0.09	1.45	0.2	2.15	0.21	3.93	0.48	4.72	0.69
	13	74.12	75	0.5078	0.56	0.06	1.16	0.1	-0.45	0.09	1.63	0.14	3.06	0.26
	15	59.85	39	0.0174	0.74	0.06	1.84	0.18	1.07	0.08	2.72	0.21	3.41	0.31
	17	73.88	67	0.2631	0.55	0.07	1.12	0.11	0.65	0.09	2.48	0.22	3.71	0.37
	20	53.92	48	0.2577	0.68	0.07	1.56	0.17	1.5	0.12	2.65	0.23	3.22	0.3
	24	19.25	14	0.1553	0.87	0.05	2.95	0.42	1.93	0.12	3.27	0.32	3.6	0.43
	26	16.97	24	0.8504	0.8	0.06	**2.23**	0.27	1.69	0.11	3.34	0.32		
	31	30.34	34	0.6484	0.76	0.06	1.97	0.23	1.63	0.11	2.88	0.24	3.56	0.36
	41	9.82	11	0.548	0.81	0.08	2.35	0.38	2.31	0.19	3.86	0.52		

Note. Marginal reliability for pattern response scores = .84

Table C4. Hallucinations Item Statistics and Parameter Estimates

SUBSCALE	ITEM	$S\text{-}\chi^2$	*df*	*p*	λ	*SE*	α	*se*	b_1	*se*	b_2	*se*	b_3	*se*
WSS Magical Ideation	5	1.45	3	0.695	0.63	0.10	1.39	0.21	1.01	0.12				
sO-LIFE Unusual Experiences	1	2.90	3	0.408	0.57	0.10	1.19	0.19	0.34	0.09				
	32	1.11	4	0.894	0.55	0.10	0.13	0.18	1.01	0.14				
CAPE Positive	33	9.91	4	0.042	0.87	0.06	3.05	0.53	1.64	0.14	2.84	0.29	3.51	0.48
	34	2.95	1	0.087	0.93	0.05	4.35	0.93	2.11	0.17	3.16	0.39		
	42	4.67	5	0.459	0.82	0.11	2.44	0.61	2.08	0.18	3.47	0.47		

Note. Marginal reliability for pattern response scores = .50

Table C5. Disorganisation / Formal Thought Disorder Item Statistics and Parameter Estimates

SUBSCALE	ITEM	*S-χ²*	*df*	*p*	λ	*SE*	α	*se*	b_1	*se*
*s*O-LIFE Cognitive Distortion	2	7.34	9	0.603	0.58	0.08	1.22	0.15	0.30	0.08
	9	6.21	9	0.720	0.43	0.09	0.80	0.12	0.52	0.12
	12	2.63	9	0.977	0.5	0.08	0.99	0.13	0.59	0.11
	16	6.77	9	0.662	0.61	0.08	1.29	0.15	0.17	0.08
	17	16.3	9	0.061	0.67	0.08	1.54	0.18	0.61	0.08
	22	5.99	9	0.742	0.62	0.08	1.35	0.16	0.46	0.08
	26	8.47	9	0.489	0.55	0.09	1.12	0.15	1.06	0.13
	36	6.32	9	0.708	0.64	0.07	1.42	0.16	0.05	0.07
	39	5.62	9	0.778	0.59	0.08	1.24	0.15	-0.12	0.08
	41	4.18	8	0.841	0.64	0.07	1.43	0.17	-0.31	0.08
	43	9.28	9	0.414	0.63	0.08	1.39	0.16	0.21	0.07

Note. Marginal reliability for pattern response scores = .74

Table C6. Body Image Aberration Item Statistics and Parameter Estimates

SUBSCALE	ITEM	*S-χ²*	*df*	*p*	λ	*SE*	α	*se*	b_1	*se*
WSS Perceptual Aberration	1	17.28	15	0.301	0.78	0.06	2.12	0.24	1.31	0.09
	2	17.37	15	0.297	0.83	0.05	2.54	0.29	1.24	0.08
	3	17.18	16	0.376	0.66	0.07	1.47	0.16	1.03	0.09
	6	14.85	16	0.537	0.49	0.08	0.97	0.13	1.33	0.16
	7	19.17	15	0.206	0.83	0.06	2.53	0.33	1.65	0.11
	8	39.24	16	0.001	0.84	0.06	2.66	0.41	1.93	0.13
	9	16.07	16	0.450	0.63	0.09	1.36	0.18	1.93	0.18
	11	16.73	15	0.337	0.61	0.07	1.30	0.14	0.82	0.09
	12	19.15	12	0.085	0.72	0.06	1.74	0.17	0.43	0.06
	14	13.95	16	0.603	0.82	0.07	2.40	0.36	1.96	0.14
	15	20.53	16	0.197	0.70	0.07	1.67	0.18	1.30	0.10
	16	11.76	14	0.626	0.87	0.05	3.04	0.42	1.64	0.10
	17	22.2	16	0.137	0.66	0.09	1.51	0.20	1.98	0.18
	18	33.73	18	0.014	0.69	0.14	1.61	0.38	3.06	0.47
	19	7.17	8	0.520	0.54	0.11	1.08	0.18	2.65	0.35
	20	19.12	16	0.262	0.80	0.07	2.26	0.32	1.92	0.14
	22	15.92	15	0.389	0.75	0.07	1.91	0.25	1.78	0.14
	23	18.82	18	0.405	0.69	0.07	1.61	0.19	1.52	0.12
	25	15.41	16	0.496	0.72	0.08	1.75	0.23	1.88	0.16
	26	20.27	17	0.260	0.66	0.10	1.49	0.24	2.38	0.26
	28	16.01	18	0.593	0.73	0.08	1.84	0.27	2.06	0.18
	29	14.51	17	0.632	0.70	0.10	1.68	0.27	2.37	0.24
	30	17.73	15	0.276	0.67	0.07	1.53	0.17	1.23	0.10
	31	10.46	16	0.8418	0.79	0.07	2.19	0.32	1.95	0.15
	32	15.37	15	0.4267	0.81	0.07	2.38	0.36	2.01	0.15
	33	13.16	15	0.5909	0.85	0.06	2.75	0.4	1.81	0.12
	34	12.12	14	0.5978	0.70	0.08	1.65	0.23	1.97	0.17
	35	13.74	17	0.686	0.68	0.07	1.60	0.18	1.47	0.12

Note. Marginal reliability for pattern response scores = .74

Table C7. Anhedonia Item Statistics and Parameter Estimates

SUBCALE	ITEM	*S-*χ^2	*df*	*p*	λ	*SE*	α	*se*	b_1	*se*
WSS	7	17.01	20	0.6535	0.34	0.11	0.61	0.14	3.47	0.71
Physical	8	24.42	18	0.1415	0.41	0.12	0.75	0.16	3.30	0.60
Anhedonia	10	29.73	21	0.0972	0.46	0.11	0.89	0.16	2.75	0.41
	12	15.31	19	0.7036	0.44	0.08	0.83	0.12	1.32	0.18
	13	27.19	21	0.1641	0.52	0.08	1.05	0.13	1.45	0.16
	14	29.48	22	0.1313	0.4	0.08	0.73	0.11	1.15	0.18
	15	19.54	16	0.241	0.82	0.07	2.47	0.36	1.80	0.12
	16	15.33	18	0.6404	0.5	0.13	0.99	0.21	3.35	0.56
	18	29.27	22	0.1368	0.45	0.1	0.87	0.14	2.25	0.30
	19	12.33	20	0.9045	0.27	0.13	0.48	0.15	4.87	1.40
	20	23.59	22	0.3706	0.41	0.09	0.77	0.12	2.07	0.29
	22	24.1	21	0.2877	0.48	0.08	0.94	0.12	1.23	0.15
	24	36.63	23	0.0354	0.36	0.11	0.65	0.14	3.29	0.63
	25	11.31	7	0.1253	0.8	0.1	2.25	0.45	2.67	0.26
	27	17.41	21	0.6867	0.41	0.08	0.76	0.11	0.30	0.11
	28	25.21	21	0.2376	0.47	0.11	0.9	0.16	2.81	0.42
	29	10.58	18	0.9115	0.5	0.13	0.99	0.2	3.27	0.53
	30	27.04	22	0.209	0.33	0.09	0.6	0.1	1.41	0.25
	31	24.57	21	0.2655	0.41	0.09	0.76	0.12	1.80	0.25
	33	13.21	18	0.7796	0.39	0.14	0.73	0.17	3.88	0.82
	35	15.85	19	0.6679	0.53	0.12	1.06	0.2	3.00	0.44
	36	10.72	18	0.9063	0.44	0.13	0.82	0.17	3.38	0.60
	37	19.48	19	0.4278	0.31	0.08	0.55	0.1	-0.66	0.18
	38	19.71	15	0.1827	0.8	0.07	2.29	0.35	2.07	0.16
	39	19.44	20	0.4947	0.61	0.08	1.30	0.17	1.78	0.17
	40	30.77	22	0.1007	0.32	0.09	0.58	0.11	2.30	0.42
	43	18.84	19	0.4686	0.37	0.13	0.67	0.16	3.83	0.82
	45	22.86	20	0.2948	0.61	0.07	1.30	0.15	1.10	0.11
	46	23.75	20	0.2527	0.57	0.10	1.17	0.18	2.41	0.28
	47	25.3	19	0.1506	0.56	0.10	1.16	0.18	2.46	0.29
	49	35.78	23	0.0433	0.46	0.09	0.89	0.14	2.15	0.28
	50	20.09	21	0.5169	0.31	0.12	0.56	0.14	3.97	0.92
	51	16.88	14	0.2618	0.47	0.16	0.90	0.24	4.07	0.9
	52	11.61	17	0.8236	0.53	0.08	1.08	0.12	-0.16	0.08
	54	25.37	20	0.1873	0.58	0.08	1.22	0.16	1.70	0.17
	56	35.15	20	0.0193	0.57	0.08	1.19	0.14	1.11	0.11
	58	23.77	20	0.2521	0.54	0.08	1.10	0.13	0.95	0.11
	59	33.48	22	0.0553	0.51	0.08	1.00	0.13	1.45	0.16
	61	15.36	19	0.7005	0.48	0.11	0.94	0.16	2.72	0.38
*s*O-LIFE Introvertive Anhedonia	8	23.81	20	0.25	0.58	0.09	1.20	0.17	1.91	0.20

SUBSCALE	ITEM	*S-*χ^2	*df*	*p*	λ	*SE*	α	*se*	b_1	*se*	b_2	*se*	b_3	*se*
CAPE Negative	37	82.92	56	0.011	0.32	0.08	0.57	0.09	-0.16	0.14	3.03	0.47	5.88	0.93

Note. Marginal reliability for pattern response scores = .76.

Table C8. Asociality Item Statistics and Parameter Estimates

SUBSCALE	ITEM	*S-χ²*	*df*	*p*	*λ*	*SE*	*α*	*se*	b_1	*se*
WSS Social Anhedonia	1	22.83	19	0.244	0.75	0.08	1.91	0.27	1.98	0.16
	2	11.01	16	0.809	0.79	0.08	2.20	0.35	2.15	0.17
	3	19.05	21	0.583	0.66	0.08	1.51	0.18	1.61	0.14
	4	23.52	24	0.491	0.42	0.08	0.79	0.11	1.54	0.21
	6	26.61	24	0.322	0.34	0.09	0.61	0.10	1.85	0.31
	7	26.39	23	0.282	0.52	0.09	1.03	0.14	1.86	0.21
	8	22.49	22	0.433	0.62	0.08	1.33	0.16	1.53	0.14
	10	22.42	20	0.317	0.51	0.07	1.00	0.11	0.36	0.10
	11	28.26	19	0.078	0.58	0.10	1.21	0.18	2.29	0.25
	12	29.42	24	0.204	0.19	0.09	0.33	0.10	3.36	0.97
	13	32.08	21	0.057	0.52	0.07	1.05	0.12	0.48	0.10
	14	23.91	21	0.297	0.53	0.07	1.07	0.12	0.48	0.10
	15	18.23	18	0.443	0.67	0.10	1.54	0.25	2.48	0.26
	16	24.02	22	0.346	0.56	0.07	1.14	0.13	0.85	0.11
	18	19.36	21	0.563	0.49	0.08	0.95	0.12	1.20	0.15
	19	10.57	16	0.836	0.74	0.09	1.89	0.29	2.20	0.19
	21	17.66	21	0.671	0.66	0.07	1.50	0.17	1.24	0.11
	22	21.85	19	0.291	0.62	0.07	1.35	0.14	0.79	0.09
	25	19.38	20	0.499	0.53	0.11	1.07	0.19	2.92	0.41
	26	34.50	22	0.044	0.45	0.10	0.86	0.14	2.31	0.31
	28	16.75	19	0.608	0.76	0.07	1.98	0.27	1.53	0.11
	29	24.70	22	0.311	0.47	0.09	0.90	0.13	1.94	0.24
	30	21.47	23	0.554	0.28	0.08	0.50	0.09	0.39	0.17
	31	28.59	23	0.194	0.41	0.09	0.77	0.11	1.79	0.25
	32	17.32	19	0.569	0.69	0.09	1.60	0.22	2.14	0.20
	33	36.82	24	0.045	0.17	0.10	0.30	0.11	4.96	1.73
	34	23.50	19	0.215	0.77	0.07	2.06	0.28	1.34	0.09
	35	18.49	21	0.619	0.45	0.08	0.85	0.11	1.00	0.14
	37	22.44	22	0.435	0.52	0.08	1.03	0.12	0.97	0.12
	38	24.48	21	0.270	0.68	0.08	1.59	0.19	1.28	0.10
	39	29.57	21	0.101	0.55	0.08	1.11	0.14	1.32	0.14
	40	22.15	21	0.393	0.55	0.08	1.11	0.13	1.23	0.13
sO-LIFE Introvertive Anhedonia	34	27.08	22	0.208	0.65	0.08	1.44	0.19	1.39	0.12

SUBSCALE	ITEM	*S-χ²*	*df*	*p*	*λ*	*SE*	*α*	*se*	b_1	*se*	b_2	*se*	b_3	*se*
CAPE Negative	16	47.49	41	0.2246	0.6	0.06	1.28	0.12	-0.33	0.09	2.39	0.19	4.65	0.52
											2.39	0.19	4.65	0.52

Note. Marginal reliability for pattern response scores = .82

Table C9. Avolition Item Statistics and Parameter Estimates

SUBSCALE	ITEM	$S\text{-}\chi^2$	*df*	*p*	λ	*SE*	α	*se*	b_1	*se*				
sO-Life Cognitive Disorganisation	39	11.61	10	0.314	0.67	0.07	1.52	0.16	-0.11	0.07				
	43	8.39	12	0.755	0.52	0.08	1.03	0.12	0.24	0.09				
SUBSCALE	**ITEM**	$S\text{-}\chi^2$	*df*	*p*	λ	*SE*	α	*se*	b_1	*se*	b_2	*se*	b_3	*se*
CAPE Negative	18	36.54	21	0.019	0.86	0.04	2.86	0.28	-1.27	0.08	0.85	0.06	2.21	0.13
	21	23.03	25	0.577	0.74	0.05	1.85	0.16	-1.27	0.1	1.24	0.09	2.72	0.19
	25	31.49	26	0.210	0.68	0.05	1.6	0.14	-0.42	0.07	1.57	0.12	3.21	0.26
	29	25.99	24	0.356	0.48	0.07	0.92	0.11	-0.08	0.1	3.48	0.38	6.06	0.82
	35	28.12	27	0.406	0.58	0.07	1.2	0.12	0.05	0.08	2.71	0.24	4.53	0.5
	36	28.44	23	0.199	0.75	0.05	1.92	0.17	-0.38	0.07	1.65	0.11	3.01	0.23

Note. Marginal reliability for pattern response scores = .81

Table C10. Blunted Affect Item Statistics and Parameter Estimates

SUBSCALE	ITEM	$S\text{-}\chi^2$	*df*	*p*	λ	*SE*	α	*se*	b_1	*se*	b_2	*se*	b_3	*se*
CAPE Negative	3	38.92	25	0.037	0.53	0.07	1.06	0.11	0.00	0.09	1.90	0.18	3.47	0.34
	8	14.11	17	0.661	0.83	0.04	2.57	0.25	0.14	0.05	1.45	0.09	2.52	0.16
	27	12.08	16	0.739	0.86	0.04	2.93	0.31	0.18	0.05	1.49	0.09	2.58	0.17
	32	21.15	19	0.328	0.81	0.04	2.37	0.22	0.17	0.06	1.73	0.11	2.81	0.20

Note. Marginal reliability for pattern response scores = .74

Table C11. Alogia Item Statistics and Parameter Estimates

SUBSCALE	ITEM	$S\text{-}\chi^2$	*df*	*p*	λ	*SE*	α	*se*	b_1	*se*				
WSS Social Anhedonia	23	11.71	2	0.427	0.57	0.27	118	0.50	0.51	0.17				
SUBSCALE	**ITEM**	$S\text{-}\chi^2$	*df*	*p*	λ	*SE*	α	*se*	b_1	*se*	b_2	*se*	b_3	*se*
CAPE Negative	4	1.71	2	0.426	0.67	0.26	1.55	0.65	-0.52	0.14	1.20	0.27	2.51	0.62

Note. Marginal reliability for pattern response scores = .46

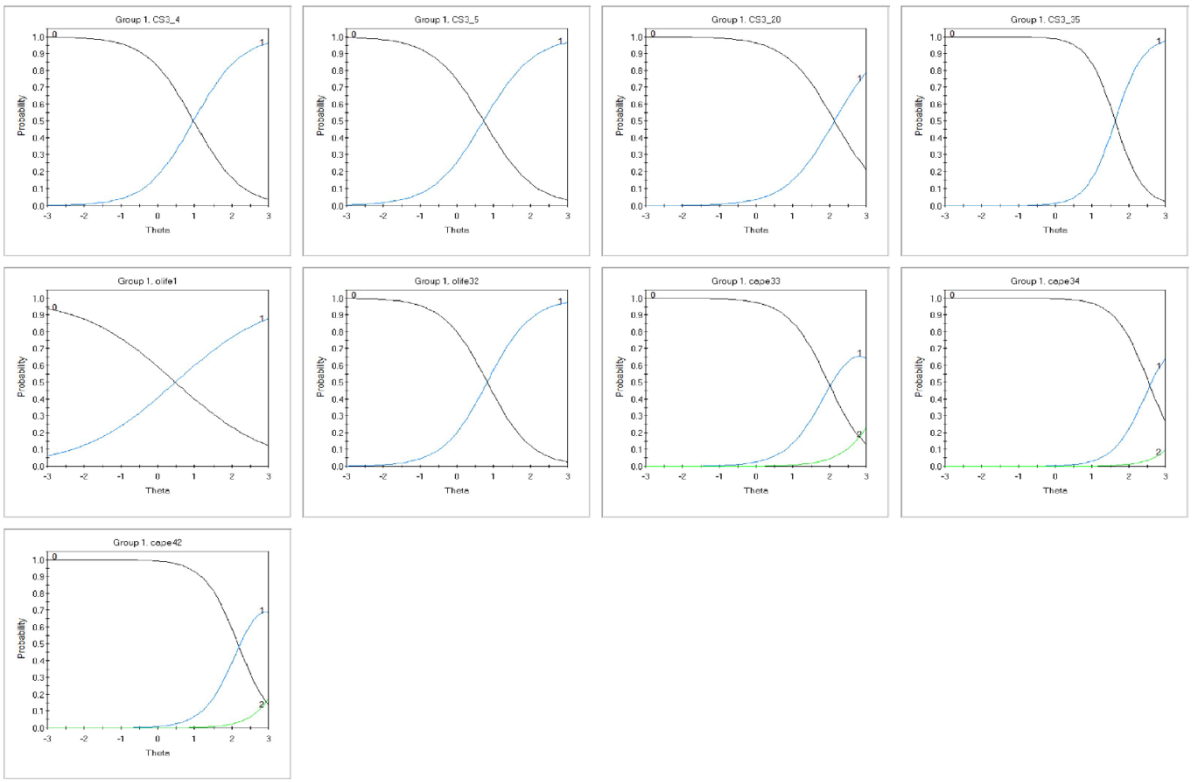

Figure C1. Option response functions (ORFs) of items included in the hallucinations dimension. Items included in this dimension included dichotomous items from Wisconsin Schizotypy Scales (denoted by the abbreviation 'CS' in graph subheadings) and sO-LIFE, and polytomous items from CAPE questionnaires.

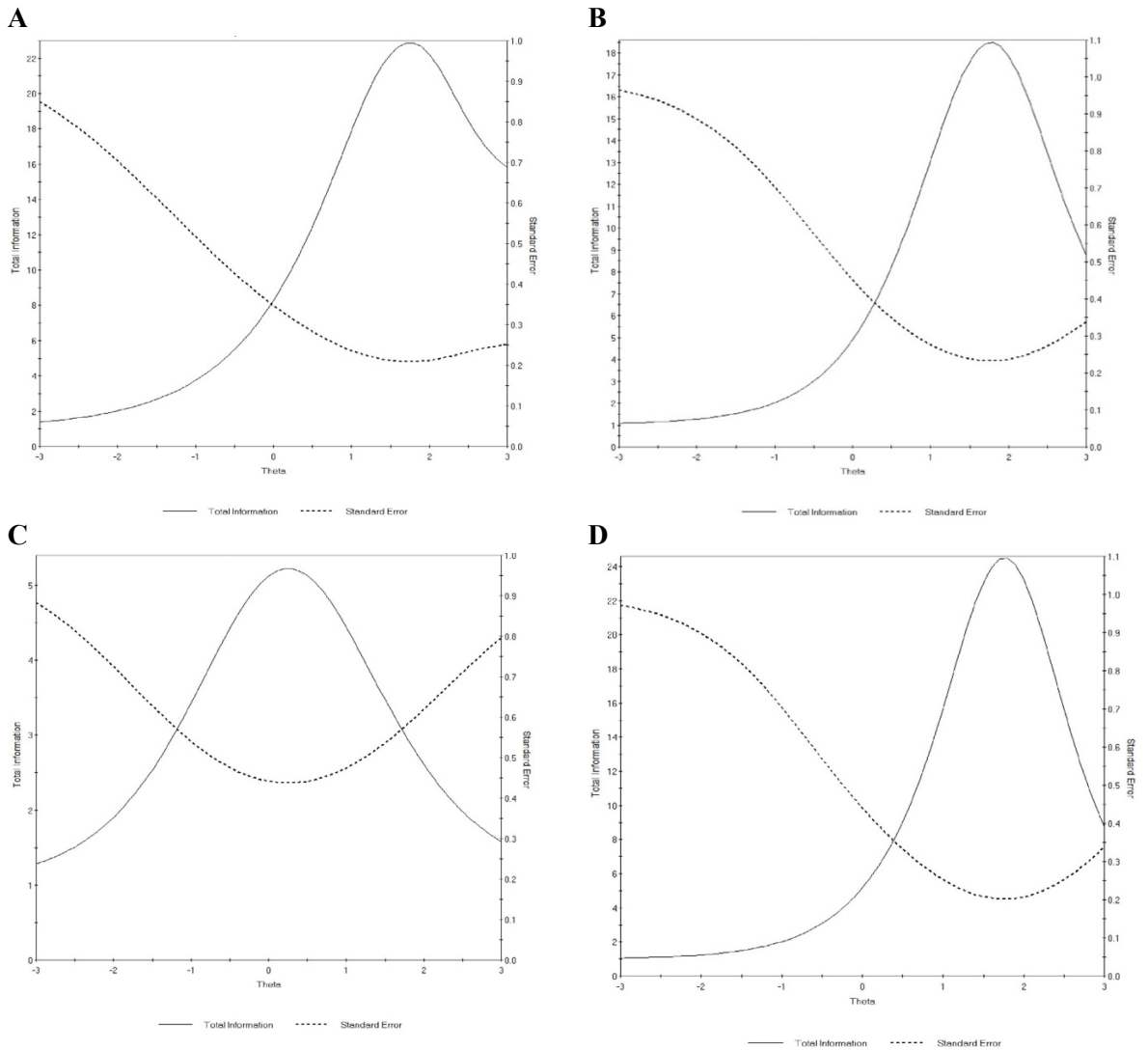

Figure C2. Test information functions for positive PLEs. Each panel corresponds to functions for (A) delusions, (B) hallucinations, (C) cognitive disorganisation, and (D) body image aberration.

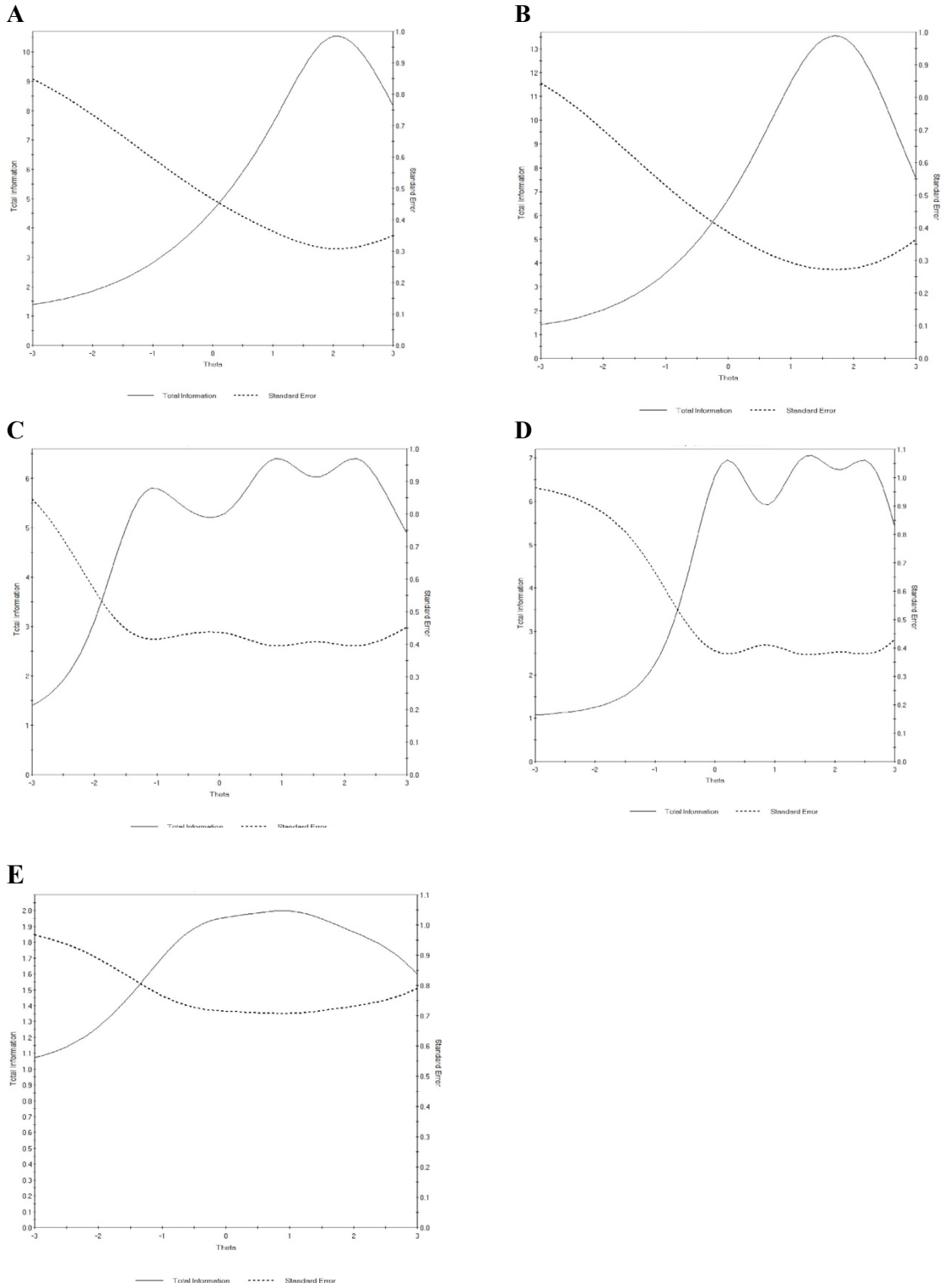

Figure C3. Test information functions for negative PLEs. Each panel corresponds to functions for (A) anhedonia, (B) asociality, (C) avolition, (D) blunted affect, and (E) alogia.

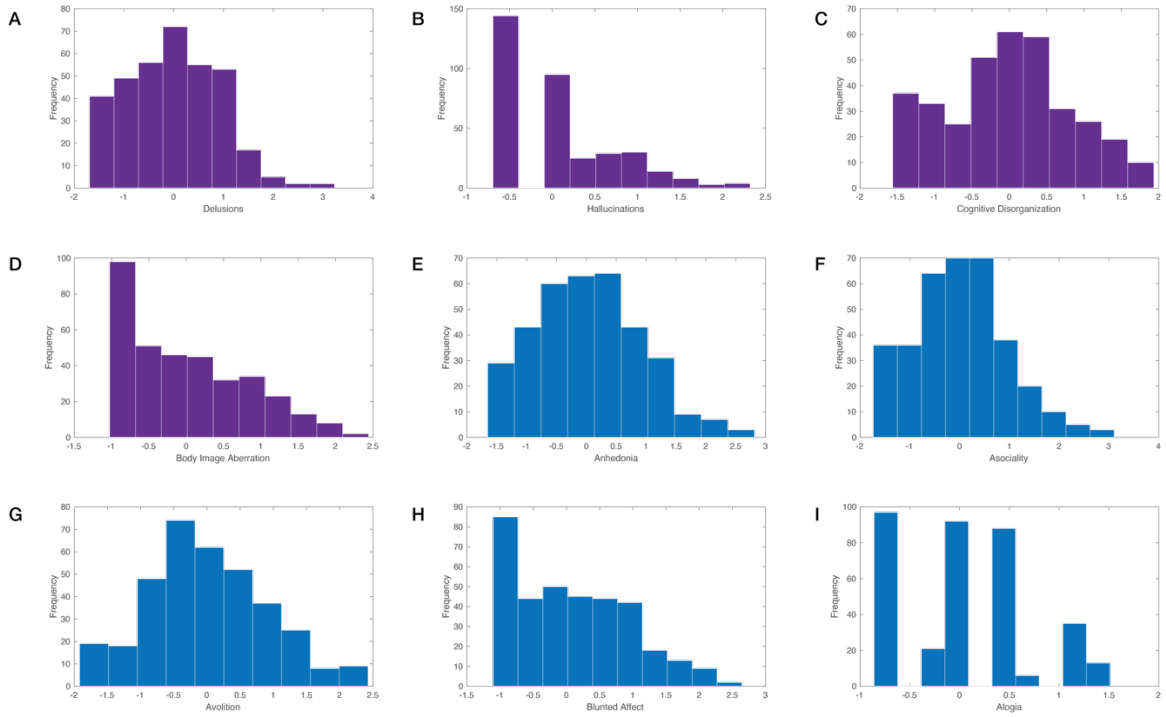

Figure C4. Histograms of item response theory scale scores estimates for positive and negative PLEs in the neuroimaging sample (n = 352). Positive PLEs are portrayed in purple histograms, depicted in panels (A) delusions, (B) hallucinations, (C) cognitive disorganisation, and (D) body image aberration. Negative PLEs are illustrated in blue histograms, depicted in panels (E) anhedonia, (F) asociality, (G) avolition, (H) blunted affect, and (I) alogia**.**

References

———

Alexander, G. E., DeLong, M. R., & Strick, P. L. (1986). Parallel organization of functionally segregated circuits linking basal ganglia and cortex. *Annual Review of Neuroscience*, *VOL. 9*, 357–381. https://doi.org/10.1146/annurev.ne.09.030186.002041

Allen, P., Chaddock, C. A., Egerton, A., Howes, O. D., Bonoldi, I., Zelaya, F., Bhattacharyya, S., Murray, R., & McGuire, P. (2016). Resting hyperperfusion of the hippocampus, midbrain, and basal ganglia in people at high risk for psychosis. *American Journal of Psychiatry*, *173*(4), 392–399. https://doi.org/10.1176/appi.ajp.2015.15040485

Allen, P., Chaddock, C. A., Howes, O. D., Egerton, A., Seal, M. L., Fusar-Poli, P., Valli, I., Day, F., & McGuire, P. K. (2012). Abnormal relationship between medial temporal lobe and subcortical dopamine function in people with an ultra high risk for psychosis. *Schizophrenia Bulletin*, *38*(5), 1040–1049. https://doi.org/10.1093/schbul/sbr017

Allen, P., Luigjes, J., Howes, O. D., Egerton, A., Hirao, K., Valli, I., Kambeitz, J., Fusar-Poli, P., Broome, M., & McGuire, P. (2012). Transition to psychosis associated with prefrontal and subcortical dysfunction in ultra high-risk individuals. *Schizophrenia Bulletin*, *38*(6), 1268–1276. https://doi.org/10.1093/schbul/sbr194

Almgren, H., Van de Steen, F., Kühn, S., Razi, A., Friston, K. J., & Marinazzo, D. (2018). Variability and reliability of effective connectivity within the core default mode network: A multi-site longitudinal spectral DCM study. *NeuroImage*, *183*(July), 757–768. https://doi.org/10.1016/j.neuroimage.2018.08.053

American Psychiatric Association. (2013). *Diagnostic and statistical manual of mental disorders (DSM-5®)*. American Psychiatric Pub.

Andreasen, N. C., & Olsen, S. (1982). Negative v positive schizophrenia: Definition and validation. *Archives of General Psychiatry*, *39*(7), 789–794. https://doi.org/10.1001/archpsyc.1982.04290070025006.

Anticevic, A. (2017). Understanding the role of thalamic circuits in schizophrenia neuropathology. *Schizophrenia Research*, *180*, 1–3. https://doi.org/10.1016/j.schres.2016.11.044

Anticevic, A., Cole, M. W., Repovs, G., Murray, J. D., Brumbaugh, M. S., Winkler, A. M.,

Savic, A., Krystal, J. H., Pearlson, G. D., & Glahn, D. C. (2014). Characterizing thalamo-cortical disturbances in schizophrenia and bipolar illness. *Cerebral Cortex*, *24*(12), 3116–3130. https://doi.org/10.1093/cercor/bht165

Anticevic, A., Haut, K., Murray, J. D., Repovs, G., Yang, G. J., Diehl, C., Mcewen, S. C., Bearden, C. E., Addington, J., Goodyear, B., Cadenhead, K. S., Mcglashan, T. H., Perkins, D. O., Belger, A., Walker, E. F., Hamann, S., Woods, S. W., & Qiu, M. (2015). Association of thalamic dysconnectivity and conversion to psychosis in youth and young adults at elevated clinical risk. *JAMA Psychiatry*, *72*(9), 882–891. https://doi.org/10.1001/jamapsychiatry.2015.0566.Association

Anticevic, A., Hu, X., Xiao, Y., Hu, J., Li, F., Bi, F., Cole, M. W., Savic, A., Yang, G. J., Repovs, G., Murray, J. D., Wang, X.-J., Huang, X., Lui, S., Krystal, J. H., & Gong, Q. (2015). Early-course unmedicated schizophrenia patients exhibit elevated prefrontal connectivity associated with longitudinal change. *Journal of Neuroscience*, *35*(1), 267–286. https://doi.org/10.1523/JNEUROSCI.2310-14.2015

Anticevic, A., Tang, Y., Cho, Y. T., Repovs, G., Cole, M. W., Savic, A., Wang, F., Krystal, J. H., & Xu, K. (2014). Amygdala connectivity differs among chronic, early course, and individuals at risk for developing schizophrenia. *Schizophrenia Bulletin*, *40*(5), 1105–1116. https://doi.org/10.1093/schbul/sbt165

Arseneault, L., Cannon, M., Poulton, R., Murray, R., Caspi, A., & Moffitt, T. E. (2002). Cannabis use in adolescence and risk for adult psychosis: Longitudinal prospective study. *British Medical Journal*, *325*(7374), 1212–1213. https://doi.org/10.1136/bmj.325.7374.1212

Avants, B. B., Tustison, N. J., Song, G., Cook, P. A., Klein, A., & Gee, J. C. (2011). A reproducible evaluation of ANTs similarity metric performance in brain image registration. *NeuroImage*, *54*(3), 2033–2044. https://doi.org/10.1016/j.neuroimage.2010.09.025

Balleine, B. W., Delgado, M. R., & Hikosaka, O. (2007). The role of the dorsal striatum in reward and decision-making. *The Journal of Neuroscience*, *27*(31), 8161–8165. https://doi.org/10.1523/JNEUROSCI.1554-07.2007

Baran, J., Chen, Z., Sforazzini, F., Ferris, N., Jamadar, S., Schmitt, B., Faul, D., Shah, N. J., Cholewa, M., & Egan, G. F. (2018). Accurate hybrid template-based and MR-based attenuation correction using UTE images for simultaneous PET/MR brain imaging applications. *BMC Medical Imaging*, *18*(1), 1–16. https://doi.org/10.1186/s12880-018-0283-3

Barrantes-Vidal, N., Chun, C. A., Myin-Germeys, I., & Kwapil, T. R. (2013). Psychometric schizotypy predicts psychotic-like, paranoid, and negative symptoms in daily life. *Journal of Abnormal Psychology*, *122*(4), 1077–1087. https://doi.org/10.1037/a0034793

Barrantes-vidal, N., Grant, P., & Kwapil, T. R. (2015). *The Role of Schizotypy in the Study of*

the Etiology of Schizophrenia Spectrum Disorders. *41*(2). https://doi.org/10.1093/schbul/sbu191

Beggs, J. M., & Plenz, D. (2003). Neuronal Avalanches in Neocortical Circuits. *The Journal of Neuroscience*, *23*(35), 11167–11177. https://doi.org/10.13005/bbra/1928

Bernal-Casas, D., Lee, H. J., Weitz, A. J., & Lee, J. H. (2017). Studying Brain Circuit Function with Dynamic Causal Modeling for Optogenetic fMRI. *Neuron*, *93*(3), 522-532.e5. https://doi.org/10.1016/j.neuron.2016.12.035

Bertolino, A., Breier, A., Callicott, J. H., Adler, C., Mattay, V. S., Shapiro, M., Frank, J. A., Pickar, D., & Weinberger, D. R. (2000). The relationship between dorsolateral prefrontal neuronal N-acetylaspartate and evoked release of striatal dopamine in schizophrenia. *Neuropsychopharmacology*, *22*(2), 125–132. https://doi.org/10.1016/S0893-133X(99)00096-2

Bock, R. D., & Aitkin, M. (1981). Marginal maximum likelihood estimation of item parameters: Application of an EM algorithm. *Psychometrika*, *46*(4), 443–459. https://doi.org/10.1007/BF02293801

Bock, R. D., & Mislevy, R. J. (1982). Adaptive EAP estimation of ability in a microcomputer environment. *Applied Psychological Measurement*, *6*(4), 431–444. https://doi.org/10.1177/014662168200600405

Bora, E., Fornito, A., Radua, J., Walterfang, M., Seal, M., Wood, S. J., Yücel, M., Velakoulis, D., & Pantelis, C. (2011). Neuroanatomical abnormalities in schizophrenia: a multimodal voxelwise meta-analysis and meta-regression analysis. *Schizophrenia Research*, *127*(1–3), 46–57. https://doi.org/10.1016/j.schres.2010.12.020

Boyacioğlu, R., Schulz, J., Koopmans, P. J., Barth, M., & Norris, D. G. (2015). Improved sensitivity and specificity for resting state and task fMRI with multiband multi-echo EPI compared to multi-echo EPI at 7T. *NeuroImage*, *119*, 352–361. https://doi.org/10.1016/j.neuroimage.2015.06.089

Burgess, G. C., Kandala, S., Nolan, D., Laumann, T. O., Power, J. D., Adeyemo, B., Harms, M. P., Petersen, S. E., & Barch, D. M. (2016). Evaluation of denoising strategies to address motion-correlated artifacts in resting-state functional magnetic resonance imaging data from the human connectome project. *Brain Connectivity*, *6*(9), 669–680. https://doi.org/10.1089/brain.2016.0435

Burgos, N., Cardoso, M. J., Thielemans, K., Modat, M., Pedemonte, S., Dickson, J., Barnes, A., Ahmed, R., Mahoney, C. J., Schott, J. M., Duncan, J. S., Atkinson, D., Arridge, S. R., Hutton, B. F., & Ourselin, S. (2014). Attenuation correction synthesis for hybrid PET-MR scanners: Application to brain studies. *IEEE Transactions on Medical Imaging*, *33*(12), 2332–2341. https://doi.org/10.1109/TMI.2014.2340135

Buxton, R. B., Wong, E. C., & Frank, L. R. (1998). Dynamics of blood flow and oxygenation changes during brain activation: The balloon model. *Magnetic Resonance in Medicine*,

39(6), 855–864. https://doi.org/10.1002/mrm.1910390602

Cadena, E. J., White, D. M., Kraguljac, N. V., Reid, M. A., & Lahti, A. C. (2018). Evaluation of fronto-striatal networks during cognitive control in unmedicated patients with schizophrenia and the effect of antipsychotic medication. *NPJ Schizophrenia*, *4*(1), 1–8. https://doi.org/10.1038/s41537-018-0051-y

Cai, L., Thissen, D., & du Toit, S. H. C. (2011). IRTPRO for windows [Computer software manual]. *Lincolnwood, IL: Scientific Software International*.

Cannon, T. D., Cornblatt, B., & McGorry, P. (2007). Editor's introduction: The empirical status of the ultra high-risk (prodromal) research paradigm. *Schizophrenia Bulletin*, *33*(3), 661–664. https://doi.org/10.1093/schbul/sbm031

Cardno, A. G., & Gottesman, I. I. (2000). Twin studies of schizophrenia: From bow-and-arrow concordances to star wars Mx and functional genomics. *American Journal of Medical Genetics - Seminars in Medical Genetics*, *97*(1), 12–17. https://doi.org/10.1002/(SICI)1096-8628(200021)97:1<12::AID-AJMG3>3.0.CO;2-U

Carlsson, A., Waters, N., & Carlsson, M. (1999). Neurotransmitter interactions in schizophrenia-therapeutic implications. *Biol Psychiatry*, *46*(10), 1388–1395. https://doi.org/http://dx.doi.org/10.1016/S0006-3223(99)00117-1

Carlsson, M., & Carlsson, A. (1990). Interactions between glutamatergic and monoaminergic systems within the basal ganglia-implications for schizophrenia and Parkinson's disease. *Trends in Neurosciences*, *13*(7), 272–276. https://doi.org/10.1016/0166-2236(90)90108-M

Cassidy, C. M., Balsam, P. D., Weinstein, J. J., Rosengard, R. J., Slifstein, M., Daw, N. D., Abi-Dargham, A., & Horga, G. (2018). A perceptual inference mechanism for hallucinations linked to striatal dopamine. *Current Biology*, *28*(4), 503-514.e4. https://doi.org/10.1016/j.cub.2017.12.059

Chahine, G., Richter, A., Wolter, S., Goya-Maldonado, R., & Gruber, O. (2017). Disruptions in the left frontoparietal network underlie resting state endophenotypic markers in Schizophrenia. *Human Brain Mapping*, *38*(4), 1741–1750. https://doi.org/10.1002/hbm.23477

Chang, C. H., & Grace, A. A. (2014). Amygdala-ventral pallidum pathway decreases dopamine activity after chronic mild stress in rats. *Biological Psychiatry*, *76*(3), 223–230. https://doi.org/10.1016/j.biopsych.2013.09.020

Chapman, L. J., Chapman, J. P., & Raulin, M. L. (1976). Scales for physical and social anhedonia. *Journal of Abnormal Psychology*, *85*(4), 374–382. https://doi.org/10.1037/0021-843X.85.4.374

Chapman, L. J., Chapman, J. P., & Raulin, M. L. (1978a). Body-image aberration in schizophrenia. In *Journal of Abnormal Psychology* (Vol. 87, Issue 4, pp. 399–407).

https://doi.org/10.1037//0021-843x.87.4.399

Chapman, L. J., Chapman, J. P., & Raulin, M. L. (1978b). Body image aberration in schizophrenia. *Journal of Abnormal Psychology*, *87*(4), 399–407. https://doi.org/10.1037//0021-843X.87.4.399

Chen, Z., Sforazzini, F., Baran, J., Close, T., Shah, N. J., & Egan, G. F. (2019). MR-PET head motion correction based on co-registration of multicontrast MR images. *Human Brain Mapping*, *August 2018*, 1–11. https://doi.org/10.1002/hbm.24497

Chesney, E., Goodwin, G. M., & Fazel, S. (2014). Risks of all-cause and suicide mortality in mental disorders: A meta-review. *World Psychiatry*, *13*(2), 153–160. https://doi.org/10.1002/wps.20128

Ciric, R., Wolf, D. H., Power, J. D., Roalf, D. R., Baum, G. L., Ruparel, K., Shinohara, R. T., Elliott, M. A., Eickhoff, S. B., Davatzikos, C., Gur, R. C., Gur, R. E., Bassett, D. S., & Satterthwaite, T. D. (2017). Benchmarking of participant-level confound regression strategies for the control of motion artifact in studies of functional connectivity. *NeuroImage*, *154*, 174–187. https://doi.org/10.1016/j.neuroimage.2017.03.020

Clark, L. A., & Watson, D. (2019). Constructing validity: New developments in creating objective measuring instruments. *Psychological Assessment*, *31*(12), 1412. https://doi.org/10.1037/pas0000626

Cole, M. W., & Schneider, W. (2007). The cognitive control network: Integrated cortical regions with dissociable functions. *NeuroImage*, *37*(1), 343–360. https://doi.org/10.1016/j.neuroimage.2007.03.071

Corlett, P. R., & Fletcher, P. C. (2012). The neurobiology of schizotypy: fronto-striatal prediction error signal correlates with delusion-like beliefs in healthy people. *Neuropsychologia*, *50*(14), 3612–3620. https://doi.org/10.1016/j.neuropsychologia.2012.09.045

Corlett, P. R., Honey, G. D., Aitken, M. R. F., Dickinson, A., Shanks, D. R., Absalom, A. R., Lee, M., Pomarol-Clotet, E., Murray, G. K., McKenna, P. J., Robbins, T. W., Bullmore, E. T., & Fletcher, P. C. (2006). Frontal responses during learning predict vulnerability to the psychotogenic effects of ketamine: Linking cognition, brain activity, and psychosis. *Archives of General Psychiatry*, *63*(6), 611–621. https://doi.org/10.1001/archpsyc.63.6.611

Corlett, P. R., Horga, G., Fletcher, P. C., Alderson-Day, B., Schmack, K., & Powers, A. R. (2019). Hallucinations and Strong Priors. *Trends in Cognitive Sciences*, *23*(2), 114–127. https://doi.org/10.1016/j.tics.2018.12.001

Corlett, P. R., Taylor, J. R., Wang, X. J., Fletcher, P. C., & Krystal, J. H. (2010). Toward a neurobiology of delusions. *Progress in Neurobiology*, *92*(3), 345–369. https://doi.org/10.1016/j.pneurobio.2010.06.007

Cougnard, A., Marcelis, M., Myin-Germeys, I., De Graaf, R., Vollebergh, W., Krabbendam, L., Lieb, R., Wittchen, H.-U., Henquet, C., Spauwen, J., & van Os, J. (2007). Does normal developmental expression of psychosis combine with environmental risk to cause persistence of psychosis? A psychosis proneness-persistence model. *Psychological Medicine*, *37*(4), 513–527. https://doi.org/10.1017/S0033291706009731

Cui, L. B., Liu, J., Wang, L. X., Li, C., Xi, Y. Bin, Guo, F., Wang, H. N., Zhang, L. C., Liu, W. M., He, H., Tian, P., Yin, H., & Lu, H. (2015). Anterior cingulate cortex-related connectivity in first-episode schizophrenia: A spectral dynamic causal modeling study with functional magnetic resonance imaging. *Frontiers in Human Neuroscience*, *9*(NOVEMBER), 1–10. https://doi.org/10.3389/fnhum.2015.00589

Dandash, O., Fornito, A., Lee, J., Keefe, R. S. E., Chee, M. W. L., Adcock, R. A., Pantelis, C., Wood, S. J., & Harrison, B. J. (2014). Altered striatal functional connectivity in subjects with an at-risk mental state for psychosis. *Schizophrenia Bulletin*, *40*(4), 904–913. https://doi.org/10.1093/schbul/sbt093

Dandash, O., Harrison, B. J., Adapa, R., Gaillard, R., Giorlando, F., Wood, S. J., Fletcher, P. C., & Fornito, A. (2014). Selective Augmentation of Striatal Functional Connectivity Following NMDA Receptor Antagonism: Implications for Psychosis. *Neuropsychopharmacology : Official Publication of the American College of Neuropsychopharmacology*, *40*(3), 1–10. https://doi.org/10.1038/npp.2014.210

Dandash, O., Pantelis, C., & Fornito, A. (2017). Dopamine, fronto-striato-thalamic circuits and risk for psychosis. *Schizophrenia Research*, *180*, 48–57. https://doi.org/10.1016/j.schres.2016.08.020

Dandash, O., Yücel, M., Daglas, R., Pantelis, C., McGorry, P., Berk, M., & Fornito, A. (2018). Differential effect of quetiapine and lithium on functional connectivity of the striatum in first episode mania. *Translational Psychiatry*, *8*(1). https://doi.org/10.1038/s41398-018-0108-8

Dazzan, P., Morgan, K. D., Orr, K. G., Hutchinson, G., Chitnis, X., Suckling, J., Fearon, P., Salvo, J., McGuire, P. K., Mallett, R. M., Jones, P. B., Leff, J., & Murray, R. M. (2004). The structural brain correlates of neurological soft signs in ÆSOP first-episode psychoses study. *Brain*, *127*(1), 143–153. https://doi.org/10.1093/brain/awh015

Dazzi, F., Shafer, A., & Lauriola, M. (2016). Meta-analysis of the Brief Psychiatric Rating Scale – Expanded (BPRS-E) structure and arguments for a new version. *Journal of Psychiatric Research*, *81*, 140–151. https://doi.org/10.1016/j.jpsychires.2016.07.001

De la Fuente-Fernández, R., Phillips, A. G., Zamburlini, M., Sossi, V., Calne, D. B., Ruth, T. J., & Stoessl, A. J. (2002). Dopamine release in human ventral striatum and expectation of reward. *Behavioural Brain Research*. https://doi.org/10.1016/S0166-4328(02)00130-4

Debbané, M., Van Der Linden, M., Gex-Fabry, M., & Eliez, S. (2009). Cognitive and

emotional associations to positive schizotypy during adolescence. *Journal of Child Psychology and Psychiatry and Allied Disciplines*, *50*(3), 326–334. https://doi.org/10.1111/j.1469-7610.2008.01961.x

DeRosse, P., & Karlsgodt, K. H. (2015). Examining the Psychosis Continuum. *Current Behavioral Neuroscience Reports*, *2*(2), 80–89. https://doi.org/10.1007/s40473-015-0040-7

Di Martino, A., Scheres, A., Margulies, D. S., Kelly, A. M. C., Uddin, L. Q., Shehzad, Z., Biswal, B., Walters, J. R., Castellanos, F. X., & Milham, M. P. (2008). Functional connectivity of human striatum: A resting state fMRI study. *Cerebral Cortex*, *18*(12), 2735–2747. https://doi.org/10.1093/cercor/bhn041

Diederen, K. M. J., Daalman, K., De Weijer, A. D., Neggers, S. F. W., Van Gastel, W., Blom, J. D., Kahn, R. S., & Sommer, I. E. C. (2012). Auditory hallucinations elicit similar brain activation in psychotic and nonpsychotic individuals. *Schizophrenia Bulletin*, *38*(5), 1074–1082. https://doi.org/10.1093/schbul/sbr033

Diedrichsen, J., Balsters, J. H., Flavell, J., Cussans, E., & Ramnani, N. (2009). A probabilistic MR atlas of the human cerebellum. *NeuroImage*, *46*(1), 39–46. https://doi.org/10.1016/j.neuroimage.2009.01.045

DiStefano, C., Zhu, M., & Mindrila, D. (2009). Understanding and using factor scores: considerations for the applied researcher. *Practical Assessment, Research & Evaluation*, *14*(20), 1–11. https://doi.org/10.1.1.460.8553

Dong, D., Wang, Y., Chang, X., Luo, C., & Yao, D. (2018). Dysfunction of Large-Scale Brain Networks in Schizophrenia: A Meta-analysis of Resting-State Functional Connectivity. *Schizophrenia Bulletin*, *44*(1), 168–181. https://doi.org/10.1093/schbul/sbx034

Dosenbach, N. U. F., Nardos, B., Cohen, A. L., Fair, D. A., Power, J. D., Church, J. A., Nelson, S. M., Wig, G. S., Vogel, A. C., Lessov-Schlaggar, C. N., Barnes, K. A., Dubis, J. W., Feczko, E., Coalson, R. S., Pruett, J. R., Barch, D. M., Petersen, S. E., & Schlaggar, B. L. (2010). Prediction of individual brain maturity using fMRI. *Science*, *329*(5997), 1358–1361. https://doi.org/10.1126/science.1194144

Draganski, B., Kherif, F., Klöppel, S., Cook, P. A., Alexander, D. C., Parker, G. J. M., Deichmann, R., Ashburner, J., & Frackowiak, R. S. J. (2008). Evidence for segregated and integrative connectivity patterns in the human basal ganglia. *The Journal of Neuroscience : The Official Journal of the Society for Neuroscience*, *28*(28), 7143–7152. https://doi.org/10.1523/JNEUROSCI.1486-08.2008

Eckblad, M., & Chapman, L. J. (1983). Magical ideation as an indicator of schizotypy. *Journal of Consulting and Clinical Psychology*, *51*(2), 215–225. https://doi.org/10.1037/0022-006X.51.2.215

Edelen, M. O., & Reeve, B. B. (2007). Applying item response theory (IRT) modeling to

questionnaire development, evaluation, and refinement. *Quality of Life Research*, *16*(1), 5. https://doi.org/10.1007/s11136-007-9198-0

Edwards, M. C. (2009). An introduction to item response theory using the need for cognition scale. *Social and Personality Psychology Compass*, *3*(4), 507–529. https://doi.org/10.4314/gjedr.v16i2.2

Egerton, A., Chaddock, C. A., Winton-Brown, T. T., Bloomfield, M. A. P., Bhattacharyya, S., Allen, P., McGuire, P. K., & Howes, O. D. (2013). Presynaptic striatal dopamine dysfunction in people at ultra-high risk for psychosis: Findings in a second cohort. *Biological Psychiatry*, *74*(2), 106–112. https://doi.org/10.1016/j.biopsych.2012.11.017

Egerton, A., Howes, O. D., Houle, S., McKenzie, K., Valmaggia, L. R., Bagby, M. R., Tseng, H. H., Bloomfield, M. A. P., Kenk, M., Bhattacharyya, S., Suridjan, I., Chaddock, C. A., Winton-Brown, T. T., Allen, P., Rusjan, P., Remington, G., Meyer-Lindenberg, A., McGuire, P. K., & Mizrahi, R. (2017). Elevated striatal dopamine function in immigrants and their children: a risk mechanism for psychosis. *Schizophrenia Bulletin*, *43*(2), 293–301. https://doi.org/10.1093/schbul/sbw181

Emsley, R., Rabinowitz, J., Torreman, M., Schooler, N., Kapala, L., Davidson, M., & McGory, P. (2003). The factor structure for the Positive and Negative Syndrome Scale (PANSS) in recent-onset psychosis. *Schizophrenia Research*, *61*(1), 47–57. https://doi.org/10.1016/S0920-9964(02)00302-X

Essen, C. B., Idaka, I. E., & Metibemu, M. A. (2017). Item level diagnostics and model-data fit in item response theory (IRT) using BILOG-MG v3. 0 and IRTPRO v3. 0 programmes. *Global Journal of Educational Research*, *16*(2), 87–94.

Essen, V., & Tononi, G. (2016). An Introduction to Brain Networks. In *Fundamentals of Brain Network Analysis*. Elsevier. https://doi.org/10.1016/b978-0-12-407908-3.00001-7

Esteban, O., Birman, D., Schaer, M., Koyejo, O. O., Poldrack, R. A., & Gorgolewski, K. J. (2017). MRIQC: Advancing the automatic prediction of image quality in MRI from unseen sites. *PloS One*, *12*(9), e0184661. https://doi.org/10.1371/journal.pone.0184661

Esteban, O., Markiewicz, C. J., Blair, R. W., Moodie, C. A., Isik, A. I., Erramuzpe, A., Kent, J. D., Goncalves, M., DuPre, E., Snyder, M., Oya, H., Ghosh, S. S., Wright, J., Durnez, J., Poldrack, R. A., & Gorgolewski, K. J. (2019). fMRIPrep: a robust preprocessing pipeline for functional MRI. *Nature Methods*, *16*(1), 111–116. https://doi.org/10.1038/s41592-018-0235-4

Esterman, M., Tamber-Rosenau, B. J., Chiu, Y. C., & Yantis, S. (2010). Avoiding non-independence in fMRI data analysis: leave one subject out. *NeuroImage*, *50*(2), 572–576. https://doi.org/10.1016/j.neuroimage.2009.10.092

Ettinger, U., Meyhöfer, I., Steffens, M., Wagner, M., & Koutsouleris, N. (2014). Genetics, cognition, and neurobiology of schizotypal personality: a review of the overlap with schizophrenia. *Frontiers in Psychiatry*, *5*(18), 1–16.

https://doi.org/10.3389/fpsyt.2014.00018

Ettinger, U., Williams, S. C. R., Meisenzahl, E. M., Möller, H. J., Kumari, V., & Koutsouleris, N. (2012). Association between brain structure and psychometric schizotypy in healthy individuals. *World Journal of Biological Psychiatry*, *13*(7), 544–549. https://doi.org/10.3109/15622975.2011.559269

Feinberg, I., & Guazzelli, M. (1999). Schizophrenia - A disorder of the corollary discharge systems that integrate the motor systems of thought with the sensory systems of consciousness. *British Journal of Psychiatry*, *174*(MAR.), 196–204. https://doi.org/10.1192/bjp.174.3.196

Fischl, B., Salat, D. H., Busa, E., Albert, M., Dieterich, M., Haselgrove, C., Kouwe, A. Van Der, Killiany, R., Kennedy, D., Klaveness, S., Montillo, A., Makris, N., Rosen, B., & Dale, A. M. (2002). Whole brain segmentation: neurotechnique automated labeling of neuroanatomical structures in the human brain. *Neuron*, *33*, 341–355. https://doi.org/10.1016/S0896-6273(02)00569-X

Floresco, S. B., West, A. R., Ash, B., Moorel, H., & Grace, A. A. (2003). Afferent modulation of dopamine neuron firing differentially regulates tonic and phasic dopamine transmission. *Nature Neuroscience*. https://doi.org/10.1038/nn1103

Fornito, A., & Bullmore, E. T. (2010). What can spontaneous fluctuations of the blood oxygenation-level-dependent signal tell us about psychiatric disorders? *Current Opinion in Psychiatry*, *23*(3), 239–249. https://doi.org/10.1097/YCO.0b013e328337d78d

Fornito, A., Harrison, B. J., Goodby, E., Dean, A., Ooi, C., Nathan, P. J., Lennox, B. R., Jones, P. B., Suckling, J., & Bullmore, E. T. (2013). Functional dysconnectivity of corticostriatal circuitry as a risk phenotype for psychosis. *JAMA Psychiatry*, *70*(11), 1143–1151. https://doi.org/10.1001/jamapsychiatry.2013.1976

Fornito, A., Yücel, M., Patti, J., Wood, S. J., & Pantelis, C. (2009). Mapping grey matter reductions in schizophrenia: an anatomical likelihood estimation analysis of voxel-based morphometry studies. *Schizophrenia Research*, *108*(1–3), 104–113. https://doi.org/10.1016/j.schres.2008.12.011

Fornito, A., Yücel, M., Wood, S. J., Adamson, C., Velakoulis, D., Saling, M. M., McGorry, P. D., & Pantelis, C. (2008). Surface-based morphometry of the anterior cingulate cortex in first episode schizophrenia. *Human Brain Mapping*, *29*(4), 478–489. https://doi.org/10.1002/hbm.20412

Fornito, A., Yung, A. R., Wood, S. J., Phillips, L. J., Nelson, B., Cotton, S., Velakoulis, D., McGorry, P. D., Pantelis, C., & Yücel, M. (2008). Anatomic abnormalities of the anterior cingulate cortex before psychosis onset: an MRI study of ultra-high-risk individuals. *Biological Psychiatry*, *64*(9), 758–765. https://doi.org/10.1016/j.biopsych.2008.05.032

Fornito, A., Zalesky, A., & Breakspear, M. (2015). The connectomics of brain disorders.

Nature Reviews Neuroscience, *16*(3), 159–172. https://doi.org/10.1038/nrn3901

Fornito, A., Zalesky, A., Pantelis, C., & Bullmore, E. T. (2012). Schizophrenia, neuroimaging and connectomics. *NeuroImage*, *62*(4), 2296–2314. https://doi.org/10.1016/j.neuroimage.2011.12.090

Fox, M. D., Snyder, A. Z., Vincent, J. L., Corbetta, M., Van Essen, D. C., & Raichle, M. E. (2005). The human brain is intrinsically organized into dynamic, anticorrelated functional networks. *Proceedings of the National Academy of Sciences of the United States of America*, *102*(27), 9673–9678. https://doi.org/10.1073/pnas.0504136102

Francey, S. M., O'Donoghue, B., Nelson, B., Graham, J., Baldwin, L., Yuen, H. P., Kerr, M. J., Ratheesh, A., Allott, K., Alvarez-Jimenez, M., Fornito, A., Harrigan, S., Thompson, A. D., Wood, S., Berk, M., & McGorry, P. D. (2020). Psychosocial Intervention With or Without Antipsychotic Medication for First-Episode Psychosis: A Randomized Noninferiority Clinical Trial. *Schizophrenia Bulletin Open*, *1*(1), 1–11. https://doi.org/10.1093/schizbullopen/sgaa015

Frässle, S., Lomakina, E. I., Razi, A., Friston, K. J., Buhmann, J. M., & Stephan, K. E. (2017). Regression DCM for fMRI. *NeuroImage*, *155*(November 2016), 406–421. https://doi.org/10.1016/j.neuroimage.2017.02.090

French, L., Gray, C., Leonard, G., Perron, M., Pike, G. B., Richer, L., Séguin, J. R., Veillette, S., Evans, C. J., Artiges, E., Banaschewski, T., Bokde, A. W. L., Bromberg, U., Bruehl, R., Buchel, C., Cattrell, A., Conrod, P. J., Flor, H., Frouin, V., … Paus, T. (2015). Early Cannabis Use, Polygenic Risk Score for Schizophrenia and Brain Maturation in Adolescence. *JAMA Psychiatry*, *72*(10), 1002–1011. https://doi.org/10.1001/jamapsychiatry.2015.1131

Friston, K. J. (1994). Functional and effective connectivity in neuroimaging: A synthesis. *Human Brain Mapping*, *2*(1–2), 56–78. https://doi.org/10.1002/hbm.460020107

Friston, K. J. (1999). Schizophrenia and the disconnection hypothesis. *Acta Psychiatrica Scandinavica, Supplement*, *99*(395), 68–79. https://doi.org/10.1111/j.1600-0447.1999.tb05985.x

Friston, K. J. (2011). Functional and Effective Connectivity: A Review. *Brain Connectivity*, *1*(1), 13–36. https://doi.org/10.1089/brain.2011.0008

Friston, K. J., Harrison, L., & Penny, W. (2003). Dynamic causal modelling. *NeuroImage*, *19*(4), 1273–1302. https://doi.org/10.1016/S1053-8119(03)00202-7

Friston, K. J., Kahan, J., Biswal, B., & Razi, A. (2014). A DCM for resting state fMRI. *NeuroImage*, *94*(August 2014), 396–407. https://doi.org/10.1016/j.neuroimage.2013.12.009

Friston, K. J., Litvak, V., Oswal, A., Razi, A., Stephan, K. E., Van Wijk, B. C. M., Ziegler, G., & Zeidman, P. (2016). Bayesian model reduction and empirical Bayes for group

(DCM) studies. *NeuroImage*, *128*, 413–431. https://doi.org/10.1016/j.neuroimage.2015.11.015

Friston, K. J., Mattout, J., Trujillo-Barreto, N., Ashburner, J., & Penny, W. (2007). Variational free energy and the Laplace approximation. *NeuroImage*, *34*(1), 220–234. https://doi.org/10.1016/j.neuroimage.2006.08.035

Friston, K. J., Moran, R., & Seth, A. K. (2013). Analysing connectivity with Granger causality and dynamic causal modelling. *Current Opinion in Neurobiology*, *23*(2), 172–178. https://doi.org/10.1016/j.conb.2012.11.010

Frith, C. (2005). The neural basis of hallucinations and delusions. *Comptes Rendus - Biologies*, *328*(2), 169–175. https://doi.org/10.1016/j.crvi.2004.10.012

Fukuda, Y., Katthagen, T., Deserno, L., Shayegan, L., Kaminski, J., Heinz, A., & Schlagenhauf, F. (2019). Reduced parietofrontal effective connectivity during a working-memory task in people with high delusional ideation. *Journal of Psychiatry and Neuroscience*, *44*(3), 195–204. https://doi.org/10.1503/jpn.180043

Fusar-Poli, P., Broome, M. R., Matthiasson, P., Woolley, J. B., Johns, L. C., Tabraham, P., Bramon, E., Valmaggia, L., Williams, S. C., & McGuire, P. (2010). Spatial working memory in individuals at high risk for psychosis: longitudinal fMRI study. *Schizophrenia Research*, *123*(1), 45–52. https://doi.org/10.1016/j.schres.2010.06.008

Fusar-Poli, P., Howes, O. D., Allen, P., Broome, M., Valli, I., & Asselin, M. (2010). Abnormal frontostriatal interactions in people with prodromal signs of psychosis: a multimodal imaging study. *Archives of General Psychiatry*, *67*(7), 683–691. https://doi.org/10.1001/archgenpsychiatry.2010.77

Fusar-Poli, P., Howes, O. D., Allen, P., Broome, M., Valli, I., Asselin, M. C., Montgomery, A. J., Grasby, P. M., & McGuire, P. (2011). Abnormal prefrontal activation directly related to pre-synaptic striatal dopamine dysfunction in people at clinical high risk for psychosis. *Mol Psychiatry*, *16*(1), 67–75. https://doi.org/10.1038/mp.2009.108

Fusar-Poli, P., McGorry, P. D., & Kane, J. M. (2017). Improving outcomes of first-episode psychosis: an overview. *World Psychiatry*, *16*(3), 251–265. https://doi.org/10.1002/wps.20446

Galderisi, S., Merlotti, E., & Mucci, A. (2015). Neurobiological background of negative symptoms. *European Archives of Psychiatry and Clinical Neuroscience*, *265*(7), 543–558. https://doi.org/10.1007/s00406-015-0590-4

Garrity, A. G., Pearlson, G. D., McKiernan, K., Lloyd, D., Kiehl, K. A., & Calhoun, V. D. (2007). Aberrant "default mode" functional connectivity in schizophrenia. *American Journal of Psychiatry*, *164*(3), 450–457. https://doi.org/10.1176/ajp.2007.164.3.450

Gee, D. G., Karlsgodt, K. H., van Erp, T. G. M., Bearden, C. E., Lieberman, M. D., Belger, A., Perkins, D. O., Olvet, D. M., Cornblatt, B. A., Constable, T., Woods, S. W.,

Addington, J., Cadenhead, K. S., McGlashan, T. H., Seidman, L. J., Tsuang, M. T., Walker, E. F., & Cannon, T. D. (2012). Altered age-related trajectories of amygdala-prefrontal circuitry in adolescents at clinical high risk for psychosis: A preliminary study. *Schizophrenia Research*, *134*(1), 1–9. https://doi.org/10.1016/j.schres.2011.10.005

Gerfen, C. R., & Bolam, J. P. (2010). The Neuroanatomical Organization of the Basal Ganglia. In *Handbook of Behavioral Neuroscience: Vol. Volume 20*. Elsevier Inc. https://doi.org/http://dx.doi.org/10.1016/B978-0-12-374767-9.00001-9

Gerfen, C. R., & Surmeier, D. J. (2011). Modulation of Striatal Projection Systems by Dopamine. *Annual Review of Neuroscience*, *34*(1), 441–466. https://doi.org/10.1146/annurev-neuro-061010-113641

Goldman-Rakic, P. S., & Brown, R. M. (1982). Postnatal development of monoamine content and synthesis in the cerebral cortex of rhesus monkeys. *Developmental Brain Research*, *4*(3), 339–349. https://doi.org/10.1016/0165-3806(82)90146-8

Goldman, P. S., & Alexander, G. E. (1977). Maturation of prefrontal cortex in the monkey revealed by local reversible cryogenic depression. *Nature*, *267*(5612), 613–615. https://doi.org/10.1038/267613a0

Gordon, E. M., Laumann, T. O., Adeyemo, B., Huckins, J. F., Kelley, W. M., & Petersen, S. E. (2016). Generation and Evaluation of a Cortical Area Parcellation from Resting-State Correlations. *Cerebral Cortex*, *26*(1), 288–303. https://doi.org/10.1093/cercor/bhu239

Goulding, S. M., Holtzman, C. W., Trotman, H. D., Ryan, A. T., MacDonald, A. N., Shapiro, D. I., Brasfield, J. L., & Walker, E. F. (2013). The Prodrome and Clinical Risk for Psychotic Disorders. *Child and Adolescent Psychiatric Clinics of North America*, *22*(4), 557–567. https://doi.org/10.1016/j.chc.2013.04.002

Grace, A. A. (1991). Phasic versus tonic dopamine release and the modulation of dopamine system responsivity: A hypothesis for the etiology of schizophrenia. *Neuroscience*, *41*(1), 1–24. https://doi.org/10.1016/0306-4522(91)90196-U

Grace, A. A. (2016). Dysregulation of the dopamine system in the pathophysiology of schizophrenia and depression. In *Nature Reviews Neuroscience* (Vol. 17, Issue 8, pp. 524–532). https://doi.org/10.1038/nrn.2016.57

Grace, A. A., & Bunney, B. S. (1984). The control of firing pattern in nigral dopamine neurons: single spike firing. *Journal of Neuroscience*, *4*(11), 2866–2876. https://doi.org/10.1039/CT9140501039

Grace, A. A., & Bunney, B. S. (1985). Opposing effects of striatonigral feedback pathways on midbrain dopamine cell activity. *Brain Research*, *333*(2), 271–284. https://doi.org/10.1016/0006-8993(85)91581-1

Grace, S. A., Labuschagne, I., Kaplan, R. A., & Rossell, S. L. (2017). The neurobiology of

body dysmorphic disorder: A systematic review and theoretical model. *Neuroscience and Biobehavioral Reviews*, *83*(October), 83–96. https://doi.org/10.1016/j.neubiorev.2017.10.003

Grant, P., Green, M. J., & Mason, O. J. (2018). Models of schizotypy: the importance of conceptual clarity. *Schizophrenia Bulletin*, 1–8. https://doi.org/10.1093/schbul/sby012

Grant, P., & Hennig, J. (2020). Schizotypy, social stress and the emergence of psychotic-like states - A case for benign schizotypy? *Schizophrenia Research*, *216*(xxxx), 435–442. https://doi.org/10.1016/j.schres.2019.10.052

Grant, P., Kuepper, Y., Mueller, E. A., Wielpuetz, C., Mason, O. J., & Hennig, J. (2013). Dopaminergic foundations of schizotypy as measured by the German version of the Oxford-Liverpool Inventory of Feelings and Experiences (O-LIFE)-a suitable endophenotype of schizophrenia. *Frontiers in Human Neuroscience*, *7*(January), 1. https://doi.org/10.3389/fnhum.2013.00001

Graybiel, A. M. (1998). The basal ganglia and chunking of action repertoires. *Neurobiology of Learning and Memory*, *70*(1–2), 119–136. https://doi.org/10.1006/nlme.1998.3843

Griffanti, L., Douaud, G., Bijsterbosch, J., Evangelisti, S., Alfaro-Almagro, F., Glasser, M. F., Duff, E. P., Fitzgibbon, S., Westphal, R., Carone, D., Beckmann, C. F., & Smith, S. M. (2017). Hand classification of fMRI ICA noise components. *NeuroImage*, *154*, 188–205. https://doi.org/10.1016/j.neuroimage.2016.12.036

Griffanti, L., Salimi-Khorshidi, G., Beckmann, C. F., Auerbach, E. J., Douaud, G., Sexton, C. E., Zsoldos, E., Ebmeier, K. P., Filippini, N., Mackay, C. E., Moeller, S., Xu, J., Yacoub, E., Baselli, G., Ugurbil, K., Miller, K. L., & Smith, S. M. (2014). ICA-based artefact removal and accelerated fMRI acquisition for improved resting state network imaging. *NeuroImage*, *95*, 232–247. https://doi.org/10.1016/j.neuroimage.2014.03.034

Guloksuz, S., & Van Os, J. (2018). The slow death of the concept of schizophrenia and the painful birth of the psychosis spectrum. In *Psychological Medicine* (Vol. 48, Issue 2). https://doi.org/10.1017/S0033291717001775

Gurin, L., & Blum, S. (2017). Delusions and the right hemisphere: A review of the case for the right hemisphere as a mediator of reality-based belief. *Journal of Neuropsychiatry and Clinical Neurosciences*, *29*(3), 225–235. https://doi.org/10.1176/appi.neuropsych.16060118

Haber, S. N. (2003). The primate basal ganglia: Parallel and integrative networks. *Journal of Chemical Neuroanatomy*, *26*(4), 317–330. https://doi.org/10.1016/j.jchemneu.2003.10.003

Haber, S. N. (2010). Integrative Networks Across Basal Ganglia Circuits. In *Handbook of Basal Ganglia Structure and Function* (Vol. 20). Elsevier Inc. https://doi.org/10.1016/B978-0-12-374767-9.00024-X

Haber, S. N. (2016). Corticostriatal circuitry. *Dialogues in Clinical Neuroscience*, *18*(1), 7–21. https://doi.org/10.1007/978-3-642-40308-8_2

Haber, S. N., Fudge, J. L., & McFarland, N. R. (2000). Striatonigrostriatal pathways in primates form an ascending spiral from the shell to the dorsolateral striatum. *The Journal of Neuroscience : The Official Journal of the Society for Neuroscience*, *20*(6), 2369–2382. https://doi.org/http://www.jneurosci.org/content/20/6/2369

Haber, S. N., & Knutson, B. (2009). The reward circuit: linking primate anatomy and human imaging. *Neuropsychopharmacology*, *35*(1), 1–23. https://doi.org/10.1038/npp.2009.129

Haber, S. N., & McFarland, N. R. (2001). The place of the thalamus in frontal cortical-basal ganglia circuits. *Neuroscientist*, *7*(4), 315–324. https://doi.org/10.1177/107385840100700408

Hadley, J. A., Nenert, R., Kraguljac, N. V., Bolding, M. S., White, D. M., Skidmore, F. M., Visscher, K. M., & Lahti, A. C. (2014). Ventral tegmental area/midbrain functional connectivity and response to antipsychotic medication in schizophrenia. *Neuropsychopharmacology*, *39*(4), 1020–1030. https://doi.org/10.1038/npp.2013.305

Hanssen, M., Krabbendam, L., Vollema, M., Delespaul, P., & van Os, J. (2006). Evidence for instrument and family-specific variation of subclinical psychosis dimensions in the general population. *Journal of Abnormal Psychology*, *115*(1), 5–14. https://doi.org/10.1037/0021-843X.115.1.5

Harrison, P. J. (2004). The hippocampus in schizophrenia: A review of the neuropathological evidence and its pathophysiological implications. *Psychopharmacology*, *174*(1), 151–162. https://doi.org/10.1007/s00213-003-1761-y

Heckers, S., & Konradi, C. (2015). GABAergic mechanisms of hippocampal hyperactivity in schizophrenia. *Schizophrenia Research*, *167*(1–3), 4–11. https://doi.org/10.1016/j.schres.2014.09.041

Heinz, A., & Schlagenhauf, F. (2010). Dopaminergic dysfunction in schizophrenia: Salience attribution revisited. *Schizophrenia Bulletin*, *36*(3), 472–485. https://doi.org/10.1093/schbul/sbq031

Henseler, I., Falkai, P., & Gruber, O. (2010). Disturbed functional connectivity within brain networks subserving domain-specific subcomponents of working memory in schizophrenia: relation to performance and clinical symptoms. *Journal of Psychiatric Research*, *44*(6), 364–372. https://doi.org/10.1016/j.jpsychires.2009.09.003

Hoffman, J. M., Meiega, W., Hawk, T., Grafton, S., Mahoney, D. K., Barrio, J. R., Mazziotta, J. C., & Phelps, M. E. (1992). The Effectsof Carbidopa Administration on Kinetics in Positron Emission Tomography. *Journal of Nuclear Medicine*, *33*(8), 1472–1477. https://pubmed.ncbi.nlm.nih.gov/1634937/

Horan, W. P., Brown, S. A., & Blanchard, J. J. (2007). Social anhedonia and schizotypy: The

contribution of individual differences in affective traits, stress, and coping. *Psychiatry Research*, *149*(1–3), 147–156. https://doi.org/10.1016/j.psychres.2006.06.002

Horga, G., Cassidy, C. M., Xu, X., Moore, H., Slifstein, M., Van Snellenberg, J. X., & Abi-Dargham, A. (2016). Dopamine-Related Disruption of Functional Topography of Striatal Connections in Unmedicated Patients With Schizophrenia. *JAMA Psychiatry*, *10032*. https://doi.org/10.1001/jamapsychiatry.2016.0178

Howes, O. D., Bose, S. K., Turkheimer, F., Valli, I., Egerton, A., Valmaggia, L. R., Murray, R. M., McGuire, P., Ph, D., & Psych, F. R. C. (2011). Dopamine Synthesis Capacity Before Onset of Psychosis: A Prospective [18F]-DOPA PET Imaging Study. *American Journal of Psychiatry*, *11*, 1311–1317. https://doi.org/10.1176/appi.ajp.2011.11010160

Howes, O. D., Bose, S., Turkheimer, F., Valli, I., Egerton, A., Stahl, D., Valmaggia, L., Allen, P., Murray, R., & McGuire, P. (2011). Progressive increase in striatal dopamine synthesis capacity as patients develop psychosis: a PET study. *Molecular Psychiatry*, *16*(9), 885–886. https://doi.org/10.1038/mp.2011.20

Howes, O. D., McCutcheon, R., & Stone, J. (2015). Glutamate and dopamine in schizophrenia: An update for the 21st century. *J Psychopharmacol*, *29*(2), 97–115. https://doi.org/10.1177/0269881114563634

Howes, O. D., Montgomery, A. J., Asselin, M. C., Murray, R. M., Valli, I., Tabraham, P., Bramon-Bosch, E., Valmaggia, L., Johns, L., Broome, M., McGuire, P. K., & Grasby, P. M. (2009). Elevated striatal dopamine function linked to prodromal signs of schizophenia. *Archives of General Psychiatry*, *66*(1), 13–20. https://doi.org/10.1001/archgenpsychiatry.2008.514

Howes, O. D., Williams, M., Ibrahim, K., Leung, G., Egerton, A., McGuire, P. K., & Turkheimer, F. (2013). Midbrain dopamine function in schizophrenia and depression: A post-mortem and positron emission tomographic imaging study. *Brain*, *136*(11), 3242–3251. https://doi.org/10.1093/brain/awt264

Hurd, Y. L., & Hall, H. (2005). Chapter IX Human forebrain dopamine systems: Characterization of the normal brain and in relation to psychiatric disorders. *Handbook of Chemical Neuroanatomy*, *21*, 525–571. https://doi.org/10.1016/S0924-8196(05)80013-2

Huttunen, J., Heinimaa, M., Svirskis, T., Nyman, M., Kajander, J., Forsback, S., Solin, O., Ilonen, T., Korkeila, J., Ristkari, T., McGlashan, T., Salokangas, R. K. R., & Hietala, J. (2008). Striatal dopamine synthesis in first-degree relatives of patients with schizophrenia. *Biological Psychiatry*, *63*(1), 114–117. https://doi.org/10.1016/j.biopsych.2007.04.017

Jablensky, A. (2000). Epidemiology of schizophrenia: The global burden of disease and disability. *European Archives of Psychiatric and Clinical Neuroscience*, *250*(6), 274 – 285. https://doi.org/10.1007/s004060070002

Jacobson, S., Kelleher, I., Harley, M., Murtagh, A., Clarke, M., Blanchard, M., Connolly, C., O'Hanlon, E., Garavan, H., & Cannon, M. (2010). Structural and functional brain correlates of subclinical psychotic symptoms in 11-13 year old schoolchildren. *NeuroImage*, *49*(2), 1875–1885. https://doi.org/10.1016/j.neuroimage.2009.09.015

Jalbrzikowski, M., Murty, V. P., Tervo-Clemmens, B., Foran, W., & Luna, B. (2019). Age-associated deviations of amygdala functional connectivity in youths with psychosis spectrum disorders: Relevance to psychotic symptoms. *American Journal of Psychiatry*, *176*(3), 196–207. https://doi.org/10.1176/appi.ajp.2018.18040443

Jauhar, S., McCutcheon, R., Borgan, F., Veronese, M., Nour, M., Pepper, F., Rogdaki, M., Stone, J., Egerton, A., Turkheimer, F., McGuire, P., & Howes, O. D. (2018). The relationship between cortical glutamate and striatal dopamine in first-episode psychosis: a cross-sectional multimodal PET and magnetic resonance spectroscopy imaging study. *The Lancet Psychiatry*, *5*(10), 816–823. https://doi.org/10.1016/S2215-0366(18)30268-2

Jenkinson, M., Bannister, P., Brady, M., & Smith, S. (2002). *Improved Optimization for the Robust and Accurate Linear Registration and Motion Correction of Brain Images*. *841*, 825–841. https://doi.org/10.1006/nimg.2002.1132

Joel, D., & Weiner, I. (2000). The connections of the dopaminergic system with the striatum in rats and primates: An analysis with respect to the functional and compartmental organization of the striatum. *Neuroscience*, *96*(3), 451–474. https://doi.org/10.1016/S0306-4522(99)00575-8

Joel, S. E., Caffo, B. S., Van Zijl, P. C. M., & Pekar, J. J. (2011). On the relationship between seed-based and ICA-based measures of functional connectivity. *Magnetic Resonance in Medicine*, *66*(3), 644–657. https://doi.org/10.1002/mrm.22818

Johnstone, E. C., Owens, D. G. C., Faith, C. D., & Crow, T. J. (1986). The Relative Stability of Positive and Negative Features in Chronic Schizophrenia. *The British Journal of Psychiatry*, *150*(1), 60–64. https://doi.org/10.1192/bjp.150.1.60

Jones, H. J., Stergiakouli, E., Tansey, K. E., Hubbard, L., Heron, J., Cannon, M., Holmans, P., Lewis, G., Linden, D. E. J., Jones, P. B., Davey Smith, G., O'Donovan, M. C., Owen, M. J., Walters, J. T., & Zammit, S. (2016). Phenotypic Manifestation of Genetic Risk for Schizophrenia During Adolescence in the General Population. *JAMA Psychiatry*, *73*(3), 221–228. https://doi.org/10.1001/jamapsychiatry.2015.3058

Juckel, G., Schlagenhauf, F., Koslowski, M., Wüstenberg, T., Villringer, A., Knutson, B., Wrase, J., & Heinz, A. (2006). Dysfunction of ventral striatal reward prediction in schizophrenia. *NeuroImage*, *29*(2), 409–416. https://doi.org/10.1016/j.neuroimage.2005.07.051

Kafkas, A., & Montaldi, D. (2015). Striatal and midbrain connectivity with the hippocampus selectively boosts memory for contextual novelty. *Hippocampus*, *25*(11), 1262–1273. https://doi.org/10.1002/hipo.22434

Kaiser, H. F. (1974). An index of factorial simplicity. *Psychometrika*, *39*(1), 31–36. https://doi.org/10.1007/BF02291575

Kapur, S. (2003). Psychosis as a state of aberrant salience: a framework linking biology, phenomenology, and pharmacology in schizophrenia. *American Journal of Psychiatry*, *160*(1), 13–23. https://doi.org/10.1176/appi.ajp.160.1.13

Karreman, M., & Moghaddam, B. (1996). The prefrontal cortex regulates the basal release of dopamine in the limbic striatum: An effect mediated by ventral tegmental area. *Journal of Neurochemistry*, *66*(2), 589–598. https://doi.org/10.1046/j.1471-4159.1996.66020589.x

Kaymaz, N., Drukker, M., Lieb, R., Wittchen, H. U., Werbeloff, N., Weiser, M., Lataster, T., & van Os, J. (2012). Do subthreshold psychotic experiences predict clinical outcomes in unselected non-help-seeking population-based samples? A systematic review and meta-analysis, enriched with new results. *Psychological Medicine*, *42*(11), 2239–2253. https://doi.org/https://doi.org/10.1017/S003329171100291

Keeler, J. F., Pretsell, D. O., & Robbins, T. W. (2014). Functional implications of dopamine D1 vs. D2 receptors: A “prepare and select” model of the striatal direct vs. indirect pathways. In *Neuroscience*. https://doi.org/10.1016/j.neuroscience.2014.07.021

Kegeles, L. S., Abi-Dargham, A., Frankle, W. G., Gil, R., Cooper, T. B., Slifstein, M., Hwang, D. R., Huang, Y., Haber, S. N., & Laruelle, M. (2010). Increased synaptic dopamine function in associative regions of the striatum in schizophrenia. *Arch Gen Psychiatry*, *67*(3), 231–239. https://doi.org/10.1001/archgenpsychiatry.2010.10

Kelleher, I, & Cannon, M. (2011). Psychotic-like experiences in the general population: characterizing a high-risk group for psychosis. *Psychological Medicine*, *41*(1), 1–6. https://doi.org/10.1017/S0033291710001005

Kelleher, Ian, & Cannon, M. (2016). Putting Psychosis in Its Place. *American Journal of Psychiatry*, *173*(10), 951–952. https://doi.org/10.1176/appi.ajp.2016.16070810

Kemp, J. M., & Powell, T. P. S. (1971). The structure of the caudate nucleus of the cat: light and electron microscopy. *Philosophical Transactions of the Royal Society of London. B, Biological Sciences*, *262*(845), 383–401. https://doi.org/10.1098/rstb.1971.0102

Kerns, J. G. (2006). Schizotypy facets, cognitive control, and emotion. *Journal of Abnormal Psychology*, *115*(3), 418–427. https://doi.org/10.1037/0021-843X.115.3.418

Keshavan, M. S., Nasrallah, H. A., & Tandon, R. (2011). Schizophrenia, “Just the Facts” 6. Moving ahead with the schizophrenia concept: From the elephant to the mouse. *Schizophrenia Research*, *127*(1–3), 3–13. https://doi.org/10.1016/j.schres.2011.01.011

Kim, J., & Yoon, K. S. (1998). Stress: Metaplastic effects in the hippocampus. *Trends in Neurosciences*, *21*(12), 505–509. https://doi.org/10.1016/S0166-2236(98)01322-8

Kim, W. S., Shen, G., Liu, C., Kang, N. I., Lee, K. H., Sui, J., & Chung, Y. C. (2020).

Altered amygdala-based functional connectivity in individuals with attenuated psychosis syndrome and first-episode schizophrenia. *Scientific Reports*, *10*(1), 1–9. https://doi.org/10.1038/s41598-020-74771-w

Kindler, J., Schultze-Lutter, F., Hauf, M., Dierks, T., Federspiel, A., Walther, S., Schimmelmann, B. G., & Hubl, D. (2017). Increased Striatal and Reduced Prefrontal Cerebral Blood Flow in Clinical High Risk for Psychosis. *Schizophrenia Bulletin*, 1–11. https://doi.org/10.1093/schbul/sbx070

Kirkpatrick, B., Fenton, W. S., Carpenter, W. T., & Marder, S. R. (2006). The NIMH-MATRICS consensus statement on negative symptoms. *Schizophrenia Bulletin*, *32*(2), 214–219. https://doi.org/10.1093/schbul/sbj053

Kitaichi, Y., Inoue, T., Izumi, T., Nakagawa, S., Kato, A., & Koyama, T. (2005). Subchronic milnacipran treatment increases basal extracellular noradrenaline concentrations in the medial prefrontal cortex of rats. *European Journal of Pharmacology*, *520*(1–3), 37–42. https://doi.org/10.1016/j.ejphar.2005.08.004

Kotov, R., Waszczuk, M. A., Krueger, R. F., Forbes, M. K., Watson, D., Clark, L. A., Achenbach, T. M., Althoff, R. R., Ivanova, M. Y., Michael Bagby, R., Brown, T. A., Carpenter, W. T., Caspi, A., Moffitt, T. E., Eaton, N. R., Forbush, K. T., Goldberg, D., Hasin, D., Hyman, S. E., … Zimmerman, M. (2017). The hierarchical taxonomy of psychopathology (HiTOP): A dimensional alternative to traditional nosologies. *Journal of Abnormal Psychology*, *126*(4), 454–477. https://doi.org/10.1037/abn0000258

Kozhuharova, P., Saviola, F., Diaconescu, A., & Allen, P. (2020). High schizotypy traits are associated with reduced hippocampal resting state functional connectivity. *Psychiatry Research: Neuroimaging*, 111215. https://doi.org/10.1016/j.pscychresns.2020.111215

Kraemer, H. C., Noda, A., & O'Hara, R. (2004). Categorical versus dimensional approaches to diagnosis: Methodological challenges. *Journal of Psychiatric Research*, *38*(1), 17–25. https://doi.org/10.1016/S0022-3956(03)00097-9

Kraguljac, N. V., White, D. M., Hadley, N., Hadley, J. A., Hoef, L. Ver, Davis, E., & Lahti, A. C. (2016). Aberrant hippocampal connectivity in unmedicated patients with schizophrenia and effects of antipsychotic medication: A longitudinal resting state functional mri study. *Schizophrenia Bulletin*, *42*(4), 1046–1055. https://doi.org/10.1093/schbul/sbv228

Kriegeskorte, N., Simmons, W. K., Bellgowan, P. S., & Baker, C. I. (2009). Circular analysis in systems neuroscience: the dangers of double dipping. *Nature Neuroscience*, *12*(5), 535–540. https://doi.org/10.1038/nn.2303

Kumakura, Y., Cumming, P., Vernaleken, I., Buchholz, H. G., Siessmeier, T., Heinz, A., Kienast, T., Bartenstein, P., & Gründer, G. (2007). Elevated [18F]fluorodopamine turnover in brain of patients with schizophrenia: An [18F]fluorodopa/positron emission tomography study. *Journal of Neuroscience*, *27*(30), 8080–8087.

https://doi.org/10.1523/JNEUROSCI.0805-07.2007

Kwapil, T. R., & Barrantes-Vidal, N. (2015). Schizotypy: looking back and moving forward. *Schizophrenia Bulletin*, *41*(2), S366–S373. https://doi.org/10.1093/schbul/sbu186

Kwapil, T. R., Gross, G. M., Silvia, P. J., & Barrantes-Vidal, N. (2013). Prediction of psychopathology and functional impairment by positive and negative schizotypy in the chapmans' ten-year longitudinal study. *Journal of Abnormal Psychology*, *122*(3), 807–815. https://doi.org/10.1037/a0033759

Lancaster, T. M., Ihssen, N., Brindley, L. M., Tansey, K. E., Mantripragada, K., O'Donovan, M. C., Owen, M. J., & Linden, D. E. J. (2016). Associations between polygenic risk for schizophrenia and brain function during probabilistic learning in healthy individuals. *Human Brain Mapping*, *37*(2), 491–500. https://doi.org/10.1002/hbm.23044

Larsen, B., Olafsson, V., Calabro, F., Laymon, C., Tervo-Clemmens, B., Campbell, E., Minhas, D., Montez, D., Price, J., & Luna, B. (2020). Maturation of the human striatal dopamine system revealed by PET and quantitative MRI. *Nature Communications*, *11*(1), 1–10. https://doi.org/10.1038/s41467-020-14693-3

Laursen, T. M., Munk-Olsen, T., & Vestergaard, M. (2012). Life expectancy and cardiovascular mortality in persons with schizophrenia. *Current Opinion in Psychiatry*, *25*, 83–88. https://doi.org/10.1097/YCO.0b013e32835035ca

Laviolette, S. R., & Grace, A. A. (2006). The roles of cannabinoid and dopamine receptor systems in neural emotional learning circuits: Implications for schizophrenia and addiction. *Cellular and Molecular Life Sciences*, *63*(14), 1597–1613. https://doi.org/10.1007/s00018-006-6027-5

Lee, S. H., DeCandia, T. R., Ripke, S., Yang, J., Sullivan, P. F., Goddard, M. E., Keller, M. C., Visscher, P. M., & Wray, N. R. (2012). Estimating the proportion of variation in susceptibility to schizophrenia captured by common SNPs. *Nature Genetics*, *44*(3), 247–250. https://doi.org/10.1038/ng.1108

Lenzenweger, M. F. (2006). Schizotypy: An organizing framework for schizophrenia research. *Current Directions in Psychological Sciences*, *15*(4), 162–166.

Lerner, T. N., Shilyansky, C., Davidson, T. J., Evans, K. E., Beier, K. T., Zalocusky, K. A., Crow, A. K., Malenka, R. C., Luo, L., Tomer, R., & Deisseroth, K. (2015). Intact-Brain Analyses Reveal Distinct Information Carried by SNc Dopamine Subcircuits. *Cell*, *162*(3), 635–647. https://doi.org/10.1016/j.cell.2015.07.014

Leucht, S., Kane, J. M., Kissling, W., Hamann, J., Etschel, E., & Engel, R. (2005). Clinical implications of Brief Psychiatric Rating Scale scores. *British Journal of Psychiatry*, *187*(OCT.), 366–371. https://doi.org/10.1192/bjp.187.4.366

Lewandowski, K. E., Cohen, B. M., & Ongur, D. (2011). Evolution of neuropsychological dysfunction during the course of schizophrenia and bipolar disorder. *Psychological*

Medicine, *41*(2), 225–241. https://doi.org/10.1017/S0033291710001042

Lewandowski, K. E., McCarthy, J. M., Öngür, D., Norris, L. A., Liu, G. Z., Juelich, R. J., & Baker, J. T. (2019). Functional connectivity in distinct cognitive subtypes in psychosis. *Schizophrenia Research*, *204*, 120–126. https://doi.org/10.1016/j.schres.2018.08.013

Li, T., Wang, Q., Zhang, J., Rolls, E. T., Yang, W., Palaniyappan, L., Zhang, L., Cheng, W., Yao, Y., Liu, Z., Gong, X., Luo, Q., Tang, Y., Crow, T. J., Broome, M. R., Xu, K., Li, C., Wang, J., Liu, Z., … Feng, J. (2017). Brain-Wide Analysis of Functional Connectivity in First-Episode and Chronic Stages of Schizophrenia. *Schizophrenia Bulletin*, *43*(2), 436–448. https://doi.org/10.1093/schbul/sbw099

Liddle, P. F. (1987). The symptoms of chronic schizophrenia. A re-examination of the positive-negative dichotomy. *British Journal of Psychiatry*, *151*(2), 145–151. https://doi.org/10.1192/bjp.151.2.145

Lidsky, T. I. (1995). Reevaluation of the mesolimbic hypothesis of antipsychotic drug action. *Schizophrenia Bulletin*, *21*(1), 67–74. https://doi.org/10.1093/schbul/21.1.67

Lieberman, J. A., Girgis, R. R., Brucato, G., Moore, H., Provenzano, F., Kegeles, L., Javitt, D., Kantrowitz, J., Wall, M. M., Corcoran, C. M., Schobel, S. A., & Small, S. A. (2018). Hippocampal dysfunction in the pathophysiology of schizophrenia: a selective review and hypothesis for early detection and intervention. *Molecular Psychiatry*, *23*(8), 1764–1772. https://doi.org/10.1038/mp.2017.249

Lieberman, J. A., Kane, J. M., & Alvir, J. (1987). Provocative tests with psychostimulant drugs in schizophrenia. *Psychopharmacology*. https://doi.org/10.1007/BF00216006

Liégeois, F., & Elward, R. (2020). Functional magnetic resonance imaging. In *Handbook of Clinical Neurology* (Vol. 174, pp. 265–275). https://doi.org/10.1016/B978-0-444-64148-9.00019-3

Lincoln, T. M., Dollfus, S., & Lyne, J. (2017). Current developments and challenges in the assessment of negative symptoms. *Schizophrenia Research*, *186*, 8–18. https://doi.org/10.1016/j.schres.2016.02.035

Linney, Y. M., Murray, R. M., Peters, E. R., MacDonald, A. M., Rijsdijk, F., & Sham, P. C. (2003). A quantitative genetic analysis of schizotypal personality traits. *Psychological Medicine*, *33*(5), 803–816. https://doi.org/10.1017/S0033291703007906

Lipska, B. K., Weinberger, D. R., Swerdlow, N. R., Geyer, M. A., Braff, D. L., & Jaskiw, G. E. (1995). Neonatal excitotoxic hippocampal damage in rats causes post-pubertal changes in prepulse inhibition of startle and its disruption by apomorphine. *Psychopharmacology*, *122*(1), 35–43. https://doi.org/10.1007/BF02246439

Little, R. J. A. (1988). A test of missing completely at random for multivariate data with missing values. *Journal of the American Statistical Association*. https://doi.org/10.1080/01621459.1988.10478722

Lodge, D. J., & Grace, A. A. (2006). The hippocampus modulates dopamine neuron responsivity by regulating the intensity of phasic neuron activation. *Neuropsychopharmacology*, *31*(7), 1356–1361. https://doi.org/10.1038/sj.npp.1300963

Lodge, D. J., & Grace, A. A. (2007). Aberrant hippocampal activity underlies the dopamine dysregulation in an animal model of schizophrenia. *Journal of Neuroscience*, *27*(42), 11424–11430. https://doi.org/10.1523/JNEUROSCI.2847-07.2007

Lodge, D. J., & Grace, A. A. (2011). Hippocampal dysregulation of dopamine system function and the pathophysiology of schizophrenia. *Trends in Pharmacological Sciences*, *32*(9), 507–513. https://doi.org/10.1016/j.tips.2011.05.001

Lodge, D. J., & Grace, A. A. (2012). Divergent activation of ventromedial and ventrolateral dopamine systems in animal models of amphetamine sensitization and schizophrenia. *International Journal of Neuropsychopharmacology*, *15*(1), 69–76. https://doi.org/10.1017/S1461145711000113

López-González, F. J., Paredes-Pacheco, J., Thurnhofer-Hemsi, K., Rossi, C., Enciso, M., Toro-Flores, D., Murcia-Casas, B., Gutiérrez-Cardo, A. L., & Roé-Vellvé, N. (2019). QModeling: a Multiplatform, Easy-to-Use and Open-Source Toolbox for PET Kinetic Analysis. *Neuroinformatics*, *17*(1), 103–114. https://doi.org/10.1007/s12021-018-9384-y

Loranger, A. W. (1984). Sex difference in age at onset of schizophrenia. *Archives of General Psychiatry*, *41*(2), 157–161. https://doi.org/10.1001/archpsyc.1984.01790130053007

Lord, L.-D., Allen, P., Expert, P., Howes, O. D., Broome, M., Lambiotte, R., Fusar-Poli, P., Valli, I., Mcguire, P., & Turkheimer, F. E. (2012). Functional brain networks before the onset of psychosis: A prospective fMRI study with graph theoretical analysis. *NeuroImage: Clinical*, *1*(1), 91–98. https://doi.org/10.1016/j.nicl.2012.09.008

Luna, B., Thulborn, K. R., Munoz, D. P., Merriam, E. P., Garver, K. E., Minshew, N. J., Keshavan, M. S., Genovese, C. R., Eddy, W. F., & Sweeney, J. A. (2001). Maturation of widely distributed brain function subserves cognitive development. *NeuroImage*, *13*(5), 786–793. https://doi.org/10.1006/nimg.2000.0743

MacDonald, A. W., Pogue-Geile, M. F., Debski, T. T., & Manuck, S. (2001). Genetic and environmental influences on schizotypy: a community-based twin study. *Schizophrenia Bulletin*, *27*(1), 47–58. https://doi.org/10.1093/oxfordjournals.schbul.a006859

Maia, T. V., & Frank, M. J. (2017). An Integrative Perspective on the Role of Dopamine in Schizophrenia. *Biological Psychiatry*, *81*(1), 52–66. https://doi.org/10.1016/j.biopsych.2016.05.021

Makowski, C., Bodnar, M., Shenker, J. J., Malla, A. K., Joober, R., Chakravarty, M. M., & Lepage, M. (2017). Linking persistent negative symptoms to amygdala–hippocampus structure in first-episode psychosis. *Translational Psychiatry*, *7*(8). https://doi.org/10.1038/tp.2017.168

Malla, A., & Payne, J. (2005). First-episode psychosis: Psychopathology, quality of life, and functional outcome. *Schizophrenia Bulletin*, *31*(3), 650–671. https://doi.org/10.1093/schbul/sbi031

Marquand, A. F., Haak, K. V., & Beckmann, C. F. (2017). Functional corticostriatal connection topographies predict goal-directed behaviour in humans. *Nature Human Behaviour*, *1*(8), 1–9. https://doi.org/10.1038/s41562-017-0146

Mason, O., & Claridge, G. (2006). The Oxford-Liverpool Inventory of Feelings and Experiences (O-LIFE): Further description and extended norms. *Schizophrenia Research*, *82*(2–3), 203–211. https://doi.org/10.1016/j.schres.2005.12.845

Mason, O., Linney, Y., & Claridge, G. (2005). Short scales for measuring schizotypy. *Schizophrenia Research*, *78*(2–3), 293–296. https://doi.org/10.1016/j.schres.2005.06.020

Maydeu-Olivares, A. (2015). Evaluating the fit of IRT models. *Handbook of Item Response Theory Modeling: Applications to Typical Performance Assessment*, 111–127.

Maydeu-Olivares, A., & Joe, H. (2014). Assessing approximate fit in categorical data analysis. *Multivariate Behavioral Research*, *49*(4), 305–328. https://doi.org/10.1080/00273171.2014.911075

McCutcheon, R. A., Abi-Dargham, A., & Howes, O. D. (2019). Schizophrenia, Dopamine and the Striatum: From Biology to Symptoms. *Trends in Neurosciences*, *42*(3), 205–220. https://doi.org/10.1016/j.tins.2018.12.004

McGowan, S., Lawrence, A. D., Sales, T., Quested, D., & Grasby, P. (2004). Presynaptic Dopaminergic Dysfunction in Schizophrenia. *Archives of General Psychiatry*, *61*(2), 134. https://doi.org/10.1001/archpsyc.61.2.134

McIntosh, A. M., Gow, A., Luciano, M., Davies, G., Liewald, D. C., Harris, S. E., Corley, J., Hall, J., Starr, J. M., Porteous, D. J., Tenesa, A., Visscher, P. M., & Deary, I. J. (2013). Polygenic risk for schizophrenia is associated with cognitive change between childhood and old age. *Biol Psychiatry*, *73*(10), 938–943. https://doi.org/10.1016/j.biopsych.2013.01.011

Meyer-Lindenberg, A., Miletich, R. S., Kohn, P. D., Esposito, G., Carson, R. E., Quarantelli, M., Weinberger, D. R., & Berman, K. F. (2002a). Reduced prefrontal activity predicts exaggerated striatal dopaminergic function in schizophrenia. *Nature Neuroscience*, *5*(3), 267–271. https://doi.org/10.1038/nn804

Meyer-Lindenberg, A., Miletich, R. S., Kohn, P. D., Esposito, G., Carson, R. E., Quarantelli, M., Weinberger, D. R., & Berman, K. F. (2002b). Reduced prefrontal activity predicts exaggerated striatal dopaminergic function in schizophrenia. *Nature Neuroscience*, *5*(3), 267–271. https://doi.org/10.1038/nn804

Miall, R. C., & Wolpert., D. M. (1996). Forward models for physiological motor control. *Neural Networks*, *9*(8), 1265–1279. https://doi.org/10.1016/S0893-6080(96)00035-4

Mistry, S., Harrison, J. R., Smith, D. J., Escott-Price, V., & Zammit, S. (2018). The use of polygenic risk scores to identify phenotypes associated with genetic risk of schizophrenia: Systematic review. *Schizophrenia Research*, *197*, 2–8. https://doi.org/10.1016/j.schres.2017.10.037

Mizrahi, R., Kenk, M., Suridjan, I., Boileau, I., George, T. P., McKenzie, K., Wilson, A. A., Houle, S., & Rusjan, P. (2014). Stress-induced dopamine response in subjects at clinical high risk for schizophrenia with and without concurrent cannabis use. *Neuropsychopharmacology*, *39*(6), 1479–1489. https://doi.org/10.1038/npp.2013.347

Modinos, G., Allen, P., Grace, A. A., & McGuire, P. (2015). Translating the MAM model of psychosis to humans. *Trends in Neurosciences*, *38*(3), 129–138. https://doi.org/10.1016/j.tins.2014.12.005

Modinos, G., Şimşek, F., Azis, M., Bossong, M., Bonoldi, I., Samson, C., Quinn, B., Perez, J., Broome, M. R., Zelaya, F., Lythgoe, D. J., Howes, O. D., Stone, J. M., Grace, A. A., Allen, P., & McGuire, P. (2018). Prefrontal GABA levels, hippocampal resting perfusion and the risk of psychosis. In *Neuropsychopharmacology* (Vol. 43, Issue 13). https://doi.org/10.1038/s41386-017-0004-6

Mohanty, A., Herrington, J. D., Koven, N. S., Fisher, J. E., Wenzel, E. A., Webb, A. G., Heller, W., Banich, M. T., & Miller, G. A. (2005). Neural mechanisms of affective interference in schizotypy. *Journal of Abnormal Psychology*, *114*(1), 16–27. https://doi.org/10.1037/0021-843X.114.1.16

Mohr, C., & Claridge, G. (2015). Schizotypy - Do not worry, it is not all worrisome. *Schizophrenia Bulletin*, *41*(2), S436–S443. https://doi.org/10.1093/schbul/sbu185

Moore, R. Y., Whone, A. L., McGowan, S., & Brooks, D. J. (2003). Monoamine neuron innervation of the normal human brain: An 18F-DOPA PET study. *Brain Research*, *982*(2), 137–145. https://doi.org/10.1016/S0006-8993(03)02721-5

Morris, R. W., Vercammen, a, Lenroot, R., Moore, L., Langton, J. M., Short, B., Kulkarni, J., Curtis, J., O'Donnell, M., Weickert, C. S., & Weickert, T. W. (2012). Disambiguating ventral striatum fMRI-related bold signal during reward prediction in schizophrenia. *Molecular Psychiatry*, *17*(3), 280–289. https://doi.org/10.1038/mp.2011.75

Murray, G. K., Corlett, P. R., Clark, L., Pessiglione, M., Blackwell, A. D., Honey, G., Jones, P. B., Bullmore, E. T., Robbins, T. W., & Fletcher, P. C. (2008). Substantia nigra/ventral tegmental reward prediction error disruption in psychosis. *Molecular Psychiatry*, *13*(3), 239, 267–276. https://doi.org/10.1038/sj.mp.4002058

Murty, V. P., Shermohammed, M., Smith, D. V., Carter, R. M. K., Huettel, S. A., & Adcock, R. A. (2014). Resting state networks distinguish human ventral tegmental area from substantia nigra. *NeuroImage*, *100*, 580–589. https://doi.org/10.1016/j.neuroimage.2014.06.047

Nelson, M. T., Seal, M. L., Pantelis, C., & Phillips, L. J. (2013). Evidence of a dimensional

relationship between schizotypy and schizophrenia: A systematic review. *Neuroscience and Biobehavioral Reviews*, *37*(3), 317–327. https://doi.org/10.1016/j.neubiorev.2013.01.004

Nour, M. M., Dahoun, T., Schwartenbeck, P., Adams, R. A., FitzGerald, T. H. B., Coello, C., Wall, M. B., Dolan, R. J., & Howes, O. D. (2018). Dopaminergic basis for signaling belief updates, but not surprise, and the link to paranoia. *Proceedings of the National Academy of Sciences of the United States of America*, *115*(43), E10167–E10176. https://doi.org/10.1073/pnas.1809298115

O'Doherty, J., Dayan, P., Schultz, J., Deichmann, R., Friston, K. J., & Dolan, R. J. (2004). Dissociable roles of ventral and dorsal striatum in instrumental conditioning. *Science*, *304*(5669), 452–454. https://doi.org/10.1126/science.1094285

Olypher, A. V., Klement, D., & Fenton, A. A. (2006). Cognitive disorganization in hippocampus: A physiological model of the disorganization in psychosis. *Journal of Neuroscience*, *26*(1), 158–168. https://doi.org/10.1523/JNEUROSCI.2064-05.2006

Orlando, M., & Thissen, D. (2003). Further investigation of the performance of S-X2: An item fit index for use with dichotomous item response theory models. *Applied Psychological Measurement*, *27*(4), 289–298. https://doi.org/10.1177/0146621603027004004

Osborne, J. W., & Costello, A. B. (2005). Best practices in exploratory factor analysis: four recommendations for getting the most from your analysis. *Pan-Pacific Management Review*, *2*(2), 131–146. https://doi.org/10.1.1.110.9154

Østby, Y., Tamnes, C. K., Fjell, A. M., Westlye, L. T., Due-Tønnessen, P., & Walhovd, K. B. (2009). Heterogeneity in subcortical brain development: A structural magnetic resonance imaging study of brain maturation from 8 to 30 years. *Journal of Neuroscience*, *29*(38), 11772–11782. https://doi.org/10.1523/JNEUROSCI.1242-09.2009

Owen, M. J., Sawa, A., & Mortensen, P. B. (2016). Schizophrenia. *The Lancet*, *6736*(15), 1–12. https://doi.org/10.1016/S0140-6736(15)01121-6

Pani, S. M., Sabaroedin, K., Tiego, J., Bellgrove, M. A., & Fornito, A. (2020). A multivariate analysis of the association between corticostriatal functional connectivity and psychosis-like experiences in the general community. *Psychiatry Research - Neuroimaging*, *October*, 111202. https://doi.org/10.1016/j.pscychresns.2020.111202

Pantelis, C., Barnes, T. R. E., & Nelson, H. E. (1992). Is the concept of frontal-subcortical dementia relevant to schizophrenia? In *British Journal of Psychiatry* (Vol. 160, Issue APR., pp. 442–460). https://doi.org/10.1192/bjp.160.4.442

Pantelis, C., Barnes, T. R., Nelson, H. E., Tanner, S., Weatherley, L., Owen, A. M., & Robbins, T. W. (1997). Frontal-striatal cognitive deficits in patients with chronic schizophrenia. *Brain*. https://doi.org/10.1093/brain/120.10.1823

Pantelis, C., & Brewer, W. (1996). Neurocognitive and neurobehavioural patterns and the syndromes of schizophrenia: role of frontal-subcortical networks. In C. Pantelis, T. Barnes, & N. HE (Eds.), *Schizophrenia: A Neuropsychological Perspective* (pp. 317–343). John Wiley & Sons.

Papanastasiou, E., Mouchlianitis, E., Joyce, D. W., McGuire, P., Banaschewski, T., Bokde, A. L. W., Bromberg, U., Büchel, C., Quinlan, E. B., Desrivières, S., Flor, H., Frouin, V., Garavan, H., Spechler, P., Gowland, P., Heinz, A., Ittermann, B., Martinot, J.-L., Paillère Martinot, M.-L., … Shergill, S. (2018). Examination of the neural basis of psychoticlike experiences in adolescence during reward processing. *JAMA Psychiatry*, 1–9. https://doi.org/10.1001/jamapsychiatry.2018.1973

Parkes, L., Fulcher, B. D., Yücel, M., & Fornito, A. (2017). Transcriptional signatures of connectomic subregions of the human striatum. *Genes, Brain and Behavior*, *16*(7), 647–663. https://doi.org/10.1111/gbb.12386

Parkes, L., Fulcher, B. D., Yücel, M., & Fornito, A. (2018). An evaluation of the efficacy, reliability, and sensitivity of motion correction strategies for resting-state functional MRI. *NeuroImage*, *171*, 415–436. https://doi.org/10.1016/j.neuroimage.2017.12.073

Patlak, C. S., & Blasberg, R. G. (1985). Graphical evaluation of blood-to-brain transfer constants from multiple-time uptake data. *Journal of Cerebral Blood Flow and Metabolism*, *5*(4), 584–590. https://doi.org/10.1038/jcbfm.1985.87

Pavlova, B., & Uher, R. (2020). Self-report and clinician-rated measures of depression severity: Can one replace the other? *JAMA Psychiatry*, *77*(6), 557–558. https://doi.org/10.1002/da.21993

Peters, E., Joseph, S., Day, S., & Garety, P. (2004). Measuring delusional ideation: the 21-Item Peters et al. Delusions Inventory. *Schizophrenia Bulletin*, *30*(4), 1005–1022. https://doi.org/10.1037/t03329-000

Pettersson-Yeo, W., Allen, P., Benetti, S., McGuire, P., & Mechelli, A. (2011). Dysconnectivity in schizophrenia: Where are we now? *Neuroscience and Biobehavioral Reviews*, *35*(5), 1110–1124. https://doi.org/10.1016/j.neubiorev.2010.11.004

Phillips, W. A., & Silverstein, S. M. (2003). Convergence of biological and psychological perspectives on cognitive coordination in schizophrenia. *Behavioral and Brain Sciences*, *26*(1), 65–138. https://doi.org/10.1017/S0140525X03480023

Pinar, A., Hawi, Z., Cummins, T., Johnson, B., Pauper, M., Tong, J., Tiego, J., Finlay, A., Klein, M., Franke, B., Fornito, A., & Bellgrove, M. A. (2018). Genome-wide association study reveals novel genetic locus associated with intra- individual variability in response time. *Translational Psychiatry*, *8*(1), 207. https://doi.org/10.1038/s41398-018-0262-z

Plomin, R., Haworth, C. M., & Davis, O. S. P. (2009). Quantitative Traits. *Nature Reviews Genetics*, *10*(12), 872–878. https://doi.org/10.1038/nrg2670

Poldrack, R. A., Congdon, E., Triplett, W., Gorgolewski, K. J., Karlsgodt, K. H., Mumford, J. A., Sabb, F. W., Freimer, N. B., London, E. D., Cannon, T. D., & Bilder, R. M. (2016). A phenome-wide examination of neural and cognitive function. *Scientific Data*, *3*, 1–12. https://doi.org/10.1038/sdata.2016.110

Postuma, R. B., & Dagher, A. (2006). Basal ganglia functional connectivity based on a meta-analysis of 126 positron emission tomography and functional magnetic resonance imaging publications. *Cerebral Cortex*, *16*(10), 1508–1521. https://doi.org/10.1093/cercor/bhj088

Potkin, S. G., Turner, J. A., Brown, G. G., McCarthy, G., Greve, D. N., Glover, G. H., Manoach, D. S., Belger, A., Diaz, M., Wible, C. G., Ford, J. M., Mathalon, D. H., Gollub, R., Lauriello, J., O'Leary, D., Van Erp, T. G. M., Toga, A. W., Preda, A., & Lim, K. O. (2009). Working memory and DLPFC inefficiency in schizophrenia: The FBIRN study. *Schizophrenia Bulletin*, *35*(1), 19–31. https://doi.org/10.1093/schbul/sbn162

Power, J. D., Barnes, K. A., Snyder, A. Z., Schlaggar, B. L., & Petersen, S. E. (2012). Spurious but systematic correlations in functional connectivity MRI networks arise from subject motion. *NeuroImage*, *59*(3), 2142–2154. https://doi.org/10.1016/j.neuroimage.2011.10.018

Power, J. D., Plitt, M., Laumann, T. O., & Martin, A. (2017). Sources and implications of whole-brain fMRI signals in humans. *NeuroImage*, *146*, 609–625. https://doi.org/10.1016/j.neuroimage.2016.09.038

Powers, A. R., Mathys, C., & Corlett, P. R. (2017). Pavlovian conditioning–induced hallucinations result from overweighting of perceptual priors. *Science*, *357*(6351), 596–600. https://doi.org/10.1126/science.aan3458

Preller, K. H., Razi, A., Zeidman, P., Stämpfli, P., Friston, K. J., & Vollenweider, F. X. (2019). Effective connectivity changes in LSD-induced altered states of consciousness in humans. *Proceedings of the National Academy of Sciences of the United States of America*, *116*(7), 2743–2748. https://doi.org/10.1073/pnas.1815129116

Priebe, S., & Röhricht, F. (2001). Specific body image pathology in acute schizophrenia. *Psychiatry Research*, *101*(3), 289–301. https://doi.org/10.1016/S0165-1781(01)00214-1

Pruim, R. H. R., Mennes, M., van Rooij, D., Llera, A., Buitelaar, J. K., & Beckmann, C. F. (2015). ICA-AROMA: A robust ICA-based strategy for removing motion artifacts from fMRI data. *NeuroImage*, *112*, 267–277. https://doi.org/10.1016/j.neuroimage.2015.02.064

Purcell, S. S. M., Wray, N. R. N., Stone, J. J. L., Visscher, P. M., O'Donovan, M. C., Sullivan, P. F., & Sklar, P. (2009). Common polygenic variation contributes to risk of schizophrenia and bipolar disorder. *Nature*, *460*(7256), 748–752.

Pycock, C. J., Kerwin, R. W., & Carter, C. J. (1980). Effect of lesion of cortical dopamine

terminals on subcortical dopamine receptors in rats. *Nature*, *286*(5768), 74–77. https://doi.org/10.1038/286074a0

Quartarone, A., Cacciola, A., Milardi, D., Ghilardi, M. F., Calamuneri, A., Chillemi, G., Anastasi, G., & Rothwell, J. (2019). New insights into cortico-basal-cerebellar connectome: clinical and physiological considerations. *Brain : A Journal of Neurology*, 1–11. https://doi.org/10.1093/brain/awz310

Razi, A., & Friston, K. J. (2016). The connected brain: causality, models, and intrinsic dynamics. *IEEE Signal Processing Magazine*, *33*(3), 14–35. https://doi.org/10.1126/science.342.6158.577

Razi, A., Kahan, J., Rees, G., & Friston, K. J. (2015). Construct validation of a DCM for resting state fMRI. *NeuroImage*, *106*, 1–14. https://doi.org/10.1016/j.neuroimage.2014.11.027

Reid, M. A., Stoeckel, L. E., White, D. M., Avsar, K. B., Bolding, M. S., Akella, N. S., Knowlton, R. C., Den Hollander, J. A., & Lahti, A. C. (2010). Assessments of function and biochemistry of the anterior cingulate cortex in schizophrenia. *Biological Psychiatry*, *68*(7), 625–633. https://doi.org/10.1016/j.biopsych.2010.04.013

Reise, S. P., Ainsworth, A. T., & Haviland, M. G. (2005). Item response theory: Fundamentals, applications, and promise in psychological research. *Current Directions in Psychological Sciences*, *14*(2), 95–101. https://doi.org/10.1111/j.0963-7214.2005.00342.x

Reise, S. P., & Rodriguez, A. (2016). Item response theory and the measurement of psychiatric constructs: some empirical and conceptual issues and challenges. *Psychological Medicine*, *46*(10), 2025. https://doi.org/10.1017/S0033291716000520

Reise, S. P., & Waller, N. G. (2009). Item response theory and clinical measurement. *Annual Review of Clinical Psychology*, *5*, 27–48. https://doi.org/10.1146/annurev.clinpsy.032408.153553

Repovs, G., Csernansky, J. G., & Barch, D. M. (2011). Brain network connectivity in individuals with schizophrenia and their siblings. *Biological Psychiatry*, *69*(10), 967–973. https://doi.org/10.1016/j.biopsych.2010.11.009

Ripke, S., Neale, B. M., Corvin, A., Walters, J. T. R., Farh, K.-H., Holmans, P. a., Lee, P., Bulik-Sullivan, B., Collier, D. a., Huang, H., Pers, T. H., Agartz, I., Agerbo, E., Albus, M., Alexander, M., Amin, F., Bacanu, S. a., Begemann, M., Belliveau Jr, R. a., … O'Donovan, M. C. (2014). Biological insights from 108 schizophrenia-associated genetic loci. *Nature*, *511*, 421–427. https://doi.org/10.1038/nature13595

Robbins, T. W., & Everitt, B. J. (1992). Functions of dopamine in the dorsal and ventral striatum. *Seminars in Neuroscience*, *4*(2), 119–127. https://doi.org/10.1016/1044-5765(92)90010-Y

Roiser, J. P., Howes, O. D., Chaddock, C. A., Joyce, E. M., & McGuire, P. (2013). Neural and behavioral correlates of aberrant salience in individuals at risk for psychosis. *Schizophrenia Bulletin*, *39*(6), 1328–1336. https://doi.org/10.1093/schbul/sbs147

Rosenheck, R., Leslie, D., Keefe, R., McEvoy, J., Swartz, M., Perkins, D., Stroup, S., Hsiao, J. K., & Lieberman, J. (2006). Barriers to employment for people with schizophrenia. *American Journal of Psychiatry*, *163*(3), 411–417. https://doi.org/10.1176/appi.ajp.163.3.411

Rössler, W., Riecher-Rössler, A., Angst, J., Murray, R., Gamma, A., Eich, D., van Os, J., & Gross, V. A. (2007). Psychotic experiences in the general population: a twenty-year prospective community study. *Schizophrenia Research*, *92*(1–3), 1–14. https://doi.org/10.1016/j.schres.2007.01.002

Ruottinen, H. M., Rinne, J. O., Ruotsalainen, U. H., Bergman, J. R., Oikonen, V. J., Haaparanta, M. T., Solin, O. H., Laihinen, A. O., & Rinne, U. K. (1995). Striatal [18F]fluorodopa utilization after COMT inhibition with entacapone studied with PET in advanced Parkinson's disease. *Journal of Neural Transmission - Parkinson's Disease and Dementia Section*, *10*(2–3), 91–106. https://doi.org/10.1007/BF02251225

Sabaroedin, K., Tiego, J., Parkes, L., Sforazzini, F., Finlay, A., Johnson, B., Pinar, A., Cropley, V., Harrison, B. J., Zalesky, A., Pantelis, C., Bellgrove, M., & Fornito, A. (2019). Functional connectivity of corticostriatal circuitry and psychosis-like experiences in the general community. *Biological Psychiatry*, *86*(1), 16–24. https://doi.org/10.1016/j.biopsych.2019.02.013

Sahakyan, L., Meller, T., Evermann, U., Schmitt, S., Pfarr, J.-K., Sommer, J., Kwapil, T. R., & Nenadić, I. (2020). Anterior vs Posterior Hippocampal Subfields in an Extended Psychosis Phenotype of Multidimensional Schizotypy in a Nonclinical Sample. *Schizophrenia Bulletin*. https://doi.org/10.1093/schbul/sbaa099

Salimi-Khorshidi, G., Douaud, G., Beckmann, C. F., Glasser, M. F., Griffanti, L., & Smith, S. M. (2014). Automatic denoising of functional MRI data: combining independent component analysis and hierarchical fusion of classifiers. *NeuroImage*, *90*, 449–468. https://doi.org/10.1016/j.neuroimage.2013.11.046

Samejima, F. (1969). Estimation of latent ability using a response pattern of graded scores. *Psychometrika Monograph Supplement*. https://doi.org/https://doi.org/10.1007/BF02291411

Sarpal, D. K., Robinson, D. G., Fales, C., Lencz, T., Argyelan, M., Karlsgodt, K. H., Gallego, J. A., John, M., Kane, J. M., Szeszko, P. R., & Malhotra, A. K. (2017). Relationship between Duration of Untreated Psychosis and Intrinsic Corticostriatal Connectivity in Patients with Early Phase Schizophrenia. *Neuropsychopharmacology*, *42*(11), 2214–2221. https://doi.org/10.1038/npp.2017.55

Sarpal, D. K., Robinson, D. G., Lencz, T., Argyelan, M., Ikuta, T., Karlsgodt, K., Gallego, J.

A., Kane, J. M., Szeszko, P. R., & Malhotra, A. K. (2015). Antipsychotic treatment and functional connectivity of the striatum in first-episode schizophrenia. *JAMA Psychiatry*, *72*(1), 5–13. https://doi.org/10.1001/jamapsychiatry.2014.1734

Satterthwaite, T. D., Wolf, D. H., Loughead, J., Ruparel, K., Elliott, M. A., Hakonarson, H., Gur, R. C., & Gur, R. E. (2012). Impact of in-scanner head motion on multiple measures of functional connectivity: relevance for studies of neurodevelopment in youth. *NeuroImage*, *60*(1), 623–632. https://doi.org/10.1016/j.neuroimage.2011.12.063

Satterthwaite, T D, Vandekar, S. N., Wolf, D. H., Bassett, D. S., Ruparel, K., Shehzad, Z., Craddock, R. C., Shinohara, R. T., Moore, T. M., Gennatas, E. D., Jackson, C., Roalf, D. R., Milham, M. P., Calkins, M. E., Hakonarson, H., Gur, R. C., & Gur, R. E. (2015). Connectome-wide network analysis of youth with Psychosis-Spectrum symptoms. *Molecular Psychiatry*, *20*(12), 1508–1515. https://doi.org/10.1038/mp.2015.66

Satterthwaite, Theodore D., Elliott, M. A., Gerraty, R. T., Ruparel, K., Loughead, J., Calkins, M. E., Eickhoff, S. B., Hakonarson, H., Gur, R. C., Gur, R. E., & Wolf, D. H. (2013). An improved framework for confound regression and filtering for control of motion artifact in the preprocessing of resting-state functional connectivity data. *NeuroImage*, *64*(1), 240–256. https://doi.org/10.1016/j.neuroimage.2012.08.052

Schlier, B., Jaya, E. S., Moritz, S., & Lincoln, T. M. (2015). The Community Assessment of Psychic Experiences measures nine clusters of psychosis-like experiences: A validation of the German version of the CAPE. *Schizophrenia Research*, *169*(1–3), 274–279. https://doi.org/10.1016/j.schres.2015.10.034

Schultz, W., Apicella, P., & Ljungberg, T. (1993). Responses of monkey dopamine neurons to reward and conditioned stimuli during successive steps of learning a delayed response task. *Journal of Neuroscience*, *13*(3), 900–913. https://doi.org/10.1523/jneurosci.13-03-00900.1993

Schultz, Wolfram. (2016). Reward functions of the basal ganglia. In *Journal of Neural Transmission*. https://doi.org/10.1007/s00702-016-1510-0

Seeman, A. P., & Lee, T. (1975). Antipsychotic drugs: Direct correlation between clinical potency and presynaptic action on dopamine neurons. *Science*, *188*(4194), 1217–1219. https://doi.org/10.1126/science.1145194

Seeman, P. (1992). Dopamine receptor sequences. Therapeutic levels of neuroleptics occupy D2 receptors, clozapine occupies D4. *Neuropsychopharmacology : Official Publication of the American College of Neuropsychopharmacology*, *7*(4), 261–284.

Sekar, A., Bialas, A. R., de Rivera, H., Davis, A., Hammond, T. R., Kamitaki, N., Tooley, K., Presumey, J., Baum, M., Van Doren, V., Genovese, G., Rose, S. A., Handsaker, R. E., Daly, M. J., Carroll, M. C., Stevens, B., & McCarroll, S. A. (2016). Schizophrenia risk from complex variation of complement component 4. *Nature*, 1–17. https://doi.org/10.1038/nature16549

Sheffield, J. M., Kandala, S., Burgess, G. C., Harms, M. P., & Barch, D. M. (2016). Cingulo-opercular network efficiency mediates the association between psychotic-like experiences and cognitive ability in the general population. *Biological Psychiatry: Cognitive Neuroscience and Neuroimaging*, *1*(6), 498–506. https://doi.org/10.1016/j.bpsc.2016.03.009

Sherman, S. M. (2016). Thalamus plays a central role in ongoing cortical functioning. *Nature Neuroscience*, *19*(4), 533–541. https://doi.org/10.1038/nn.4269

Shin, C. W., & Kim, S. (2006). Self-organized criticality and scale-free properties in emergent functional neural networks. *Physical Review E - Statistical, Nonlinear, and Soft Matter Physics*, *74*(4), 1–4. https://doi.org/10.1103/PhysRevE.74.045101

Skåtun, K. C., Kaufmann, T., Doan, N. T., Alnæs, D., Córdova-Palomera, A., Jönsson, E. G., Fatouros-Bergman, H., Flyckt, L., Melle, I., Andreassen, O. A., Agartz, I., & Westlye, L. T. (2017). Consistent Functional Connectivity Alterations in Schizophrenia Spectrum Disorder: A Multisite Study. *Schizophrenia Bulletin*, *43*(4), 914–924. https://doi.org/10.1093/schbul/sbw145

Skene, N. G., Bryois, J., Bakken, T. E., Breen, G., Crowley, J. J., Gaspar, H. A., Giusti-Rodriguez, P., Hodge, R. D., Miller, J. A., Muñoz-Manchado, A. B., O'Donovan, M. C., Owen, M. J., Pardiñas, A. F., Ryge, J., Walters, J. T. R., Linnarsson, S., Lein, E. S., Sullivan, P. F., & Hjerling-Leffler, J. (2018). Genetic identification of brain cell types underlying schizophrenia. *Nature Genetics*, *50*(6), 825–833. https://doi.org/10.1038/s41588-018-0129-5

Skudlarski, P., Schretlen, D. J., Thaker, G. K., Stevens, M. C., Keshavan, M. S., Sweeney, J. a, Tamminga, C. a, Clementz, B. a, O'Neil, K., & Pearlson, G. D. (2013). Diffusion tensor imaging white matter endophenotypes in patients with schizophrenia or psychotic bipolar disorder and their relatives. *American Journal of Psychiatry*, *170*(8), 886–898. https://doi.org/10.1176/appi.ajp.2013.12111448

Slifstein, M., Van De Giessen, E., Van Snellenberg, J., Thompson, J. L., Narendran, R., Gil, R., Hackett, E., Girgis, R., Ojeil, N., Moore, H., D'Souza, D., Malison, R. T., Huang, Y., Lim, K., Nabulsi, N., Carson, R. E., Lieberman, J. A., & Abi-Dargham, A. (2015). Deficits in prefrontal cortical and extrastriatal dopamine release in schizophrenia a positron emission tomographic functional magnetic resonance imaging study. *JAMA Psychiatry*, *72*(4), 316–324. https://doi.org/10.1001/jamapsychiatry.2014.2414

Small, S. A., Schobel, S. A., Buxton, R. B., & Witter, M. P. (2011). A pathophysiological framework of hippocampal dysfunction in ageing and disease. *Nature Reviews Neuroscience*, *12*(10), 585–601. https://doi.org/10.1038/nrn3085

Smith, S. M., & Nichols, T. E. (2009). Threshold-free cluster enhancement: addressing problems of smoothing, threshold dependence and localisation in cluster inference. *Neuroimage*, *44*(1), 83–98. https://doi.org/10.1016/j.neuroimage.2008.03.061

Snaith, R. (2003). “The Hospital Anxiety and Depression Scale”. *Health Qual Life Outcomes*, *1*(6), 29. https://doi.org/10.1186/1477-7525-1-29

Soliman, A., O’Driscoll, G. A., Pruessner, J., Holahan, A. L. V., Boileau, I., Gagnon, D., & Dagher, A. (2008). Stress-induced dopamine release in humans at risk of psychosis: A [11C] raclopride PET study. *Neuropsychopharmacology*, *33*(8), 2033–2041. https://doi.org/10.1038/sj.npp.1301597

Soliman, A., O’Driscoll, G. A., Pruessner, J., Joober, R., Ditto, B., Streicker, E., Goldberg, Y., Caro, J., Rekkas, P. V., & Dagher, A. (2011). Limbic response to psychosocial stress in schizotypy: A functional magnetic resonance imaging study. *Schizophrenia Research*, *131*(1–3), 184–191. https://doi.org/10.1016/j.schres.2011.05.016

Sporns, O. (2013). Structure and function of complex brain networks. *Dialogues in Clinical Neuroscience*, *15*(3), 247–262. https://doi.org/10.31887/dcns.2013.15.3/osporns

Sporns, O., Chialvo, D. R., Kaiser, M., & Hilgetag, C. C. (2004). Organization, development and function of complex brain networks. In *Trends in Cognitive Sciences* (Vol. 8, Issue 9, pp. 418–425). https://doi.org/10.1016/j.tics.2004.07.008

Stam, C. J., & De Bruin, E. A. (2004). Scale-free dynamics of global functional connectivity in the human brain. *Human Brain Mapping*, *22*(2), 97–109. https://doi.org/10.1002/hbm.20016

Stefanis, N. C., Hanssen, M., Smirnis, N. K., Avramopoulos, D. A., Evdokimidis, I. K., Stefanis, C. N., Verdoux, H., & Van Os, J. (2002). Evidence that three dimensions of psychosis have a distribution in the general population. *Psychological Medicine*, *32*(02), 347–358. https://doi.org/10.1017/S0033291701005141

Stegmayer, K., Horn, H., Federspiel, A., Razavi, N., Bracht, T., Laimb??ck, K., Strik, W., Dierks, T., Wiest, R., M??ller, T. J., & Walther, S. (2014). Ventral striatum gray matter density reduction in patients with schizophrenia and psychotic emotional dysregulation. *NeuroImage: Clinical*, *4*, 232–239. https://doi.org/10.1016/j.nicl.2013.12.007

Stone, C. A., & Zhang, B. (2003). Assessing goodness of fit of item response theory models: A comparison of traditional and alternative procedures. *Journal of Educational Measurement*, *40*(4), 331–352. https://doi.org/10.1111/j.1745-3984.2003.tb01150.x

Stone, J. M., Howes, O. D., Egerton, A., Kambeitz, J., Allen, P., Lythgoe, D. J., O’Gorman, R. L., McLean, M. A., Barker, G. J., & McGuire, P. (2010). Altered relationship between hippocampal glutamate levels and striatal dopamine function in subjects at ultra high risk of psychosis. *Biological Psychiatry*, *68*(7), 599–602. https://doi.org/10.1016/j.biopsych.2010.05.034

Strauss, G. P., Ahmed, A. O., Young, J. W., & Kirkpatrick, B. (2019). Reconsidering the latent structure of negative symptoms in schizophrenia: A review of evidence supporting the 5 consensus domains. *Schizophrenia Bulletin*, *45*(4), 725–729. https://doi.org/10.1093/schbul/sby169

Strauss, G. P., Esfahlani, F. Z., Galderisi, S., Mucci, A., Rossi, A., Bucci, P., Rocca, P., Maj, M., Kirkpatrick, B., Ruiz, I., & Sayama, H. (2019). Network analysis reveals the latent structure of negative symptoms in schizophrenia. *Schizophrenia Bulletin*, *45*(5), 1033–1041. https://doi.org/10.1093/schbul/sby133

Strauss, G. P., Nuñez, A., Ahmed, A. O., Barchard, K. A., Granholm, E., Kirkpatrick, B., Gold, J. M., & Allen, D. N. (2018). The latent structure of negative symptoms in schizophrenia. *JAMA Psychiatry*, *75*(12), 1303. https://doi.org/10.1001/jamapsychiatry.2018.2475

Surmeier, D. J., Ding, J., Day, M., Wang, Z., & Shen, W. (2007). D1 and D2 dopamine-receptor modulation of striatal glutamatergic signaling in striatal medium spiny neurons. *Trends in Neurosciences*, *30*(5), 228–235. https://doi.org/10.1016/j.tins.2007.03.008

Sussman, D., Leung, R. C., Chakravarty, M. M., Lerch, J. P., & Taylor, M. J. (2016). Developing human brain: Age-related changes in cortical, subcortical, and cerebellar anatomy. *Brain and Behavior*, *6*(4), 1–15. https://doi.org/10.1002/brb3.457

Tansey, K. E., Rees, E., Linden, D. E., Ripke, S., Chambert, K. D., Moran, J. L., McCarroll, S. A., Holmans, P., Kirov, G., Walters, J., Owen, M. J., & O'Donovan, M. C. (2015). Common alleles contribute to schizophrenia in CNV carriers. *Molecular Psychiatry*, *21*(8), 1085–1089. https://doi.org/10.1038/mp.2015.143

Taylor, J. H., Calkins, M. E., & Gur, R. E. (2020). Markers of Psychosis Risk in the General Population. *Biological Psychiatry*. https://doi.org/10.1016/j.biopsych.2020.02.002

Thierry, A. M., Tassin, J. P., Blanc, G., & Glowinski, J. (1976). Selective activation of the mesocortical DA system by stress. *Nature*, *263*(5574), 242–244. https://doi.org/10.1038/263242a0

Thomas, M. L. (2011). The value of item response theory in clinical assessment: a review. *Assessment*, *18*(3), 291–307. https://doi.org/10.1177/1073191110374797

Thompson, J. L., Pogue-Geile, M. F., & Grace, A. A. (2004). Developmental pathology, dopamine, and stress: A model for the age of onset of schizophrenia symptoms. *Schizophrenia Bulletin*, *30*(4), 875–900. https://doi.org/10.1093/oxfordjournals.schbul.a007139

Toland, M. D. (2014). Practical Guide to Conducting an Item Response Theory Analysis. In *Journal of Early Adolescence* (Vol. 34, Issue 1). https://doi.org/10.1177/0272431613511332

Treiber, J. M., White, N. S., Steed, T. C., Bartsch, H., Holland, D., Farid, N., McDonald, C. R., Carter, B. S., Dale, A. M., & Chen, C. C. (2016). Characterization and correction of geometric distortions in 814 Diffusion Weighted Images. *PLoS ONE*, *11*(3). https://doi.org/10.1371/journal.pone.0152472

Upthegrove, R., Birchwood, M., Ross, K., Brunett, K., McCollum, R., & Jones, L. (2010).

The evolution of depression and suicidality in first episode psychosis. *Acta Psychiatrica Scandinavica*, *122*(3), 211–218. https://doi.org/10.1111/j.1600-0447.2009.01506.x

Uscatescu, L.-C., Kronbichler, L., Stelzig-Schoeler, R., Pearce, B.-G., Said-Yuerekli, S., Reich, L. A., Weber, S., Aichhorn, W., & Kronbichler, M. (2020). Effective connectivity of the hippocampus can differentiate patients with schizophrenia from healthy controls: a spectral DCM approach. *MedRxiv*. https://doi.org/10.1101/2020.01.12.20017293

Van Dellen, E., Bohlken, M. M., Draaisma, L., Tewarie, P. K., Van Lutterveld, R., Mandl, R., Stam, C. J., & Sommer, I. E. (2016). Structural brain network disturbances in the psychosis spectrum. *Schizophrenia Bulletin*, *42*(3), 782–789. https://doi.org/10.1093/schbul/sbv178

van der Sluis, S., Verhage, M., Posthuma, D., & Dolan, C. V. (2010). Phenotypic complexity, measurement bias, and poor phenotypic resolution contribute to the missing heritability problem in genetic association studies. *PLoS ONE*, *5*(11). https://doi.org/10.1371/journal.pone.0013929

van Os, J, Linscott, R. J., Myin-Germeys, I., Delespaul, P., & Krabbendam, L. (2009). A systematic review and meta-analysis of the psychosis continuum: evidence for a psychosis proneness-persistence-impairment model of psychotic disorder. *Psychological Medicine*, *39*(2), 179–195. https://doi.org/10.1017/S0033291708003814

van Os, Jim, & Kapur, S. (2009). Schizophrenia. *The Lancet*, *374*(9690), 635–645. https://doi.org/10.1016/S0140-6736(09)60995-8

Velthorst, E., Koeter, M., Van Der Gaag, M., Nieman, D. H., Fett, A.-K. J., Smit, F., Staring, A. B. P., Meijer, C., & de Haan, L. (2014). Adapted cognitive-behavioural therapy required for targeting negative symptoms in schizophrenia: Meta-analysis and meta-regression. *Psychological Medicine*, *45*, 453–465. https://doi.org/10.1017/S0033291714001147

Verdoux, H., & Van Os, J. (2002). Psychotic symptoms in non-clinical populations and the continuum of psychosis. *Schizophrenia Research*, *54*(1–2), 59–65. https://doi.org/10.1016/S0920-9964(01)00352-8

Visscher, P. M., Hill, W. G., & Wray, N. R. (2008). Heritability in the genomics era — concepts and misconceptions. *Nature Reviews Genetics*, *9*(4), 255–266. https://doi.org/10.1038/nrg2322

Vollema, M. G., Sitskoorn, M. M., Appels, M. C., & Kahn, R. S. (2002). Does the Schizotypal Personality Questionnaire reflect the biological-genetic vulnerability to schizophrenia? *Schizophr Res*, *54*(1–2), 39-45. https://doi.org/10.1016/S0920-9964(01)00350-4

Vul, E., Harris, C., Winkielman, P., & Pashler, H. (2017). Puzzlingly high correlations in fMRI studies of emotion, personality, and social cognition. *Perspectives on*

Psychological Science, *4*(3), 274–290. https://doi.org/10.1111/j.1745-6924.2009.01125.x

Vul, E., & Pashler, H. (2012). Voodoo and circularity errors. *NeuroImage*, *62*(2), 945–948. https://doi.org/10.1016/j.neuroimage.2012.01.027

Vulink, N. C., Planting, R. S., Figee, M., Booij, J., & Denys, D. (2016). Reduced striatal dopamine D2/3 receptor availability in Body Dysmorphic Disorder. *European Neuropsychopharmacology*, *26*(2), 350–356. https://doi.org/10.1016/j.euroneuro.2015.11.018

Walther, S., & Strik, W. (2012). Motor symptoms and schizophrenia. *Neuropsychobiology*, *66*(2), 77–92. https://doi.org/10.1159/000339456

Walton, E., Geisler, D., Lee, P. H., Hass, J., Turner, J. A., Liu, J., Sponheim, S. R., White, T., Wassink, T. H., Roessner, V., Gollub, R. L., Calhoun, V. D., & Ehrlich, S. (2014). Prefrontal inefficiency is associated with polygenic risk for schizophrenia. *Schizophrenia Bulletin*, *40*(6), 1263–1271. https://doi.org/10.1093/schbul/sbt174

Wang, X., Xia, M., Lai, Y., Dai, Z., Cao, Q., Cheng, Z., Han, X., Yang, L., Yuan, Y., Zhang, Y., Li, K., Ma, H., Shi, C., Hong, N., Szeszko, P., Yu, X., & He, Y. (2014). Disrupted resting-state functional connectivity in minimally treated chronic schizophrenia. *Schizophrenia Research*, *156*(2–3), 150–156. https://doi.org/10.1016/j.schres.2014.03.033

Wang, Y, Liu, W. H., Li, Z., Wei, X. H., Jiang, X. Q., Geng, F. L., Zou, L. Q., Lui, S. S., Cheung, E. F., Pantelis, C., & Chan, R. C. (2016). Altered corticostriatal functional connectivity in individuals with high social anhedonia. *Psychological Medicine*, *46*(1), 125–135. https://doi.org/10.1017/S0033291715001592

Wang, Yi, Ettinger, U., Meindl, T., & Chan, R. C. K. (2018). Association of schizotypy with striatocortical functional connectivity and its asymmetry in healthy adults. *Human Brain Mapping*, *39*(1), 288–299. https://doi.org/10.1002/hbm.23842

Wechsler, D. (2011). Wechsler Abbreviated Scale of Intelligence--Second Edition. In *Wechsler Abbreviated Scale of Intelligence--Second Edition (WASI-II)*. NCS Pearson.

Weinberger, D. R. (1987). Implications of Normal Brain Development for the Pathogenesis of Schizophrenia. *Archives of General Psychiatry*, *45*(11), 1055. https://doi.org/10.1001/archpsyc.1988.01800350089019

Weinstein, J. J., Chohan, M. O., Slifstein, M., Kegeles, L. S., Moore, H., & Abi-Dargham, A. (2017). Pathway-Specific Dopamine Abnormalities in Schizophrenia. *Biological Psychiatry*, *81*(1), 31–42. https://doi.org/10.1016/j.biopsych.2016.03.2104

Welsh, R. C., Chen, A. C., & Taylor, S. F. (2010). Low-frequency BOLD fluctuations demonstrate altered thalamocortical connectivity in schizophrenia. *Schizophrenia Bulletin*, *36*(4), 713–722. https://doi.org/10.1093/schbul/sbn145

Werbeloff, N., Drukker, M., Dohrenwend, B. P., Levav, I., Yoffe, R., van Os, J., Davidson, M., & Weiser, M. (2012). Self-reported attenuated psychotic symptoms as forerunners of severe mental disorders later in life. *Archives of General Psychiatry*, *69*(5), 467–475. https://doi.org/10.1001/archgenpsychiatry.2011.1580

White, T. P., Joseph, V., Francis, S. T., & Liddle, P. F. (2010). Aberrant salience network (bilateral insula and anterior cingulate cortex) connectivity during information processing in schizophrenia. *Schizophrenia Research*, *123*(2–3), 105–115. https://doi.org/10.1016/j.schres.2010.07.020

Whitfield-Gabrieli, S., Thermenos, H. W., Milanovic, S., Tsuang, M. T., Faraone, S. V., McCarley, R. W., Shenton, M. E., Green, A. I., Nieto-Castanon, A., LaViolette, P., Wojcik, J., Gabrieli, J. D. E., & Seidman, L. J. (2009). Hyperactivity and hyperconnectivity of the default network in schizophrenia and in first-degree relatives of persons with schizophrenia. *Proceedings of the National Academy of Sciences*, *106*(4), 1279–1284. https://doi.org/10.1073/pnas.0809141106

Winkler, A. M., Ridgway, G. R., Webster, M. A., Smith, S. M., & Nichols, T. E. (2014). Permutation inference for the general linear model. *NeuroImage*, *92*, 381–397. https://doi.org/10.1016/j.neuroimage.2014.01.060

Winton-Brown, T. T., Fusar-Poli, P., Ungless, M. A., & Howes, O. D. (2014). Dopaminergic basis of salience dysregulation in psychosis. *Trends in Neurosciences*, *37*(2), 85–94. https://doi.org/10.1016/j.tins.2013.11.003

Winton-Brown, T. T., Schmidt, A., Roiser, J. P., Howes, O. D., Egerton, A., Fusar-Poli, P., Bunzeck, N., Grace, A. A., Duzel, E., Kapur, S., & McGuire, P. (2017). Altered activation and connectivity in a hippocampal-basal ganglia-midbrain circuit during salience processing in subjects at ultra high risk for psychosis. *Translational Psychiatry*, *7*(10), 1–8. https://doi.org/10.1038/tp.2017.174

Wolf, D. H., Satterthwaite, T. D., Calkins, M. E., Ruparel, K., Elliott, M. a, Hopson, R. D., Jackson, C. T., Prabhakaran, K., Bilker, W. B., Hakonarson, H., Gur, R. C., & Gur, R. E. (2015). Functional neuroimaging abnormalities in youth with psychosis spectrum symptoms. *JAMA Psychiatry*, *72*(5), 456–465. https://doi.org/10.1001/jamapsychiatry.2014.3169

Wolthusen, R. P. F., Coombs, G., Boeke, E. A., Ehrlich, S., DeCross, S. N., Nasr, S., & Holt, D. J. (2018). Correlation between levels of delusional beliefs and perfusion of the hippocampus and an associated network in a non–help-seeking population. *Biological Psychiatry: Cognitive Neuroscience and Neuroimaging*, *3*(2), 178–186. https://doi.org/10.1016/j.bpsc.2017.06.007

Wood, S. J., Yung, A. R., McGorry, P. D., & Pantelis, C. (2011). Neuroimaging and treatment evidence for clinical staging in psychotic disorders: From the at-risk mental state to chronic schizophrenia. *Biological Psychiatry*, *70*(7), 619–625.

https://doi.org/10.1016/j.biopsych.2011.05.034

Woodward, N. D., Cowan, R. L., Park, S., Ansari, M. S., Baldwin, R. M., Li, R., Doop, M., Kessler, R. M., & Zald, D. H. (2011). Correlation of individual differences in schizotypal personality traits with amphetamine-induced dopamine release in striatal and extrastriatal brain regions. *American Journal of Psychiatry*, *168*(4), 418–426. https://doi.org/10.1176/appi.ajp.2010.10020165

Woodward, N. D., & Heckers, S. (2016). Mapping thalamocortical functional connectivity in chronic and early stages of psychotic disorders. *Biological Psychiatry*, *79*(12), 1016–1025. https://doi.org/10.1016/j.biopsych.2015.06.026

Yan, C., Wang, Y., Su, L., Xu, T., Yin, D., Fan, M., Deng, C., Wang, Z., Lui, S. S. Y., Cheung, E. F. C., & Chan, R. C. K. (2016). Differential mesolimbic and prefrontal alterations during reward anticipation and consummation in positive and negative schizotypy. *Psychiatry Research - Neuroimaging*, *254*, 127–136. https://doi.org/10.1016/j.pscychresns.2016.06.014

Yang, Q., Khoury, M. J., Friedman, J. M., Little, J., & Flanders, D. W. (2005). How many genes underlie the occurrence of common complex diseases in the population? *International Journal of Epidemiology*, *34*(5), 1129–1137. https://doi.org/10.1093/ije/dyi130

Yoon, J. H., Minzenberg, M. J., Raouf, S., D'Esposito, M., & Carter, C. S. (2013). Impaired prefrontal-basal ganglia functional connectivity and substantia nigra hyperactivity in schizophrenia. *Biological Psychiatry*, *74*(2), 122–129. https://doi.org/10.1016/j.biopsych.2012.11.018

Yung, A. R., & McGorry, P. D. (1996). The prodromal phase of first-episode psychosis: past and current conceptualizations. *Schizophrenia Bulletin*, *22*(2), 353–370. https://doi.org/10.1093/schbul/22.2.353

Yung, A. R., Yuen, H. P., Phillips, L. J., Francey, S., & McGorry, P. D. (2005). Mapping the onset of psychosis: The comprehensive assessment of at risk mental states (CAARMS). *Schizophrenia Research*, *60*(1), 30–31. https://doi.org/10.1016/S0920-9964(03)80090-7

Zeidman, P., Jafarian, A., Corbin, N., Seghier, M. L., Razi, A., Cathy, J., & Friston, K. J. (2019). A tutorial on group effective connectivity analysis , part 1 : first level analysis with DCM for fMRI 1 Introduction. *ArXiv Preprint*, *1902.1059*.

Zeidman, P., & Maguire, E. A. (2017). Anterior hippocampus: the anatomy of perception, imagination and episodic memory. *Nature Reviews Neuroscience*, *17*(3), 173–182. https://doi.org/10.1038/nrn.2015.24.Anterior

Zhou, Y., Friston, K. J., Zeidman, P., Chen, J., Li, S., & Razi, A. (2017). The Hierarchical Organization of the Default, Dorsal Attention and Salience Networks in Adolescents and Young Adults. *Cerebral Cortex*, *November*, 1–12. https://doi.org/10.1093/cercor/bhx307

Zhou, Y., Shu, N., Liu, Y., Song, M., Hao, Y., Liu, H., Yu, C., Liu, Z., & Jiang, T. (2008). Altered resting-state functional connectivity and anatomical connectivity of hippocampus in schizophrenia. *Schizophrenia Research*, *100*(1–3), 120–132. https://doi.org/10.1016/j.schres.2007.11.039